# Peatland restoration on the North York Moors: implications for hydrological functioning and water quality

Thesis submitted in accordance with the requirements of the University of Liverpool for the degree of Doctor in Philosophy

by

Hannah Tabea Lehnhart-Barnett

May 2022

Abstract

Increased recognition of the ecosystem services, such as climate regulation and supply of drinking water, provided by intact peatlands and the damaging impacts of peat afforestation on runoff regimes, water quality and carbon storage are driving forest-to-bog restoration initiatives within the UK and elsewhere. However, restoration programmes accompanied by long-term reference data remain scarce, limiting our current understanding of the timescales and mechanisms involved in post-forestry peatland restoration and the extent of hydrological and biogeochemical recovery attainable.

This research is set on May Moss, a 1.5 km^2 ombrotrophic open low-relief blanket mire in the North York Moors (NE England) and Site of Special Scientific Interest (SSSI). The water-shedding mire comprises two basins, one of which drains mainly intact and protected blanket bog, forming the headwater catchment for the Eller Beck (0.63 km^2). The second basin drains towards the Long Grain (1.53 km^2) and was afforested between 1975 and 1983 to form a lodgepole pine (*Pinus contorta*) plantation. Most of the forestry plantation within the Long Grain catchment was removed between 2009 and 2012 as part of a SITA Trust *Enriching Nature* funded blanket bog restoration program, which involved forest clearance, carried out through a combination of felling and mulching or pulverising, and drain blocking with peat plugs and timber weirs. A weather station was installed on the intact bog watershed in 2010 to enable long-term micrometeorological monitoring. A four-year paired catchment hydrological monitoring programme was initiated in spring 2017 through the installation of V-notch weirs and dipwells in both catchments, and expanded in summer 2018 through a two-year paired water sampling campaign for stream-water chemistry analysis. This research is thus based on a paired catchment study, comparing an "intact" blanket bog catchment with a "restored" catchment, ten years after rewetting. The main aims of this study were 1) to use the long-term hydrometeorological time-series to assess the hydrological functioning of an intact upland ombrotrophic mire, and 2) to examine the effects of peatland restoration from former conifer plantation on blanket bog functioning. These were assessed through three main objectives:

I. A characterisation of the hydrological functioning of May Moss based on the long-term micro-meteorological series (20/08/2010 – 01/07/2021) to examine the key drivers in water balance behaviour.

II. A comparison in hydrological functioning between the "intact" and "restored" catchments based on a four-year (14/03/2017 – 01/07/2021) paired runoff and

water table depth (WTD) series, supported by the long-term meteorological series for May Moss, to assess the hydrological recovery of the Long Grain catchment.

III. A comparison in stream-water chemistry between the "intact" and "restored" catchments based on a two-year (18/07/2018 – 27/08/2020) paired sampling campaign, supported by the simultaneous hydrological and meteorological series.

These three objectives produced the following key results:

I. Variations in average WTD between years are primarily related to variations in the average available energy (net radiation – soil heat flux), while variation in WTD over monthly timescales are driven mainly by changes in the vapour pressure deficit. Changes in peat water storage across the summer (June – August) are driven by summer water availability (precipitation – evapotranspiration), while more frequent, highly evaporative days ($\geq 25°C$) in summer are the main determinant in driving more severe water table drawdown events.

II. A decade after rewetting, storm runoff was significantly less "flashy" in the "restored" catchment, with a 35% reduction in peak flow, compared to the "intact" catchment, although the "restored" catchment releases proportionally higher baseflow. Water levels were near surface level (< 5cm) 45% of the time at the "restored" sites, compared to 60% at the "intact" site. Both sites showed good recovery after the 2018 drought summer, although runoff/rainfall coefficients suggest lower water retention and a longer post-drought recovery time at the "restored" catchment.

III. The "restored" site had significantly lower dissolved organic carbon (DOC) concentrations and water discolouration relative to the "intact" site, which may be related to factors such as recovery, enhanced flushing or differences in DOC production or mobility. Element enrichments in dry masses extracted from the water samples at the "restored" site are indicative of disturbance to the upper peat profile.

The research presented here indicates present hydrological resilience of an intact and recovering blanket mire to a drought event, though current climate trends may indicate vulnerability to the impacts of climate change. Given the relative reduction in storm runoff intensity and fluvial carbon loss in the recovering catchment of Long Grain within a decade of rewetting, this research advocates further and larger-scale forest-to-bog restoration, particularly of sites most at risk of drying, in order to sustain future hydrological resilience and ensure net carbon storage under a changing climate.

Acknowledgements

This has been an incredible journey. I would first and foremost like to convey my sincere gratitude to my supervisor Richard Chiverrell for giving me the opportunity to work with him on this project. He has provided me with continued support and guidance, as well as the time and patience in reading an endless supply of drafts and more drafts. During my PhD, he has also been actively supportive in opening new doors for me, such as applying for funds for our Arduino ventures. This has all been an immensely fun and rewarding experience, made even better with plenty of May Moss fieldtrips, sunny Yorkshire weather, epic breakfasts and the occasional adder! Thank you Rich!

I would also like to thank my secondary supervisors Neil Macdonald and Andy Morse for their insight and advice, as well as Cath Bashworth for providing us with the Forestry Commission collaboration and further financial support for the project. My sincere thanks also go to Claire Mahaffey for teaching and assisting me in DOC analysis and to Sabena Blackbird for laboratory analysis of POC and PN. My thanks also go to Jen and Luke, for making (sometimes tedious) lab work so much more entertaining, thanks guys!

I am also incredible grateful to my undergraduate supervisor Susan Waldron for inspiring and encouraging me to pursue a PhD in the first place!

This journey would not have been possible without a number of important people in my life.

A massive thanks to my amazing PhD pals Hazel, Grace, Maddy, Fi, Simon and Chris for being such a great support throughout – what a trip this has been! A special shout-out goes to Hazel for being the best flatmate I could ask for!

My gratitude also goes to Thomas and Katja, Rosemary, John, David and Judith, Julia, Milan, Lewi, and Oma Heidrun, Opa Werner, Onkel Marcus and Nelly, John and Gill, Alice, Frances and Peter, and my wild and lovable family across the pond: Sofi, Siri, Damian, Sam, John, Alex, tias Sheri and Chabu, tios David and Peter, uncle Chris and aunt Elizabeth. You have all been there in the background, supporting and cheering me on, so thank you!

I would like to convey my gratitude to three people in particular.

To my mother, Susan, I am grateful to you beyond words for your unwavering love, support and encouragement of me, you are amazing and so strong, and an inspiration to me, so thank you! I would also like to thank Klaus for enriching us with new adventure and giddy laughs!

James, thank you for your love and wholehearted support. Your creativity, strength, drive and passion for the natural world are an inspiration to me and I feel incredibly lucky to have you in my life. I'm excited to see what the next chapter holds!

TABLE OF CONTENTS

6

List of Figures

13

15

LIST OF TABLES

17

Chapter 1. Introduction

1.1 MOTIVATION OF RESEARCH

Anthropogenic pressures on the natural environment have led to major disruption to most of Earth's ecosystems and climate. Peatlands have become a prime example of resource exploitation ranging from palm oil plantations to peat extraction and commercial forestry. These industries generally depend on the drainage of peatlands and are associated with a variety of negative impacts, ranging from habitat loss to severe carbon emissions, thus exacerbating anthropogenic pressures on the climate system (Moore, 2002; Frolking et al., 2011).

Peatlands are wetland environments in which organic matter – peat – has accumulated over thousands of years and preserved by permanently water saturated, anoxic conditions (Rydin and Jeglum, 2013). Despite covering only 3% of the world's terrestrial land surface (Xu et al., 2018), peatlands contain between 500 and 700 Gt C (Yu et al., 2010), making them the largest terrestrial carbon store and important regulators of the global climate (Bonn et al., 2016). Ombrotrophic peatlands, or bogs, derive all their water and nutrient supply from precipitation, leading to their poor nutrient status and acidic condition (Charman, 2002), and are often located within headwater catchments that are important sources for drinking water (Ritson et al., 2014).

Peatlands are estimated to cover 11% of the UK (Joosten et al., 2017) (Figure 1.1), with an estimated carbon pool of 2302 Mt C (Billett et al., 2010). Blanket bogs, so called for the way that they blanket the upland landscape, are the most prominent peatland type in the UK, making up 82% of the UK's peatland area (Joosten et al., 2017). In addition, Britain is estimated to contain 10-15% of the world's total blanket bog area (Lindsay, 1995). However, large-scale drainage and afforestation of peatlands, particularly between the 1950s and 1980s (Hargreaves et al., 2003; Sloan et al., 2018a), led to the conversion of approximately 9 – 10% of deep peat areas in the UK to forestry plantations, contributing to the wide-ranging modifications of UK peatland today (Figure 1.2). In the UK, peatland afforestation tends to be carried out on open bogs and involves the ploughing of regularly spaced furrows as well as deeper drains which lead surface waters off the site and channel them to streams, which effectively lowers water levels in the peat (Anderson and Peace, 2017). Prepared sites are then planted typically with the North American species *Pinus contorta* (lodgepole pine) or *Picea sitchensis* (Sitka spruce) (Cannell et al., 1993; Tanneberger et al., 2017).
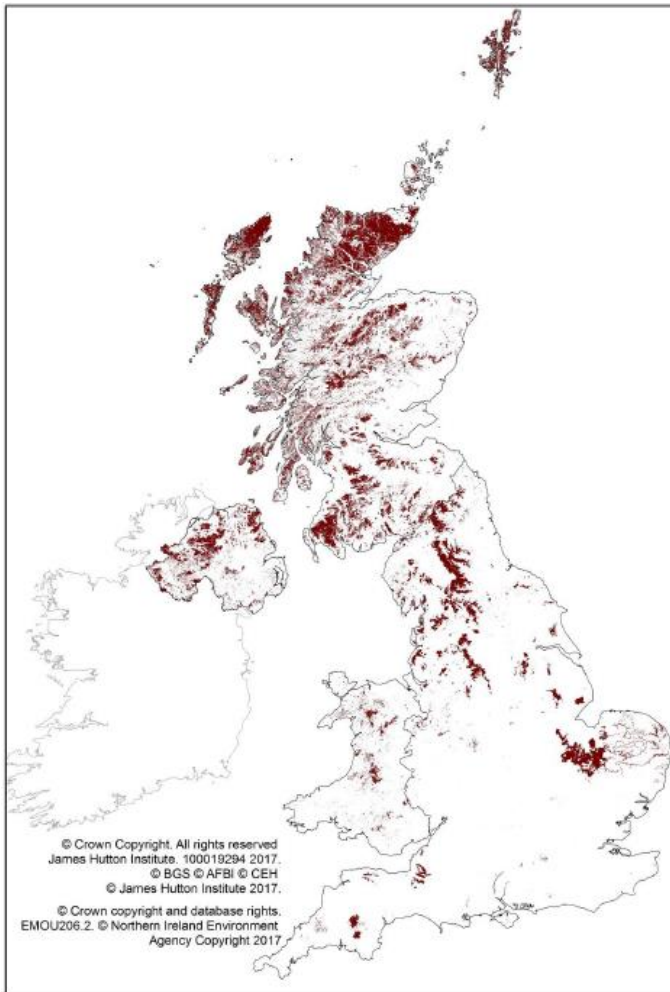
Figure 1.1. Map showing peat cover in the United Kingdom (Artz et al., 2019).
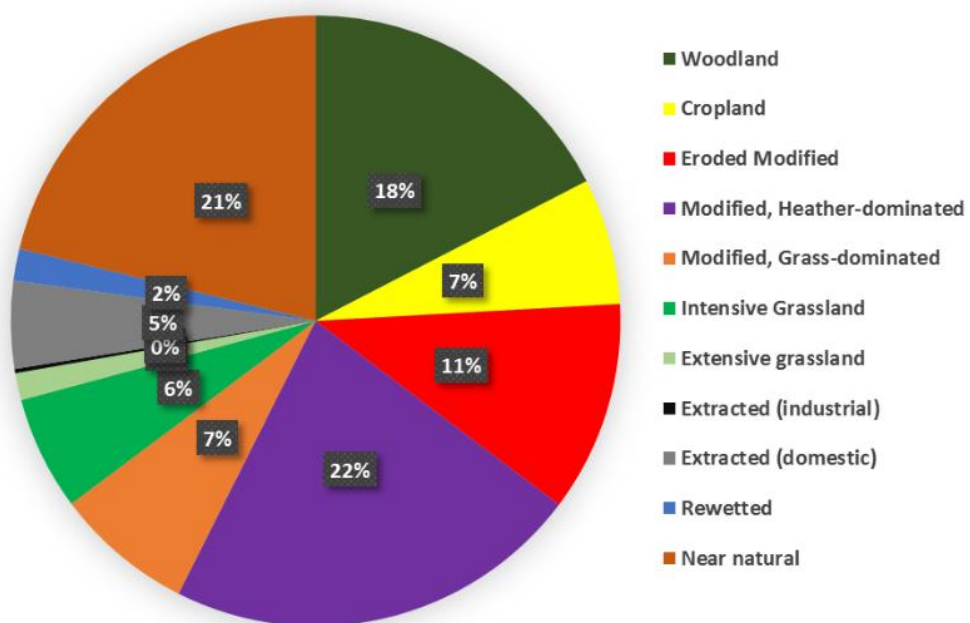
Figure 1.2. State of UK peatlands (Artz et al., 2019).

Awareness of the impact of drainage on the hydrology of peatlands goes back to the mid-20th century. For example, Conway and Millar (1960) offer an early example of a paired catchment study in the northern Pennines, UK, in which they highlight a reduced water storage capacity within a drained peatland relative to a near "natural" bog with abundant *Sphagnum* cover. Similarly, Burke (1975) found that drainage increased runoff from a blanket bog in Co. Mayo, Ireland, which in turn led to the combined water losses through runoff and evaporation exceeding inputs from precipitation, resulting in a progressive drying of the bog. Since then, mounting evidence has pointed towards the damaging effects of peatland drainage and afforestation, particularly concerning habitat loss (Lavers and Haines-Young, 1997; Hancock et al., 2020; Strobl et al., 2020), water quality, through the heightened release of nutrients and dissolved organic carbon (Rodgers et al., 2010; Asam et al., 2014b; a; Nieminen et al., 2015, 2017a; b; Marttila et al., 2018) and carbon emissions from drainage-induced peat decomposition (Meyer et al., 2013; Günther et al., 2020; Jovani-Sancho et al., 2021), with global CO_2 emissions from drained peatlands estimated to have increased by 20% between 1990 and 2008 (Joosten, 2009).

The concept and practice of peatland restoration have been developing over the past 30 years to encompass not only the rewetting of drained peatlands to form new wetland habitat to benefit wildlife, but also more recently to re-establish their "active" status as carbon sinks after commercial practices, such as forestry and peat harvesting, have ceased. An early example is the rewetting project of the ca. 2 km^2 Hasenmoor in Schleswig-Holstein, northern Germany, which was commercially mined from 1921 to 1970 and subsequently rewetted by blocking drainage ditches to raise the bog's water levels (Eigner, 1975). Increasing recognition of the importance of intact peatlands in global carbon cycling, sequestration, and storage, as well as the negative impacts of peatland degradation have led to the initiation of monitoring programmes and promoted peatland restoration projects in the UK and around the world (Erwin, 2009; Field et al., 2020). Such restoration aims to assist the recovery of peatland hydrological and biogeochemical functioning to facilitate peat accumulation, biodiversity and other ecosystem services, with the overall aim of mitigating climate change (Bonn et al., 2016). More recent developments have included the concept of "natural capital" – the economic valuation of ecosystem services (Potschin and Haines-Young, 2011). In Payment for Ecosystem Services (PES) schemes, individuals and organisations deliver payment for ecosystem services on a voluntary basis to the provider (e.g. landowner, steward, organisation, etc.) who is turn funds the sustainable land management necessary for the continued provision of such services (Reed et al., 2017). An example of such a PES

scheme is the UK Peatland Code (IUCN, 2022), developed and published by the International Union for Conservation of Nature (IUCN) UK Peatland Programme. The UK Peatland Code is designed to provide a basis for business sponsorship of UK peatland restoration and carbon finance, motivated by corporate social responsibility, as a means to deliver climate change mitigation benefits alongside other ecosystem services (Reed et al., 2013; IUCN, 2022).

In the UK, there has been a growing wealth in research focused on the restoration of eroding peatland over the last several decades (Phillips et al., 1981; Evans and Warburton, 2010; Shuttleworth et al., 2015). More recently, interest and funding towards peatland restoration has targeted the recovery of former "active" bogs from commercial afforestation, also known as forest-to-bog restoration (Anderson, 2010; Howson et al., 2021b). Such restoration activities typically involve the removal of trees and blocking of drainage ditches to raise water levels (Anderson, 2010), though best-practises are still being developed (Anderson and Peace, 2017; Gaffney et al., 2022). To fully assess the extent of ecosystem recovery, rewetting projects require long-term (> 5 years) studies in conjunction with baseline or reference data (Andersen et al., 2017), while their recovery is foremost examined in terms their ecological, hydrological and biogeochemical functioning (Gilbert, 2013; Creevy et al., 2020; Mazzola et al., 2020; Pravia et al., 2020; Howson et al., 2021b), necessary to assess the extent of restoration "success" in the (re-)establishment of ecosystem services. This ultimately informs commercial and government bodies on their efficacy, with the aim to stimulate further investment in peatland restoration (Glenk and Martin-Ortega, 2018).

Given that forest-to-bog restoration is a relatively novel approach, there have been calls for further research into the extent of recovery attainable (Alderson et al., 2019) and the timeframes and mechanisms involved (Martin-Ortega et al., 2014; Glenk et al., 2021), by crucially involving baseline or control sites to assess their relative success in re-establishing "natural" hydrological and biogeochemical functioning (Andersen et al., 2017). This research provides valuable baseline and reference data based on a decade of hydro-meteorological monitoring of an "intact" blanket bog, May Moss, coinciding with a four-year paired catchment study involving the "intact" and a "restored" catchment, to assess hydrological and biogeochemical recovery a decade after rewetting took place.

1.2 MAY MOSS

The study is centred on May Moss (54° 21' 4" N, 0° 39' 16" W, elev. 253 m) (Figure 1.3), a 1.5 km^2 ombrotrophic blanket bog in the eastern North York Moors, protected as part of the

North York Moors Site of Special Scientific Interest (SSSI)/Special Protection Area (SPA) and managed by Forestry England, Natural England (Figure 1.4). The full extent of the water-shedding mire is larger than the remaining intact bog (0.63 km^2), originally comprising two basins which feed the headwaters of the northward draining Eller Beck (EB) and southward flowing Long Grain (LG) (Figure 1.4). Eller Beck forms a first order stream contributing to the River Esk catchment, which empties directly into the North Sea at the town of Whitby. Long Grain, likewise a first order stream, drains into the southward flowing Upper Derwent, which itself contributes to the flood-prone River Ouse, which flows through the city of York, before joining the River Trent and entering the Humber Estuary.

The bog habitat at May Moss is classified as a *Sphagnum magellanicum – Andromeda polifolia* (M18a) sub-community under the National Vegetation Classification (NVC) (Elkington et al., 2001). There is an abundant presence of *Calluna vulgaris*, *Erica tetralix*, *Eriophorum vaginatum*, *Eriophorum augustifolia*, *Vaccinium myrtillus*, *Empetrum nigrum* and *Hypnum jutlandicum* (Chiverrell, 2001) and scattered incidence of *Drosera rotundifolia*. The bog furthermore supports intermittent bog pools (Figure 1.5) and populations of Adders (*Vipera berus*) and the Large Heath (*Coenonympha tullia*) butterfly. The site borders an extensive area of upland wet heathland to the north and grass moorland to the northwest and northeast (Figure 1.4). The land is administered by the Forestry Commission to the south and east, and the Ministry of Defence (RAF Fylingdales) to the north-west, rendering it largely inaccessible to the public.

Peat development at May Moss initiated separately within the two basins over the underlying Kellaways Rock, a brown ferruginous mid-Jurassic sandstone, approximately 9 ka during the early Holocene (Atherden, 1979), followed by paludification in which peat expanded to cover the watershed between the basins from 3.5 to 3 ka (Chiverrell, 2001). The deepest peats are > 5 m and centre in those basins, with Atherden (1979) recording a maximum peat depth of 6.4 m, while 3 m of ombrotrophic peat cover parts of the watershed between the two basins (Figure 1.3) (Chiverrell, 2001). Peat cores taken from May Moss and analysed for light transmittance present a gradual increase in humification down the peat profile (Figure 1.6), reflecting continued peat decomposition towards greater depths. However, the cores have also revealed both vertical and horizontal inconsistencies in the humification stratigraphy, which may be related to the presence of *Sphagnum* (more resistant to decay) during wetter conditions, differing rates of accumulation and acrotelm characteristics, and local variation in bacterial populations (Chiverrell, 2001). While historical botanical data have indicated a drying trend at May Moss during the 20th century, in response

to nearby forestry land use or climate change (Atherden, 1972), reconstructions of surface wetness have identified repeated changes between wetter and drier conditions, highlighting that May Moss has endured a variable climate over the past 2000 years (Chiverrell, 2001).
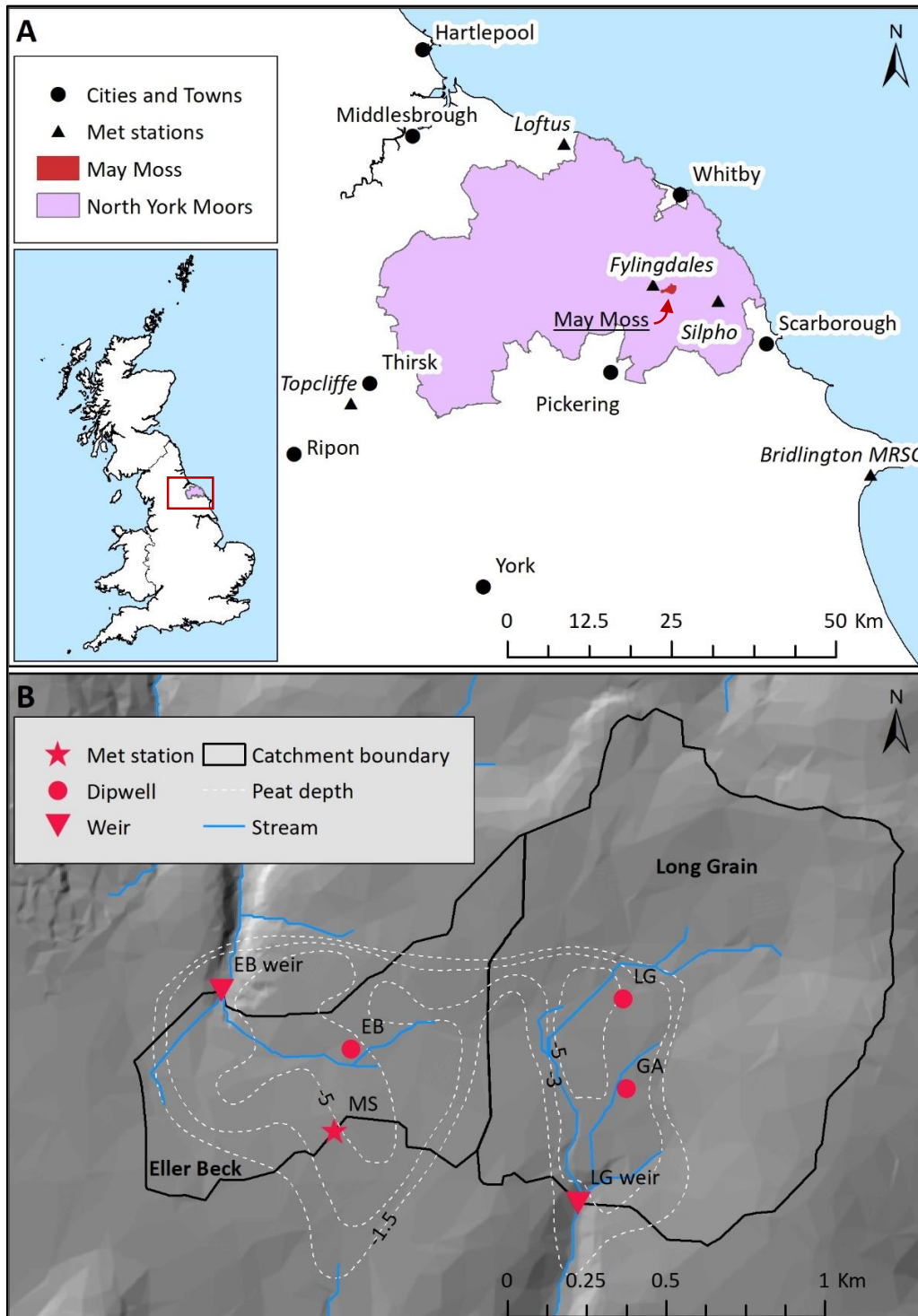
Figure 1.3. A) Regional map of the study site May Moss, situated within the North York Moors, UK, and nearby MIDAS meteorological stations (black triangles and labels in italics). B) Site map of May Moss, showing peat depths (Chiverrell, 2001) across the Eller Beck and Long Grain catchments and monitoring stations.
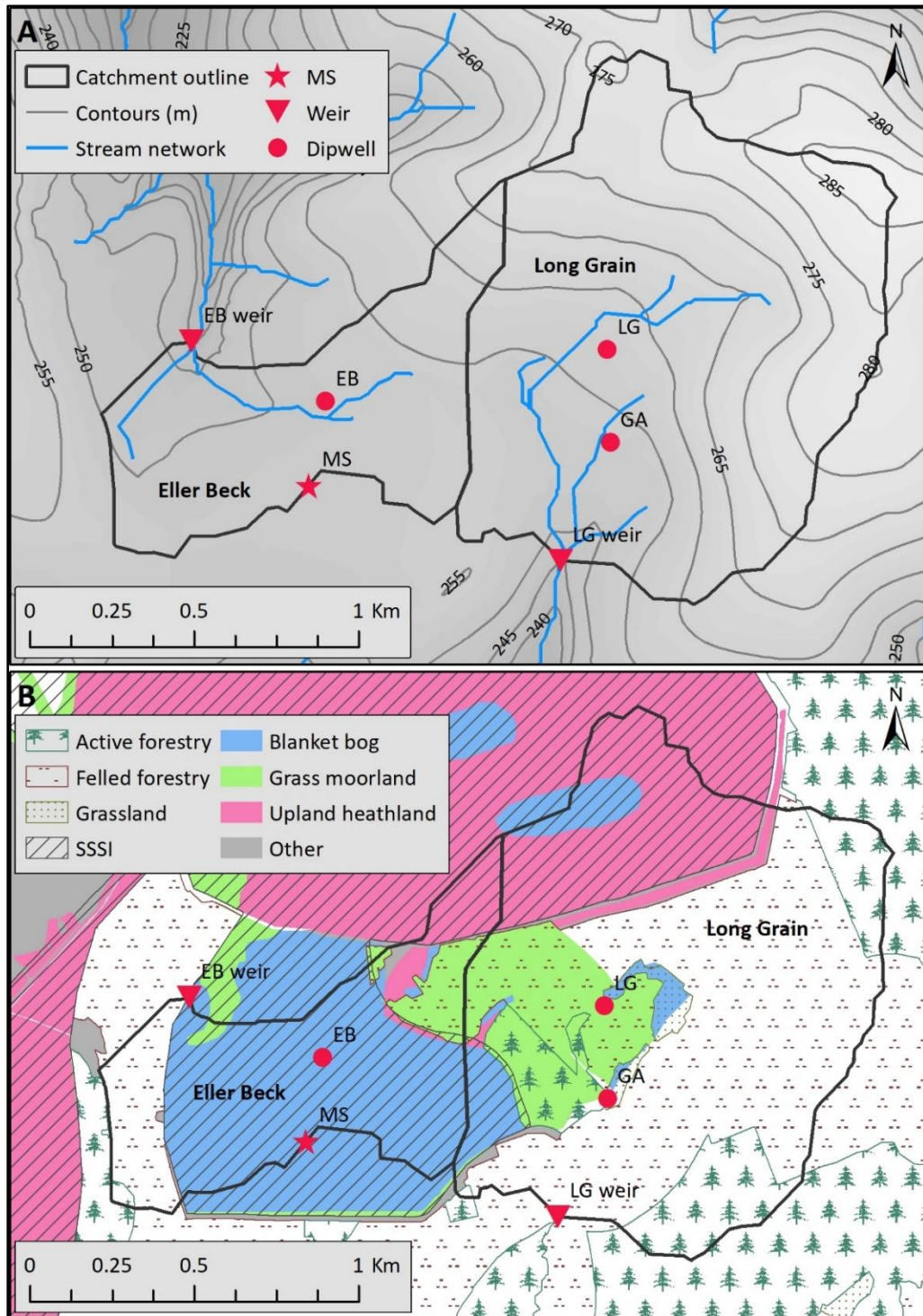
Figure 1.4. A) Topography (Ordnance Survey, 2020) and stream network of the Eller Beck and Long Grain catchments. B) Hashed lines depict area designated as SSSI; Surface cover categories shown according to the Priority Habitat Inventory (Natural England, 2019) and the National Forestry Inventory (Forestry Commission, 2019). Both maps depict the catchment outlines and monitoring sites.
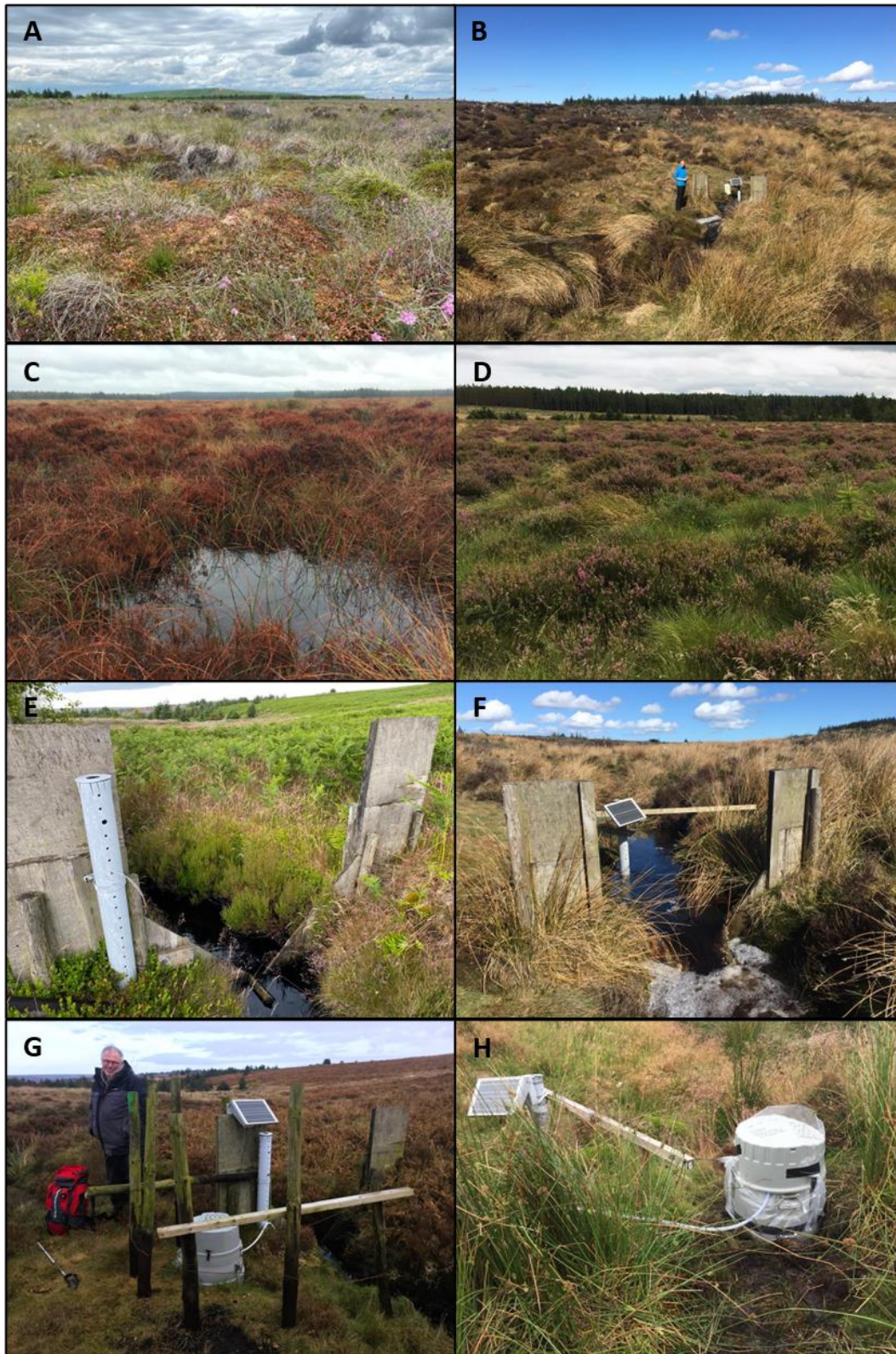
Figure 1.5. Images from May Moss. A) The intact bog in summer; B) The recovering bog and weir on Long Grain; C) A bog pool on the intact bog, D) The recovering bog in summer; E) Close-up of the weir on Eller Beck; F) Close-up of the weir on Long Grain; G) The autosampler at Eller Beck weir; and H) The autosampler at Long Grain weir. © Richard Chiverrell and Hannah Lehnhart-Barnett.
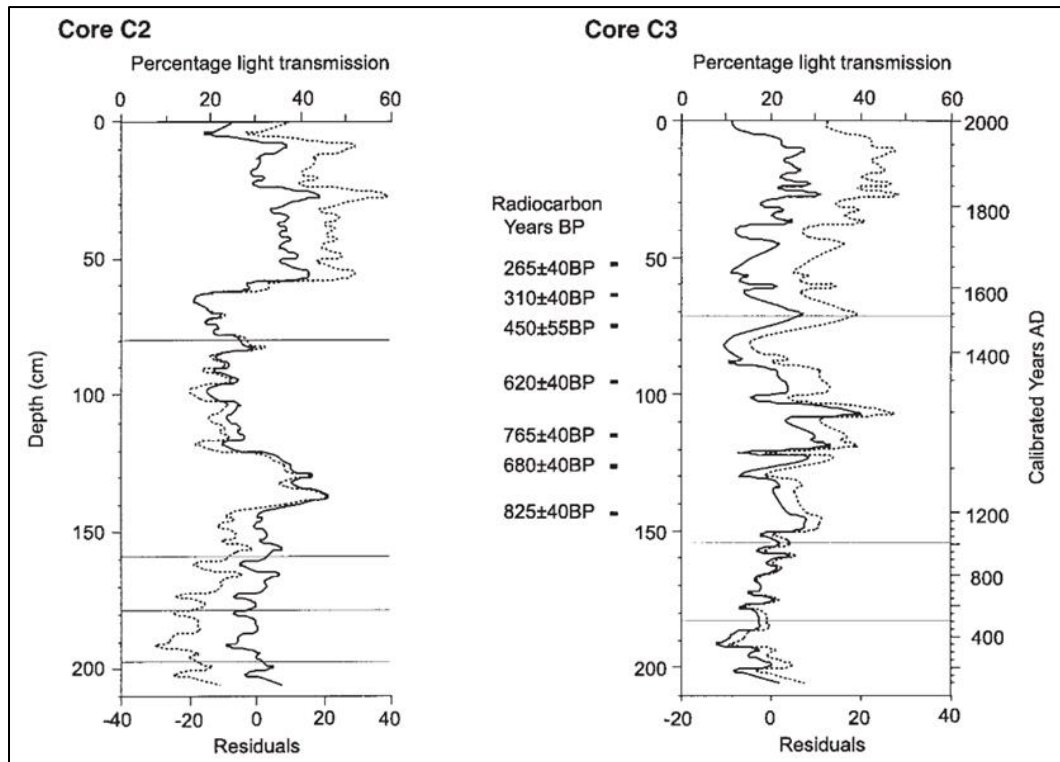
Figure 1.6. Percentage light transmission data from May Moss cores C2 and C3 from Chiverrell (2001). The dashed line presents the percentage light transmission, and the solid line presents the residual values after removal of the long-term trend. A low percentage of light transmission denotes well-humified peat and a high percentage denotes poorly humified peat (Chiverrell, 2001).

Like many other peatland areas in the UK, large parts of the Long Grain catchment were afforested between 1975 and 1983 to form a Lodgepole pine (*Pinus contorta*) plantation, managed by the Forestry Commission. SITA Trust *Enriching Nature* funding enabled the launch of a 0.7 km^2 restoration program across the Long Grain catchment between 2009 and 2012 to restore the "lost" half of May Moss (Cris et al., 2012), with the hope of facilitating carbon storage and alleviating the severity of downstream flooding through natural flood management (slowing-the-flow) (Foster, 2012). Restoration work involved forest clearance, carried out through a combination of felling and mulching or pulverising, and drain blocking with peat plugs and timber weirs, while planting ridges and furrows were left intact and largely remain in place (Figure 1.7). The Eller Beck catchment remains largely intact, mainly draining the SSSI protected blanket bog (Figure 1.4).

A monitoring program on the intact bog was launched in August 2010 (Figure 1.8), with a meteorological station installed near the centre of the intact bog and the watershed of the Eller Beck catchment (Figure 1.3 and Figure 1.4), providing hourly air temperature, relative humidity, and wind profiles, as well as net radiation, photosynthetic active radiation, soil heat flux, atmospheric pressure, precipitation and water table depth. Based on hydro-meteorological data (2010 – 2019) from the May Moss meteorological station, the mire is

characterised by an average annual temperature of 8.1°C and average annual precipitation of 922 mm. This places the mire below the lower margin of annual precipitation amounts (> 1000 mm) considered necessary for the continued development of a bog (Lindsay, 1995).

Figure 1.7. A) A digger mulches timber in the Long Grain catchment © Tony Bartholomew. B) Long Grain after forest clearance and ditch-blocking © Forestry Commission.

9 – 3 ka	1975 – 1983	2009 – 2012	August 2010	March 2017	July 2018
•Peat initiation and paludification at May Moss	•Afforestation of eastern section of May Moss	•Rewetting of 70.6 ha of former blanket bog	•Installation of the hydro-meteorological station on the intact bog •Start of monitoring programme	•Installation of weirs and dipwells on the intact and rewetted sites •Start of paired hydrological monitoring	•Installation of autosamplers on the intact and rewetted sites •Start of paired stream-water chemistry monitoring

Figure 1.8. Timeline of the origin, land use change and monitoring programme at May Moss.

In March 2017, V-notch weirs with dipwells, recording the water stage directly upstream, were installed on the Eller Beck and Long Grain streams where they exit the area of deep peat (Figure 1.3 and Figure 1.4). Three additional dipwells were also installed within the peat: "EB" within the Eller Beck catchment, supplementing the long-term dipwell "MS" at the meteorological station, "LG" within the Long Grain catchment, and "GA" adjacent to a bog pool, named Great Arc, also within the Long Grain catchment (Figure 1.3 and Figure 1.4). Automatic water levels loggers were placed in all dipwells to record runoff at the weirs and peatland water table depth. A water sampling campaign was initiated in July 2018 by installing automatic water samplers adjacent to the two weirs to collect 1 L samples every couple of days for water sample analysis (Figure 1.8).

The monitored catchment areas measure 0.63 km^2 for the Eller Beck catchment and 1.53 km^2 for the Long Grain catchment. The monitored Eller Beck catchment is dominated by intact blanket bog (64.0%), with some upland heathland to the northeast, and felled recovering areas (23.4%) to the west and northeast of the catchment (Figure 1.4 and Table 1.1). The

adjacent monitored Long Grain catchment is dominated by deforested areas intended for recovering former blanket bog habitat (56.8%). Deforestation within Long Grain thus covers an area greater than 20% – a threshold recommended for the analysis of land cover change impacts on water yields within paired catchment studies (Brown et al., 2005). The Long Grain catchment also contains smaller patches of upland heathland (18.4%) to the north and some remaining active forestry plantation (15.7%) to the west along the border with intact blanket bog, as well as to the northeast and south of the catchment, with only a small proportion of intact blanket bog (5.3%) situated within the catchment (Figure 1.4 and Table 1.1). Given the dominated land covers at each respective site and for ease of recognition, the Eller Beck catchment is often referred to as the "intact" site or simply "EB", while the Long Grain catchment is discussed as the "restored" or "recovering" site or simply as "LG" in this thesis.

Table 1.1. Catchment area and percentage land covers of the Eller Beck and Long Grain catchments.

Characteristic	Eller Beck	Long Grain
Catchment area (km^2)	0.63	1.53
Land cover (%)		
Blanket bog	64.0	5.3
Active forestry	0.6	15.7
Felled forestry	23.4	56.8
Grass moorland	0.8	0.1
Grassland	0.0	2.1
Upland heathland	9.9	18.4
Other (e.g. road)	1.3	1.6

1.3 PAIRED CATCHMENT APPROACH

This research employs a paired catchment approach, contrasting the Long Grain catchment, characterised by a forest-to-bog rewetting programme carried out a decade prior to this study, with the adjacent Eller Beck catchment, dominated by intact blanket bog (Figure 1.4). Paired catchment analysis is a widely-used method for determining effects of land-use changes on runoff by comparing a treated catchment with a control (Conway and Millar, 1960; Brown et al., 2005; Bathurst et al., 2018). A key advantage of paired catchment studies is the exclusion of climate variability as a controlling variable, as both catchments are subject to the same climatic and meteorological conditions (Brown et al., 2005). Brown et al. (2005) further highlight that paired catchments should display similarities in slope, aspect, soils and area to assess for changes in water yield solely in response to changes in vegetation. While the first three of those characteristics are comparable between the two catchments (Figure 1.4), the two-fold difference in catchment size may be considered an additional factor influencing potential differences in runoff between both sites, despite both catchments

being relatively small headwaters. Concerns over catchment size reflect the wider discussion on scale, or how well the observations within small headwater catchment reflect processes occurring within larger catchments. Extrapolation of such observations should be approached with caution and with a level of uncertainty, as for instance, hydrological responses within small catchments have been shown to be more variable compared with larger catchment (Pilgrim et al., 1982; Stott, 1997). More recently, research into the role of scale in catchment analysis has revealed greater linkages between catchments ranging in size. For example, across eight nested catchments, ranging 7 – 147 ha, in eastern Quebec, Canada, the fraction of effective rainfall routed as event water during rainstorms was insensitive to catchment size and instead related more to storm intensity (Segura et al., 2012). Likewise, Jutebring Sterte et al. (2021) have pointed to the soil characteristics, in particular hydraulic conductivity, being the critical factor influencing water travel time, rather than catchment size. However, studies have also shown the presence of linear relationships between catchment size and mean transit time (Segura et al., 2012) as well as chemical fluxes of dissolved organic carbon (DOC) and total dissolved solids (TDS) (Coch et al., 2020). To offset any influence of catchment size within this research, fluxes such as discharge and DOC are corrected by dividing them by the catchment area (Hope et al., 1997; Worrall et al., 2012), which thus allows the two catchments to be compared in terms of their fluxes per unit of area. The experimental setup across Eller Beck and Long Grain thus facilitates a paired catchment approach for investigating the influence of forest-to-bog restoration on hydrological and biogeochemical functioning.

1.4 RESEARCH AIM AND OBJECTIVES

The aims of this research are 1) to use the long-term hydrometeorological time-series to assess the hydrological functioning of an intact upland ombrotrophic mire, and 2) to examine the effects of peatland restoration from former conifer plantation on a blanket bog situated towards the dry end of the climate window typically associated with blanket mires. The research assesses the hydrological functioning and water quality using a paired catchment approach comparing an "intact" catchment (Eller Beck) with an adjacent "restored" catchment (Long Grain). These aims were addressed using three core objectives:

I. Quantifying and characterising the hydrological functioning and drivers governing the intact blanket bog and the main catchment draining it (Eller Beck) using a 10-year hydro-meteorological timeseries (20/08/2010 – 01/07/2021) (*Chapter 4*)

II.   A critical comparison of the hydrological functioning of the paired intact and restored catchments using a four-year hydrological series (14/03/2017 – 01/07/2021) including runoff and water table depths, a decade after rewetting (*Chapter 5*)

III.   Evaluating the impacts of restoration on stream-water quality by comparing the intact and restored catchments by conducting a two-year water sampling campaign (18/07/2018 – 27/08/2020), facilitated by the paired hydrological series (*Chapter 6*)

1.5   THESIS STRUCTURE

This thesis consists of six main chapters, with Chapters 4, 5 and 6 produced as journal articles. Chapter aims and declarations of relative contributions are summarised as follows:

Chapter 2. Literature review: Hydrology and hydrochemistry of ombrotrophic peatlands

Chapter 2 provides a review of literature on the hydrological functioning and hydrochemistry of intact ombrotrophic peatlands. The chapter begins by explaining the components of the water balance and their interrelationships. The core processes in peat accumulation, decomposition, humification and mineralisation are then explored, followed by a summary of the stream-water chemistry, particularly concerning dissolved organic carbon (DOC). The review concludes with a consideration of the role and implementation of peatland restoration research within climate change mitigation.

Contributions: **Hannah Lehnhart-Barnett**: Conceptualization, Writing - Original Draft, Review & Editing

Chapter 3. Gap filling, quality control and preliminary processing of the May Moss meteorological data

Chapter 3 encompasses a thorough description of the data cleaning and gap filling procedure carried out for the long-term micrometeorological timeseries (20/08/2010 – 01/07/2021), including air temperature, relative humidity, and wind speed profiles, as well as atmospheric pressure, net radiation, photosynthetic active radiation, soil heat flux, peat temperatures, precipitation and water table depth (WTD), to prepare the data for later analysis. The chapter also provides a review of the commonly implemented techniques for measuring and calculating evapotranspiration (ET) in peatlands, followed by a step-by-step guide for the calculation of ET using the Bowen ratio energy balance method as well as the procedure

followed for data rejection and subsequent ET gap filling. The chapter offers a consideration of the main sources of measurement error and the validity of approaches undertaken to reduce such error, and concludes with a summary of quality control procedures carried out to produce a decade-long ET time series for May Moss.

Contributions: **Hannah Lehnhart-Barnett**: Conceptualization, Methodology, Writing - Original Draft; **Richard Chiverrell**: Conceptualization, Writing - Review & Editing, Supervision, Funding acquisition; **Neil Macdonald**: Writing - Review & Editing; **Andy Morse**: Methodology

Chapter 4. Hydrological functioning of an intact blanket bog and the impact of summer heatwaves

This chapter encompasses the analysis of the long-term hydrometeorological timeseries from the May Moss meteorological station. The timeseries is used to characterise the hydrological functioning of an intact blanket bog, in terms of annual water balances and the influence of micrometeorology on water table processes. Correlations between the radiative budget, temperature, vapour pressure deficit, precipitation, and peatland water tables shed light on the key factors governing hydrological functioning over annual, seasonal, and monthly timescales. The chapter concludes with a consideration of the vulnerability of the hydrological functioning of May Moss to climatic warming.

Contributions: **Hannah Lehnhart-Barnett**: Conceptualization, Methodology, Writing - Original Draft; **Richard Chiverrell**: Conceptualization, Resources, Writing - Review & Editing, Supervision, Funding acquisition; **Neil Macdonald**: Writing - Review & Editing, Supervision

Chapter 5. Forest-to-bog restoration I. Hydrological functioning

Here, we analyse the impact of forest-to-bog restoration on the hydrological functioning of a formerly afforested blanket bog through a paired catchment study with an adjacent intact blanket mire. Annual water balances, comprising precipitation, evapotranspiration, runoff, and storage change, as well as their residuals, are quantified for three hydrological years (2017/18, 2018/19 and 2019/20). The two catchments are compared in their relative runoff partitioning into quickflow and baseflow, storm hydrograph response and water table drawdown behaviour. Peak runoff was significantly reduced, and lag times extended at the restored site relative to the intact site, resulting in storm hydrographs to be considerably subdued. Higher baseflow at the restored site suggest more enhanced hydraulic connectivity with the peat, which may be a legacy effect of previous drainage.

Contributions: **Hannah Lehnhart-Barnett**: Conceptualization, Methodology, Writing - Original Draft; **Richard Chiverrell**: Conceptualization, Resources, Writing - Review & Editing, Supervision, Funding acquisition

Chapter 6. Forest-to-bog restoration II. Stream-water chemistry

Using the paired intact and restored catchments, a two-year water sampling campaign was carried out, collecting stream-water samples every two days from streams draining the intact (EB) and restored (LG) sites. Water samples were analysed for dissolved organic carbon (DOC), dissolved nitrogen (DN), particulate organic carbon (POC), particulate nitrogen (PN), loss-on-ignition (LOI) and UV-vis absorbance. Powders collected by freeze drying the water samples were analysed for humic substances (HS) and 32 element concentrations measured by X-ray Fluorescence (XRF). Stream-water DOC concentrations and discolouration were significantly lower at the restored site, while POC concentrations were similar between both sites, suggesting that post-forestry restoration has been effective in limiting fluvial carbon loss below pristine levels. Higher element concentrations within dry masses extracted from water samples at the restored site suggest considerable disturbance-induced mixing of the upper peat profile.

Contributions: **Hannah Lehnhart-Barnett**: Conceptualization, Methodology, Writing - Original Draft; **Richard Chiverrell**: Conceptualization, Resources, Writing - Review & Editing, Supervision, Funding acquisition; **Claire Mahaffey**: Resources**; Sabena Blackbird**: Resources

Chapter 7. Synthesis

This final chapter offers a synthesis of the thesis and is divided into three parts: 1) a summary of the key results, 2) an exploration of the scope for future research and 3) a speculative discussion of the key findings within the context of wider research on palaeoclimatology, climate change and peatland restoration and management.

Contributions: **Hannah Lehnhart-Barnett**: Conceptualization, Writing - Original Draft; **Richard Chiverrell**: Writing – Review & Editing

Chapter 2. Literature review: Hydrology and hydrochemistry of ombrotrophic peatlands

2.1 INTRODUCTION

Peatlands are wetland ecosystems which contain an accumulation of peat, developed though the long-term sequestration of atmospheric carbon (C) by a water-saturated living plant layer (Rydin and Jeglum, 2013). Despite covering just 2.84% (4.23 million km^2) of Earth's land surface (Xu et al., 2018), peatlands form the largest terrestrial carbon store, estimated between 500 and 700 Gt C (gigatons of carbon), with northern peatlands dominating this stock with an estimated 547 (473 − 621) Gt C (Yu et al., 2010). In comparison, Earth's atmosphere contained approximately 829 ± 10 Gt C, mainly in the form of CO_2, in 2013 (Ciais et al., 2013). Water saturated conditions inhibit the decomposition of dead organic material, resulting in layers of accumulated peat, with northern peatlands estimated to sequester, on average, 18.6 g C m^{-2} yr^{-1} (Yu et al., 2010).

Ombrotrophic peatlands, or bogs, receive all their water and nutrient supply by precipitation, and are therefore characteristically nutrient poor as well as highly acidic (Rydin and Jeglum, 2013). Blanket bogs, which derive their name from the way they "blanket" the upland landscape, have developed primarily within cool, humid, often oceanic climates with high annual precipitation (> 1000 mm) and a high proportion of rain days (> 160 days) per year (Lindsay et al., 1988; Rydin and Jeglum, 2013). They thus form the dominant peatland type in the UK (> 80%) (Tanneberger et al., 2017), with Lunt et al. (2019) estimating an annual carbon accumulation within a blanket bog in southeast England to be equivalent to 11.77 ± 0.88 t CO_2 ha^{-1} yr^{-1}. Blanket bog habitat is likewise found across other countries in north-west Europe, particularly Ireland, Norway and Iceland, and along the northern Pacific coasts of the US, Canada, Russia and Japan, the Canadian Atlantic coast, the southern tip of South America (Tierra del Fuego), and New Zealand (Rydin and Jeglum, 2013). As such, blanket mire, which incorporates other mire types into a continuous upland wetland system, is considered the most widespread upland peat type (Evans and Warburton, 2010).

As intact peatlands form a long-term net carbon sink, they are considered important regulators of global climate (Evans et al., 2014a). In addition, upland mires can play an important role in regulating water quality by retaining nutrients (Moore et al., 2005) and metal pollutants within accumulated organic matter (Shotyk, 1997). The accumulation and

retention of these pollutants within the peat limits their loss down the catchment, reducing downstream eutrophication and costs involved in water treatment, thereby improving drinking water quality (House et al., 2010; Bonn et al., 2016). However, headwater streams draining peatlands are typically more enriched in dissolved organic carbon (DOC) (Hope et al., 1997; Aitkenhead et al., 1999), a by-product from incomplete decomposition of organic matter, which leads to their characteristic brown colour and can add to water treatment costs (Volk et al., 2002; Ferretto et al., 2021) due to the formation of carcinogenic trihalomethane compounds (Matilainen et al., 2011). DOC is typically dominated by humic substances (HS). These range in colour from the more yellow to yellow-brown lower molecular weight fulvic acids (FA), to the brown to black higher molecular weight humic acids (HA) (Thurman, 1985; Wallage et al., 2006; Klavins and Purmalis, 2013).

Given their role in global climate regulation, carbon storage and sequestration, peatlands have become a primary focus in mitigating climate change. Drained peatlands have been estimated to emit between 0.10 and 0.23 Gt C per year, primarily related to the agricultural, forestry and other land use sectors. The afforestation of peatlands in the UK, which proliferated between the 1950s and 1980s (Hargreaves et al., 2003; Sloan et al., 2018a), has led to the conversion of approximately 9 – 10% of deep peat areas in the UK to active forestry, primarily with the North American species *Pinus contorta* (lodgepole pine) or *Picea sitchensis* (Sitka spruce) (Cannell et al., 1993; Tanneberger et al., 2017). Besides leading to the loss of peatland habitat, peatland afforestation inherently leads to the drainage, further decomposition and CO_2 emission from the peat, often resulting in a positive feedback of driving peat subsidence and further drying (Sloan et al., 2018a), as well as deteriorating water quality through the further release of DOC with disturbance by machinery and greater decomposition, nutrients from fertiliser use and plant litter (Cummins and Farrell, 2003; Marttila et al., 2018) and from metal pollutants (Kaila et al., 2012; Asam et al., 2014a). In addition, afforestation has been related to a reduction in runoff, particularly baseflow, due to enhanced transpiration by tree stands as well as an increase in peak flow due to greater channelisation of runoff through drains and furrows (Anderson et al., 2000). The latest IPCC report indicates that the agriculture, forestry and other land use sectors emit 13 Gt CO_2-eq each year, amounting to 22% of anthropogenic emission, but highlights that ecosystem restoration, including of peatlands, on a global scale could achieve an offset of 4.2 – 7.4 Gt CO_2-eq yr^{-1} (IPCC, 2022). The combined implications of peatland degradation on habitat provision, the global climate, drinking water supply, as well as the potential climate benefits

achieved by net carbon sequestration through intact peatlands, have thus driven further calls for the protection and restoration of these wetlands (Field et al., 2020; Glenk et al., 2021).

This review aims to summarise the hydrological functioning of intact ombrotrophic peatlands, with a focus on northern upland blanket bogs, by examining the role of the key parameters within their water balance. This is then followed by an appraisal of the main processes involved in peat accumulation and decomposition, redox reactions, and the fluvial export of components, especially DOC. The review concludes with a consideration of some of the main knowledge gaps within peatland research, particularly ecosystem restoration within the context of climate change.

2.2 HYDROLOGY

2.2.1   Water balance

The water balance, or water budget, quantifies the inflows, outflows and storage changes in a system. Compared to other peatland types, such as fens, the water balance of bogs is simplified, as their only water input is through precipitation (P) and the main outflows are runoff (R) and precipitation (P) (Figure 2.1) (Rydin and Jeglum, 2013). Groundwater exchange is generally considered negligible (Bay, 1967; Bridgham et al., 1999). Thus, the water balance equation of blanket bogs takes the form of:

$$P = ET + R + \Delta S \qquad (2.1)$$

where P is precipitation (mm), ET is evapotranspiration (mm), R is runoff (mm) and ΔS is change in internal water storage (mm) over the time interval measured (Evans and Warburton, 2010).
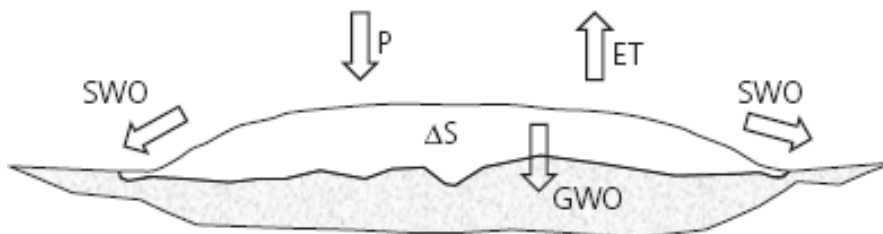
Figure 2.1. Components of the water balance for a bog (Rydin and Jeglum, 2013).

As P forms the principal input of water for bogs, it tends to dominate the annual hydrological budget, though relative proportions compared to outputs vary intra-annually through seasonal changes in ET and ΔS. For example, annual P exceeded ET by 1.55 to 1.94 times, while growing-season P/ET ratios ranged between 1.02 and 1.34 at Mer Bleue bog in south-

easter Ontario, Canada, highlighting the strong seasonality in P excess (P – ET) (Lafleur et al., 2005). The relative importance of the outputs – ET and R – likewise varies and can differ by location. In Thoreau's Bog in Massachusetts, USA, total runoff amounted to 246 mm between mid-March 1976 and June 1977 (Hemond, 1980), contributing only 19.5% to the total annual outputs (ET + R). In an ombrotrophic mire in Sweden, ET losses were 4 to 6 times higher than R during the growing season (May to October), where runoff often ceases completely during dry periods (Kellner and Halldin, 2002), while R dominated losses during two consecutive summers in a blanket bog in Newfoundland (Price, 1992b).

The annual hydrology of blanket bogs is characterised by the seasonal cycle of low evapotranspiration during the cold winter months and high evaporative losses over the warmer summer season driven by higher temperatures and biological activity. This seasonal cycle of moisture surplus and deficit tends to result in shallow, near-surface water levels in winter and water-table drawdown in summer, when evaporative losses can exceed P inputs. Under conditions of moisture surplus, the depth to water table (WTD) is determined by the surface gradient and the hydraulic conductivity of the acrotelm, the near-surface and periodically aerated "active" layer, with any excess moisture released as runoff. The length and intensity of the moisture deficit period is governed by the excess precipitation (P – ET) and greatly influences the average WTD of the year (Charman, 2007). However, intact peatlands have also been noted to be resilient to the effects of deep water-table drawdown through a decoupling of summer and winter hydrology, as winter recharge tends to compensate any losses observed over the summer drawdown period (Worrall et al., 2006).

2.2.2   Precipitation

Like all actively accumulating peatlands, ombrotrophic mires require a positive water balance (i.e., inputs exceeding outputs) with precipitation excess to inhibit decomposition and accumulate peat (Bragg and Tallis, 2001). Blanket bogs tend to develop in areas with limited drainage and a cool, wet climate, such as found in the uplands of the UK, where examples of mean annual precipitation records at blanket bogs include 2063 mm at Moor House National Nature Reserve (NNR), England (Robroek et al., 2010), 1040 mm in the north-eastern Flow Country, Scotland (Muller et al., 2015) and 1013 mm at the Kinder Scout Plateau, Southern Pennines (Shuttleworth et al., 2019). In addition, the distribution, or number of "rain days", is considered as important, if not more, as the total precipitation input (Charman, 2002). Thresholds on minimum amounts of annual precipitation and frequency of "rain days" for the continued development of blanket mires have been suggested. Lindsay et al. (1988) has

advocated a minimum of 160 "wet days" (> 1 mm d^{-1}) or 200 "rain days" (> 0.25 mm d^{-1}), and a minimum of 1000 mm of precipitation per year.

2.2.3   Evapotranspiration

Evaporation is a vaporisation process, in which liquid water is turned to water vapour by an energy input, typically from solar radiation, that equals the latent heat of vaporisation (2.45 MJ kg^{-1} at 20°C) (Oke, 1987; Novák, 2012). In addition, evaporation depends on a (vertical) vapour concentration gradient for the diffusion of the gas from an area of high vapour pressure (near the surface) upwards to an area of low vapour pressure, where atmospheric turbulence transports the vapour away in rotating parcels of air, called "eddies" (Oke, 1987; Lafleur, 2008). A higher evaporative flux is thus related to a greater vapour pressure gradient and stronger eddies.

Evapotranspiration (ET) combines the evaporative fluxes from the ground, water and vegetation surfaces with the transpiration movement of water through plant tissue and stomata to the atmosphere (Charman, 2002; Rydin and Jeglum, 2013). As evapotranspiration cannot be directly measured, several methods and techniques have been developed in order to quantify it. These range from relatively direct, but labour intensive techniques such as using lysimeters (Novák, 2012; Abtew and Melesse, 2013; Rydin and Jeglum, 2013) and simple calculations such as the Thornthwaite equation (Thornthwaite, 1948), to more intricate models such as the Penman-Monteith (PM) (Monteith, 1965) and Priestley-Taylor (PT) (Priestley and Taylor, 1972) equations, and complex micrometeorological techniques involving vertical profiles of temperature, humidity and wind, such as the Bowen ratio energy balance (BREB) method (Bowen, 1926) and more recent eddy covariance (EC), which are described in further detail in *Chapter 3*.

Being a vaporisation process, ET is tightly bound to the energy balance and is represented by the latent heat flux, λE (W m^{-2}), in the energy balance equation, which may be simplified to:

$$R_n = G + H + \lambda E \qquad\qquad (2.2)$$

where R_n is net radiation (W m^{-2}), G is the ground heat flux (W m^{-2}), H is the sensible heat flux (W m^{-2}). ET thus links the water and energy balances. As ET is influenced by a variety of factors, in addition to solar radiation inputs, including temperature, vapour pressure deficit and wind, as well as moisture availability, plant species and their physiology, transpiration strength and seasonal activity (Charman, 2002; Rydin and Jeglum, 2013), ET rates can vary considerably between day and night, from day to day and within a year (Sottocornola and

Kiely, 2010). ET rates tend to be smaller for *Sphagnum* dominated bogs, compared to other wetland types, due to more limited evaporation via capillary movement. Typical daily ET rates on blanket bogs have been reported as 0.8 – 2.8 mm day^{-1} on rain-free days at Moor House NNR, North Pennines (Worrall et al., 2015), 2.5 – 3.0 mm day^{-1} in summer from an Atlantic blanket bog in southwest Ireland (Sottocornola and Kiely, 2010) and 2.5 mm day^{-1} (Price, 1992a) and 0.9 – 2.1 mm day^{-1} during the growing season in Newfoundland, Canada (Wang et al., 2020).

As a result of changes in surface heating between day and night, ET follows a strong diurnal cycle, with peak evapotranspiration in the early afternoon driven by solar radiation and stronger vapour pressure gradients, while night-time ET losses tends to be negligible (Oke, 1987; Campbell and Williamson, 1997; Humphreys et al., 2006) or reversed due to dew formation (Lafleur, 2008). The diurnal nature of evapotranspiration can be observed through diel variations in the water table (Fahle and Dietrich, 2014; Watras et al., 2017), with a steep decline in the water level observed during daylight hours, in response to water extraction by plants for photosynthesis, and recovery during the night reflecting the break in transpiration. In addition, local variability in weather conditions can exert considerably influence on daily ET rates. Fog and rain were shown to significantly reduce ET in an ombrotrophic bog in Newfoundland, Canada. Here, ET rates averaged at 2.5 mm day^{-1} under clear weather conditions but reduced to 1.1 and 0.7 mm day^{-1} under foggy and rainy conditions, respectively (Price, 1991).

ET shows a strong seasonal pattern, governed by changes in net radiation, temperature and vapour pressure deficits, with winter ET limited by fewer daylight hours and low temperatures, while summer ET is driven by longer daylight periods, warmer temperatures, and biological activity. Despite the shorter daylight periods during the winter half-year, Lafleur et al. (2005) found October – April accounted for 24-29% of total annual ET, highlighting the importance of winter ET for annual water budgets. Brümmer et al. (2012) highlights the strong seasonal pattern by the strong positive linear correlation between monthly mean net radiation and ET for shrub-covered bog in eastern Canada. Conversely, Lafleur et al. (2005) found little correspondence between summer ET rates and solar radiation, temperature and rainfall, although the lowest summer ET losses occurred in the driest year over the monitoring period.

Vegetation type plays an important role in influencing ET losses from the bog (Charman, 2002). Watras et al. (2017) found daily mean ET rates to be significantly higher from a

forested bog (4.04 mm day^{-1}), characterised by larch (*Larix laricina*) and black spruce (*Picea mariana*), compared to a relatively open bog (3.09 mm day^{-1}), dominated by *Sphagnum* mosses and ericaceous scrubs. *Sphagnum* mosses are more sensitive to changes in water level than vascular plants, as their lack of a root system makes them dependent on capillary movement to replace water lost to evaporation in the absence of rain (Price et al., 2009). Despite this dependence on shallow water levels for *Sphagnum* to photosynthesise, the influence of the WTD on ET in bogs has been a source of debate (Lafleur, 2008). Bridgham et al. (1999) found that ET in a bog was less responsive to changes in WTD than in a fen. Conversely, at Mer Bleue Bog, Lafleur et al. (2005) observed a considerable step reduction in ET with water levels below −0.65 m below the hummock surface, suggesting that the sudden drop in ET marked a threshold at which both *Sphagnum* and vascular plant evaporation and evapotranspiration were severely affected by water availability. Similarly, at a marine blanket bog in western Newfoundland, ET decreased markedly in response to the water table lowering beyond the −0.24 m threshold (Wang et al., 2020).

2.2.4   Runoff

Water entering the mire may move on both vertically and laterally through the peat and exit the bog through a variety of pathways, including saturation excess overland flow (Holden and Burt, 2003b), seepage (Holden et al., 2017), macropore (Holden, 2009; Wallage and Holden, 2011) and pipeflow (Holden and Burt, 2002c; Smart et al., 2013), which collectively form the runoff from peat bogs. Water typically makes up around 90% of blanket peats (Evans and Warburton, 2010). The rate at which water moves through the peat is determined by Darcy's Law on hydraulic conductivity, which relates the flow of water, Q, to the hydraulic gradient, $\Delta h / \Delta l$:

$$Q = -k \frac{\Delta h}{\Delta l} \qquad (2.3)$$

where Q is discharge per unit area (m^3 s^{-1}), k is the hydraulic conductivity (m s^{-1}), Δh is the head (vertical change in height) (m), and Δl is the distance (m) (Oke, 1987; Charman, 2002; Evans and Warburton, 2010; Rydin and Jeglum, 2013). The hydraulic conductivity k of peat is strongly related to the level of humification, which often increases with depth and is positively related to bulk density, with greater bulk density resulting in reduced size and frequency of pore spaces and thus lower hydraulic conductivity (Rydin and Jeglum, 2013). Hydraulic conductivities can range between 2.8 x 10^{-4} m s^{-1} in the less decomposed fibric peats to 1.0 x 10^{-7} m s^{-1} in highly humified sapric peats (Letts et al., 2000). In addition, the

degree of humification and thus hydraulic conductivity is related to the source material, with *Sphagnum* peats tending to be more humified, with lower hydraulic conductivity, than peat composed of the remains of vascular plants, such as *Carex* spp. (Rydin and Jeglum, 2013). As the horizontal movement of water within peat becomes more restricted towards greater depths, runoff thus tends to dominate within the more permeable acrotelm (Figure 2.2) (Holden and Burt, 2003b). The permanently saturated, anoxic catotelm layer extends below the acrotelm, in which the degree of humification increases, though at a slowing rate, with depth (Ingram, 1978, 1982; Holden and Burt, 2003a). While the diplothelmic acrotelm-catotelm model (Figure 2.2) has faced critique for its two-dimensional simplicity (Morris et al., 2011), the concept nevertheless has merit in describing hydrological processes in peats (Holden and Burt, 2003a; Evans and Warburton, 2010).
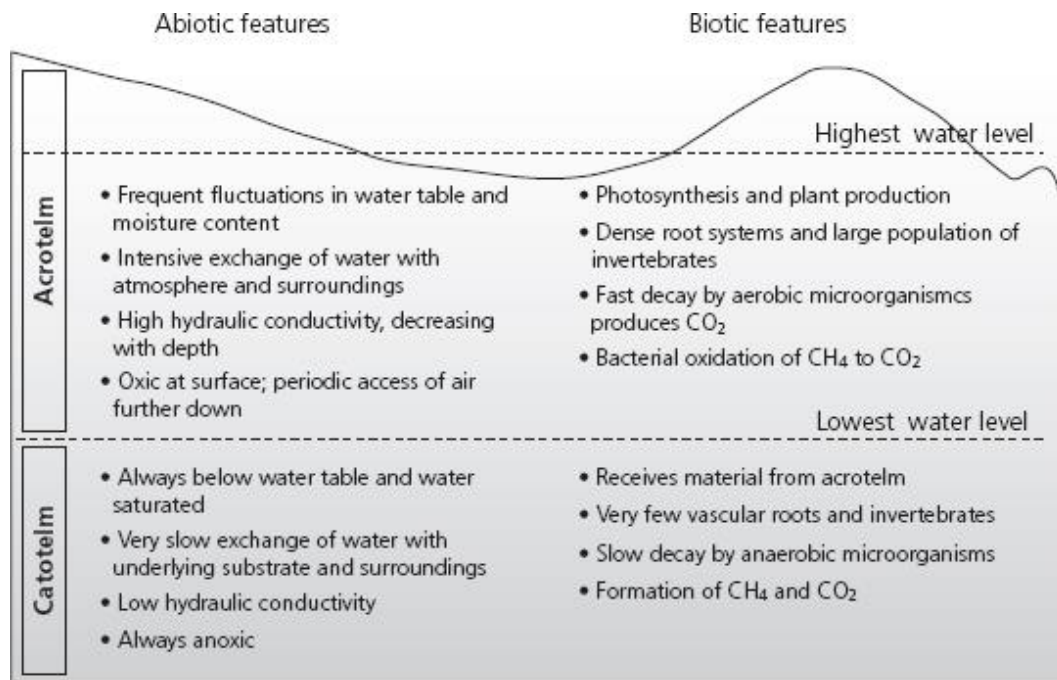
Figure 2.2. Abiotic and biotic features of the acrotelm and catotelm layers (Rydin and Jeglum, 2013).

Storm runoff from bogs, particularly upland blanket bogs, tends to be flashy (Evans et al., 1999; Holden and Burt, 2002b, 2003a; b; Flynn et al., 2021). As a result, storm hydrographs tend be steep with a sharp peak (Evans et al., 1999), with Holden and Burt (2003b) estimating mean rainfall peaks to peak discharge lag times to be between 2.1 and 3.2 hours among three blanket peat catchment of varying catchment size. The prevalence of shallow water table for most of the year result in the majority of storm flow departing as saturation excess overland flow (Holden and Burt, 2003b), with minimal baseflow produced by throughflow which may dominate during periods of low rainfall (Holden and Burt, 2002a, 2003b). An exception to this can be the network of macropores and pipes at greater depths, connected to the peat

surface, which can allow the rapid movement of water within deeper peat layers (Holden and Burt, 2002c; Holden et al., 2012; Cunliffe et al., 2013; Smart et al., 2013), with Holden and Burt (2003a) finding that the relative runoff contributions of macropores was 35% and that of pipes was 10% at Moor House NNR, while Wallage and Holden (2011) assigned at least 60% of runoff to macropore flow. Drought events have been found to considerably alter preferential flow paths, with Holden and Burt (2002b) observing an increase in microporosity after a laboratory drought experiment, with preferential flow extending deeper into the peat and limited recovery in peat structure following the experiment.

2.2.5 Water table

The water table depth (WTD) is the most commonly used parameter when monitoring and studying the hydrological status of a peatland and is generally measured using dipwells, often with automatic pressure transducers installed within them (Holden and Burt, 2002a; Bonnett et al., 2009). As already highlighted extensively in this review, the water table in bogs tends to remain shallow for most of the year. For example, Evans et al. (1999) observed water levels to be within 5 cm from the surface 93% of the time, while Wallage and Holden (2011) found that water levels were at the surface 18% of the time. The water level fluctuates primarily within the active acrotelm layer as a result of diurnal changes driven by daytime evaporation and deeper water table drawdown events, particularly in summer (Charman, 2002). Like runoff, the extent of the water level rise will be affected by the hydraulic conductivity of the peat, with less permeable peat forcing a greater water table rise, while more permeable peat will generally produce a more muted water table response (Ingram, 1967).

The historically popular belief that peatlands act like "sponges" in storing water like a reservoir and releasing it slowly, thereby dampening the flood response (Turner, 1757; Atherden, 1972; Simmons, 1990) has repeatedly been discredited over the last couple decades. While the "sponge"-like attributes of *Sphagnum* in storing water have often been highlighted (Moore, 2002; Dise, 2009), the rapid water table and runoff response to rainfall, makes bogs, compared to other wetlands, less likely to attenuate flow and reduce downstream flooding and more likely to produce "flashy" runoff response to storm events (Holden and Burt, 2003a; Ballard et al., 2012; Bacon et al., 2017). In addition, baseflow is poorly maintained, making bog streams prone to drying-up after a week without rain (Holden and Burt, 2003a; Holden, 2005b).

However, the validity of the "sponge" analogy has, more recently, been re-examined (Bathurst et al., 2018; Flynn et al., 2021a). In a paired catchment study in northern England, Bathurst et al. (2018) found that drainage ditches dug for peatland forestry enhanced flood peaks and seasonal runoff relative to an undrained upland peat grassland, suggesting that intact upland peatland can retain a seasonal, if not event, "sponge" effect in flow regulation. Similarly, Flynn et al. (2021a) have highlighted that blanket bogs can buffer against extreme precipitation immediately following dry periods, as recorded particularly in summer. Such events typically produce a rapid rise in groundwater levels but are not necessarily reflected in a rise in runoff (Flynn et al., 2021a). Thus, the "sponge" hypothesis may have some validity at the seasonal event scale.

Increased humification with depth results in a corresponding reduction in the specific yield, i.e. the rate of water table change per unit precipitation added into the saturated zone (Waddington et al., 2015; Bourgault et al., 2017). This general decline in specific yield with depths leads to a WTD feedback which helps regulate water loss during periods of very high or little rainfall (Waddington et al., 2015). During high rainfall events, when the water table suddenly rises vertically towards increasingly permeable layers, water is efficiently transported away through lateral runoff within the shallow peat layer, rather than inundating the mire. Conversely, during periods of low rainfall, the water level drops to less permeable peats, impeding lateral runoff which limits further water table drawdown and causes the mire to preserve moisture (Bragg and Tallis, 2001; Waddington et al., 2015).

The extent of summer water table drawdown can vary considerable between years, depending on the meteorological conditions. Evans et al. (1999) measured a maximum water level drop to −42 cm during the 1995 dry summer associated with a water deficit (P − ET < 0). Similarly, Lafleur et al. (2005) found mean WTD at Mer Bleue bog, south-eastern Ontario, to vary between −50.3 cm to −34.1 cm over the growing season (May to September), while dropping to −65 cm and exceeding −70 cm in 1999 and 2002, respectively, with deeper drawdown linked with extended dry periods or drought in summer. Charman (2007) used testate amoebae to relate summer water table variability to hydrometeorological variables and found that the seasonal moisture deficit (P − ET) was a much greater control on summer water table variability than temperature or precipitation alone.

However, with climate change predicted to cause a change in precipitation regimes concerning the intensity, frequency and duration of rain events (Trenberth et al., 2003), there is concern that particularly ombrotrophic peatlands, being dependent on high and

frequent precipitation, could be vulnerable to enhanced drying and carbon loss (Ise et al., 2008), which could further affect the distribution of blanket peat biome under a warmer climate (Gallego-Sala and Prentice, 2013). The afforestation of peatlands over the past decades has added to these climatic concerns, by intensifying the drying effect through large-scale drainage (Frolking et al., 2011) as well as enhanced evapotranspiration from the plantation trees (Anderson et al., 2000; Lewis et al., 2013), in effect also increasing the vulnerability of the peatland carbon sink (Loisel et al., 2021). Forest-to-bog restoration aims to reverse this drying effect by blocking drains and removing the trees in part to re-establish the peatland's "natural" hydrological processes (Anderson, 2010; Menberu et al., 2018; Howson et al., 2021b) and their resilience to climatic change (Glenk et al., 2021; Lees et al., 2021) in order to protect vital ecosystem services such as carbon storage (Leifeld and Menichetti, 2018).

2.3 HYDROCHEMISTRY

2.3.1 Peat accumulation, decomposition and humification

The biogeochemistry of peatlands is fundamentally bound to their hydrological functioning. Peat formation may be initiated by infilling or paludification within shallow basins or slopes where there is poor drainage and a sufficient supply of water to facilitate waterlogged conditions (Rydin and Jeglum, 2013). In addition, ombrotrophic peatlands are inherently nutrient poor due to their sole reliance on precipitation for external inputs, which contributes to their low primary productivity, generally dominated by *Sphagnum* mosses, compared to other wetland types (Moore, 1989). The prevalence of shallow water levels, resulting in anoxic conditions, in addition to low nutrient availability, are widely understood to be key drivers in slowing the rate of decomposition, thus facilitating the slow, net accumulation of peat within active mires (Moore, 1989; Laiho, 2006). In addition, many peatland plants, particularly *Sphagna*, are inherently resistant to decomposition by containing phenolic compounds (Freeman et al., 2001b), consisting of a hydroxyl group bonded directly to an aromatic hydrocarbon (Schlesinger and Bernhardt, 2013). While vascular plants contain lignin, a phenolic macromolecule, which acts to support their tissue structure, *Sphagnum* mosses contain alternative phenolics to retain cell structure (Rydin and Jeglum, 2013). Peat decomposition is driven by hydrolase enzymes, which do not require oxygen and can therefore be highly active in anoxic environments. However, the enzyme phenol oxidase, which can decompose phenolics, is inhibited by low oxygen availability, thus

leading to the accumulation of phenolics which in turn inhibit further decomposition of organic matter by hydrolase (Freeman et al., 2001b). These decay-inhibiting conditions and processes thus combine to facilitate the slow but net accumulation of peat, particularly carbon, within active mires. As such, the carbon accumulation within peatlands is sometimes described as an imbalance between production and decay, caused by the prevailing anoxic conditions within the peat column (Laiho, 2006).

The bulk of decomposition occurs within the active and periodically aerated 'acrotelm' layer and is primarily driven by microbial processes (Clymo et al., 1998; Laiho, 2006). Materials from plant and animal remains, including plant lignin, celluloses, proteins, carbohydrates and lipids, are transformed through a range of biochemical and abiotic pathways into decay-resistant humic substances, which include humin, humic acid (HA) and fulvic acid (FA), by a process termed humification (Charman, 2002; Zaccone et al., 2018). The production of humic compounds is heavily affected by variations in the water tables given the association with the acrotelm – catotelm structure that typifies peatlands (Clymo et al., 1998). Patterns in the humification of peat with depth are thus a complex series of responses to differences in the peat-forming vegetation, hydroclimate, peat depth, trophic status, pH, and age. The ratio of humic acids to fulvic acids (HA:FA) is often used to infer the degree of peat humification, with lower rations (< 10) indicating lesser degrees of humification while higher ratios (> 30) imply greater humification (Klavins and Purmalis, 2013). Humic substances are thought to make up a dominant proportion of DOC, which is typically released by root respiration or as a by-product of decomposition (Glatzel et al., 2003; Worrall et al., 2008). Higher HA:FA ratios thus also provide information on the relative composition of DOC, with higher ratios indicating a higher proportion of humic acids.

2.3.2   Mineralisation

While humification leads to a transformation of organic matter, mineralisation of decomposed material releases inorganic molecules for microbial activity (Biester et al., 2012; Rydin and Jeglum, 2013). Similar to humification, mineralisation processes are tightly bound to fluctuations in the water table resulting in oxic or anoxic conditions, which determine the redox potential and are largely mediated by microbial processes. Increasingly anaerobic conditions lead to a decline in redox potential, a measure of electron availability and thus an indicator whether reduction or oxidation will occur. Increasingly anaerobic conditions, i.e., rising water levels, lead to alternative electron acceptors to oxygen being used and thus bring about a sequence of chemical transformations, most notably the reduction of nitrate (NO_3^-)

to ammonium (NH_4^+), followed by the reduction of manganese dioxide (MnO_2). As oxygen levels cease completely, ferric iron (Fe^{3+}) reduces to ferrous iron (Fe^{2+}), followed by the reductions of sulphate (SO_4^{2-}) to sulphide (S^{2-}) and carbon dioxide (CO_2) to methane (CH_4) (Charman, 2002; Rydin and Jeglum, 2013). These reduced ions and compounds thus become more mobile under increasingly anoxic conditions (Rydin and Jeglum, 2013).

Mineralisation processes are most notably observed during and after water table drawdown events, as they lead to extended periods of oxygenation within subsurface peat layers often followed by rapid rewetting. The arguable most studied and reported mineralisation process within peatlands has been the conversion of labile carbon to CO_2 or CH_4 (Figure 2.3), with the two end-products commonly showing an inverse relationship and being highly sensitive to changes in water level (Laine et al., 2009). The seasonal lowering of water levels allows oxygenation of near-surface peats, facilitating the aerobic decomposition of organic matter to CO_2, although the CO_2 flux from primary production of the living plant layer, including root respiration and mineralisation of root products such as DOC (Figure 2.3), generally exceed the CO_2 emissions associated with decomposition (Crow and Wieder, 2005) largely due to prevalent waterlogged conditions, resulting in intact peatlands generally being net carbon sinks (Lafleur et al., 2001). In addition, DOC within peat soils has been found to be relatively stable to mineralisation, compared to DOC derived from forest floors and agricultural soils (Kalbitz et al., 2003).
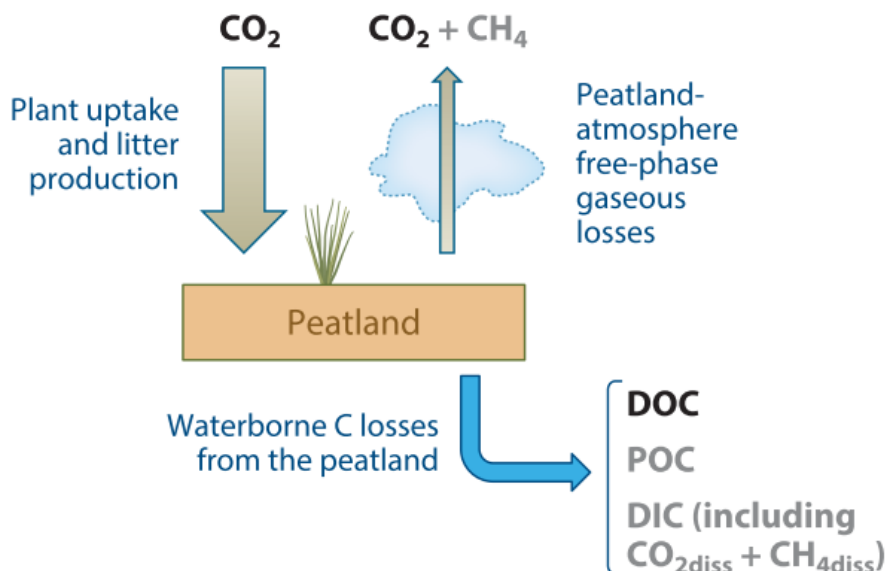
Figure 2.3. Principal components of the peatland carbon balance (Page and Baird, 2016).

The anaerobic release of CH_4 from peatlands (Figure 2.3) has been widely studied, particularly to assess the net GHG budget of intact peatlands as well as degraded and

afforested peats, given that CH_4 is 25 times more effective than CO_2 at trapping heat and is responsible for 22% of total climate forcing by all long-lived GHGs (Lelieveld et al., 1998). CH_4 emissions by methanogenesis increase within rising water levels, driven by methanogenic bacteria under anoxic conditions (Laine et al., 2009). Methanogenesis will occur under anaerobic conditions when alternative electron acceptors, such as nitrate (NO_3^-), ferric iron (Fe^{3+}) or sulphate (SO_4^{2-}), are not available (Rydin and Jeglum, 2013). Under these absences, methanogens typically use the substrates dihydrogen (H_2) and CO_2 (hydrogenotrophic methanogens) or acetate (CH_3COOH) (aceticlastic methanogens), which are then converted to CO_2 and CH_4 (Lai, 2009a). Acetate is produced from the fermentation of less decay-resistant carbohydrates (compared to lignin) into fatty acids and alcohols which then in turn converted to acetate through acetogenesis by syntrophic bacteria (Lai, 2009a). Acetoclastic methanogenesis tends to dominate within the upper peat layers where labile carbon is more abundant, while hydrogenotrophic methanogenesis predominates within deeper peat layers (Hornibrook et al., 1997). Methanogenesis is furthermore sensitive to pH and temperature, with CO_2 and CH_4 by methanogenesis increasing with higher pH and temperature (Lai, 2009a; Ye et al., 2012). The methanogenic-produced CH_4 travels upwards through the peat column by diffusion, ebullition bubbles or plants-mediated transport, while a high proportion of diffusing CH_4 may be consumed by methanotrophic bacteria within the aerobic layer (Lai, 2009a). CH_4 production and consumption peaks at an optimum pH 5.5 – 7.0 in temperate peatlands (Dunfield et al., 1993), and is thus naturally limited within highly acidic ombrotrophic *Sphagnum* bogs where the pH in peat is typically 3 – 4.5 (Dedysh, 2002). CH_4 emissions thus tend to be much lower from ombrotrophic bogs compared to more alkaline minerotrophic fens (Lai, 2009a).

2.3.3 Fluvial export

Stream systems, particularly headwaters, draining peat-dominated catchments form an important pathway for the transport of DOC, POC and pollutants (Figure 2.3). Peat-draining stream-waters are typically brown in colour, reflective of high concentrations of humic substances in DOC (Hope et al., 1997; Aitkenhead et al., 1999), and eroding peats in particular can form considerable sources for downstream sediment (Evans and Warburton, 2005; Yeloff et al., 2005).

DOC concentrations in headwater streams derived from upland peat catchments are usually high, often ranging between 5 and 30 mg L^{-1} (Koehler et al., 2009; Broder and Biester, 2015), but able to exceed 100 mg L^{-1}, particularly at sites experiencing peat erosion or drainage (Clay

et al., 2012). In addition, riverine DOC concentrations tend to be elevated in summer and autumn (Koehler et al., 2009), reflective of higher plant-mediated DOC production over the summer followed by greater mobilisation in autumn with higher runoff (Bonnett et al., 2006). Over a year Billett et al. (2010) measured DOC fluxes between 18.5 and 26.9 g C m^{-2} yr^{-1} from four peat catchments (0.2 – 3.35 km^2) across the UK.

In addition to forming a pathway for downstream export, streams may also form sites for microbially-driven autochthonous DOC production (Williamson et al., 2021), although allochthonous sources from peat tend to dominate stream DOC concentrations (Eatherall et al., 2000). DOC may also be lost by mineralisation to CO_2 through in-stream biological activity, for example Moody et al. (2013) measured the loss of DOC originating from upland peat down a catchment, finding that on average 73% of DOC was lost within 10 days, particularly in the first two days, and that between 48% and 69% of DOC was removed in a year, suggesting that peat streams could be considerable sources of CO_2.

DOC concentrations within surface water exiting peatlands have been widely reported to have increased in recent decades, though studies have related this trend to various hypotheses. These have included the effects of climate change in stimulating phenol oxidase activity and greater DOC release (Freeman et al., 2001a), the reduction in sulphur deposition in facilitating greater DOC solubility (Evans et al., 2006a, 2012; Monteith et al., 2007) and changes in land management practices (Yallop et al., 2010), leading to concerns about the future carbon balance and emissions from these peatlands.

Peat is generally highly effective at retaining nutrients and atmospheric pollutants. Peat has a high cation exchange capacity, which leads to the effective removal of many metallic ions from solution which accumulate together with successive layers of peat (Shotyk et al., 1992), thus making peat an excellent archive for palaeoenvironmental research (Barber, 1993). However, the strong tendency of metals to form complexes with dissolved organic matter (DOM) can also facilitate their mobility and export downstream (Rothwell et al., 2007). For example, Rothwell et al. (2007) found a close association between DOC export and fluxes of lead, titanium and vanadium, while Broder and Biester (2015) similarly noted a strong link between DOC, lead and arsenic. The rise in DOC concentrations from peats observed over the last decades as well as the effect of peat drainage in enhancing DOC release may thus raise concern over the heightened related export of pollutants from peatlands to waterways.

2.4 PEATLAND RESEARCH IN THE CONTEXT OF ECOSYSTEM RESTORATION

The hydrological and biogeochemical functioning of temperate ombrotrophic peatlands is tightly coupled, with a predominantly cool, humid hydroclimate facilitating their characteristically shallow water levels and long-term peat accumulation and carbon storage. However, peatland degradation and climate change are disrupting this functioning by altering peatland hydrological regimes and thus their carbon balance, leading to calls for further research particularly into the interrelating processes between peatlands, carbon and climate (Loisel et al., 2021). The importance of peatlands within global carbon cycling has driven urgent calls for their protection and restoration as an effort to mitigate climatic warming (Erwin, 2009; Field et al., 2020). Andersen et al. (2017) highlight that the number of peatland restoration projects within Europe and their accompanying research are still few in number, considering that most peatlands within Europe have been affected by anthropogenic disturbance in some way. The authors further point towards a limitation in publishing evidence of restoration progress beyond specific sites and a lack in baseline measurements to facilitate guidance on restoration targets, and suggest that systematic and standardised long-term monitoring and research targeting specific peatland functioning elements together with baselines, controls or a reference site are needed in order to establish the "success" of such restoration projects (Andersen et al., 2017). Given that peatland restoration, such as post-forestry rewetting, is still a relatively new endeavour, further research is required to understand the extent of ecosystem recovery attainable (Alderson et al., 2019), and the mechanisms and timeframes involved in facilitating large-scale implementation of restoration projects to realise their full potential for habitat recovery, water quality improvement and climate change mitigation (Martin-Ortega et al., 2014; Glenk et al., 2021).

Chapter 3. Gap filling, quality control and preliminary processing of the May Moss meteorological data

3.1 INTRODUCTION

3.1.1 The May Moss meteorological station

The closure of the hydro-climate water balance for ecological environments depends in part on the quantification of evapotranspiration (ET) using typically micrometeorological models and techniques, such as the Penman-Monteith (PM) equation or the Bowen ratio energy balance (BREB) (Drexler et al., 2004; Lafleur, 2008). Quantifying the atmospheric component of these water exchanges typically occurs alongside the recording of water tables and hydrological discharge to fluvial systems. Such evapotranspiration methods depend on the availability of near-ground measurement of temperature, humidity, wind speed, atmospheric pressure, net radiation, and soil heat flux to quantify the water vapour flux, or evapotranspiration, between the ground and the atmosphere.

A multi-level sensor array installed on May Moss, an upland ombrotrophic blanket mire, was used to facilitate the analysis of fluxes, such as ET, within the boundary layer of the atmosphere (BLA), as well as parallel monitoring of precipitation and water table depth. The data collected have enabled the closure of the water balance for this extensive (0.63 km^2) site. A 3-metre-high mast-based hydro-meteorological station (Figure 3.1) was installed in the centre of May Moss (Figure 1.3), at an elevation of 253 m, in August 2010, and collected hourly hydrological and micrometeorological data between 20/08/2010 and 01/07/2021. The system records air temperature (T), relative humidity (RH) and wind speed profiles, net radiation (R_n), photosynthetically active radiation (PAR), subsurface temperatures (at 0.12 and 0.39 m depths), soil heat flux (at 0.05 m depth), precipitation and the depth of water table using a datalogger (CR1000, Campbell Scientific). In addition, a separate pressure transducer (HOBO U20 Water Level Logger, Onset) was placed within the station's enclosure to record half-hourly atmospheric pressure since 14/03/2017.

The exchanges of energy between the surface of the bog and the near surface atmosphere were monitored directly using R_n, photosynthetically active radiation and soil heat flux sensors. Air temperature, RH and wind speed were measured at four heights: 0.4, 1.0, 2.0 and 3.0 metres above ground. The duration of these records provides a context to assess the

relationships among the vertical sensor series and near ground atmospheric boundary layer. However, since installation, sensor failure, replacement, misalignment, and occasional data loss have created gaps in the time series, ranging in duration from hours to years. These affected the air temperature, RH, wind speed, soil heat flux, R_n, soil heat flux, precipitation, and atmospheric pressure series.
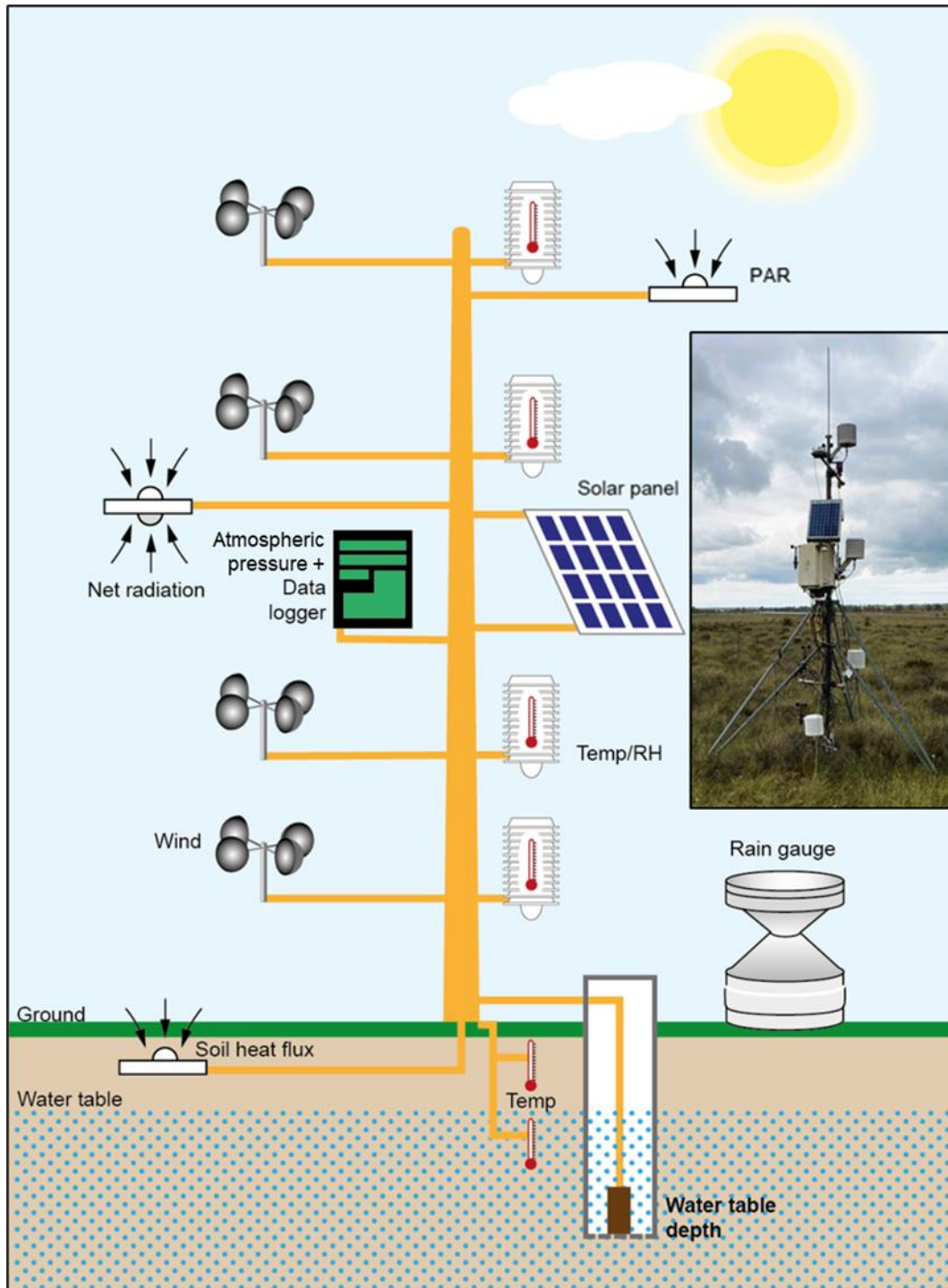
Figure 3.1. Schematic of the May Moss meteorological station and coupled sensors and loggers.

Sensor-specific procedures were applied to fill data gaps. The justification for filling the gaps rather than leaving the data as incomplete series stems from the focus on completing water balance calculations. Where possible, data gaps were filled using linear models based on the relationship with adjacent or related sensors on the station (Peterson et al., 1998). In other cases, data from nearby meteorological stations were used to produce calibration equations with the May Moss data based on simple linear regression using overlapping data. Fylingdales station (Midas station ID: 358; 54.359°N, −0.672°E), at an elevation of 262 m and 1.4 km northwest of the May Moss station, has records for hourly air temperature, RH, wind speed and precipitation (Figure 3.2). For these comparisons, the measurements at 2.0 m were used as most like the set up at the Fylingdales UK Met Office station. Simple linear regressions were fitted between hourly Fylingdales and May Moss air temperature, RH and wind speed data (01/01/2011 – 31/12/2017) to produce sensor-specific calibration equations. These time series for these two meteorological stations, in relatively proximity, show a strong comparability even for more localised parameters e.g., precipitation (Figure 3.2). Linear calibrations were applied to the Fylingdales data to fill gaps in the equivalent May Moss timeseries. The following sections describe the energy balance and its role in quantifying ET, the various methods suitable for the quantification of ET, the approaches used to address gaps in the data series and the validation techniques applied to quality assess the original and corrected data series.
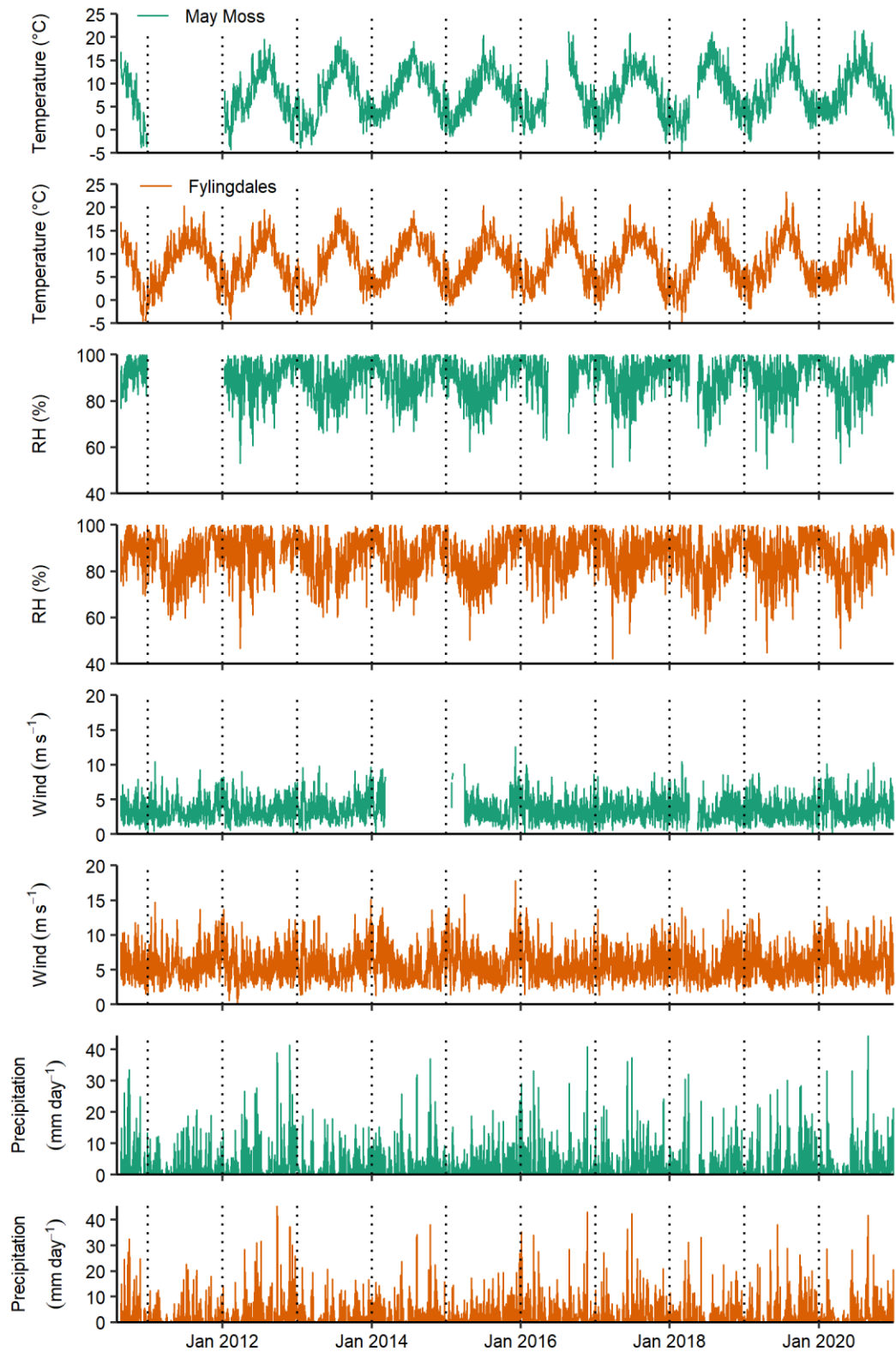
Figure 3.2. Daily average air temperature (°C), relative humidity (RH) (%), wind speed (m s^{-1}) and total precipitation (mm day^{-1}) recorded at the May Moss (green) and Fylingdales (orange) meteorological stations.

3.1.2   Energy balance theory

The exchange of energy and water between the surface and the atmosphere are tightly bound (Lafleur, 2008). The water balance of a blanket mire can be characterised as:

$$P - R - ET = \Delta S \qquad (3.1)$$

where P is precipitation, R is runoff, ET is evapotranspiration, and ΔS is the change in water stored within the system. The closure of the water balance equation is crucial for assessing the hydrological processes and budget changes over time. While P and R can be measured using simple monitoring equipment, such as tipping bucket rain gauges and water level loggers emersed in water courses, ET and ΔS are more challenging to quantify.

ET is a vaporisation process in which the state of water changes from liquid to water vapour (a gas). The process combines the evaporative fluxes of water from ground, water and vegetation surfaces and the transpiration movement of water through plant tissue to the atmosphere due to photosynthesis (Charman, 2002; Rydin and Jeglum, 2013). ET is a thermodynamic process, based on the principles of the kinetic theory of fluids, and it is tightly bound to the energy flux. For evaporation to occur, a molecule of water requires an energy input, primarily sourced from solar radiation, that equals the latent heat of vaporisation (2.45 MJ kg^{-1} at 20°C) (Oke, 1987; Novák, 2012). In addition to the availability of energy and water, evaporation depends on the presence of a vapour concentration gradient for the diffusion of water vapour to areas of lower vapour pressure. Vapour pressure typically declines with distance from the surface as atmospheric turbulence transports the vapour away (Oke, 1987). Water vapour is thus transported through the atmosphere in rotating parcels of air, called eddies. The greater the vapour pressure gradient and the stronger the eddies, the greater the evaporative flux (Lafleur, 2008).

The energy balance equivalent to the mass flux ET is the latent heat flux λE (W m^{-2}), which is the energy consumed to turn water from its liquid state into gas (water vapour), where λ is the latent heat of vaporization and E is the flux density of water vapour (kg m^{-2} s^{-1}) (Oke, 1987; Allen et al., 1998; Drexler et al., 2004; Lafleur, 2008). λE can be computed from the energy balance equation:

$$R_n = G + H + \lambda E \qquad (3.2)$$

where R_n is net radiation (W m^{-2}), G is the soil heat flux (W m^{-2}) and H is the sensible heat flux (W m^{-2}). R_n is the sum of all radiation fluxes, consisting of the incoming and outgoing longwave (thermal) radiation (3.0 − 100 μm) and the incoming and outgoing short-wave

(solar) radiation (0.15 − 3.0 µm). R_n, thus represents the energy available for heating the soil (G), biological processes, such as photosynthesis, and driving the turbulent transfer of sensible (H) and latent (λE) heat between the surface and the atmosphere (Lafleur, 2008).

Plants absorb solar radiation for photosynthesis principally across the visible blue and red bands (0.40 − 0.70 µm) of the electromagnetic spectrum, also known as photosynthetically active radiation (PAR) (Lafleur, 2008). As such, PAR directly correlates to solar radiation (Udo and Aro, 1999; Oliphant et al., 2006; Escobedo et al., 2009; García-Rodríguez et al., 2020) and to R_n (Singh et al., 2012). PAR is commonly expressed in mol m^{-2} s^{-1}, representing the photosynthetic photon flux density (PPFD) (Oke, 1987).

The diurnal variation in R_n is driven by the incoming shortwave (solar) radiation, or incident radiation, controlled by the Earth's angle in relation to the Sun (Oke, 1987). During the day, R_n comprises the sum of the four radiation streams and is positive due to a net flux downwards towards the ground during the day, driven by an increase in the incoming shortwave (solar) radiation, or incident radiation, towards midday. During night-time, R_n is dominated by the incoming and outgoing longwave (thermal) radiation, with shortwave radiation negligible, and as a result becomes negative, representing a net loss of energy from the ground into the atmosphere (Oke, 1987; Novák, 2012). The seasonal cycle echoes the diurnal pattern, with greater fluxes during the summer, when solar radiation peaks, and low fluxes during winter.

The soil heat flux (W m^{-2}) is the transfer, or conduction, of heat vertically through the soil profile and is influenced by the soil's thermal conductivity, heat capacity, thermal diffusivity, and thermal admittance. Heat is conducted downwards into the soil during the day (positive flux) and is lost upwards towards the surface and into the atmosphere by night (negative flux) (Oke, 1987). Although the soil heat flux is small compared with R_n and generally becomes negligible over a 24-hour period (Allen et al., 1998), it can be an important part of the energy exchange over hourly and shorter timescales. The soil heat flux can be challenging to quantify in peatlands due to variations in microtopography and water level affecting heat conduction along the soil profile (Lafleur, 2008). Kellner (2001) found the soil heat flux to be nearly twice as high in hollows compared to ridges in a Swedish boreal bog and was attributed to differences in peat porosity and water content.

3.1.3 ET measurement and modelling techniques

A range of methods have been developed for the measurement and calculation of ET. A brief discussion of the commonly used approaches in quantifying ET is presented here, with the

chosen method depending typically on the instrumentation available and research budget. For more in-depth reviews and explanations on the various techniques available for evapotranspiration estimation see Gilvear and Bradley (2000), Drexler et al. (2004), Novák (2012), Wang and Dickinson, (2012) and Abtew and Melesse (2013).

3.1.3.1 *Direct measurement techniques*

Direct measurement techniques of evapotranspiration include the use of evaporation pans and lysimeters. For the former, water is poured into a pan of known volume and the water-level is measured over time. As factors, such as the influence of vegetation are removed, pan evaporation can differ considerably from actual evapotranspiration in a vegetated environment, and it is therefore most suitable for the estimation of open water evaporation. A lysimeter is an open box with impermeable walls and bottom, into which a block of peat, together with its vegetation cover, are placed and the evapotranspiration losses are monitored. The use of lysimeters generally requires considerable time and effort for their continual maintenance and control of environmental parameters (Novák, 2012; Abtew and Melesse, 2013; Rydin and Jeglum, 2013).

3.1.3.2 *Micrometeorological techniques*

As methods for the direct measurement of evapotranspiration generally lack accuracy and efficiency, evapotranspiration is commonly estimated using the micrometeorological Bowen ratio energy balance (BREB) and eddy covariance (EC) techniques (Drexler et al., 2004; Rydin and Jeglum, 2013). These methods are based on the energy balance equation (Eq. 3.2). The methods require vertical gradients of temperature, humidity, and wind within the near-surface BLA, and therefore require a micrometeorological flux tower of sufficient height informed by the surface roughness (height of vegetation) (Drexler et al., 2004). Both methods assume a wide, homogenous evaporating surface; a 'fetch' of at least 50 m per metre of height above ground of the highest instrument considered generally sufficient for accurate estimation of fluxes (Drexler et al., 2004).

The ratio of sensible to latent heat flux is known as the Bowen ratio β. The BREB method (Bowen, 1926) uses vertical air temperature and vapour pressure gradients within the near surface layer to solve the energy balance equation for the latent heat flux λE by substituting the sensible heat factor H with Bowen's β:

$$\lambda E = \frac{R_n - G}{1 + \beta} \tag{3.3}$$

The calculation of Bowen's β requires simultaneous air temperature and vapour pressure measurements at two vertical heights, as determined by the vegetation height (Drexler et al., 2004), typically near the surface and at 2 metres (Novák, 2012):

$$\beta = \gamma \frac{\Delta T}{\Delta e_a} \tag{3.4}$$

where ΔT is the change in air temperature T between two heights (Δ = upper measurement – lower measurement) and Δe_a is the change in actual vapour pressure e_a between the same two heights (Δ = upper measurement – lower measurement). The psychrometric constant γ (kPa °C^{-1}) is computed from:

$$\gamma = \frac{C_p \rho}{\epsilon \lambda} \tag{3.5}$$

where C_p is the specific heat at constant pressure (1.013 x 10^{-3} MJ kg^{-1} °C^{-1}), ρ is atmospheric pressure (kPa), ϵ is the ratio of molecular weight of water vapour to dry air (0.622), and λ is the latent heat of vaporisation (2.45 MJ kg^{-1}). Actual vapour pressure (e_a) can be derived from air temperature (T) and relative humidity (RH):

$$e_s = 0.6108 exp \left[\frac{17.27T}{T + 237.3} \right] \tag{3.6}$$

$$e_a = e_s \frac{RH}{100} \tag{3.7}$$

where e_s is the saturation vapour pressure at air temperature T (kPa) and exp is the base of the natural logarithm. The latent heat flux λE from Eq. 3.3 can then be converted to the evapotranspiration flux E by dividing λE by the latent heat of vaporization (2.45 MJ kg^{-1}) (Drexler et al., 2004). Due to the requirements and assumptions for the wind fetch and surface roughness, as highlighted above, the BREB method is best suited to habitats with short vegetation and where soil water is not limited (Allen et al., 2011; Wang and Dickinson, 2012), such as wetlands (Drexler et al., 2004), although reliable estimation of λE is possible from non-saturated soils when β is less than ≈ 1.0 (Allen et al., 2011).

The BREB method is considered a relatively reliable technique for estimating ET (Drexler et al., 2004; Allen et al., 2011). The key advantage of the BREB method lies in its simplicity, only requiring T and e_a at two heights, R_n and G measurement, with half-hourly or hourly records deemed sufficient, making BREB an efficient and low-cost (compared with EC) technique for quantifying ET. The Bowen ratio β is also useful for expressing the partitioning of available energy into sensible or latent heat, i.e., the contribution of the ecosystem to the local climate (Lafleur, 2008). BREB has therefore become a widely used method for the study of ET in

wetlands (Price, 1992a; Wessel and Rouse, 1994; Campbell and Williamson, 1997; Thompson et al., 1999; Kellner, 2001; Kellner and Halldin, 2002; Peacock and Hess, 2004; Lapen et al., 2005).

Due to its simplicity, errors in calculating Bowen's β most likely stem from a dependence on accurate R_n, G, T and e_a measurements. When Δe_a in Eq. 3.4 approaches zero (i.e., a negligible vapour pressure gradient), β becomes disproportionally large (Campbell and Williamson, 1997; Drexler et al., 2004). λE estimates also become unreliable when $\beta \approx -1.0$, which causes the denominator in Eq. 3.3 to approach zero and the equation to near infinity (Drexler et al., 2004), which tends to occur during the early morning, late afternoon, during precipitation or extreme advection events (Ohmura, 1982). Errors due to negligible Δe_a can be tackled by eliminating data where Δe_a is less than or equal to the sensor resolution (Unland et al., 1996; Hu et al., 2014). The error in λE associated with $\beta \approx -1.0$ can be address by the simple elimination of data where $-1.25 < \beta < -0.75$ (Payero et al., 2003; Campbell Scientific, 2005) or $\beta < -0.75$ (Ortega-Farias et al., 1996). However, Ohmura (1982) and Perez et al. (1999) have stressed that the rejection of data should be based on the measurement accuracy (sensor resolution) and the vapour pressure gradient, and therefore the rejection interval should be variable between data points. Ohmura (1982) proposes that data should be rejected when ΔT falls within the following range:

$$-\left(\frac{\Delta e_a}{\gamma}\right) - 2\left(\frac{\delta e_a}{\gamma} + \delta T\right) < \Delta T < -\left(\frac{\Delta e_a}{\gamma}\right) + 2\left(\frac{\delta e_a}{\gamma} + \delta T\right) \qquad (3.8)$$

where δe_a and δT are the respective resolutions of the sensors used to measure absolute vapour pressure e_a (kPa) and air temperature T (°C). The method has been corroborated by others (Payero et al., 2003; Campbell Scientific, 2005; Allen et al., 2011). Perez et al. (1999) highlighted the need for a clear procedure for the rejection of data to be used in the BREB method and produced a set of rules for the acceptance (Table 3.1) and rejection (Table 3.2) of data based on the available energy, vapour pressure gradient and Bowen ratio, which involve the calculation of an exclusion interval ε around $\beta = -1.0$:

$$\varepsilon = \frac{\delta e_a - \gamma \delta T}{\Delta e_a} \qquad (3.9)$$

where Δe_a equals e_a measured at the lower level minus at the upper level of the BREB mast. The exclusions following the rules set out in Table 3.1 and Table 3.2 tend to result in the rejection of approximately 40% of data (Perez et al., 1999). However, most times when data are rejected coalesce with night-time or precipitation events, when ET is negligible (Perez et al., 1999). The conditions for accepting and rejecting data for the BREB method defined by

59

Perez et al. (1999) (outlined in Table 3.1 and Table 3.2) were corroborated by Hu et al. (2014), however the method used to develop Eq. 3.9 for the error limit estimation around $\beta = -1.0$ was critiqued by Hu et al. (2014) who argue that the denominator Δe_a must be an absolute value and adapted the equation to:

$$\varepsilon = \frac{\delta e_a + \gamma \delta T}{|\Delta e_a|} \tag{3.10}$$

where Δe_a equals e_a measured at the upper level minus at the lower level of the BREB mast. By applying their error limit equation (Eq. 3.10), Hu et al. (2014) observed an acceptance rate of 18.94% for data collected between August and October 2011 at the Aksu National Field Research Station Agro-ecosystems, Xinjiang Uygur Autonomous Region, China.

Table 3.1. Conditions which permit the use of the BREB method, where Δe_a equals the upper e_a measurement minus the lower e_a measurement, adapted from Perez et al., (1999) and Hu et al. (2014).

Condition	Available energy	Vapour pressure difference	Bowen ratio	Latent heat	Sensible heat
A	$Rn - G > 0$	$\Delta e_a < 0$	$-1 < \beta \leq 0$	$\lambda ET > 0$	$H \leq 0$
B	$Rn - G > 0$	$\Delta e_a < 0$	$\beta > 0$	$\lambda ET > 0$	$H > 0$
C	$Rn - G > 0$	$\Delta e_a > 0$	$\beta < -1$	$\lambda ET < 0$	$H > 0$
D	$Rn - G < 0$	$\Delta e_a < 0$	$\beta < -1$	$\lambda ET > 0$	$H < 0$
E	$Rn - G < 0$	$\Delta e_a > 0$	$-1 < \beta \leq 0$	$\lambda ET < 0$	$H \leq 0$
F	$Rn - G < 0$	$\Delta e_a > 0$	$\beta > 0$	$\lambda ET < 0$	$H < 0$

Table 3.2. Conditions which lead to erroneous λE under the BREB method and data are therefore rejected, where Δe_a equals the upper e_a measurement minus the lower e_a measurement, adapted from Perez et al. (1999) and Hu et al. (2014).

Error	Available energy	Vapour pressure difference	Bowen ratio
A	$Rn - G > 0$	$\Delta e_a > 0$	$\beta > -1 + |\varepsilon|$
B	$Rn - G > 0$	$\Delta e_a < 0$	$\beta < -1 - |\varepsilon|$
C	$Rn - G < 0$	$\Delta e_a > 0$	$\beta > -1 - |\varepsilon|$
D	$Rn - G < 0$	$\Delta e_a < 0$	$\beta < -1 + |\varepsilon|$

A more complex and advanced method than BREB is the eddy covariance (EC) technique, which is based on the transport of water vapour by rotating parcels of air, called eddies, driven by atmospheric turbulence. The technique depends on high resolution measurements, typically of at least ≥ 10 Hz, of vertical wind speed and humidity, averaged over 10 to 30 minutes (Drexler et al., 2004; Lafleur, 2008). The EC equation makes use of the correlation between vertical wind speed w' and humidity ρ', where the prime indicates variation from the mean, and can be simplified to:

$$\lambda E = \overline{w' \rho'} \tag{3.11}$$

The key advantage of the EC method over other techniques lies in its direct output of both the sensible and latent heat fluxes. While the EC technique has arguably become the most

widely used technique for measuring ET, largely due to decreased cost and increased automation of instrumentation (Shuttleworth, 2007; Lafleur, 2008; Allen et al., 2011), the method still faces some complications. Foken (2008) has drawn attention to the causes of problems with the energy balance closure, wherein the sum of R_n and G is larger than the sum of the turbulent sensible and latent heat fluxes due to an underestimation of the turbulent fluxes (Twine et al., 2000; Sottocornola and Kiely, 2010; Allen et al., 2011; Wang and Dickinson, 2012).

3.1.3.3 *Empirical and combination equations*

Over the past decades numerous models have been developed for the estimation of evapotranspiration, which include empirical equations, such as Thornthwaite (1948), the Penman-Monteith (PM) equation (Monteith, 1965) and the Priestley-Taylor (PT) method (Priestley and Taylor, 1972). The Thornthwaite equation (Thornthwaite, 1948) relies solely on average monthly air temperature and day length to estimate monthly potential evapotranspiration. As such, the method is only suitable for obtaining estimates of monthly or seasonal ET (Bay, 1967; Abtew and Melesse, 2013) and merely estimates the evaporative demand of the atmosphere, rather than actual ET (Drexler et al., 2004). Despite these limitations, the Thornthwaite equation is still widely used, particularly where limited temperature data are available (Bridgham et al., 1999; Lai, 2009b; Todd et al., 2013; Swinnen et al., 2019).

The Penman (Penman, 1948) and subsequent Penman-Monteith (PM) (Monteith, 1965) combination equations are widely used methods for estimating potential ET in wetlands which contain radiation, vapour pressure deficit and aerodynamic terms, commonly applied to hourly or daily timescales (Campbell and Williamson, 1997; Kellner, 2001; Peacock and Hess, 2004; Isabelle et al., 2018). The PM equation takes the form of (Allen et al., 1994):

$$\lambda ET = \frac{s(R_n - G) + \rho C_p \dfrac{(e_a - e_s)}{r_a}}{s + \gamma \left(1 + \dfrac{r_c}{r_a}\right)} \tag{3.12}$$

where s is the slope of the saturation vapour pressure curve at air temperature T (kPa °C[-1]), r_a is the aerodynamic resistance (s m^{-1}) and r_c is the canopy resistance (s m^{-1}). The computation of r_a and r_c are described by Allen et al. (1994) and Peacock and Hess (2004).

The PM method has since been modified by the United Nations Food and Agricultural Organization (FAO) to determine a reference crop evapotranspiration ET_o, referred to here at the FAO-PM method, which assumes a 0.12 m clipped grass surface with a bulk surface

resistance of 70 m s^{-1} (Allen et al., 1994; Allen et al., 1998), thereby eliminating the need to include the resistance terms from the original PM equation. The FAO-PM equation for hourly timesteps is thus expressed as:

$$ET_o = \frac{0.408s(R_n - G) + \gamma\frac{37}{T+273}u_2(e_s - e_a)}{s + \gamma(1 + 0.34u_2)}$$
(3.13)

where u_2 is wind speed at 2 metre height.

Another widely used method for the estimation of potential ET is the empirical Priestley-Taylor (PT) (Priestley and Taylor, 1972) , which has been applied in wetlands (Humphreys et al., 2006; Brümmer et al., 2012; Peichl et al., 2013; Runkle et al., 2014; Isabelle et al., 2018; Howson et al., 2021b). The PT equation simplifies the PM equation by replacing the aerodynamic terms for the vapour pressure deficit and resistance with the constant a:

$$E_{PT} = a\frac{s}{\gamma + s}(R_n - G)$$
(3.14)

where a is a coefficient with an average value of $a = 1.26$ (Novák, 2012). Drexler et al. (2004) recommend the calibration of a using Bowen's β, which thus allows for site-specific calibration where β ratios are available:

$$a = \frac{s + \gamma}{s(1 + \beta)}$$
(3.15)

As ET calculated by the PM, FAO-PM and PT methods represents potential ET (ET under conditions of no water stress), it is known to overestimate actual ET as measured by micrometeorological methods. For example, at Mer Bleue bog, ET measured by EC was approximately half of ET calculated by the PM method (Lafleur et al., 2005). Although sometimes used to compute ET entirely, both the PT and PM equations are most commonly applied to fill gaps in ET timeseries obtained using micrometeorologically methods (Drexler et al., 2004; Sottocornola and Kiely, 2010; Brümmer et al., 2012) and to examine the ratio of potential to actual ET (Campbell and Williamson, 1997; Kellner, 2001; Peacock and Hess, 2004; Lafleur et al., 2005; Moore et al., 2013; Isabelle et al., 2018).

3.1.3.4   Recommended ET techniques applied in this research

For the purposes of this research, the BREB method was selected as the most appropriate technique to compute ET, given that the May Moss meteorological mast setup provided vertical air temperature and relative humidity profiles together with the required energy balance components R_n (and PAR) and G. The wide use of the BREB method as a relatively

reliable technique for estimating ET (Drexler et al., 2004; Allen et al., 2011) within wetland research (Price, 1992a; Wessel and Rouse, 1994; Campbell and Williamson, 1997; Thompson et al., 1999; Kellner, 2001; Kellner and Halldin, 2002; Peacock and Hess, 2004; Lapen et al., 2005) also ensures repeatability and comparability with other studies.

For instances where the BREB method failed, due to inappropriate boundary layer conditions (Ohmura, 1982; Perez et al., 1999) or lack of data, the PT method was selected to model ET. The PT method relies on empirical data, while not requiring resistance terms. Instead, constant a can be calibrated for the study site using local Bowen's β ratios computed using vertical temperature and relative humidity profiles (Drexler et al., 2004). The wide use and recommendation of the PT technique in wetland research (Drexler et al., 2004; Brümmer et al., 2012; Peichl et al., 2013; Runkle et al., 2014) again ensures repeatability and comparability. The BREB technique, supported by the PT method, was thus selected to compute a continuous ET timeseries.

3.2 GAP FILLING AND QUALITY CONTROL

3.2.1 Atmospheric pressure

Atmospheric pressure was recorded at half-hourly intervals between 14/03/2017 and 01/07/2021 on a watertight pressure transducer (HOBO U20 Water Level Logger, Onset) placed inside the CR1000 enclosure. This atmospheric pressure timeseries was needed for calculations that compensate for atmospheric pressure in the processing data from a network of pressure transducers submerged in dipwells and stream gauging stations across May Moss. Ultimately, the atmospheric pressure series was also used in modelling evapotranspiration.

Gaps in the timeseries occurred between 22/10/2017 14:30 and 01/02/2018 14:30, between 05/04/2018 14:30 and 05/04/2018 15:30 and at 17/05/2018 16:30 (2450.5 hours of data gaps amounting to 18.1% of the series). The two shorter 0.5- and 1-hour gaps were filled by interpolating adjacent data points. The longer gap and the lack of data between 20/08/2010 and 13/03/2017 required deriving atmospheric pressure data from nearby weather stations. The three nearest meteorological stations to May Moss recording atmospheric pressure were Bridlington MRSC (Midas station ID: 373; 54.0938°N, −0.17413°E; 15 m elevation; 42.5 km SE of May Moss), Loftus (Midas station ID: 17344; 54.563°N, −0.864°E; 158 m elevation; 27.2 km NW of May Moss) and Topcliffe (Midas station ID: 16596; 54.205°N, −1.39°E; 25 m elevation; 50.6 km SW of May Moss) (Figure 1.3). For the period between 14/03/2017 and

21/10/2017 hourly atmospheric pressures at May Moss were regressed against equivalent data from the three meteorological stations. This revealed a broad regional coherence in hourly atmospheric pressure (Figure 3.3), with Topcliffe being least correlated (R^2 = 0.993) and Loftus being closest in distance, elevation and the station most correlated (R^2 = 0.997) with May Moss (Figure 3.4).
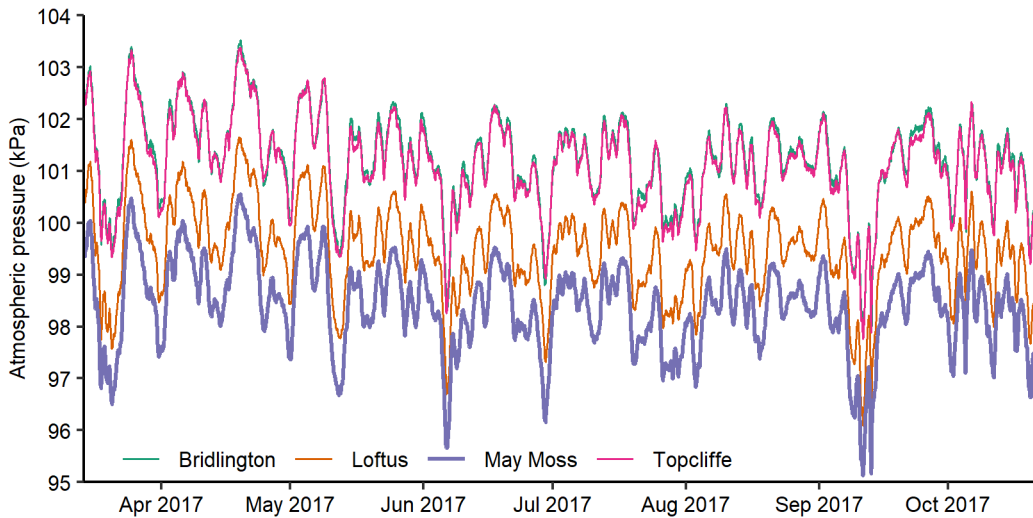
Figure 3.3. Hourly atmospheric pressures (kPa) recorded at Bridlington (MRSC), Loftus, May Moss and Topcliffe meteorological stations between 14/03/2017 and 21/10/2017. May Moss in bold grey.
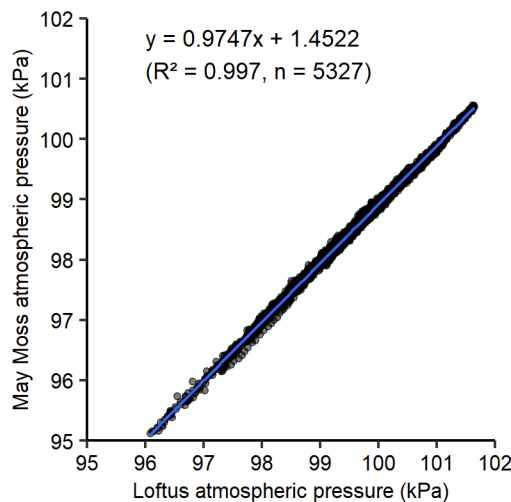
Figure 3.4. Linear regression between Loftus and May Moss hourly atmospheric pressure data (14/03/2017 – 21/10/2017).

Loftus atmospheric pressures were therefore used to fill the data gaps by linear regression. The standard error of the mean (SE) of the linear model (Figure 3.4) was 0.05, based on 5327 paired observations from the May Moss and Loftus stations. The gradient in the regression equation is either a function of systematic differences in elevation between the stations or a function of sensor differences. The equation was used to derive hourly atmospheric

pressures between 20/08/2010 and 13/03/2017 and to fill the gap between 22/10/2017 14:30 and 01/02/2018 14:30.

3.2.2 Air temperature and relative humidity

Hourly air temperature (°C) (average, minimum and maximum) and RH (%) were recorded at 0.4, 1.0, 2.0 and 3.0 metres above ground using four combined temperature and RH sensors (CS215, Campbell Scientific). During visits over the monitoring period, the performance of the CS215 sensors was assessed by placing them next to each other at several heights, with the measurements always placed within the declared sensor uncertainties. In addition, a strong consistency in the relationship with equivalent Fylingdales records was observed (Figure 3.2 and Figure 3.5). Linear regressions between the May Moss CS215 sensor records and Fylingdales air temperature and RH showed consistently decreasing slopes with the May Moss sensor height and generally increasing intercepts with sensor height (Figure 3.5 and Figure 3.6), indicating the increased influence of surface roughness with proximity to the ground among the CS215 sensors.

Average air temperature and RH at two heights were required for ET calculation. The data gaps amounted to 1.1 – 31.4% of the total records between four air temperature timeseries and 2.4 – 31.3% of the records for the four RH timeseries. For average air temperatures, gaps in the timeseries were addressed using one of the processes listed below and applied in the order of preference 1 to 3:

1. Where average temperature data were missing for an individual CS215 sensor, but minimum and maximum air temperatures were recorded for that sensor, then the gap in average temperature was filled by taking the average of the minimum and maximum air temperature (0.001 – 0.1% of series);
2. where the conditions for step 1) were not met, but the sensor lacking for data was situated between two adjacent functioning CS215 sensors, the gap was filled by taking the average of the two average air temperatures for these adjacent sensors. The average difference between the central and adjacent sensors was 0.03 ± 0.2°C, which was considered to justify this linear approach. This method was only applicable for sensors located at 1.0 and 2.0 m (2.61 – 9.95% of series);
3. where conditions for steps 1) and 2) were not met, most often but not exclusively for the lower- and upper-most sensors, the gaps were addressed by deriving average air temperature using a linear regression between the May Moss sensor and Fylingdales air temperatures. The calibration datasets for these regressions used

overlapped hourly air temperature data for each of the May Moss sensors and Fylingdales (Figure 3.5) (1.06 – 31.33% of series). The four linear regression models (Figure 3.5) based on the 3.0, 2.0, 1.0 and 0.4 m series had a SE of 0.68, 0.68, 0.90 and 1.22, respectively.
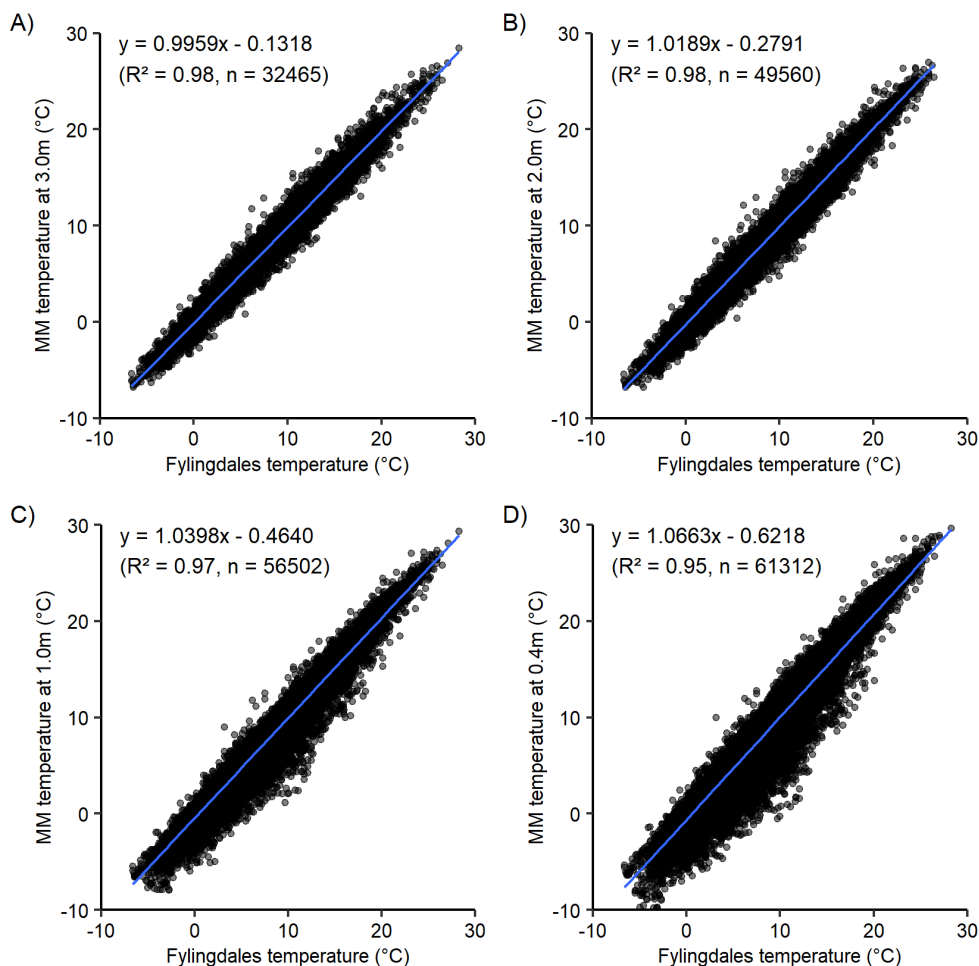
Figure 3.5. Linear regressions between hourly Fylingdales air temperature (°C) and May Moss (MM) air temperature (°C) at 3.0, 2.0, 1.0 and 0.4 m above ground, based on overlapping data from both meteorological stations between 01/01/2011 and 31/12/2017.

Gaps in the RH timeseries were filled using one of the processes listed below, applied in the order of preference 1 to 2:

1) Where RH data for an individual CS215 sensor were missing, but the sensor was situated between two adjacent functioning CS215 sensors, the gap was filled by taking the average of the RH of the two adjacent sensors. The average difference between the central and adjacent sensors was 0.09 ± 0.8%, which was considered to justify this linear approach. This method was only applicable for sensors located at 1.0 and 2.0 m (0.0 – 11.0% of series);

66

2) where conditions for step 1) were not met, the gaps were filled by deriving RH using

a linear regression between the May Moss sensor and Fylingdales RH, where all

values equalling 100% were removed for the regression. The calibration datasets for

these regressions used overlapped hourly RH data for each of the May Moss sensors

and Fylingdales (Figure 3.6). The models based on the 3.0, 2.0, 1.0 and 0.4 m series

had a SE of 3.70, 3.64, 4.05 and 5.00, respectively. Any values > 100% resulting from

the models were adjusted to 100% (2.4 – 31.3% of series).
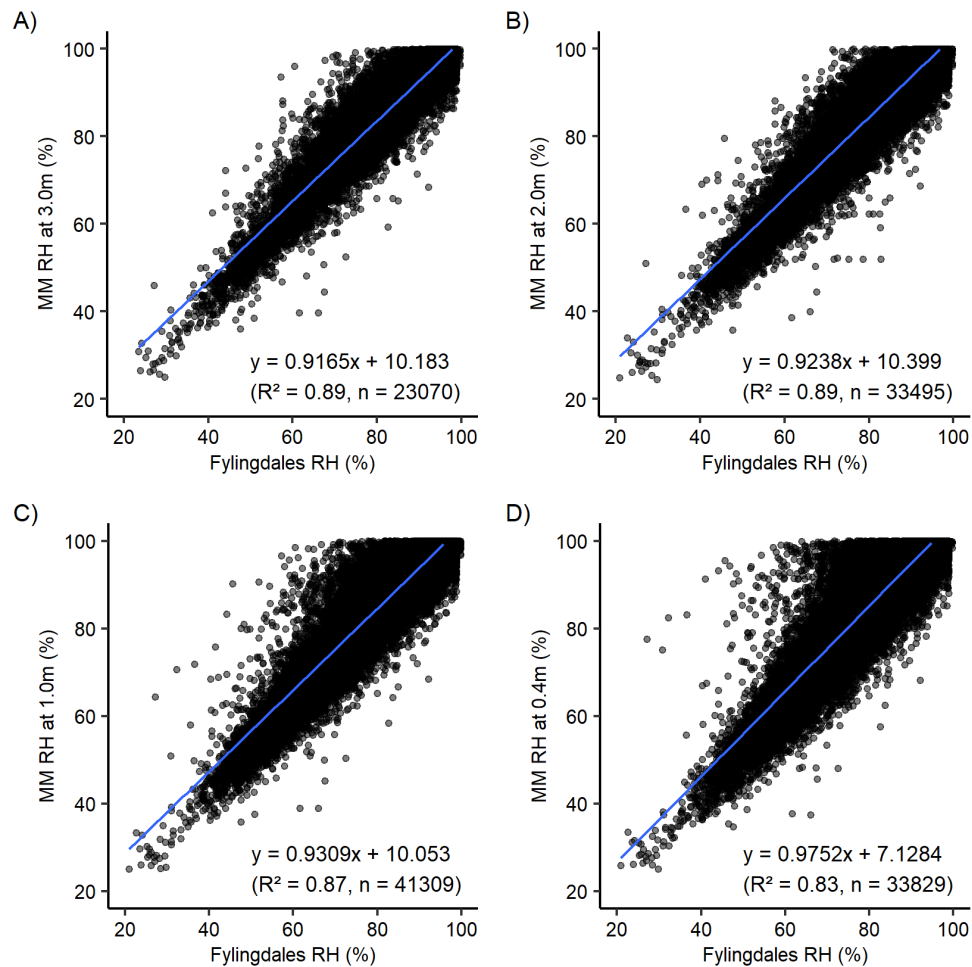
Figure 3.6. Linear regressions between hourly Fylingdales RH (%) and May Moss (MM) RH (%) at 3.0, 2.0, 1.0 and 0.4 m above ground, based on overlapping data between 01/01/2011 and 31/12/2017.

3.2.3   Wind speed

Average hourly wind speed at heights 0.4, 1.0, 2.0 and 3.0 metres were monitored using four wind sentry anemometers (03102, Campbell-Scientific). Wind speeds at two heights were required to model evapotranspiration through the eddy covariance method. Data gap occurrence ranged between 1.5 and 10.9% among the four wind-speed timeseries. Gaps in the wind speed timeseries were filled using one of the processes listed below, applied in the order of preference 1 to 2:

1) Where wind speeds from an individual anemometer was missing, but the sensor was situated between two adjacent functioning anemometers, the gap was filled using the average of the wind speeds of the two adjacent sensors (0.5 – 9.8% of series);

2) where conditions for step 1) were not met, the gap was filled by deriving wind speed using a linear regression between the May Moss sensor and Fylingdales wind speed (converted from knots to m s^{-1}). The calibration datasets for these regressions used paired hourly wind speed data from each of the May Moss sensors and Fylingdales (Figure 3.7). The models based on the 3.0, 2.0, 1.0 and 0.4 m series had SE of 0.91, 0.99, 0.78 and 0.58, respectively. The regressions displayed a reduction in gradient with proximity to the ground, demonstrating the expected influence of near ground roughness on the wind profile. Any values < 0 m s^{-1} resulting from the models were adjusted to 0 ms^{-1} to amend false negative wind speed values (1.1 – 9.3% of series).
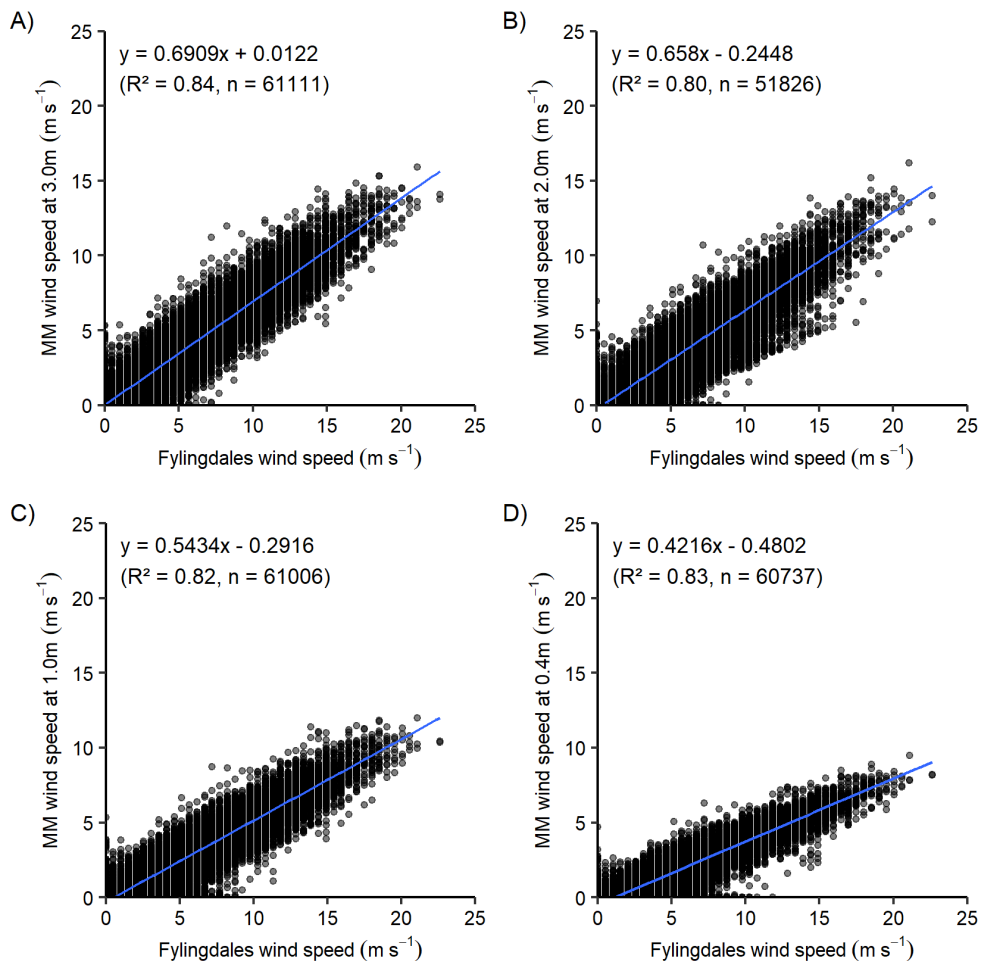
Figure 3.7. Linear regressions between hourly Fylingdales wind speed (m s^{-1}) and May Moss (MM) wind speed (m s^{-1}) at 3.0, 2.0, 1.0 and 0.4 m above ground, based on overlapping data between 01/01/2011 and 31/12/2017.

3.2.4   Precipitation

Hourly precipitation was monitored using a tipping bucket rain gauge (ARG100, Campbell Scientific) placed near (< 3 m) the May Moss meteorological station mast. Data gaps in the May Moss precipitation timeseries amounted to 1.1% of the complete series. Despite the distribution of precipitation being stochastic in nature, the May Moss and the Fylingdales (1.4 km from May Moss) precipitation series showed a strong, positive, linear correlation at a daily time-scale, with the regression model giving a SE of 1.41 based on 2463 observations (Figure 3.8). The Fylingdales precipitation series was therefore considered suitable to fill gaps in the May Moss series.
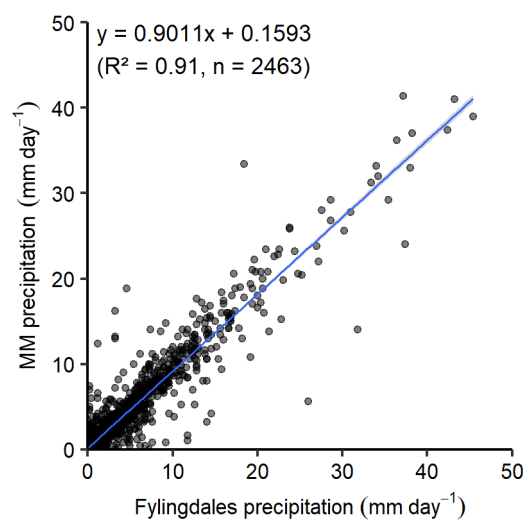
Figure 3.8. Linear correlation between Fylingdales and May Moss (MM) daily precipitation (mm day^{-1}), based on overlapping data from both meteorological stations between 01/01/2011 and 31/12/2020. Shaded region represents 95% confidence interval.

3.2.5   PAR

Photosynthetic active radiation (PAR) on May Moss was recorded at hourly timesteps using a SKP215 Quantum Sensor (Campbell Scientific) at 2.5 m height. The sensor operated continuously throughout the monitoring period, aside from one data gap between 05/04/2018 and 17/05/2018 (43 days; 1.1% of series). The timeseries displays clear diurnal and seasonal fluctuations, though minimal interannual variations. This pattern is replicated at the Leeming meteorological station (Midas station ID: 17314; 54.297N, −1.533E decimal degrees), which lies at 33 m elevation, 57.5 km west of May Moss, where repetitive seasonal cyclicity is evident, with little variation between years (Figure 3.9). As PAR dominates the R_n fraction responsible for ET, the timeseries provides a basis for addressing the more extensive data gaps in the R_n timeseries (Figure 3.10).
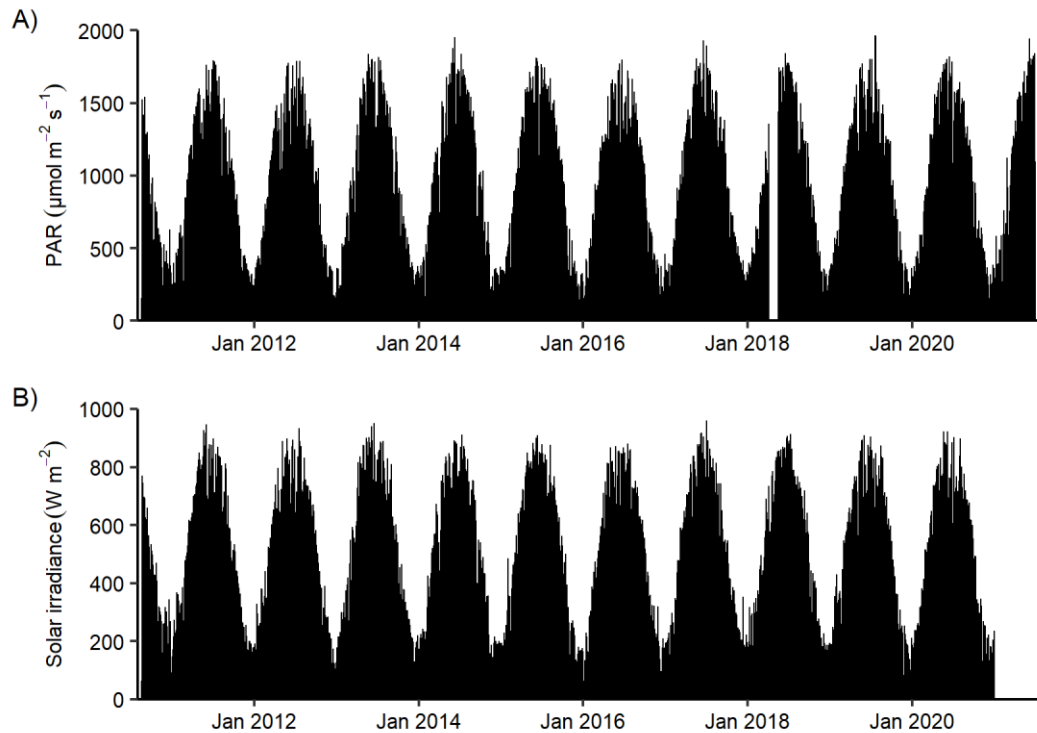
Figure 3.9. Comparison between A) Photosynthetic active radiation (PAR) (μmol m⁻² s⁻¹) timeseries at May Moss and B) Solar irradiance (W m⁻²) measured at the Leeming meteorological station.

3.2.6 Net radiation

Net radiation (R_n) was measured using a NR-LITE2 Net Radiometer (Campbell Scientific) at a height of 1.5 m to contribute to calculations of peatland evapotranspiration. Two main errors in the original R_n data (Figure 3.10) were observed:

1) A considerable change was observed in R_n progressing from 2011 to 2012 (Figure 3.10). Leeming station is the nearest meteorological station to May Moss providing independent solar irradiance (W m⁻²) records. The differences in the May Moss R_n timeseries observed comparing 2011 and 2012 do not occur in the Leeming timeseries (Figure 3.9). Hence, there appears a shift or step in the May Moss R_n timeseries that probably reflects instrument drift or changes in sensor alignment. May Moss R_n data were therefore rejected from 01/01/2012 to 01/01/2014.

2) During winter 2014, the net radiometer became detached, either through wind or bird damage. Following repositioning, the net radiometer then tilted again 13/02/2014 and collected erroneous data until 22/08/2016, when it was repositioned. Faults with the sensor between 21/05/2017 and 05/04/2018 led to the collection of further erroneous data, and the sensor failed to produce any data between 05/04/2018 and 17/05/2018 (Figure 3.10).

A new NR-LITE2 Net Radiometer (Campbell Scientific) was installed on 17/05/2018, which collected hourly R_n data not compromised by these issues thereafter (Figure 3.10).
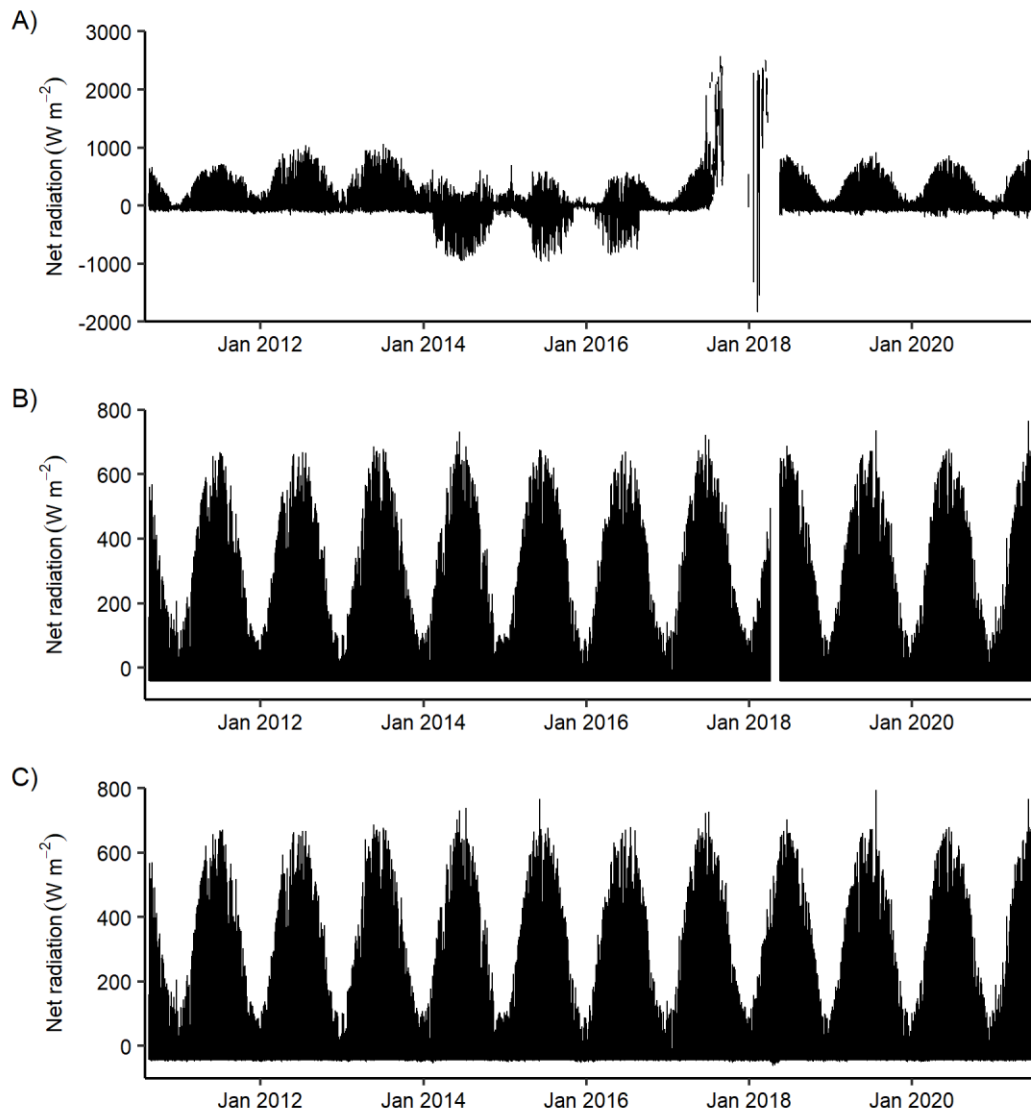
Figure 3.10. A) Uncorrected net radiation, R_n, (W m^{-2}) timeseries, B) Modelled R_n (W m^{-2}) based on linear regression with photosynthetic active radiation (PAR) (µmol m^{-2} s^{-1}) and C) Modelled R_n (W m^{-2}) with wind correction applied and gap filled with R_n based on Leeming solar radiation.

Consequently, the periods over which the May Moss R_n data remained uncorrupted were 20/08/2010 – 31/12/2011 and 18/05/2018 – 01/07/2021. Given the prevalence of erroneous R_n data (58.7% of series) and its importance in evapotranspiration calculations, a solution was sought to address this data gap. Because R_n and PAR are closely related (Oke, 1987; Singh et al., 2012), the relationship between the two series for the period where both series are uncompromised provides a basis for addressing these gaps in R_n. Previous examples of

this approach include Sottocornola and Kiely (2010) who replaced missing R_n data by applying a linear regression with PAR data (R^2 = 0.94).

The focus of the research here is the water balance of May Moss, and so this approach is defended given the dominant contribution of PAR to R_n during daylight hours, when the bulk of evapotranspiration occurs. Three linear models based on correlation between R_n and PAR were produced, and these differ only in the timing of the data included in the regressions. The regression models were restricted to any non-erroneous data series that spanned a calendar year (1st January – 31st December) for each NR-LITE2 Net Radiometer.

- Model 1 (y = 1.2113x − 0.1509; R² = 0.92; SE = 0.15) based on the time period 01/01/2011 – 31/12/2011,
- Model 2 (y = 1.3812x − 0.1557; R² = 0.96; SE = 0.11) based on the time period 01/01/2019 – 31/12/2020,
- Model 3 (y = 1.3123x − 0.1545; R² = 0.94; SE = 0.13) based on the time periods of both models 1 and model 2.

As PAR only produces values ≥ 0, the three models were limited in their negative R_n values, reaching a minimum limit for R_n of −41.92 W m^{-2} (Model 1), −43.25 W m^{-2} (Model 2) and −42.92 W m^{-2} (Model 3). These limitations constrain the nocturnal data but are negated in importance here as ET is mainly restricted to daylight hours (positive R_n) and the focus in this study is on quantifying peatland water balances at daily and lower frequency time-steps. Raw and modelled hourly R_n were therefore converted to daily averages. Wilcoxon signed rank tests were carried out between the raw, uncompromised R_n data and the model outputs over the unaffected time periods 20/08/2010 – 31/12/2011 and 18/05/2018 – 01/07/2021 to test for significant differences between the uncompromised R_n data and the model outputs. Only the outputs from model 1 (Figure 3.11) showed no significance difference (p-value = 0.6538) with the raw R_n data and were therefore selected to produce the modelled R_n timeseries.

The NR-LITE2 net radiometer displays a known sensitivity to wind speed, and so the modelled timeseries was corrected for wind speed using the following equation:

$$where\ U < 5ms^{-1}, Rn_{cor} = Rn_{obs} \tag{3.16}$$

$$where\ U > 5\ m\ s^{-1}, Rn_{cor} = Rn_{obs}\big(1.0 + A(u - 5.0)\big) \tag{3.17}$$

where Rn_{obs} is the uncorrected net radiation (W m^{-2}), Rn_{cor} is net radiation corrected for wind speed sensitivity (W m^{-2}), u is wind speed (m s^{-1}) and A is a constant (0.021286) (Campbell Scientific Inc., 2016).
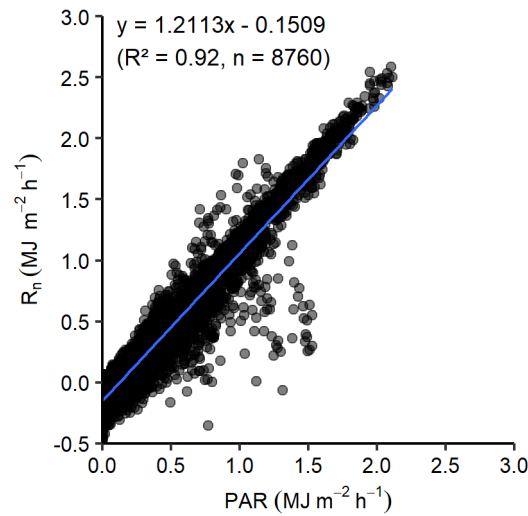
Figure 3.11. Correlation between net radiation, R_n, (MJ m^{-2} h^{-1}) and photosynthetic active radiation, PAR, (MJ m^{-2} h^{-1}) from model 1.

The hourly R_n gap between 05/04/2018 and 17/05/2018 was filled by modelling R_n based on solar radiation data from the Leeming meteorological station, following the method by Allen et al. (1994b). The May Moss and Leeming R_n timeseries were well correlated (y = 1.0502x – 16.991; R^2 = 0.89; based on overlapping daily averages 01/01/2011 – 31/12/2020). The Leeming R_n series was therefore used to fill the gap between 05/04/2018 and 17/05/2018 in the May Moss R_n (W m^{-2}) timeseries (Figure 3.10).

3.2.7   Soil temperature and heat flux

The soil heat flux was measured using a heat flux plate (HFP01, Campbell Scientific) installed 0.05 m below the vegetation surface and monitored using two soil temperature probes (107, Campbell Scientific) fitted at 0.39 m (STP1) and 0.12 m (STP2) depths. The two soil temperature probes recorded continuously throughout the period between 20/08/2010 and 04/04/2018, allowing inter-seasonal cross-validation with the soil heat flux series over the early monitoring period. Both probes exhibited clear diurnal and seasonal periodicity, with minimal variation between years. Following a period of data loss (05/04/2018 – 17/05/2018), the STP1 was accidentally dislodged from its original location on 17/05/2018, rendering the succeeding STP1 timeseries erroneous after 17/05/2018 (Figure 3.12).
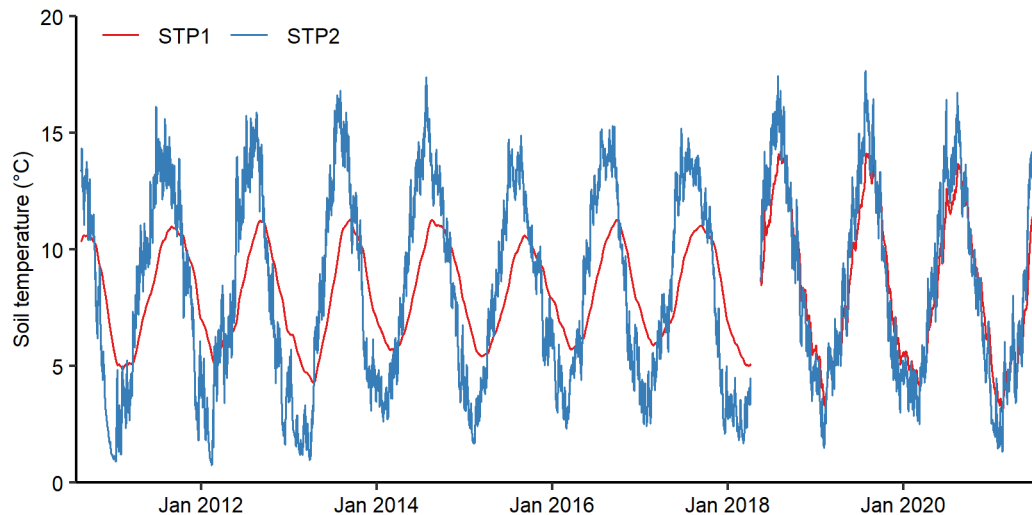
Figure 3.12. Hourly soil temperature timeseries at 0.39 cm (STP1) and 0.12 cm (STP2) depth between 20/08/2010 and 01/07/2021 .

The soil heat flux data began to show signs of a signal weakening drift from 2013 until 04/04/2018 (Figure 3.13). Over this time, the amplitude of the annual pattern near ground SHF reduced with a linear reduction in the annual standard deviation over time. Over time, vegetation development over the sensor had led to gradual burial of the heat flux plate beneath annual layers of peat, resulting in a "dampening" effect of the diurnal and seasonal heat fluxes. Data loss resulted in a gap between 05/04/2018 and 17/05/2018 (43 days; 1.1% of series). On 17/05/2018 the soil heat flux plate was recovered from this deeper position and resituated at 0.05m below ground. The repositioning resulted in a shift to a higher annual standard deviation, compared to the previous years.

Two types of data 'correction' were needed to address the drift and for the repositioning of the soil heat flux plate on 17/05/2018. To correct the annual drift evident from the year 2013 up until 04/04/2018, a correction factor was produced for each calendar year based on the average annual standard deviation (SD) of the 2011 and 2012 soil heat flux data (SD = 11.79). A linear regression was applied between the calendar years and the standard deviations of the annual data, with a SE of 0.59 (Figure 3.14). The linear equation was applied to every year and the resulting standard deviation divided by the average annual standard deviation of 2011 and 2012. The resulting annual correction factors were multiplied with the original data from 01/01/2013 to 04/04/2018. Data between 18/05/2018 and 01/07/2021 displayed a clear shift with an increase in SD from previous years (Figure 3.13). The correction factor for this time was determined by dividing the average SD (11.79) of 2011 and 2012 by the average SD (18.67) of 2019 and 2020. The data values were multiplied with the resulting correction factor (0.63) to produce the corrected soil heat flux for that time.
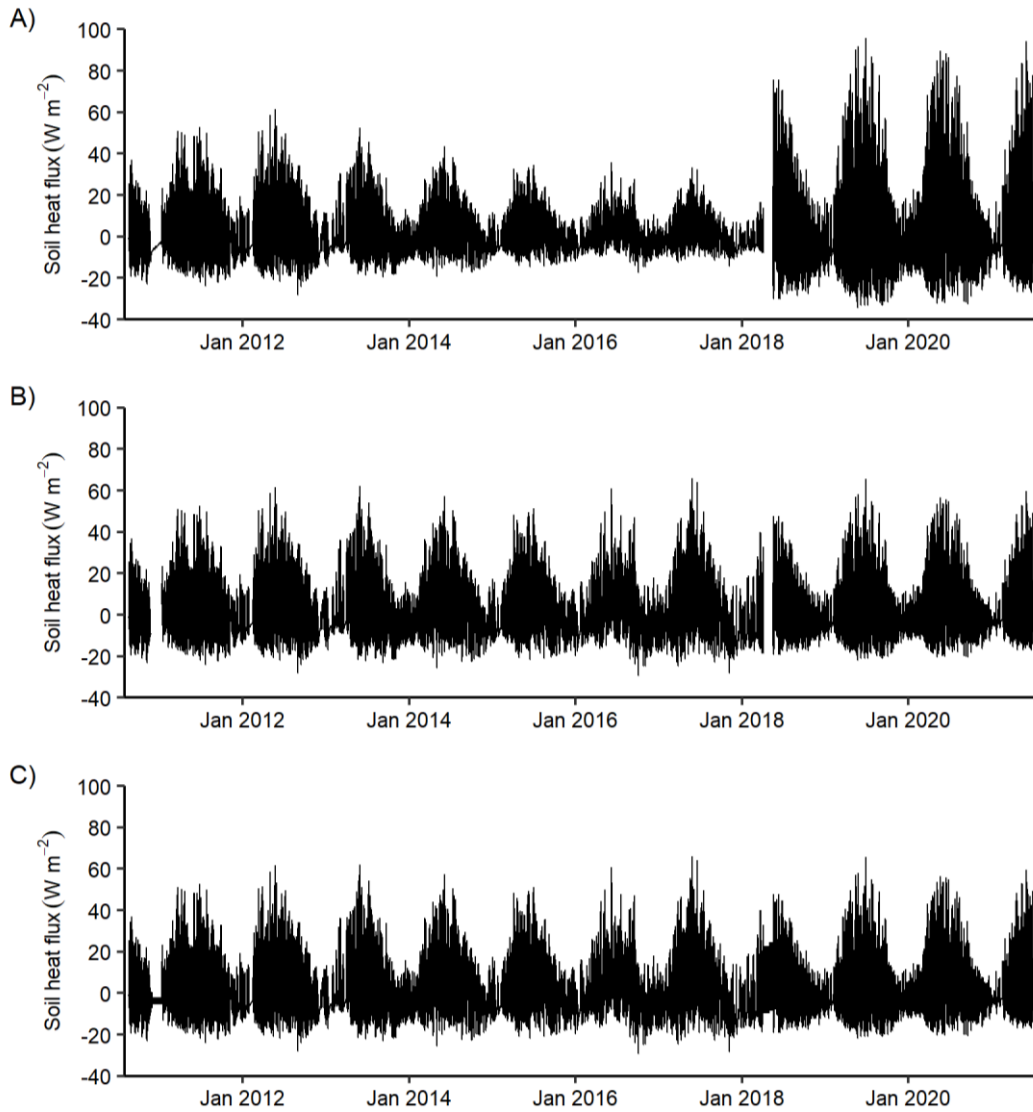
Figure 3.13. A) Uncorrected hourly soil heat flux (W m^{-2}) timeseries, B) Corrected hourly soil heat flux (W m^{-2}) timeseries and C) Corrected hourly soil heat flux (W m^{-2}) timeseries with gaps filled.

$$y = -1.003x + 2029$$
$$(R^2 = 0.94, n = 7)$$
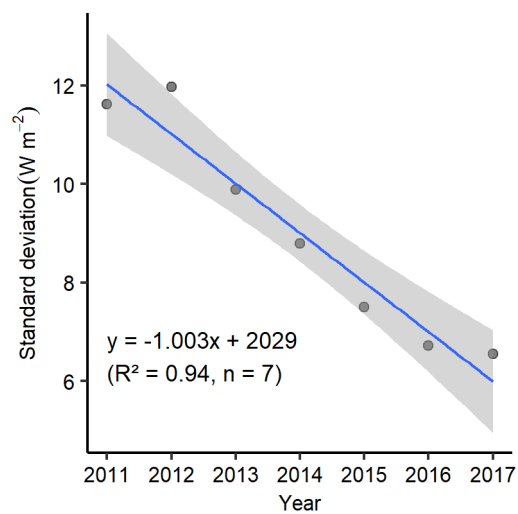
Figure 3.14. Linear regression between monitoring year and the standard deviation of annual soil heat flux data. Shaded region represents 95% confidence interval.

Data gaps during the periods 24/11/2010 – 12/01/2011 and 05/04/2018 – 17/05/2018 (2.3% of series) were the result of instrument malfunctioning and data loss. These gaps were filled by obtaining average hourly soil heat flux for each hour of the day for each of the five affected calendar months, an approach which has been applied by others (e.g., Sottocornola and Kiely, 2010), to produce a continuous hourly soil heat flux timeseries (Figure 3.13).

3.2.8   Water table depth

Hourly peat water levels were monitored using a submersible vented pressure transducer (PDCR 1830, Campbell Scientific) placed inside a 1.8 m length dipwell next (< 3m) to the May Moss meteorological station mast recording directly to the CR1000 datalogger. The sensor collected continuous water level data between 20/08/2010 and 01/07/2021, apart from a 1-hour gap on 24/08/2016, which was filled by interpolating adjacent data point, and a longer gap between 05/04/2018 – 17/05/2018 due to data loss, which amounted to 1.1% of the complete timeseries. Between 23/08/2016 12:00 and 13:00 a shift in the water level data occurred caused by an adjustment of the transducer during a sensor check-up, resulting in an average 0.08 m lowering of the sensor (average difference between the 12:00 level and the following three levels at 13:00, 14:00 and 15:00) (Figure 3.15). To correct this level shift, a correction of 0.08 m was added to water levels after 23/08/2016 12:00 (Figure 3.15).

Manual water table depths were measured periodically from 24/05/2019 to calibrate the sensor outputs to actual water table depth. Sensor outputs and manual water table depths were regressed (R^2 = 0.99, SE = 0.006) (Figure 3.16) and the linear equation applied to the sensor data. The gap 05/04/2018 – 17/05/2018 was filled by regressing the corrected water table timeseries against a water table timeseries from the Eller Beck dipwell water level logger on May Moss, 300 m north of the May Moss meteorological station (R^2 = 0.93) to produce a water table timeseries for the May Moss meteorological station between 20/08/2010 and 01/07/2021 (Figure 3.15).
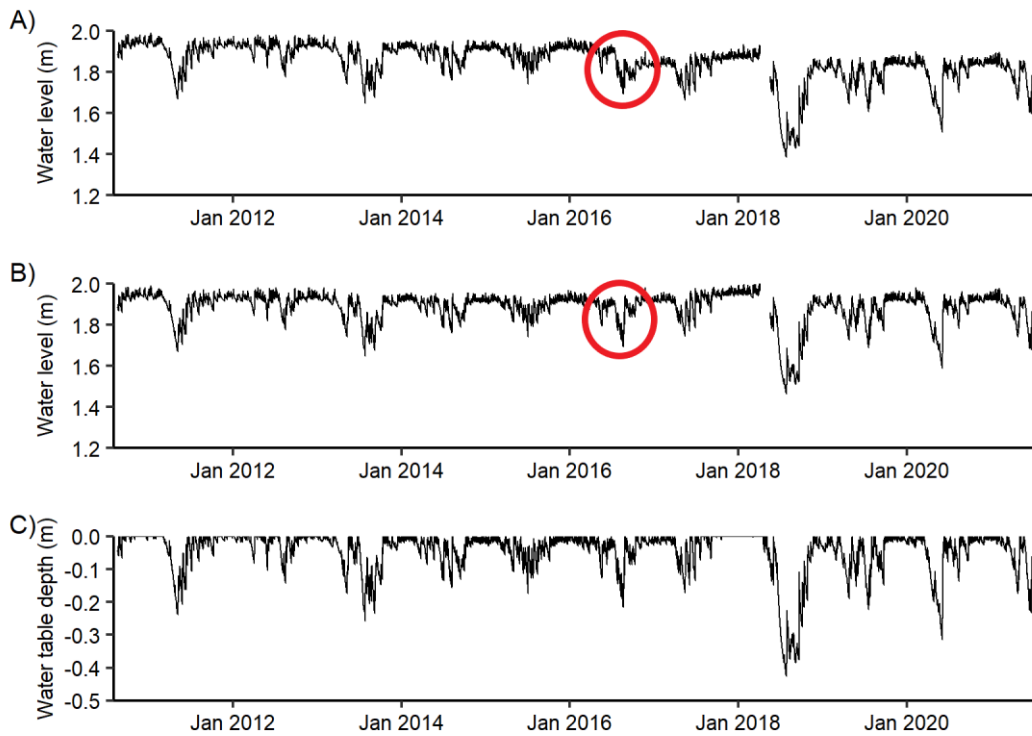
Figure 3.15. A) Uncorrected water level timeseries at the May Moss meteorological station. The level shift on 23/08/2016 is encircled in red. B) the water level timeseries with the 0.08 m adjustment from 23/08/2016 13:00 onwards, with the level shift encircled in red. C) The adjusted, corrected and gap filled water table depth timeseries.
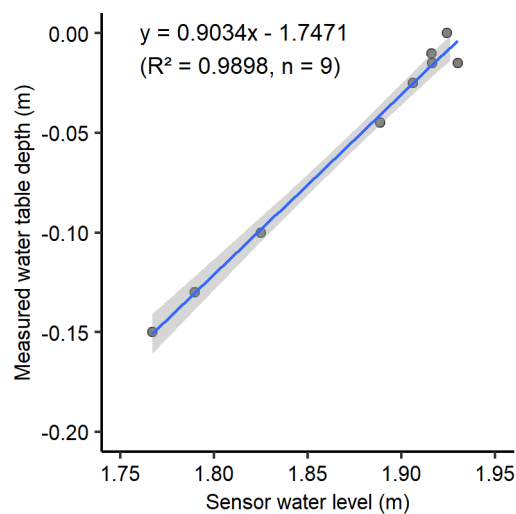
Figure 3.16. Linear regression between the pressure transducer sensor water level output (m) and the measured water table depth (m) at the May Moss meteorological station. Shaded region represents 95% confidence interval.

3.3 MODELLING EVAPOTRANSPIRATION (ET)

The May Moss micrometeorological timeseries lends itself well to the BREB method with its hourly records of net radiation, soil heat flux, atmospheric pressure, and vertical profiles for T and RH. The station has a 'fetch' of at least 240 m and a roughness length (taken as a tenth of the mean vegetation height (Oke, 1987) of 0.04 m. Two out of the four combined

77

temperature and RH sensors (CS215) were required for the Bowen ratio equation, however simultaneous availability of long-term data from two sensors was limited by individual sensor malfunction (Table 3.3). The filling of data gaps in the T and RH timeseries through interpolation or modelling, as discussed above, was intended for short continuous data gaps between 1 and 48 hours long. Out of the four measurement heights (0.4, 1.0, 2.0 and 3.0 m), sensor measurements at 0.4 and 3.0 m were selected to calculate the vertical T and e_a gradient for the BREB equation due to the lowest frequency of simultaneous error and to meet an adequate height between them to detect gradients in temperature and vapour pressure (Drexler et al., 2004). Due to an extended malfunctioning of the sensor at 3.0 m during the period 10/05/2013 – 24/08/2016, data from the sensor at 2.0 m was used as a replacement for 3.0 m sensor during the period 10/05/2013 – 09/09/2015, however a data gap remained for the period 10/09/2015 – 24/08/2016, for which λE could not be computed using the BREB method.

Table 3.3. Time periods during which long-term (> 24 hours) T and RH sensor data are available (X) or unavailable (O) at the four sensor heights 3.0, 2.0, 1.0 and 0.4 m and the sensor heights selected during each period for the BREB method.

Time period	3.0	2.0	1.0	0.4	Height of sensors selected
20/08/2010 – 24/12/2010	X	X	X	X	3.0 and 0.4
25/12/2010 – 23/03/2011	X	O	X	X	3.0 and 0.4
24/03/2011 – 14/05/2011	X	O	O	X	3.0 and 0.4
15/05/2011 – 11/01/2012	X	O	X	X	3.0 and 0.4
12/01/2012 – 09/05/2013	X	X	X	X	3.0 and 0.4
10/05/2013 – 09/09/2015	O	X	X	X	2.0 and 0.4
10/09/2015 – 10/05/2016	O	X	X	O	–
11/05/2016 – 24/08/2016	O	O	X	O	–
25/08/2016 – 04/04/2018	X	X	X	X	3.0 and 0.4
05/04/2018 – 17/05/2018	O	O	O	O	–
18/05/2018 – 01/07/2021	X	X	X	X	3.0 and 0.4

Following the gap filling and quality control of sensor data, T and RH at 3.0, 2.0 and 0.4, using the selection listed in Table 3.3, atmospheric pressure, soil heat flux and R_n were used to calculate λE using the BREB equation. Once Bowen's β were computed for all data points, data were eliminated using the rejection criteria (Table 3.1 and Table 3.2) defined by Perez et al. (1999), with the error limit adapted by Hu et al. (2014). In addition, any data points where both ΔT and Δe_a were equal to zero (stable BLA conditions) were removed to avoid division by zero (0.1% of series) (Table 3.4). Any negative λE values were converted to zero (27.9% of series). Positive λE (W m^{-2}) fluxes were only available for the hours between 04:00 and 21:00, with the bulk of data available around midday (26.1% of series) (Figure 3.17).

Table 3.4. Total number and proportions of data rejected due to stable conditions (lack of temperature and vapour pressure gradient), not fulfilling any of the data acceptance conditions required for the BREB method or fulfilling conditions requiring data rejection, following the procedures outlined by Perez et al. (1999) and Hu et al. (2014). Note: Values do not add up to totals due to overlapping rejection through different criteria. Data gaps amounted to 8.8% of the timeseries.

Criteria	Rejected (hours)	Rejected (% of timeseries)
Stable conditions	68	0.1
Conditions required for data acceptance according to Table 1	26801	28.1
Conditions requiring data rejection according to Table 2	9961	10.5
Total	35493	37.3
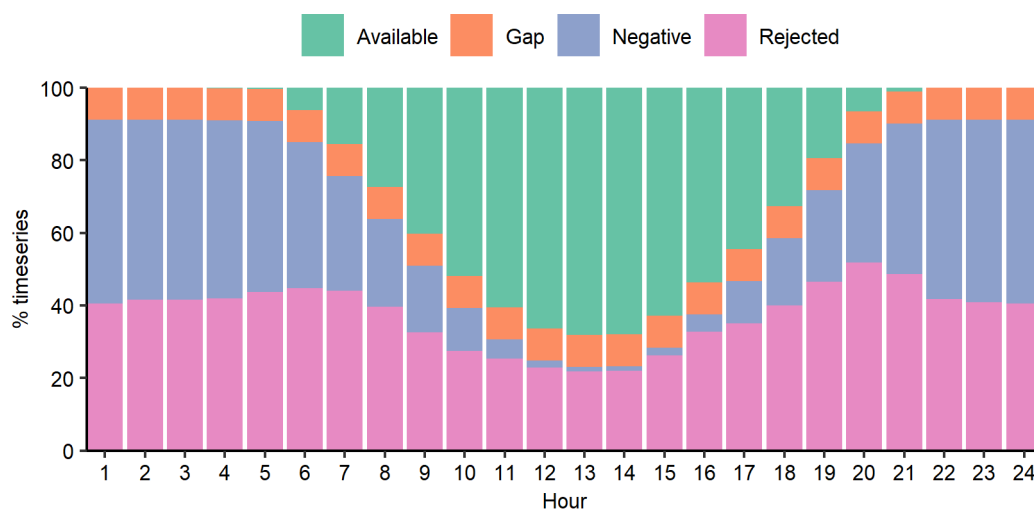
Figure 3.17. Percentage of timeseries data available for the BREB method and percentage of data gaps, negative fluxes (converted to zero) and data rejected following the procedures by Perez et al. (1999) and Hu et al. (2014) or because of stable BLA conditions for every hour.

The Priestley-Taylor (PT) equation was used to fill hourly data gaps caused by the data rejection procedure outlined above and the gap 10/09/2015 – 24/08/2016 during the CS215 sensor malfunction. The constant a was calibrated using the method by Drexler et al. (2004) and derived from the average a (0.80) based on hourly non-rejected data 01/01/2011 – 31/12/2020. Average daily λE (W m^{-2}) from the BREB and PT methods, derived from overlapping data (01/01/2011 – 31/12/2020), correlate well (Figure 3.18). This linear regression was used to correct the PT-modelled λE. Again, negative λE fluxes, occurring predominately by night, were converted to zero (34.8% of series). Positive λE fluxes derived using the PT equation thus made up 11.3% of the complete λE timeseries.
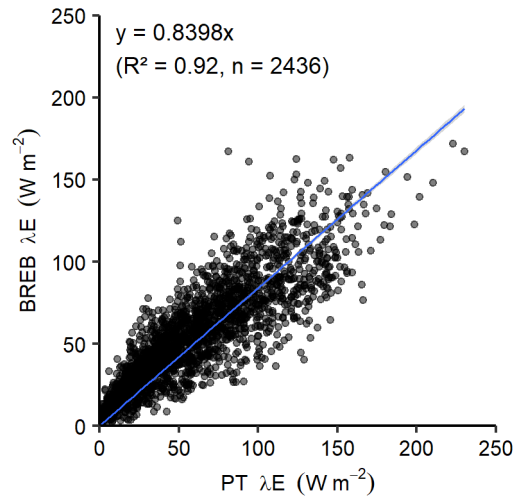
Figure 3.18. Linear regression (through origin) between the latent heat flux, λE, (W m^{-2}) computed using the Bowen ratio energy balance (BREB) method and Priestley-Taylor (PT) equation.

The evapotranspiration rates ET (mm hr^{-1}) were computed by multiplying hourly λE (W m^{-2}) by 0.0036 (conversion factor to MJ m^{-2} hr^{-1}) and dividing by the latent heat of vaporisation, 2.45 MJ m^{-2} (Oke, 1987):

$$\text{ET (mm hr}^{-1}) = \frac{\lambda E \times 0.0036}{2.45} \tag{3.18}$$

The complete ET timeseries (Figure 3.19), following data validation for the BREB method and gap filling using the PT method, shows a strong seasonal ET pattern, with lull years during 2011, 2016 and 2021, and strong ET years in 2012, 2014, particularly during the 2018 summer heatwave.
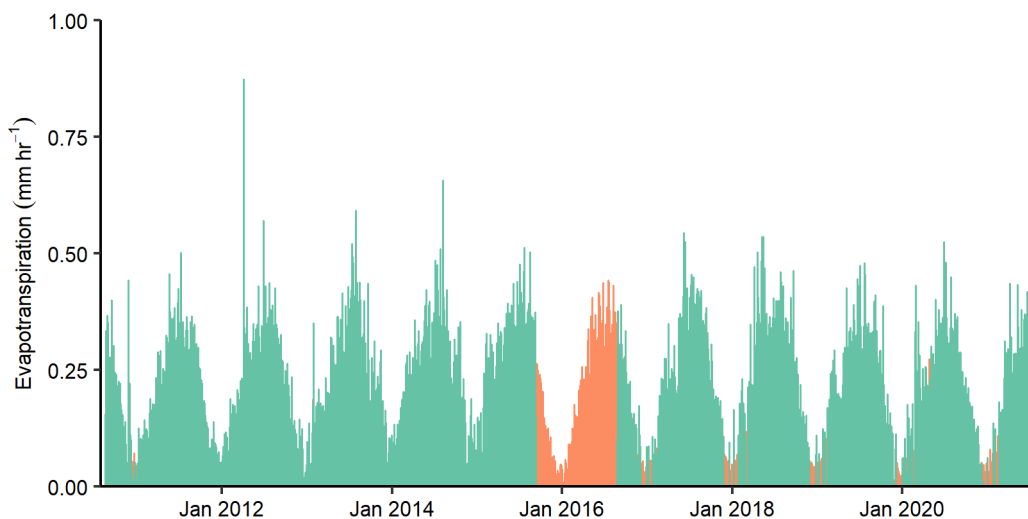
Figure 3.19. Evapotranspiration (ET) (mm hr^{-1}), based on the Bowen ratio energy balance method. Data in green were computed using the BREB method. Data in orange are former gaps filled using the PT method.

The relationships between vertical wind speed (upper − lower measurement), air temperature and ET, and between the four terms of the energy balance equation (R_n, G, H and λE) were explored over four days with contrasting meteorological conditions identified in 2017 (Figure 3.20). These typologies of day were selected to present the differing diurnal structures typical of the meteorological year and explore their influence over ET (mm hr⁻¹). Warm (mean 17.2°C) sunny conditions (25/05/2017; Figure 3.20A) persisting through the day produced an extended duration of vertical heat transfer between 6:30 and 19:30 hours and a peak ET flux of 0.35 mm hr⁻¹. This transfer of heat and water vapour is dampened under warm overcast conditions, though two hours of sunshine around 15:00 hours quickly increased the vertical heat transfer and ET to 0.29 mm hr⁻¹ (19/07/2017; Figure 3.20B). Cooler (mean 7.5°C) sunny autumnal or winter days (27/10/2017; Figure 3.20C) reduce the duration of strong vertical heat transfer between 9:00 and 17:00 and lower peak ET fluxes to < 0.2 mm hr⁻¹. Under winter cold overcast conditions (10/12/2017; Figure 3.20D) the vertical transfer of heat and the ET fluxes become negligible. In summary, the intensity and duration of incoming radiation and strong vertical heat transfer that develops governs the ET fluxes at a diurnal and annual scale.

Air temperature and vertical wind speed are closely linked through the vertical transfer of sensible heat, as eddies, particularly visible during unstable conditions by day. During these updraft conditions, temperature increases with vertical wind speed, whilst temperatures decrease under downdraft conditions (Oke, 1987). The ET flux is highest during warm, sunny days, driven by a greater energy flux towards the surface, and becomes almost negligible under cold, overcast conditions with minimal radiative input (Figure 3.20). R_n, H and λE follow a similarly defined diurnal pattern (though less pronounced during overcast days), while G does not vary greatly between night and day, and typically lags the three other energy fluxes as the soil absorbs heat more slowly by day and releases it gradually by night. This behaviour is amplified over annual timescales, with R_n, H and λE reaching maximum rates during the summer, while G increases over the summer months, before gradually reducing over the autumn as the soil loses its heat store (Oke, 1987).
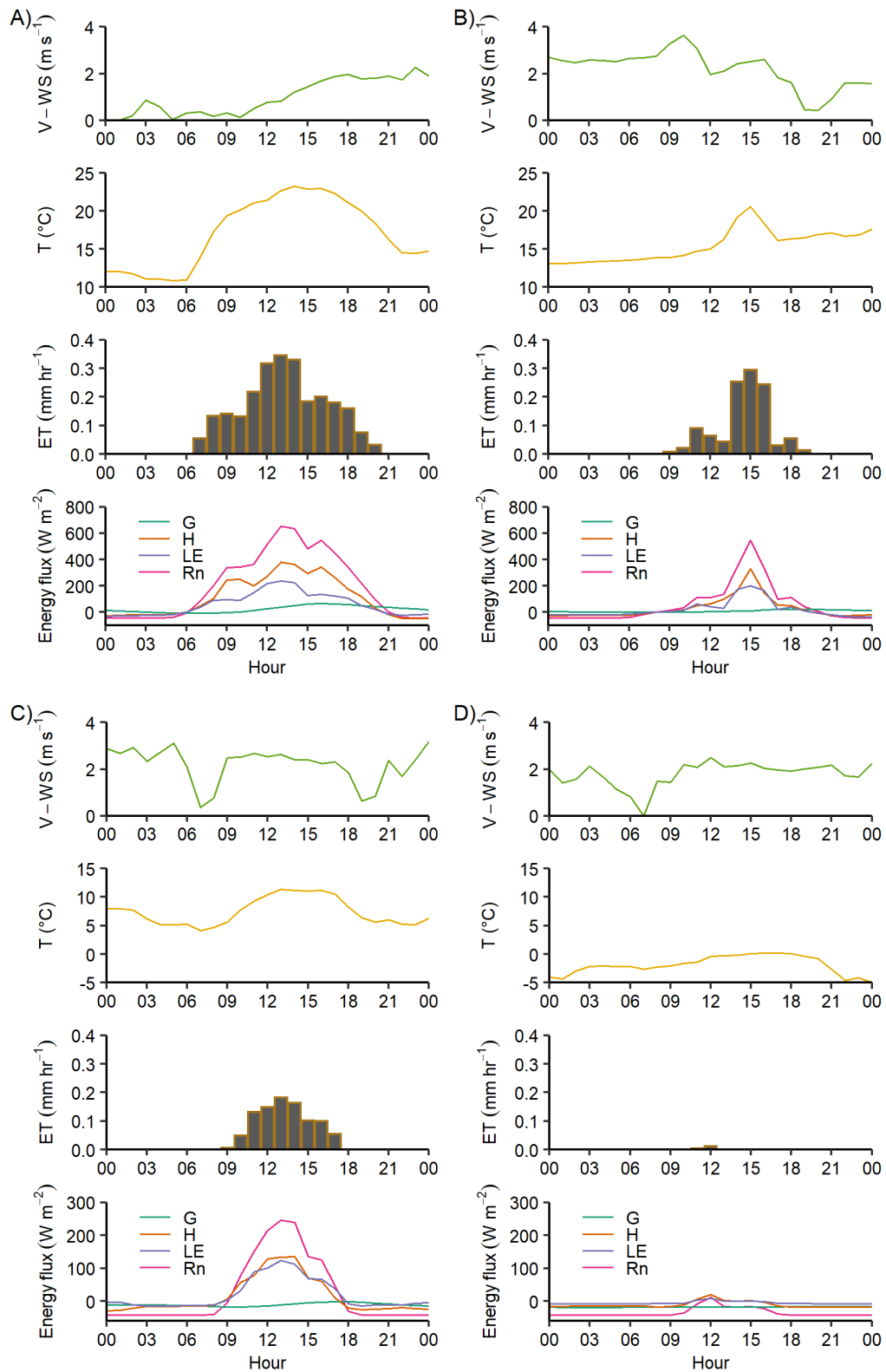
Figure 3.20. Relationship between vertical wind speed (V-WS) (m s⁻¹), air temperature (T) (°C), evapotranspiration (ET) (mm hr⁻¹) and the energy fluxes of net radiation (R_n), soil heat flux (G), sensible heat (H) and latent heat (LE) (W m⁻²) on four days: A) 25/05/2017 – a warm, sunny day, B) 19/07/2017 – a warm, overcast day, C) 27/10/2017 – a cold, sunny day, and D) 10/12/2017 – a cold, overcast day.

3.4 MEASUREMENT ERROR

Error is an intrinsic part of environmental monitoring. Sensor manufacturing defects or calibration error, leading to drift in observations, are examples of systematic error. Such errors may be addressed by using correction factors. Random errors may occur in any order and without a discernible source and include instrument malfunction, limitations, calibration and programming, as well as environmental factors. Data recording, transfer, processing, and storage may furthermore lead to process errors (Abtew and Melesse, 2013).

Error may be reduced through quality control measures (Abtew and Melesse, 2013), such as those outlined here for the various measurements taken at the May Moss meteorological station. Individual sensors were calibrated during the initial installation of the station and regularly tested for accuracy during field visits. For example, the performance of the temperature and relative humidity sensors (CS215, Campbell Scientific) was assessed by placing them next to each other at several heights, with the measurements always placed within the declared sensor uncertainties (Table 3.5). Likewise, the raingauge (ARG100, Campbell Scientific) was inspected during site visits to clear any debris and ensure the gauge was correctly levelled by pouring a known quantity of water through the gauge and counting the number of tips. In addition, air temperatures always remained within the sensor's declared operating temperatures, where specified (Figure 3.2 and Table 3.5).

The main sources of error regarding the May Moss meteorological station were instrument malfunction and drift. Sensor malfunction affected most sensors, often producing lengthy gaps in the timeseries, and was particularly evident for net radiation (NR-LITE2 Net Radiometer, Campbell Scientific). To fill these gaps, linear regression of the affected timeseries against related series (e.g., PAR for net radiation) and against equivalent series from the Fylingdales station was commonly applied. Error resulting from sensor drift was evident in the soil heat flux timeseries (Figure 3.13) and was addressed using a correction factor computed by regressing annual standard deviations of the data against measurement years (Figure 3.14). All these regressions were characterised by high coefficients of determination ($R^2 > 0.8$) and low standard error (SE ≤ 5.00), indicating a low level of process error through the low dispersion of the modelled values from the original timeseries, thus providing a high degree of confidence that the modelled values approximate the data gaps in the original series.

Further sources of error relate to the sensitivity of the individual types of sensors installed on the May Moss meteorological station (Table 3.5). For example, the tipping bucket

raingauge (ARG100, Campbell Scientific), used to quantify hourly precipitation, has a sensitivity and resolution of 0.2 mm/tip, which places a limit on the detection of low rainfall events. During high intensity rainfall events, extra volumes of water may be lost due to spillage, which reduced the accuracy of the gauge by 4% at rainfall rates of 25 mm hr^{-1} and by 8% at 133 mm hr^{-1} (Table 3.5) (Campbell Scientific, 2010). However, as the most intense rainfall events recorded in an hour over the monitoring period was 15 mm hr^{-1} (on 23/08/2017), measurement error of the raingauge records was kept below 4%.

Table 3.5. Sensor specifications and uncertainty values.

Measurement	Sensor (Manufacturer)	Measurement range (Operating temperature)	Resolution (R) / Sensitivity (S)	Accuracy
Atmospheric pressure	HOBO U20 (Onset)	0 – 207 kPa	R: < 0.02 kPa	Typical: ± 0.05% Max: ± 1.0%
Air temperature	CS215 (Campbell Scientific)	-40° to +70°C	R: 0.01°C	± 0.3°C (at 25°C) ± 0.4°C (5° to 40°C) ± 0.9°C (-40° to +70°C)
Relative humidity	CS215 (Campbell Scientific)	0 – 100% RH (-20° to +60°C)	R: 0.03% RH	± 2% (10% to 90%) at 25°C ± 4% (0% to 100%) at 25°C
Wind speed	03102 (Campbell Scientific)	Range: 0 – 50 m s^{-1} Gust: 60 m s^{-1} (-50° to +50°C)	R: 0.5 m s^{-1}	± 0.5 m s^{-1}
Precipitation	ARG100 (Campbell Scientific)	0.2 – 500 mm hr^{-1}	R/S: 0.2 mm/tip	Degradation in accuracy is typically: 4% at 25 mm/hr 8% at 133 mm/hr
PAR	SKP215 (Campbell Scientific / Skye Instruments)	400 and 700 nm (at -35°C to +75°C)	S: 10µV µmol^{-1} m^{-2} s^{-1}	Accuracy/absolute calibration error: ± 5% (typically < ± 3%)
Net radiation	NR-LITE2 (Campbell Scientific)	± 2000 W m^{-2} (-40° to +80°C)	S: 10 µV W^{-1} m^{-2} (nominal)	Non-linearity (over full range): < 1%
Soil heat flux	HFP01 (Campbell Scientific)	± 2000 W m^{-2} (-40° to +80°C)	S: 50 µV W^{-1} m^{-2} (nominal)	Within -15% to +5% in most common soils (12-hour totals)
Water table depth	PDCR 1830 (Campbell Scientific)	0.75 to 600 mH20 (-20° to 60°C)	R: < 0.01 cm	± 0.1%

Intrinsic accuracy limits of the various sensors as well as the use of multiple different sensors for the quantification of ET inevitably leads to uncertainty in the ET series and the broader water balance of May Moss. In the following chapters, the water balance equation (Eq. 3.1) is rearranged to:

$$P - ET - R - \Delta S = \varepsilon \qquad (3.19)$$

where ε is the water balance residual (mm). A positive residual term, ε, implies that water gains (P) are exceeding water outflows ($ET + R$ and storage change, ΔS) (Isabelle et al., 2018). However, ε is also representative of the measurement error derived from the four main water balance components. In their energy and water balance estimation for a Swedish mire, Kellner and Halldin (2002) give error estimates of 5% for precipitation, 20% for runoff and $20-30$% for ET using the BREB technique. These estimated error values were accommodated within the analysis and interpretation of annual water balances and their residuals for May Moss.

3.5 SUMMARY

The closure of the water and energy balance typically requires the quantification of evapotranspiration (ET), or the latent heat flux (λE), using micrometeorological techniques. Gaps and errors among the May Moss micrometeorological sensor data for air temperatures, RH, wind speed, precipitation, PAR, R_n, soil heat flux and water level were filled and corrected, often through linear regression with adjacent sensors or with data from nearby meteorological stations, or by simple replacement with equivalent data from the Fylingdales meteorological station, where appropriate (Table 3.6). While some corrections (e.g., soil heat flux) were simple, others (e.g., R_n) required extensive modelling to obtain a complete timeseries necessary for evaluating ET. The gap filling and data correction facilitated the quantification of ET using the Bowen ratio energy balance (BREB) method. As the BREB method is prone to intrinsic errors, unsuitable data were rejected following the method by Perez et al. (1999), with the error limit equation (around $\beta = -1$) developed by Hu et al. (2014). Consequent gaps in the λE timeseries were filled using the Priestley-Taylor (PT) equation. In sum, the BREB method made up 53.9% of the ET timeseries and the PT method filled the remaining 46.1%. When analysing micrometeorological profiles, higher temperatures, and radiative input, accompanied by gradients in vertical wind speed which accelerate the dispersal of water vapour, encourage greater energy fluxes (R_n, G, H and λE) and ET. These strong interrelationships between energy fluxes and micrometeorological factors, such as wind, humidity, and air temperature, are thus displayed in their clear diurnal and seasonal patterns and cycles, with the potential for vast hydrological impacts as a result of meteorological events (e.g., heatwaves) or climate change.

Table 3.6. Summary of meteorological time series, their measurement interval, the number of hours of missing data and percentage of series, the duration (hours) of the longest data gap per series, and the method used to fill these gaps.

Series (Number of sensors)	Interval	Hours of missing data (% of series)	Longest gap duration (hours)	Gap filling method applied
Atmospheric pressure (1)	0.5 hour	2450.5 (18.1%)	2448	Linear regression with the Loftus station atmospheric pressure series.
Air temperature (4)	1 hour	3.0m: 29889 (31.4%) 2.0m: 12923 (13.6%) 1.0m: 5826 (6.1%) 0.4m: 1012 (1.1%)	3.0m: 17016 2.0m: 9171 1.0m: 1230 0.4m: 1010	In order of preference: 1) average of min and max temperature data, 2) interpolation of adjacent sensor temperature data, 3) linear regression with Fylingdales station air temperature series.
Relative humidity (4)	1 hour	3.0m: 29837 (31.3%) 2.0m: 12722 (13.4%) 1.0m: 2329 (2.4%) 0.4m: 9393 (9.9%)	3.0m: 28825 2.0m: 9168 1.0m: 1229 0.4m: 8383	In order of preference: 1) interpolation of adjacent sensor RH data, 2) linear regression with Fylingdales station RH series.
Wind speed (4)	1 hour	3.0m: 8886 (9.3%) 2.0m: 10354 (10.9%) 1.0m: 1452 (1.5%) 0.4m: 2413 (2.5%)	3.0m: 7875 2.0m: 9327 1.0m: 1010 0.4m: 1982	In order of preference: 1) interpolation of adjacent sensor wind speed data, 2) linear regression with Fylingdales station wind speed series.
Precipitation (1)	1 hour	1011 (1.1%)	1010	Gaps replaced with Fylingdales station precipitation records.
PAR (1)	1 hour	1010 (1.1%)	1010	NA
Net radiation (1)	1 hour	55920 (58.7%)	55920	The prevalence of erroneous data meant the entire series had to be modelled, based on linear regression with PAR data, followed by Leeming station solar radiation series.
Soil heat flux (1)	1 hour	2223 (2.3%) continuous drift	1010	The drift in the data was approached by using an annual standard deviation correction factor. Data gaps were filled using hourly averages for each affected month.
Water table depth (1)	1 hour	1011 (1.1%)	1010	Interpolation for 1-hour gap; Long gap filled by interpolation with Eller Beck dipwell series.

Chapter 4. Hydrological functioning of an intact blanket bog

ABSTRACT

The capacity of peatlands to sequester and store atmospheric carbon is tightly coupled to their hydrological functioning. Climate change is predicted to increase the frequency and severity of extreme weather events, such as heatwaves and droughts, across Europe. Here, we use a decade-long hydro-meteorological series spanning 2010/11 − 2019/20 to characterise the hydrological functioning of an intact water-shedding ombrotrophic blanket bog. The period investigated thus includes a substantial drawdown of water tables (−427 mm) during the 2018 summer heatwave. Annual water balances were calculated for three consecutive hydrological years (2017/18, 2018/19 and 2019/20) and comprised, on average, 930 mm of precipitation, 335 mm of evapotranspiration losses, 371 mm of runoff losses and a storage change of −7 mm, with the annual residual averaging at +268 mm. Correlations between the radiative budget, temperature, vapour pressure deficit, precipitation and peatland water tables (WT) shed light on the key factors governing hydrological functioning over annual, seasonal and monthly timescales. Average annual WT depth (WTD) is primarily related to average available energy (net radiation − soil heat flux, $R_n − G$), while monthly average WTD is driven mainly by VPD, which in turn is strongly coupled with available energy ($R_n − G$). Summer water availability (P − ET) is controlled more by precipitation than evapotranspiration and is the key driver of summer change in water storage (ΔS). However, the deeper summer WT drawdown is associated with greater incidence of warm, highly evaporative days. Thus, the duration and extent of the 2018 summer drawdown reflects the combined impacts of low water availability (P − ET) and high incidence of evaporative days. The water balance of May Moss had recovered a year after the 2018 summer drought. That said with the predicted increase in the frequency of summer heatwaves in Europe together with a local reduction in winter and spring precipitation and average winter warming, and given a location in the drier eastern England, the water balance of May Moss may be vulnerable to climate change.

4.1 INTRODUCTION

The global peatland area sustains between 500 and 700 Gt of carbon (C), with northern peatlands sequestering an average of 18.6 g C m^{-2} yr^{-1} (Yu et al., 2010). The capacity of peatlands to sequester atmospheric carbon is tightly coupled with their hydrological functioning (Limpens et al., 2008; Bell et al., 2018). While peatlands have been resilient to minor climatic changes over the past 10,000 years (Page and Baird, 2016), sudden disruptions in their hydrological functioning due to extreme weather events (e.g., heatwaves, droughts, and floods) or climatic change over the longer-term can lead to alterations in their biogeochemical functioning with impacts on their capacity for long-term carbon sequestration and storage (Bridgham et al., 2008; Ratcliffe et al., 2018).

Anthropogenically-driven climate change is predicted to increase the variability of the summer climate in Europe and increase the frequency of summer heatwaves (Seneviratne et al., 2006), with annual mean temperatures already shown as increasing at a faster rate in the UK compared to the global mean (Kennedy-Asser et al., 2021). The 2018 summer heatwave in the UK is a recent example of an extreme weather event and was the combined result of an anticyclonic circulation system and high sea surface temperatures near the UK, culminating in the joint warmest summer (June, July, August) on record since 1884 (McCarthy et al., 2019b).

In the UK, with its temperate and maritime climate, 11% of the land surface is covered by deep peat, with blanket bogs accounting for 82% of this area (Joosten et al., 2017). Blanket bogs are a type of ombrotrophic ("rain-fed") peatland which depend on atmospheric deposition, primarily through precipitation, for their supply of water and nutrients (Charman, 2002; Rydin and Jeglum, 2013). Blanket bogs thus tend to develop in areas subject to high rainfall with a temperate climate (Tallis, 1998), with limited evaporative losses (Sottocornola and Kiely, 2010). A near-surface water table is maintained by regular, high precipitation, low hydraulic conductivity of peat and low evapotranspiration, and is vital to the growth and long-term survival of *Sphagnum* mosses, essential for the continued accumulation of peat and the development of these temperate *Sphagnum*-dominated peatlands (van Breemen, 1995).

Peatlands are naturally resilient to mild droughts through the desiccation-resistant properties of *Sphagnum* (van Breemen, 1995) and the process of "mire breathing", in which the water level naturally adjusts after drying-induced peat subsidence (Dise, 2009). However, more severe drought events can have significant impacts on the hydrological functioning of

peatlands (Holden and Burt, 2002a). Previous research on the impacts of droughts have found changes to peat structure (Holden and Burt, 2002b), resulting in changes in hydrological pathways (Worrall et al., 2006), such as via macropores and pipes (Holden and Burt, 2002b), in addition to exceptional water table drawdown (Lafleur et al., 2005).

Multi-year studies on peatlands which encompass the entire water budget are scarce. This has limited the comprehensive examination of the timescales and relative controls of hydrometeorological variables in driving peatland hydrological processes, such as water table drawdown, and the effects of extreme weather events, such as heatwaves and droughts. This lack of data has induced calls for further research into the impacts of drought events on the hydrological functioning of peatlands to identify their resilience to temperature and rainfall thresholds (Holden and Burt, 2002a).

The aim here is to characterise the hydrological functioning of an intact blanket bog using a decade-long hydro-meteorological time series (20/08/2010 – 01/07/2021), including a four-year runoff series (14/03/2017 – 01/07/2021), as a baseline to explore the key drivers of the extreme 2018 summer heatwave WT drawdown. The hydrometeorological array at May Moss, on the North York Moors (NE England), collects parameters (e.g. hourly net radiation, soil heat flux, and vertical profile for air temperature and relative humidity) that facilitate the use of Bowen ratio equation (Bowen, 1926) to calculate ET (Price, 1992a; Wessel and Rouse, 1994; Campbell and Williamson, 1997; Thompson et al., 1999; Kellner, 2001; Peacock and Hess, 2004; Lapen et al., 2005). By measuring the hydrological inputs, outputs and storage change, these measurements enable the quantification and exploration of the water balance for three consecutive hydrological years bracketing the 2018 heatwave.

4.2 METHOD

4.2.1 Site description

May Moss (54° 21' 4" N, 0° 39' 16" W, elev. 253 m) is an intact upland blanket bog situated within the North York Moors National Park (UK). The peatland is protected as a Site of Special Scientific Interest (SSSI) and sustains peat depths up to 6.4 m (Atherden, 1979). The peat has accumulated on Jurassic sandstone, in the broadly flat headwater basins of the northward draining Eller Beck (EB) and the southward flowing Long Grain (LG) (Atherden, 1979). As such, May Moss lies on the watershed between these two catchments. At 0.63 km^2, May Moss is the largest area of actively-accumulating blanket bog in the North York Moors (Chiverrell, 2001) and has not been subject to managed burning or grazing.

Spatial land cover datasets, containing habitat and land use classifications, were obtained from the Priority Habitat Inventory (Natural England, 2019) and the National Forest Inventory (Forestry Commission, 2019). The bog is classified as a *Sphagnum magellanicum – Andromeda polifolia* (M18a) sub-community under the National Vegetation Classification (NVC) (Elkington et al., 2001), with abundant presence of *Calluna vulgaris*, *Erica tetralix*, *Eriophorum vaginatum*, *Eriophorum augustifolia*, *Vaccinium myrtillus*, *Empetrum nigrum* and *Hypnum jutlandicum* (Chiverrell, 2001) and scattered incidence of *Drosera rotundifolia*. The site borders an extensive area of upland wet heathland to the north, grass moorland to the northwest and northeast, and the land is administered by the Forestry Commission to the south and east and the Ministry of Defence (RAF Fylingdales) to the north-west, rendering it largely inaccessible to the public.

Though largely intact, the Eller Beck stream draining the intact May Moss peatland began to be affected by a single single-thread gully that was blocked and restored across the period 2013-14 by Moors for the Future. The gully extended ≈330 m east across May Moss some 250 m north of the meteorological station. The gully for the most part was 1 m in width and < 0.5 m deep but increasing to < 5 m width and ≈3-4 m depth at the edge of the site. The gully was blocked with ≈4 wooden dams and numerous heather bales in summer 2013, and has since stabilised and infilled with peat. Research and management activities at May Moss are supported by the National Park Authority, Natural England, and the Forestry Commission. These interests reflect that the North York Moors upland area between the Vale of Cleveland (to the north) and the Vales of Pickering & York (to the south) are designated as a SAC (Special Area of Conservation) and forms the largest inland SSSI (Site of Special Scientific Interest) in the UK.

4.2.2   The May Moss meteorological station

Hourly hydro-meteorological data were collected from the May Moss meteorological station, consisting of a micrometeorological mast, rain gauge and water level sensor, between 20/08/2010 and 01/07/2021. The station is situated centrally on the intact bog, on the watershed of the Eller Beck catchment with an uninterrupted blanket bog cover wind fetch of over 240 m in all directions, and the closest forestry plantation to the south. Hourly data were recorded using the Campbell Scientific CR1000 datalogger. Average, minimum, and maximum temperature (°C) and relative humidity (%) were measured at 0.4, 1.0, 2.0 and 3.0 m heights using four temperature and relative humidity sensors (Campbell Scientific CS215) and four rotary cup anemometers (Campbell Scientific 03102) were fixed at the same

heights. A net radiometer (NR-LITE2 Net Radiometer, Campbell Scientific), PAR-sensor (SKP215 Quantum Sensor, Campbell Scientific) and soil heat flux plate (HFP01, Campbell Scientific) were used to monitor energy fluxes. A rain gauge (ARG100, Campbell Scientific) collected hourly total precipitation (mm). Hourly peat water levels were monitored using a submersible vented pressure transducer (PDCR 1830, Campbell Scientific) placed inside a 1.8 m length dipwell next to the May Moss meteorological station. Data gaps in the hydrometeorological time series were filled using largely linear regression (Peterson et al., 1998), where possible with adjacent sensors or otherwise with equivalent sensor data from the Fylingdales meteorological station. The methods used in the preparation of data from all sensors are outlined in detail in *Chapter 3*. The May Moss hydrometeorological data were analysed based on the UK hydrological year (1st October to 30th September) (e.g., Holden and Burt (2003a); Worrall et al. (2015)). Hence, calendar years (1st January – 31st December) are referred to specifically as "calendar years", while the use of the simple terms "year" and "annual" refer to the hydrological year.

4.2.3 Historical data acquisition

To examine the May Moss time series within a historical context, daily air temperature (Met Office, 2021b; d) and precipitation (Met Office, 2021a; c) data from 1961 to 2010 were obtained from the Centre for Environmental Data Analysis (CEDA). Air temperature and precipitation data between 01/01/1961 and 31/12/1983 were sourced from the Silpho Moor meteorological station (54° 20' 16.08" N, 0° 31' 40.44" E, elev. 203 m), 8.3 km southeast of the May Moss station, and data between 01/01/1984 and 19/08/2010 were sourced from the Fylingdales station (54° 21' 30.96" N, 0° 40' 11.96" E, elev. 262 m), 1.4 km northwest of the May Moss station. Consistencies in daily air temperature and precipitation data between stations were examined by linear regression of overlapping data.

4.2.4 Evapotranspiration

With the availability of hourly net radiation, soil heat flux, air temperature and relative humidity profiles, the Bowen ratio energy balance (BREB) method (Bowen, 1926) was used to quantify hourly evapotranspiration (ET):

$$\lambda E = \frac{R_n - G}{1 + \beta} \tag{4.1}$$

where λE is the latent heat flux (W m^{-2}), R_n is net radiation (W m^{-2}), G is soil heat flux (W m^{-2}) and β is the Bowen ratio quantified from simultaneous air temperature and vapour pressure measurements at two vertical heights:

$$\beta = \gamma \frac{\Delta T}{\Delta e_a} \tag{4.2}$$

where ΔT is the change in air temperature T between two heights (Δ = upper measurement – lower measurement) and Δe_a is the change in actual vapour pressure e_a between the same two heights. The psychrometric constant γ (kPa °C^{-1}) is computed from:

$$\gamma = \frac{C_p \rho}{\epsilon \lambda} \tag{4.3}$$

where C_p is the specific heat at constant pressure (1.013 x 10^{-3} MJ kg^{-1} °C^{-1}), ρ is atmospheric pressure (kPa), ϵ is the ratio of molecular weight of water vapour to dry air (0.622), and λ is the latent heat of vaporisation (2.45 MJ kg^{-1}). Actual vapour pressure (e_a) can be derived from air temperature (T) and relative humidity (RH):

$$e_s = 0.6108 exp \left[\frac{17.27T}{T + 237.3} \right] \tag{4.4}$$

$$e_a = e_s \frac{RH}{100} \tag{4.5}$$

where e_s is the saturation vapour pressure at air temperature T (kPa) and exp is the base of the natural logarithm. The latent heat flux λE was then divided by the latent heat of vaporization (2.45 MJ kg^{-1}) to obtain the evapotranspiration flux ET (mm hr^{-1}) (Drexler et al., 2004). Further rationale behind the selection of the BREB method is outlined in *Chapter 3*. Data not suited for the BREB method were identified using the method outlined by Perez et al. (1999) with the error limit equation adapted by Hu et al. (2014). These ET gaps were filled using the Priestley-Taylor equation (Priestley and Taylor, 1972):

$$ET_{PT} = a \frac{s}{\gamma + s} (R_n - G) \tag{4.6}$$

where ET_{PT} is evapotranspiration (mm h^{-1}) determined by the Priestley-Taylor (PT) method and s is the slope of the saturation vapour pressure curve at air temperature T (kPa °C^{-1}). Constant a represents aerodynamic terms for the vapour pressure deficit (VPD) and resistance (Abtew and Melesse, 2013) and was calibrated using the method recommended by Drexler et al. (2004). The ET_{PT} output was then adjusted using a linear regression with BREB-derived ET (R^2 = 0.92).

4.2.5 Runoff

The intact mire is largely situated within the Eller Beck catchment. The Eller Beck catchment area and stream network were delineated in ArcGIS using an OS Terrain 5 DTM (Ordnance Survey, 2020). A 90° triangular v-notch weir was constructed on Eller Beck where the stream exits the area of blanket bog to the north-west. A water-proof pressure transducer (HOBO U20 Water Level Logger, ONSET) was placed within a dipwell fitted to the weir on 13/03/2017, which has recorded sensor depths at half-hourly intervals until 01/07/2021. Sixteen manual head measurements (height between the v-notch and the water surface) were taken over the monitoring period. Sensor depths were converted to water levels using a linear regression (R^2 = 0.91) between sensor depths and the manual water levels. Half-hourly discharge (Q) was calculated using the Kindsvater-Shen equation (The British Standards Institution, 2017):

$$Q = C_d \frac{8}{15} \tan\frac{\alpha}{2} \sqrt{2g} h_e^{5/2} \tag{4.7}$$

where C_d is the coefficient of discharge, α is the notch angle (90 degrees), g is the acceleration due to gravity (9.81 m s^{-1}) and h_e is the effective head (m). The coefficient of discharge, C_d, was estimated as 0.578, based on the formula recommended by (Edwards, 2014) and validated by the calibration graph (Figure 4.1) provided in the British Standards ISO 1438:2008 (The British Standards Institution, 2017).
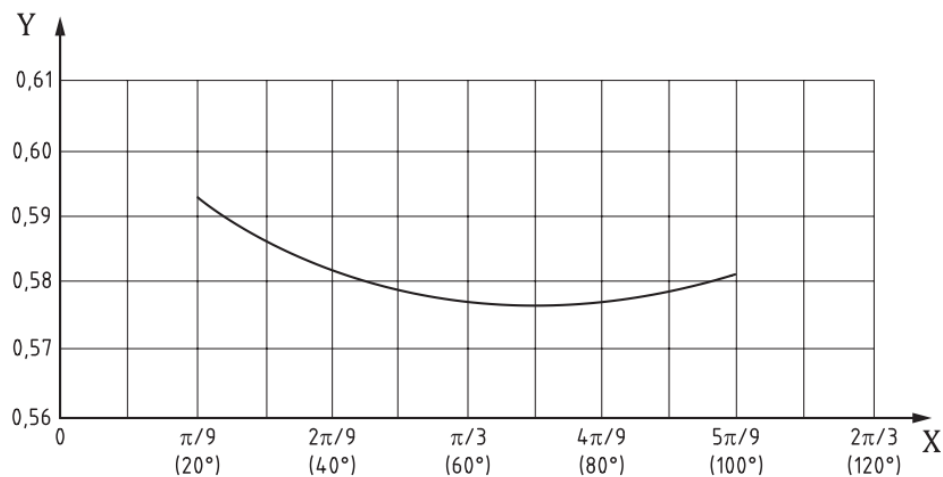
Key

X   value of notch angle, α (radians)

Y   value of C_d

Figure 4.1. Coefficient of discharge, C_d, calibration curve for the V-notch weir, related to notch angle, α (The British Standards Institution, 2017).

The effective head, h_e, from Eq. 4.7 was quantified as:

$$h_e = h + k_h \qquad (4.8)$$

Where h is the measured head (m) and k_h is a constant value of 0.00085 m for 90° v-notch weirs (The British Standards Institution, 2017). Discharge data ($m^3\ s^{-1}$) were divided by the Eller Beck catchment area (0.63 km^2) to quantify area-specific runoff (mm hr^{-1}).

The runoff time series was interrupted by a data gap between 22/10/2017 and 01/02/2018 (7% of series) which would have affected the monthly water balance for the affected months and for the hydrological year 2017/18. The gap was therefore filled by linear regressions between WTD and runoff (R^2 = 0.39), where WTD < 0, based on data collected from the affected months (October – February) in the calendar years 2017 and 2018.

4.2.6 Water balance

The annual water balance equation for a bog takes the form of:

$$P = ET - R - \Delta S \qquad (4.9)$$

where P is precipitation (mm), ET is evapotranspiration (mm), R is runoff (mm) and ΔS is the change in storage, here quantified as the change in water level between the start and end of the water balance time interval. The equation was rearranged to solve for the residual, ε:

$$P - ET - R - \Delta S = \varepsilon \qquad (4.10)$$

A positive residual term, ε, implies that water gains (P) are exceeding water outflows ($ET + R$ and storage change, ΔS), and that the system is therefore unbalanced, or the water budget is not closed. As bogs are ombrotrophic, receiving all water inputs through precipitation and with other inflows such as groundwater recharge considered negligible, the residual most likely represents error or uncertainty in the measured terms, or an unknown outflow term or "leak" (Isabelle et al., 2018; Safeeq et al., 2021), such as discharge through peat pipes, or additional changes in storage associated with the swelling or shrinking of the underlying peat with "mire breathing" (Kellner and Halldin, 2002). All water balance terms were based on hourly recordings. As runoff is typically flashy within upland blanket mires (Holden and Burt, 2003b), under-sampling of runoff extremes in the hourly timeseries is therefore likely to form a large proportion of residuals. In addition, infiltration through the stream bed and slow diffusion from the peat to the bedrock could also contribute to unaccounted residual losses. The water balance terms, as well as annual and monthly residuals, were summarised for the three complete hydrological years 2017/18, 2018/19 and 2019/20.

4.2.7 Correlation analysis

Correlations between energy, meteorological and hydrological variables were tested at annual, monthly and summer timescales to assess their relative importance in driving variability in the water balance of May Moss, in particular regarding water table depth and storage. The data included encompassed the complete hydrological years (01/10/2010 – 30/09/2020) available from the timeseries. The specific variables analysed were the available energy (net radiation – soil heat flux, Rn – G), photosynthetic active radiation (PAR), average (avg), minimum (min) and maximum (max) air temperature (T) measured at 2.0 m height, the number of days in a year recording a maximum air temperature of at least 25°C (N days ≥ 25°C) (for annual and summer periods), vapour pressure deficit (VPD) at 2.0 m height, total precipitation (mm), percentage of rain days (≥ 0.2 mm per day) (% rain days), percentage of wet days (≥ 1.0 mm per day) (% wet days), total evapotranspiration (ET), available water (precipitation – evapotranspiration, P – ET), average water table depth (avg WTD), minimum (lowest) water table depth (min WTD) and the change in storage (ΔS) over the specified period. Average and minimum WTD are given as negative values (mm below the surface), where lower values signify greater depth from the surface.

The Shapiro-Wilk test was used to confirm whether data series were normally distributed to ensure the use of appropriate correlation tests, with a p-value < 0.05 indicating that values differed significantly from a normal distribution. Monthly series were overwhelmingly non-normally distributed and therefore the non-parametric Kendall's tau correlation test was used on all monthly variables. Annual and summer data were normally distributed, with the exceptions of minimum temperature (Min T) in the annual series, and average (Avg WTD) and minimum (Min WTD) water table depth in the summer series. Pearson's test was applied to analyse correlations between normally distributed variables and Kendall's tau test was applied where one or both variables had non-normal distributions. P-values were adjusted for the False Discovery Rate (FDR), which measures the proportion of false positives, using the Benjamini-Hochberg method (Benjamini and Hochberg, 1995), which is less conservative than the commonly used Bonferroni method and therefore less likely to reject true hypotheses (Pike, 2011).

4.3 RESULTS

4.3.1 Historical context

Daily hydroclimate records from the Silpho Moor (01/01/1961 – 31/12/1983), Fylingdales (01/01/1984 – 19/08/2010) and May Moss (20/08/2010 – 31/12/2020) meteorological stations correlate well (Figure 4.2). The records combine to provide a longer-term context of air temperature and precipitation for May Moss and the southeast of the North York Moors (Figure 4.3). The area is characterised by an average annual air temperature of 8.0 ± 0.7°C and an average annual total precipitation of 935 ± 137 mm, based on daily records between 1961 and 2020. Winter temperatures, with an average of 2.8°C, are more variable (coefficient of variation, CV = 36%) than summer temperatures, averaging at 13.6°C (CV = 7%). The average annual (CV = 8%) and summer air temperatures thus remain relatively stable across the time series.
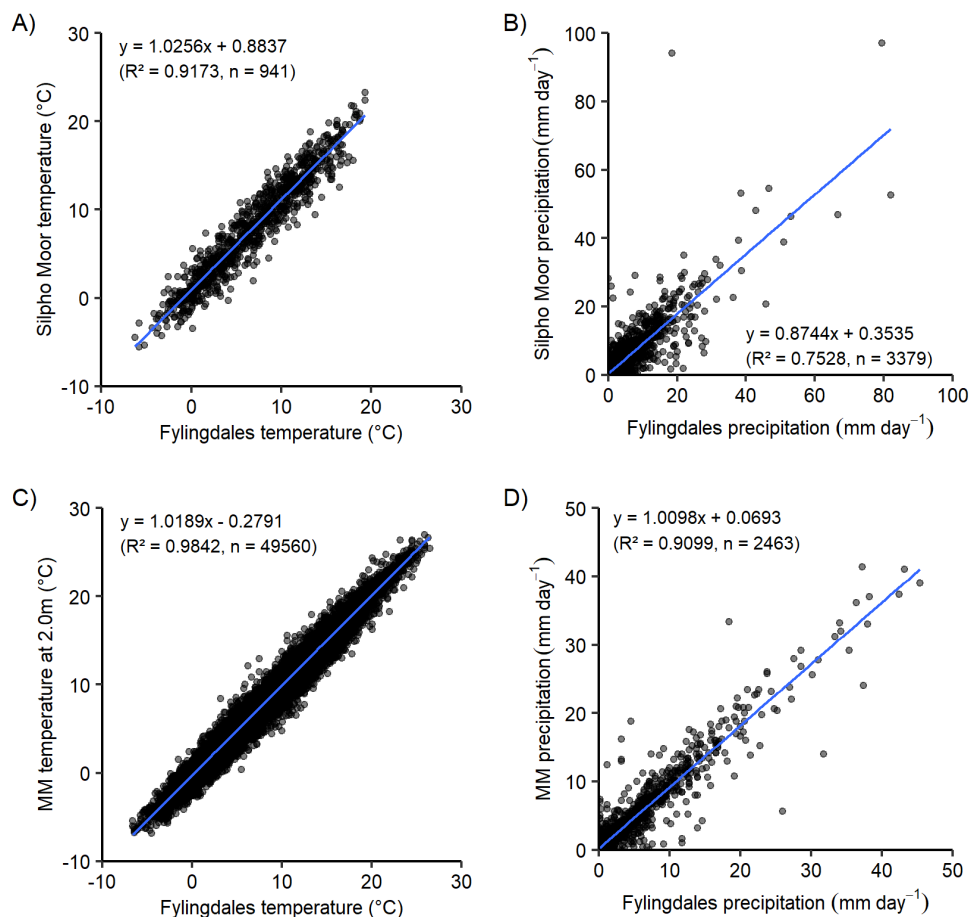
Figure 4.2. Linear regressions between overlapping daily average air temperature (°C) and daily total precipitation (mm day^{-1}) data from the Silpho Moor, Fylingdales and May Moss (MM) meteorological stations, based on overlapping records spanning A) 01/01/1984 – 30/07/1986, B) 01/02/1976 – 31/07/1986, C) 01/01/2011 – 31/12/2017 and D) 01/01/2011 – 31/12/2017.

Maximum air temperatures recorded each year over the 1961 – 2020 series have ranged between 22.0 and 31.7 (CV = 8%), with the latest record measured in 2019. Precipitation varies between years, with annual total precipitation (1961 – 2020) ranging between 596.8 and 1359.7 mm (CV = 15%). Summer total precipitation is more variable than the annual total, ranging between 39.7 and 439.7 mm (CV = 3%5) and making up 4.3 – 40.5% of annual total precipitation (1961 – 2020). Notable dry years occurred in 1964, 1976, 1984, 1995, 2003 and 2018 (Figure 4.3). Compared with the 1961 – 1990 reference, the latest decade (2011 – 2020) is, on average, 0.3°C warmer, driven by a 0.6°C warming of average winter temperatures, while average summer temperatures have not varied significantly. Average annual total precipitation over 2011 – 2020 has increased by 3% compared to the 1961 – 1990 reference, driven by wetter summers (+17%) and autumns (+15%), while winter (−9%) and spring (−11%) months have become drier.
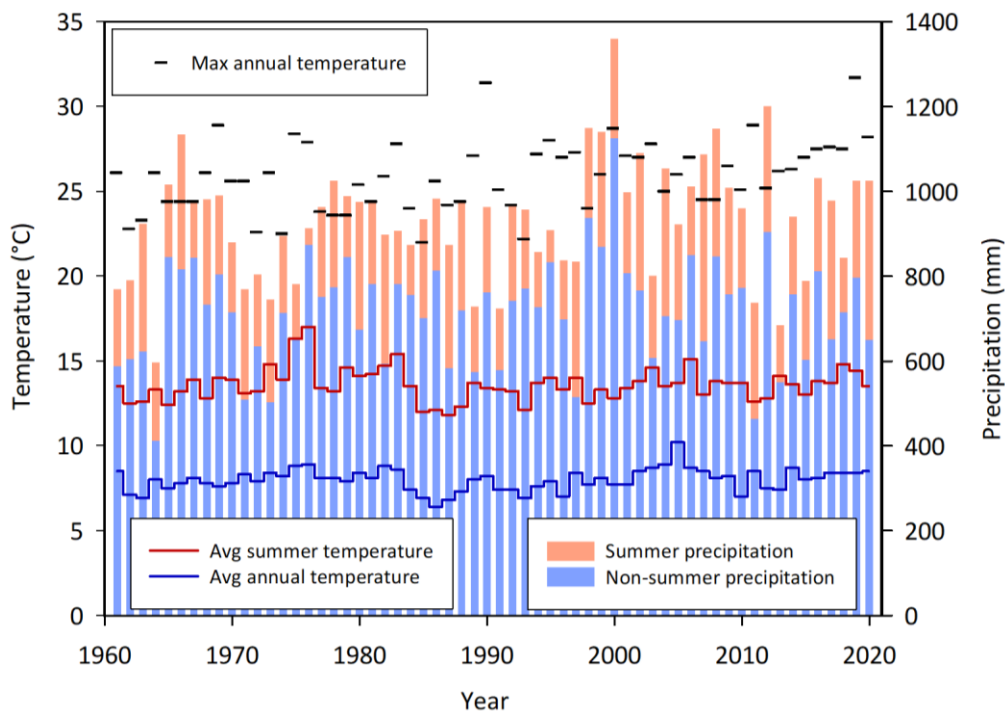
Figure 4.3. Maximum (max) annual, average (avg) annual and average summer air temperature, and total summer (June, July, August) and total non-summer precipitation (mm) per calendar year between 1961 and 2020. Records obtained from the Silpho Moor (Jan 1961 – Dec 1983), Fylingdales (Jan 1984 – Aug 2010) and May Moss (Sept 2010 – Dec 2020) meteorological stations.

4.3.2   Hydroclimate of May Moss

The decade-long hydrometeorological series on May Moss, spanning the hydrological years 2010/11 – 2019/20, is characterised by strong seasonality in air temperature, ET and WTD, which follow a similar pattern, while precipitation is more stochastic (Figure 4.4). Average

annual temperature varied little (CV = 6%) between hydrological years, ranging between 7.1 and 8.7°C, with an average of 8.1°C (Table 4.1). The lowest temperature (−11.7°C) was recorded in the first year of monitoring both on 20/12/2010 and 21/12/2010, while the highest (31.7°C) was observed on 25/07/2019 during a heatwave.
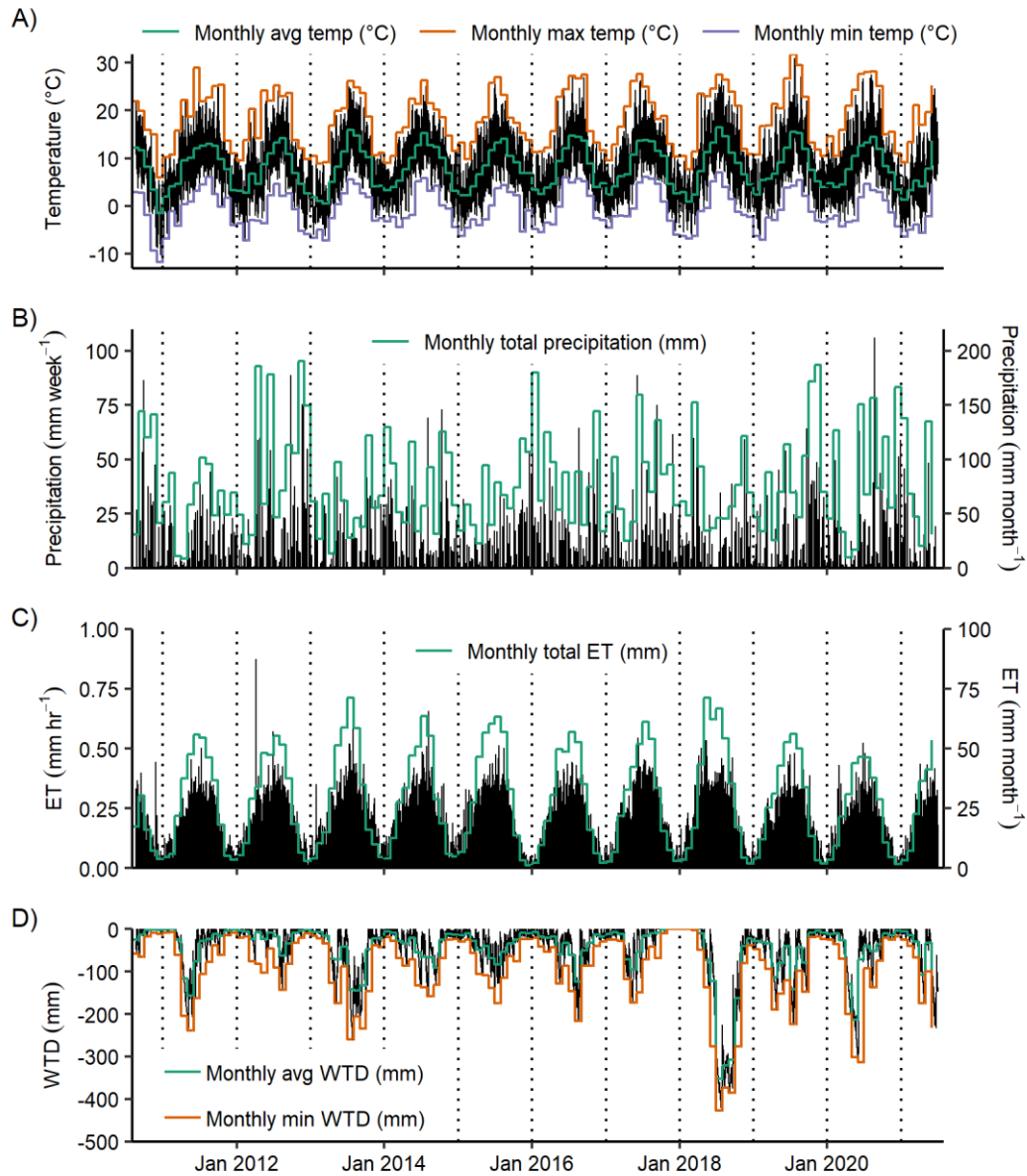
Figure 4.4. A) Hourly average (black line) and monthly average (avg), maximum (max) and minimum (min) air temperature (°C), B) weekly total (black line) and monthly total precipitation (mm), C) hourly (black line) and monthly total evapotranspiration (ET) (mm) and D) hourly average (black line) and monthly average (avg) and minimum (min) water table depth (mm) between August 2010 and July 2021. Vertical dotted lines mark calendar years.

Annual total precipitation varied between 779 and 1110 mm (average = 922 mm), with 2015/16 and 2019/20 being particularly wet (Table 4.1). Hydrological years contained, on average, 243 rain days (≥ 0.2 mm) or 148 wet days (≥ 1 mm) (CV = 5%). The most intense precipitation event across the monitoring period comprised 15 mm hr^{-1} on 23/08/2017, while

April 2011 was the driest month, with only 8 mm of rain spread across 6 days. Total annual evapotranspiration (ET) varied between 287 mm (2019/20) and 395 mm (2014/15), with an average of 345 mm (CV = 9%). The average daily ET rate was 0.9 mm day^{-1}, with a maximum rate of 4.2 mm day^{-1}. The WTD remained relatively near the surface for most of the year, with the average annual WT fluctuating at depths of between −17 and −100 mm. However, the extent of summertime water table drawdown differed considerably between years and the WTD time series is marked by an exceptionally deep draw-down event, reaching −427 mm, during the 2018 summer heatwave (Figure 4.4). While this deep drawdown resulted in a ΔS of −255 mm over the 2017/18 hydrological year, this deficit was offset by the following year with a +253 mm increase in ΔS (Table 4.1). Despite these considerable variations in water levels, annual ΔS remains relatively balanced, averaging at +1 mm over the ten monitored hydrological years (2010/11 – 2019/20) (Table 4.1).

Table 4.1. Annual average (avg), maximum (max) and minimum (min) air temperature (T), total precipitation (P), total evapotranspiration (ET), actual (P − ET) and relative (ET/P) available water, average (avg) and minimum (min) water table depth (WTD) and the storage change (ΔS) across each hydrological year (hydro year). The hydrological year is defined as beginning on the 1st October and ending on the 31st September the following year. *The dataset analysed concluded on 01/07/2021 and data for 2020/21 are therefore incomplete. **Excludes data from 2020/21 due to data deficiency.

Hydro Year	Avg T (°C)	Max T (°C)	Min T (°C)	P (mm)	ET (mm)	P − ET (mm)	ET/P	Avg WTD (mm)	Min WTD (mm)	ΔS (mm)
2010/11	7.6	28.9	-11.7	853	337	516	0.40	-37	-239	-35
2011/12	8.0	25.4	-7.2	944	345	599	0.37	-17	-142	+24
2012/13	7.1	26.2	-7.2	887	365	522	0.41	-54	-259	-119
2013/14	8.5	26.3	-4.4	895	353	542	0.39	-39	-157	+103
2014/15	7.8	27.0	-6.3	779	395	385	0.51	-36	-174	-9
2015/16	8.5	27.5	-5.5	1077	323	754	0.30	-36	-216	+4
2016/17	8.4	27.6	-4.6	992	331	661	0.33	-29	-172	+67
2017/18	8.2	27.5	-6.8	816	387	428	0.47	-100	-427	-255
2018/19	8.7	31.7	-7.0	865	331	535	0.38	-68	-276	+253
2019/20	8.4	28.2	-4.3	1110	287	823	0.26	-51	-314	-20
2020/21*	6.1	25.3	-6.4	783	182	601	0.23	-41	-233	-131
Average**	8.1	27.6	-6.5	922	345	576	0.38	-47	-238	+1

Pearson's correlation tests were applied to all annual variables, apart from those involving minimum annual air temperature (Min T) which had a non-normal distribution and therefore involved the non-parametric Kendall's tau correlation test. Significance was determined by FDR-adjusted p-values < 0.05. Higher annual average VPD was significantly related to higher energy availability (Rn − G) (p < 0.05) and a lower incidence of wet days (≥ 1.0 mm per day) in a year (p < 0.05). Total annual precipitation (P) and evapotranspiration (ET) were significantly negatively related (p < 0.05) and the available water (P − ET) appeared to be driven more by precipitation (p < 0.01) than evapotranspiration (p < 0.01). On average, deeper annual WTDs were significantly related to higher annual available energy (Rn − G) (p

< 0.05) and lower minimum WTD coincided significantly with lower average WTD (p < 0.01) (Table 4.2).

Table 4.2. Pearson's (non-italics) and Kendall's tau (*italics,* all correlations with Min T) correlation coefficients between annual radiative and hydro-meteorological variables. Yellow shading indicates FDR-adjusted p < 0.05, red shading indicates FDR-adjusted p < 0.01.

	Rn – G	PAR	Avg T	Max T	Min T	N days ≥ 25°C	VPD	P	% rain days	% wet days	ET	P – ET	Avg WTD	Min WTD
PAR	1.00													
Avg T	-0.10	-0.15												
Max T	0.45	0.63	0.41											
Min T	*0.02*	*0.06*	*0.38*	*0.11*										
N days >25°C	0.54	0.45	0.51	0.69	*0.12*									
VPD	0.84	0.76	-0.22	0.51	*-0.29*	0.34								
P	-0.51	-0.40	0.37	-0.06	*0.29*	0.26	-0.66							
% rain days	-0.66	-0.58	0.68	-0.17	*0.38*	0.02	-0.79	0.63						
% wet days	-0.69	-0.54	0.54	-0.06	*0.45*	0.06	-0.84	0.73	0.85					
ET	0.37	0.10	-0.42	-0.35	*-0.16*	-0.36	0.37	-0.85	-0.46	-0.53				
P – ET	-0.49	-0.34	0.39	0.04	*0.33*	0.29	-0.61	0.99	0.61	0.70	-0.91			
Avg WTD	-0.83	-0.75	-0.09	-0.40	*-0.07*	-0.68	-0.69	0.32	0.51	0.46	-0.27	0.32		
Min WTD	-0.78	-0.63	-0.01	-0.37	*0.02*	-0.72	-0.67	0.09	0.53	0.45	-0.04	0.08	0.92	
ΔS	-0.34	0.14	0.55	0.47	*0.20*	0.07	-0.30	0.15	0.55	0.48	-0.42	0.22	0.40	0.55

At monthly timescales, seasonally-patterned variables, such as temperature, VPD, ET, P – ET, average and minimum WTD were significantly related to energy variables (Rn – G, PAR), while precipitation was unrelated. ET was most correlated with energy variables, followed by VPD and then temperature variables (p < 0.01), and was unrelated to precipitation. Monthly P – ET appeared to be driven more by precipitation than ET. Average and minimum WTD correlated best with VPD, followed by energy variables, then maximum temperature and ET, while the change in storage (ΔS) over a month was most related to total precipitation, followed by the percentage of wet days and P – ET (Table 4.3).

Table 4.3. Kendall's tau correlation coefficients between monthly radiative and hydro-meteorological variables. Yellow shading indicates FDR-adjusted p < 0.05, red shading indicates FDR-adjusted p < 0.01. Correlations are based on monthly data from October 2010 to September 2020.

	Rn-G	PAR	Avg T	Max T	Min T	VPD	P	% rain days	% wet days	ET	P – ET	Avg WTD	Min WTD
PAR	0.97												
Avg T	0.52	0.53											
Max T	0.60	0.61	0.75										
Min T	0.42	0.44	0.76	0.58									
VPD	0.80	0.79	0.61	0.67	0.48								
P	-0.15	-0.14	-0.02	-0.07	0.04	-0.20							
% rain days	-0.44	-0.43	-0.24	-0.33	-0.16	-0.47	0.48						
% wet days	-0.27	-0.25	-0.10	-0.15	-0.02	-0.30	0.63	0.61					
ET	0.83	0.84	0.61	0.63	0.51	0.79	-0.11	-0.39	-0.21				
P – ET	-0.43	-0.42	-0.26	-0.31	-0.19	-0.48	0.71	0.59	0.61	-0.40			
Avg WTD	-0.54	-0.53	-0.48	-0.52	-0.38	-0.57	0.25	0.41	0.30	-0.50	0.44		
Min WTD	-0.61	-0.61	-0.53	-0.58	-0.43	-0.63	0.17	0.39	0.25	-0.57	0.40	0.85	
ΔS	-0.08	-0.08	0.05	0.01	0.09	-0.09	0.38	0.25	0.35	-0.05	0.35	0.02	-0.02

Average summer (JJA) temperatures ranged between 12.6 and 14.8°C (Table 4.4) and warmer summers (Avg T) were associated with a higher incidence of days recording at least 25°C (N days ≥ 25°C) (p < 0.05). While VPD and ET had significant positive correlations with available energy (Rn – G) and PAR (p < 0.01), precipitation variables (P, % rain days and % wet days) were significantly negatively related to energy terms (Rn – G and PAR) (p < 0.01) (Table 4.5). VPD was furthermore negatively related to precipitation variables and available water (P – ET) (p < 0.05) but was positively correlated with ET (p < 0.05). Wetter summers (P) were associated significantly with lower summer ET (p < 0.01), with higher summer ET being significantly related to higher VPD (p < 0.05) and a lower incidence of wet days (≥ 1.0 mm per day) (p < 0.01) across the summer. The available water (P – ET), ranging between -55 and 244 mm across the ten fully monitored summers (Table 4.4), appeared to be driven more by P than ET (p < 0.01) (Table 4.5).

Table 4.4. Summer (JJA) average (avg), maximum (max) and minimum (min) air temperature (T), total precipitation (P), total evapotranspiration (ET), actual (P – ET) and relative (ET/P) available water, average (avg) and minimum (min) water table depth (WTD) and the storage change (ΔS). *The dataset analysed concluded on 01/07/2021 and data for 2020/21 are therefore incomplete. **Excludes data from 2020/21 due to data deficiency.

Hydro year	Avg T (°C)	Max T (°C)	Min T (°C)	P (mm)	ET (mm)	P – ET (mm)	ET/P	Avg WTD (mm)	Min WTD (mm)	ΔS (mm)
2010/11	12.6	28.9	3.1	275	157	119	0.57	-42	-162	85
2011/12	12.8	25.2	2.1	296	154	142	0.52	-30	-142	17
2012/13	14.1	26.2	2.6	136	188	-53	1.39	-110	-259	-162
2013/14	13.6	26.3	3.1	184	170	14	0.92	-62	-157	-60
2014/15	13.0	27.0	0.1	186	180	5	0.97	-69	-174	-28
2015/16	13.8	27.2	4.9	219	158	61	0.72	-73	-216	-15
2016/17	13.7	27.6	4.9	327	167	160	0.51	-26	-148	94
2017/18	14.8	27.5	3.9	128	183	-55	1.43	-267	-427	-207
2018/19	14.4	31.7	3.8	230	159	71	0.69	-76	-224	13
2019/20	13.5	28.2	1.9	375	131	244	0.35	-54	-314	285
2020/21*	13.6	25.3	4.6	31	54	-24	1.76	-147	-233	-79
Average**	13.6	27.6	3.0	236	165	71	0.81	-81	-222	2

Table 4.5. Pearson's (non-italics) and Kendall's tau (italics, all correlations with Avg WTD and Min WTD) correlation coefficients between summer (JJA) radiative and hydro-meteorological variables. Yellow shading indicates FDR-adjusted $p < 0.05$, red shading indicates FDR-adjusted $p < 0.01$.

	Rn – G	PAR	Avg T	Max T	Min T	N days ≥ 25°C	VPD	P	% rain days	% wet days	ET	P – ET	Avg WTD	Min WTD
PAR	0.99													
Avg T	0.60	0.59												
Max T	0.00	-0.04	0.30											
Min T	-0.02	0.01	0.50	0.27										
N days ≥ 25°C	0.21	0.16	0.75	0.69	0.27									
VPD	0.98	0.97	0.65	0.15	0.11	0.30								
P	-0.85	-0.87	-0.49	0.17	0.01	-0.03	-0.81							
% rain days	-0.92	-0.93	-0.67	-0.02	-0.13	-0.29	-0.92	0.71						
% wet days	-0.96	-0.94	-0.55	0.12	0.15	-0.15	-0.90	0.89	0.80					
ET	0.84	0.88	0.36	-0.29	-0.01	-0.16	0.81	-0.86	-0.71	-0.84				
P – ET	-0.87	-0.89	-0.47	0.19	0.01	0.00	-0.83	1.00	0.73	0.90	-0.90			
Avg WTD	*-0.60*	*-0.56*	*-0.60*	*-0.02*	*-0.07*	*-0.44*	*-0.60*	*0.60*	*0.58*	*0.52*	*-0.47*	*0.64*		
Min WTD	*-0.38*	*-0.33*	*-0.47*	*-0.24*	*-0.02*	*-0.63*	*-0.38*	*0.29*	*0.36*	*0.30*	*-0.24*	*0.33*	*0.69*	
ΔS	-0.77	-0.79	-0.49	0.29	-0.13	0.03	-0.74	0.94	0.61	0.83	-0.89	0.95	*0.59*	*0.24*

Average summer WTDs ranged between -267 and -26 mm, while the deepest summer WTD recorded -427 mm in summer 2018 (Table 4.4). Like their annual equivalents and despite

considerable variation between years, average summer ΔS was relatively balanced, with a mean of 2 mm over the ten fully monitored hydrological years (2010/11 – 2019/20) (Table 4.4). Lower average summer WTDs were significantly related to higher available energy (Rn – G) and summer air temperatures ($p < 0.05$), and lower summer precipitation and incidence of rain days (% rain days) ($p < 0.05$), particularly lower water availability (P – ET) ($p < 0.05$) (Table 4.5). Similarly, the change in storage (ΔS) across the summer was most related to summer water availability (P – ET) ($p < 0.01$), followed by summer precipitation (P) and ET ($p < 0.01$), and % wet days, PAR, Rn – G and VPD ($p < 0.05$) (Table 4.5). The largest summer water table drawdown (Min WTD) correlated with the summer average WTD ($p < 0.05$) and was significantly associated with the incidence of days recording at least 25°C ($p < 0.05$) (Table 4.5).

4.3.3   Water balance

Runoff data were recorded using a waterproof pressure transducer inside a dipwell, placed directly upstream from the Eller Beck v-notch weir, and spanned the period 14/03/2017 – 01/07/2021 (Figure 4.5). The availability of the runoff series facilitated calculations to close the water balance for the Eller Beck catchment for that period. The water balance equation for an ombrotrophic blanket bog assumes that precipitation equals the water losses though runoff, evapotranspiration and change in storage. Rearranging the water balance equation (P − ET − R − ΔS = ε) allows the quantification of residuals (ε), with positive residuals representing a greater net unaccounted water loss, including measurement uncertainty, within the water balance calculation.

Annual residuals, ε, for the three complete hydrological years amounted to +450 mm in 2017/18, +70 mm in 2018/19 and +285 mm in 2019/20, with monthly averages of +32 mm in 2017/18, +3 mm in 2018/19 and +22 mm in 2019/20 (Table 4.6), implying that inputs exceeded outputs and storage change for most of the year. Residuals were positive in 77.8% of the months across the hydrological years 2017/18, 2018/19 and 2019/20. Negative residuals, ε, occurred mainly in summer, specifically in June, July and September 2017, July, September and October 2018, April, June, July and September 2019 and June 2020. Exceptionally high, negative residuals occurred in October 2018 (−166 mm) and June 2020 (−223), while particularly high, positive residuals were observed in June 2018 (+101 mm) and May 2020 (+126 mm). Kendall's correlation tests revealed that monthly residuals were unrelated to precipitation inputs ($\tau = -0.14$, $p = 0.1437$), ET losses ($\tau = -0.12$, $p = 0.1966$) and

available water, P – ET, ($\tau = -0.05$, $p = 0.5863$), but increased significantly with more negative ΔS, i.e., net water table drawdown ($\tau = -0.53$, $p < 0.001$).
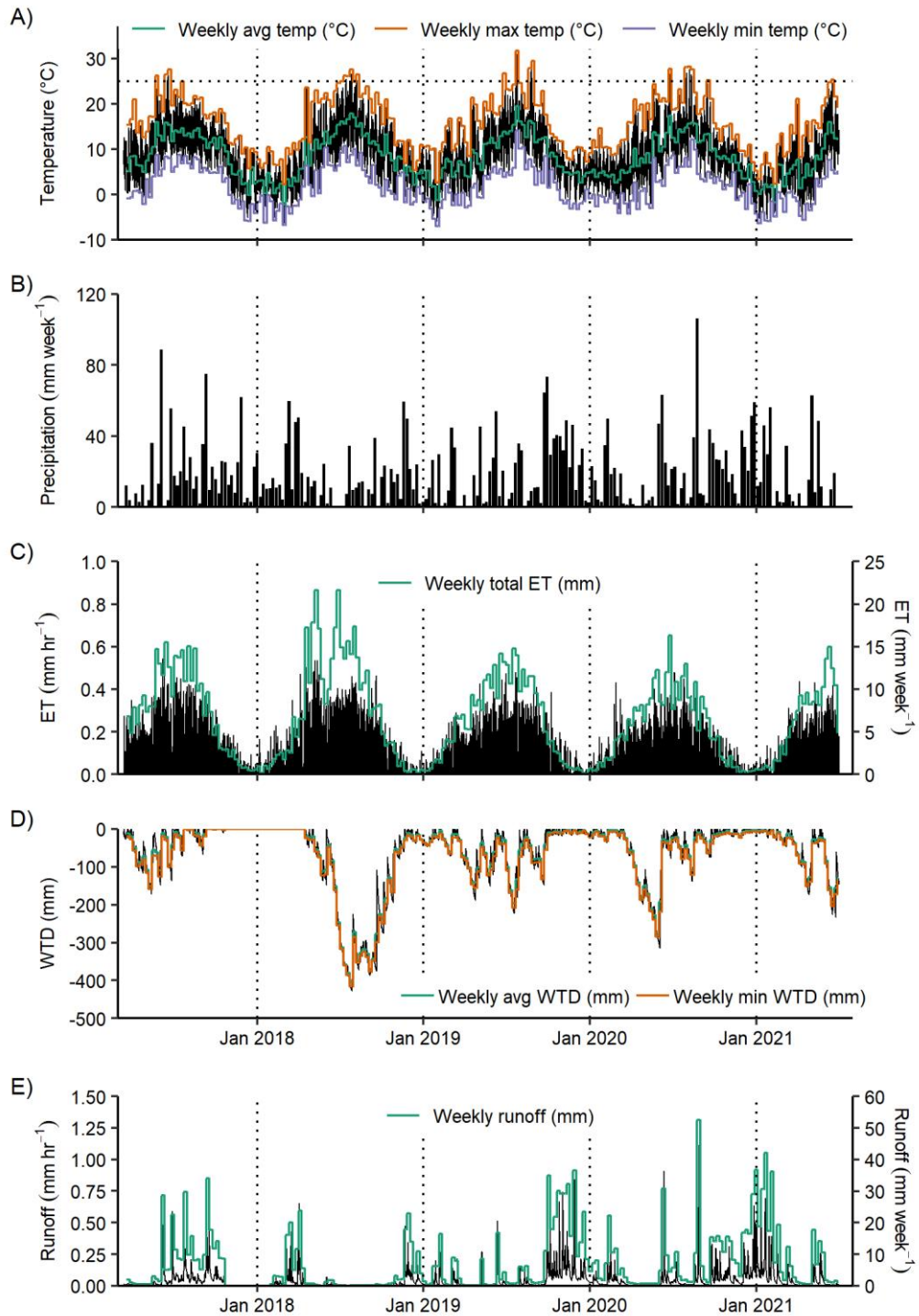
Figure 4.5. A) Hourly average (black line) and weekly average (avg), maximum (max) and minimum (min) air temperature (°C), B) weekly precipitation (mm), C) hourly (black line) and weekly total evapotranspiration (ET), D) hourly average (black line) and weekly average (avg) and minimum (min) water table depth (WTD) (mm) and E) hourly (black line) and weekly total runoff (mm) (includes data gap of winter 2017/18). Vertical dotted lines mark calendar years and the horizontal dotted line in A) marks the 25°C threshold.

Table 4.6. Water balance components and residuals for 2017/18, 2018/19 and 2019/20. Summer (JJA) data are shown in brackets.

Water year	P (mm)	ET (mm)	R (mm)	ΔS (mm)	Residual (mm)	Monthly average residual ± SD (mm)
2017/18	816 (128)	387 (183)	233 (6)	-255 (-207)	+450 (+123)	+32 ± 53 (+37 ± 83)
2018/19	865 (230)	331 (159)	211 (47)	+253 (+13)	+70 (+34)	+3 ± 62 (+6 ± 36)
2019/20	1110 (375)	287 (131)	558 (140)	-20 (+285)	+285 (-91)	+22 ± 84 (-62 ± 140)
Average	930 (245)	335 (158)	371 (34)	-7 (+31)	+268 (+22)	+19 ± 67 (-6 ± 94)

As is characteristic for an ombrotrophic bog, the water budget of May Moss is driven by precipitation, with peaks in runoff closely coupled with periods of intense precipitation (Figure 4.5). Among the three complete hydrological years, 2017/18 experienced the lowest precipitation inputs and highest ET losses, while the opposite was observed for 2019/20. Runoff was lowest in 2018/19 and highest in 2019/20, along with precipitation (Table 4.6). Similarly, summer 2018 had the lowest precipitation and highest ET, with the reverse in summer 2020. Runoff was exceptionally low in summer 2018 and greatest in summer 2020 (Table 4.6). Water losses were thus dominated by ET in 2017/18 and 2018/19 and by runoff in 2019/20 (Table 4.6). Average ΔS for the three hydrological years was -7 mm (Table 4.6), highlighting that, despite the 2018 heatwave, the bog remained near balanced.

On monthly timescales, the relative dominance between ET and runoff was nearly balanced, with runoff dominating in 17 out of the 36 months (47.2%), primarily in autumn and winter, and ET dominating in 19 months (52.8%), mainly in spring and summer (Figure 4.6). Water deficits (P − ET < 0) occurred in 8 out of 36 months (22.2%) over the three complete hydrological years, specifically in May − August 2018, April and August 2019, and April and May 2020. Positive or neutral ΔS (≥ 0) were observed in 20 out of the 36 months (56%) (Figure 4.6), highlighting that water levels were recharging or at surface level for most of the year.
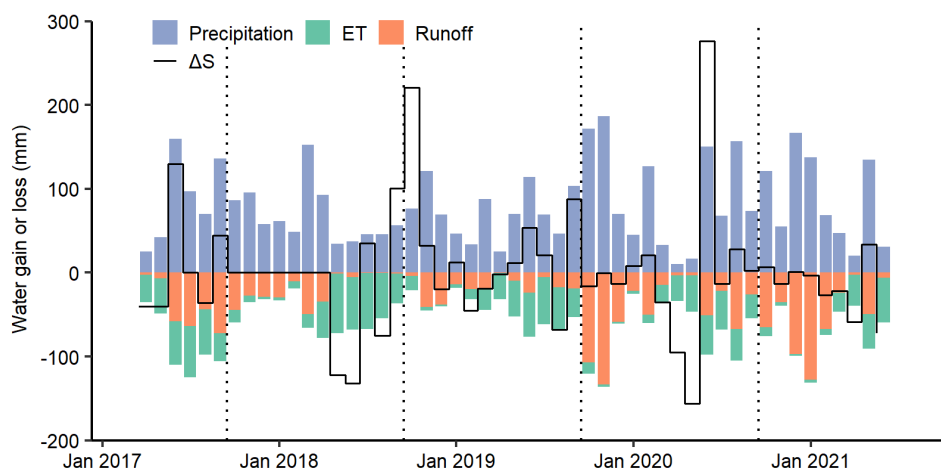
Figure 4.6. Monthly water balance terms between March 2017 and June 2021. Positive values denote water gain and negative values signify water losses. Dotted lines mark hydrological years.

4.3.4   The 2018 heatwave

The maximum daily temperature threshold defining a heatwave varies between counties in the UK, although in all counties this temperature threshold must be met or exceeded for at least three consecutive days to be classed as a heatwave (McCarthy et al., 2019a). Across the 1961 – 2020 temperature record obtained from Silpho Moor, Fylingdales and May Moss, the incidence of days with a maximum air temperature at or exceeding the North Yorkshire temperature threshold of 25°C (McCarthy et al., 2019a) has generally increased, particularly within the last decade. The incidence of heatwaves is sporadic between 1961 and 2016, occurring every six to ten years, followed by a period with successive annual heatwaves in the summers of 2017, 2018, 2019 and 2020 (Figure 4.7).

The summer of 2018 was the warmest (average summer air temperature) and driest (total summer precipitation) among the monitored years (2011 – 2020) with an average air temperature of 14.8°C, a total of 128 mm of rain across June, July and August, and evaporative losses amounting to 183 mm, above the summer average of 165 mm observed over the monitoring period (2011 – 2020). Across the 1961 – 2020 series, the summer of 2018 was the fifth driest and warmest (average summer air temperature), and the driest summer since 1995 and the warmest since 1983 (Figure 4.7).
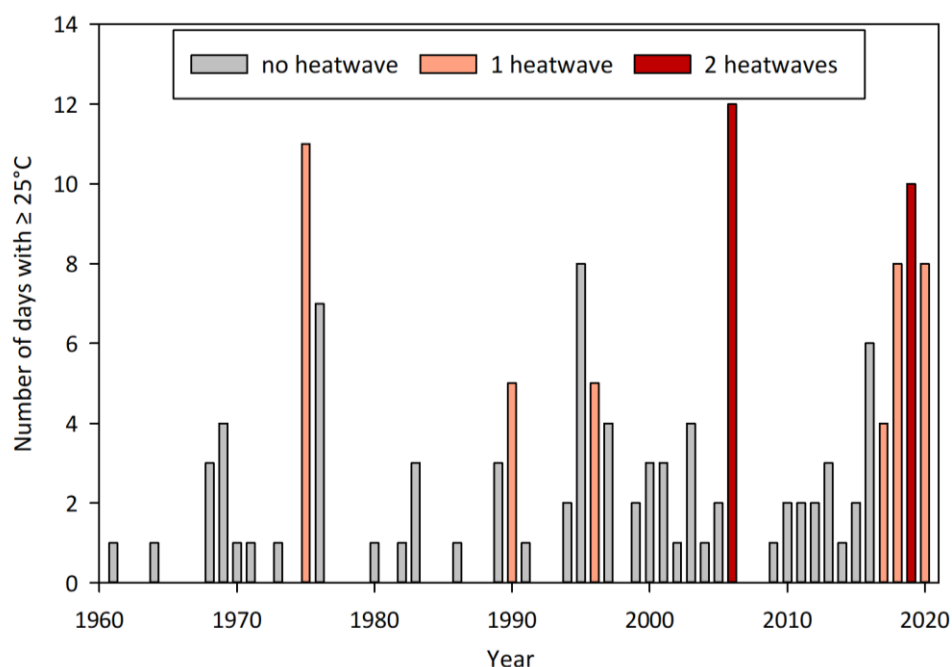
Figure 4.7. Number of days in a year recording a maximum air temperature of at least 25°C and occurrence of heatwaves in those years. Data based on daily maximum air temperature records obtained from the Silpho Moor (01/01/1961 – 31/12/1983), Fylingdales (01/01/1984 – 19/08/2010) and May Moss (20/08/2010 – 31/12/2020) meteorological stations.

At the May Moss meteorological station, the summer 2018 heatwave culminated in the deepest water table drawdown over the monitoring period, reaching a minimum WTD of −427 mm on 27/07/2018 21:00 (Table 4.4). The 40 days preceding this date experienced a total of only 10 mm of rain. June 2018 had only 9 rainy days, compared with the average of 20 rainy days per month over the monitoring period and an average of 18 rainy days for the month of June (2011 – 2021). June 2018 was thus the joint second driest month across the entire monitoring period.

The onset of the 2018 heatwave reveals the micrometeorological conditions that typically drive water table draw-down. The last substantial summer rainfall in 2018 (4.8 mm) was on the 16/06/2018, with an isolated precipitation event (7.2 mm) on 17/07/2018. The week commencing 16/06/2018, early in the dry spell, contains four types of micrometeorological behaviours governing ET (Figure 4.8).

1) Precipitation on 16/06/2018 reduced the VPD gradient limiting ET and producing a brief water table recharge.

2) Overcast conditions (relatively low net radiation, Rn) on the 16th, 17th and 20th June with low VPD limited ET losses.

3) Conversely, clear sunny conditions on the 18th, 19th, 21st and 22nd June facilitating prolonged and higher ET rates.

4) Lower net radiation and vertical wind speeds in morning and evening of the 19th appear to limit ET.

In summary, over these day-to-week timescales it is warm, dry conditions with negative VPD indicating lower atmospheric saturation with distance from the surface that drives greater ET. ET is also greatest when the vertical wind speed indicates steeper gradient in wind speed with distance from the surface. Higher wind speeds transport more water vapour away, thus increasing the VPD gradient and driving more ET. Thus, a combination of conditions with a strongly negative VPD gradient and high vertical wind speeds are conducive to rapid transport of water vapour away from the peatland.
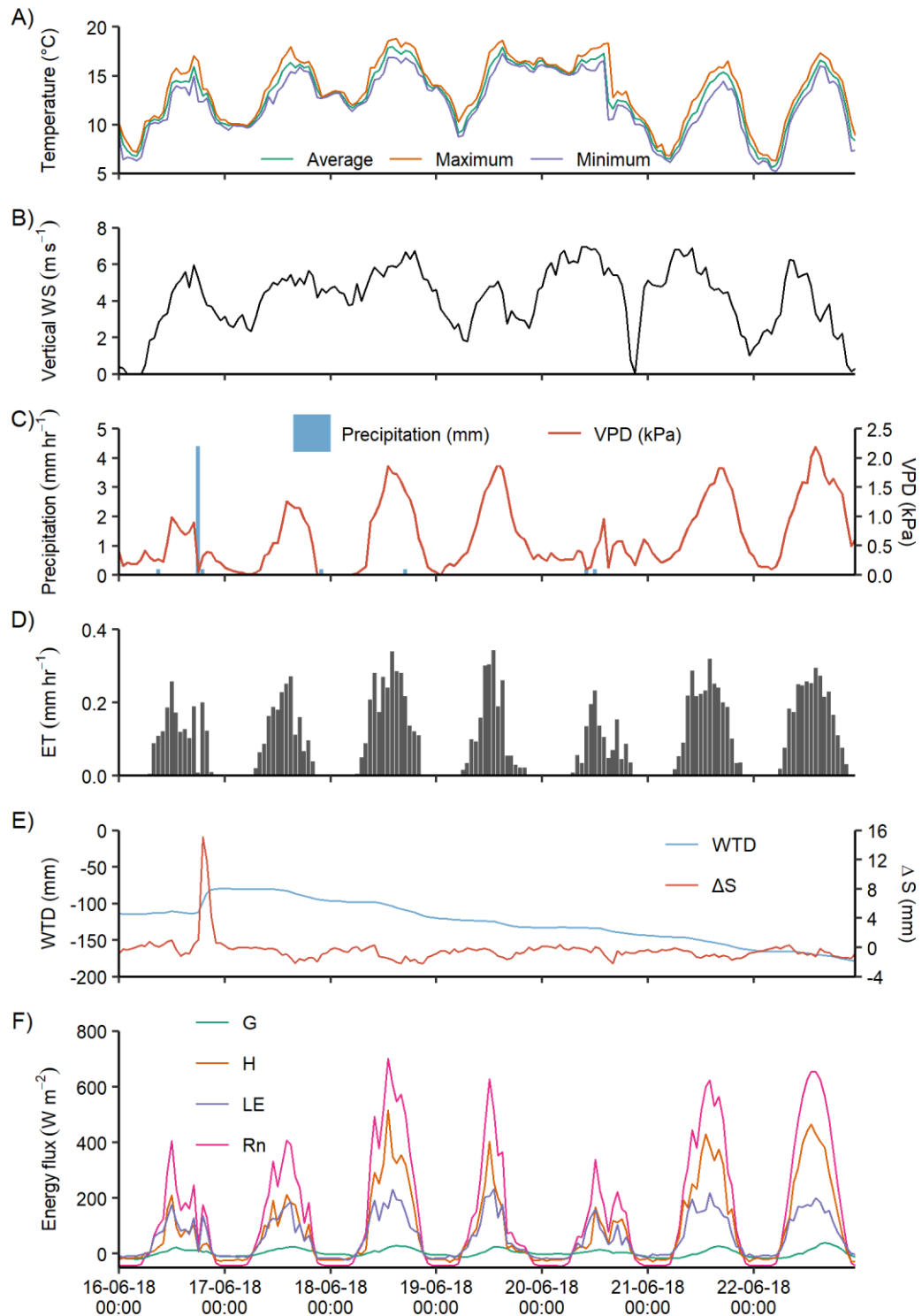
Figure 4.8. Hourly boundary layer functioning between 16/06/2018 00:00 and 22/06/2018 23:00, at the onset of the dry period. A) Average, maximum and minimum air temperature (°C), B) vertical wind speed (WS) (m s^{-1}) between 3.0 m and 0.4 m, C) precipitation (mm) and vapour pressure deficit (VPD) (kPa), D) evapotranspiration (ET) (mm), E) water table depth (WTD) (mm) and change in storage (ΔS), and F) the energy balance components, consisting of soil heat flux (G), sensible heat flux (H), latent heat flux (LE) and net radiation (Rn) (W m^{-2}).

Marked changes in water storage (ΔS) were observed over the recovery period following the 2018 heatwave and water deficit, particularly between June (ΔS = -132 mm) and July (ΔS = +35 mm) and from August (ΔS = -75 mm) to September (ΔS = +101 mm) and October (ΔS = +221 mm) (Figure 4.6). The positive change in monthly storage between June and July 2018 (+167 mm) was most likely the result of heavy rainfall during the last week of July, recording 38.2 mm over the course of seven days (24th – 30th July) (Figure 4.5), which made up 83% of total precipitation inputs that month. While ET losses were high in July 2018 (67 mm), low runoff (0.6 mm) losses in conjunction with high precipitation at the end of the month facilitated the rapid rise in water levels and positive storage change (Figure 4.6). However, in August rainfall inputs (46 mm) fell short of ET losses (54 mm) again, which likely drove further storage deficits (-75 mm) that month. Subsequent rises in rainfall (57 and 76 mm) and reductions in ET (35 and 17 mm) consequently led to the recovery of water levels through September (+101 mm) and October (+221 mm) (Figure 4.6). It took approximately 14 weeks for average weekly water levels to recover from their lowest stage to be within 10 cm of the surface, and a further 3 weeks to reach 5 cm below the surface (Figure 4.5).

4.4 Discussion

4.4.1 The hydroclimate of May Moss

4.4.1.1 Temperature

The annual air temperature at May Moss is cool, with an average of 8.6°C (2010/11 – 2019/20). Compared to the historical reference temperature from 1961 – 1990, based on records from the nearby Silpho Moor and Fylingdales meteorological stations, the latest decade (2011 – 2020) is, on average, 0.3°C warmer, driven by a 0.6°C warming of average winter temperatures. The average temperature warming at May Moss is slightly less than the UK-wide average warming of 0.9°C between the 1961 – 1990 reference and the 2010 – 2019 decade (Kendon et al., 2020). However, the increase in average winter temperatures at May Moss corroborates the more pronounced winter warming at an upland peatland meteorological station at Moor House, northern England, observed through a 23% reduction in days with air frost from 1991–2006 relative to 1953–1980, compared to summer warming and nearby lowland temperature records from Durham (Holden and Rose, 2011). Winter warming at May Moss is furthermore reflective of the UK-wide 16% reduction in days with ground frost in the 2010 – 2019 decade compared with the 1961 – 1990 reference (Kendon et al., 2020).

4.4.1.2 Precipitation

Based on ten years of micro-meteorological data (2010/11 – 2019/20), the hydroclimate of May Moss, with an average of 922 mm (779 – 1110 mm) of annual precipitation, is relatively dry for an ombrotrophic blanket mire, most likely due to the "rain shadow" barrier formed by the Pennines (Wheeler, 2013). Blanket bogs typically require at least 1000 mm of annual precipitation for their development (Lindsay et al., 1988). For example, Moor House (North Pennines, UK) receives between 1345 and 3372 mm of precipitation in a year (Holden and Burt, 2002a). In Ireland, annual precipitation ranges between 1313 and 1999 mm across blanket bogs in the Garron, Letterunshin and Cuilcagh catchments (Flynn et al., 2021b) and between 2423 and 2776 mm (2002/03 – 2006/07) in an Atlantic blanket bog near Glencar, Co. Kerry (Sottocornola and Kiely, 2010). Total annual precipitation, though important, has been argued to be equally or less crucial than the annual distribution of precipitation for the development of blanket bogs and the retainment of a near surface water table (Lindsay et al., 1988; Evans et al., 1999). In this respect, the precipitation distribution across a year at May Moss, with an average of 243 rain days (≥ 0.2 mm per day) and 148 wet days (≥ 1.0 mm per day), is comparable to Moor House, where an average of 247 precipitation days have been noted (Holden and Burt, 2002a) and to blanket bogs in Ireland, with 238 – 259 rain days (> 0.2 mm per day) and 191 – 218 wet days (> 1.0 mm per day) (Flynn et al., 2021b).

In the UK, the decade of 2010 – 2019 was, on average, 5% wetter than the 1961 – 1990 UK reference period, with summers being 13% wetter and winters being 12% wetter (Kendon et al., 2020). This is similarly reflected at May Moss, with the latest decade (2011-2020) being 3% wetter than the 1961 – 1990 reference (Silpho Moor and Fylingdales records) and summer rainfall having increased 17% between the two time periods. Conversely to the UK average, winters at May Moss have become drier, with a 9% reduction in precipitation between 1961 – 1990 and 2011 – 2020. Annual precipitation amounts in the north-east of England and Yorkshire are influenced by the "rain shadow" effect due to Pennines forming a meteorological barrier from prevailing westerlies (Wheeler, 2013). Similarly, Fowler and Kilsby (2002b) have noted higher winter precipitation in eastern parts of the North York Moors, compared to more western areas of Yorkshire, associated with a negative North Atlantic Oscillation (NAO). A negative NAO is typically associated with weaker than usual differences in pressure and drier winters in Europe (Hurrell et al., 2003), but allows for relatively stronger easterlies and northerlies in bringing rainfall to the east coast of the UK (Wheeler, 2013). The reduction in winter precipitation at May Moss may thus be related to a relative strengthening of NOA between the two time periods compared and reinforces the

uncertainty surrounding future precipitation regimes in the UK uplands (Murphy et al., 2019).

4.4.1.3 Evapotranspiration

Over the ten hydrological years monitored (2010/11 – 2019/20), the average daily ET rate at May Moss meteorological station was 0.9 mm day^{-1}, with a maximum rate of 4.2 mm day^{-1} recorded. This resembles rates of 0.3 – 4.5 mm day^{-1} recorded at a blanket bog in Newfoundland, Canada (Price, 1992b) and rates of 0.1 – 0.5 mm day^{-1} on a typical day, with 4 – 5 mm day^{-1} common in summer, at a shrub-covered bog in south-eastern Ontario, Canada (Lafleur et al., 2005). Likewise, Sottocornola and Kiely (2010) recorded ET rates of 0.1 – 3.0 mm day^{-1} at an Atlantic blanket bog in Co. Kerry, Ireland, and Worrall et al. (2015) observed a median ET rate of 1.6 mm day^{-1}, with an interquartile range of 0.8 – 2.8 mm day^{-1}, at Moor House, UK.

Annual ET at May Moss ranged between 287 and 395 mm yr^{-1} (average = 345 mm; CV = 9%), which overlaps estimates at an Atlantic blanket bog in the southwest of Ireland (369 – 424 mm) (Sottocornola and Kiely, 2010) and is considerably lower than at a shrub-covered bog in south-eastern Ontario, Canada (414 – 458 mm) (Brümmer et al., 2012). Unlike the findings by Lafleur et al. (2005), higher annual ET losses at May Moss were significantly related to lower annual precipitation (Table 4.2). Although at shorter monthly timescales, we observed no significant correlation between ET and P at May Moss, similar to the findings by Lafleur et al. (2005) on a seasonal timescale. This may reflect a closer coupling between precipitation and ET in a more humid oceanic climate, such as at May Moss, as opposed to a continental climate (e.g., SE Ontario). Over the shorter monthly timescales, higher available energy (Rn – G), PAR, VPD and temperature appeared to be more closely coupled to ET losses. Precipitation and VPD were significantly, negatively related over monthly timescales and particularly in summer (Table 4.3 and Table 4.5). Rainfall events cause water vapour concentrations in air to reach saturation (Oke, 1987; Price, 1991), resulting in a reduced or negligible VPD gradient which limits ET to negligible rates (Price, 1991; Allen et al., 1998; Kellner, 2001; Wang et al., 2020), thus years experiencing higher than average precipitation are likely to be associated with a reduction in ET.

Summer (JJA) ET at May Moss was slightly more variable (CV = 10%) than annual ET and made up 45 – 52% of annual totals. Growing season (April – September) ET made up 79 – 86% of annual ET at May Moss, more than at an Atlantic blanket bog in southwest Ireland (64 – 71%) (Sottocornola and Kiely, 2010). Higher summer ET was highly correlated with available

energy (Rn – G) and PAR (Table 4.5), reflective of the stark contrast in available energy (Rn – G) in summer compared to the rest of the year which drives ET (Kellner, 2001). Higher ET was also significantly related to lower summer precipitation, the proportion of wet days and higher VPD (Table 4.5), suggesting that a lower incidence and sum of rainfall with a related increase in VPD gradients could facilitate higher ET losses on a seasonal scale in summer.

4.4.1.4   *Available water and storage change*

The available water (P – ET) varied considerably between years (385 – 823 mm; average = 576 mm) and was driven more by the precipitation gains than ET losses across all analysed timescales (Table 4.2, Table 4.3, Table 4.5). The ET/P ratio, with higher ratios signifying greater water stress, was generally about twice, though in two instances (2012/13 and 2017/18) it was three times as high in summer compared to the annual average. Annual (0.26 – 0.51) and summer (0.35 – 1.43) ET/P ratios were considerably higher and more variable than ET/P ratios measured at an Atlantic blanket bog in Co. Kerry, Ireland, with annual ranges of 0.14 – 0.17 and summer ranges of 0.23 – 0.30 (Sottocornola and Kiely, 2010), but resemble the average growing season ET/P of 0.82 at a bog in south-eastern Ontario, Canada (Lafleur et al., 2005).

The decade of hydrometeorological monitoring (2010/11 – 2019/20) saw annual ΔS fluctuating between -255 mm and +253 mm (Table 4.1). Despite considerable variations in water levels over the monitoring period, annual ΔS remained relatively balanced, averaging at +1 mm (Table 4.1). ΔS reflects the net inputs and outputs of the water balance equation, with ΔS = zero signifying a system in hydrological equilibrium where inputs equal outputs. As average annual ΔS = +1 mm, we can infer that the centre of the blanket bog May Moss is hydrologically balanced over the ten-year period, despite being situated within a relatively dry area in the North York Moors, with mean annual P < 1000 mm, and subject to at least one severe drawdown event within the monitoring period (summer 2018). This state of equilibrium could thus reflect a hydrological resilience of May Moss, as commonly found with intact peatlands, in response to short-term impacts, such as drought (Page and Baird, 2016).

4.4.2   Water balance

4.4.2.1   *Water balance residuals*

Multi-year studies on blanket bog hydrology which measure all components of the water balance over entire years are scarce. Here, we quantify annual water balance components (P, ET, R and ΔS) and residuals (ε) for 2017/18, 2018/19 and 2019/20. While precipitation (P),

evapotranspiration (ET) and water storage change (ΔS) were measured at the May Moss meteorological station, situated on the intact, low-relief open bog, near the Eller Beck catchment watershed, runoff (R) was based on discharge measurements of the Eller Beck, where the stream exits the area of deep peat (Figure 1.4). Water balance estimates therefore do not account for spatial variability across the bog but should capture net lateral flows lost by runoff. The location of estimates near the watershed thus facilitates a characterisation of water level behaviour in response to precipitation gains, ET and runoff losses, without the supplementing influence of incoming lateral flow.

The water balance of May Moss comprised, on average, 930 mm of P inputs, 335 mm of ET losses, 371 mm of R losses and a ΔS of −7 mm, with the annual residual averaging at +268 mm. Annual and monthly residuals (ε) tended to be positive, initially implying that inputs exceeded outputs and storage change for most of the year, and water budgets were therefore generally positive, as is necessary for the continued development of an active mire (Lindsay, 1995). However, as well as incorporating unmeasured terms, residuals also contain the net sum of all errors in the measured components of the water balance (Kondolf and Matthews, 1991). Unmeasured terms could take the form of unknown outflows, such as peat pipes (Holden and Burt, 2002c; Holden, 2005a) discharging beyond the weir site. Error in the water balance terms reflects measurement uncertainty among the terms themselves and the contributory sensor measurements, particularly for ET (Isabelle et al., 2018).

An underestimation of ET could stem from an underestimation of night-time ET, when a high proportion of Bowen ratios are rejected (*Chapter 3*) (Perez et al., 1999), although others have noted that night-time ET from ombrotrophic peats is largely negligible (Campbell and Williamson, 1997; Thompson et al., 1999; Shuttleworth, 2007). In addition, soil moisture and surface water storage were not measured as part of this study, so direct evaporation from the bog surface and open water pools is not known. A study by Watras et al. (2017) found that evaporation from a 0.6 ha bog pool was 20% higher than the surrounding open bog in Wisconsin, USA. While no such sizeable pools occur on May Moss, the cumulative effect of multiple small bog pools could have led to considerable underestimation of ET. The difference of 20% noted by Watras et al. (2017) would be within the 20 − 30% uncertainty range noted by Kellner and Halldin (2002) for ET estimates based on the BREB method.

The significant negative correlation between residuals and ΔS implied that greater unaccounted losses coincided with net water table drawdown. This suggests that peat moisture loss could have explained a proportion of the higher residuals related to greater

water table drawdown. Change in peat water storage comprises both the water lost or gained through water table fluctuations as well as the reduction or increase in peat moisture (McCarter and Price, 2013). Within the shallow peat layer below hollows, peat water content was found to reduce from complete saturation (100%) to 55% when water levels dropped to around 20 cm below the surface at a *Sphagnum* bog in central Sweden (Kellner and Halldin, 2002). Thus, storage change, associated with variations in peat moisture, could also have explained a considerable proportion of water balance residuals.

An underestimation of runoff could have resulted from, for example, unaccounted losses to the bedrock subsurface from beneath the stream bed or through the slow loss from peat to deeper subsurface layers. Upland blanket mire streams have a notoriously "flashy" runoff regime, particularly following high intensity rainfall events (Holden and Burt, 2003b). As our runoff estimates are based on hourly timesteps, the most likely source of runoff residuals would therefore be the under-capturing of peak runoff under high flow conditions from the site.

In a study on unmeasured residuals in sediment budgets, Kondolf and Matthews (1991) highlight that residuals not only incorporate unmeasured terms but also the net sum of errors in the measured components. Kellner and Halldin (2002) estimate that water balance components may be subject to errors of 5% for precipitation, 20% for runoff and 30% for ET using the BREB technique. When applying these error estimates to our annual water balance estimates (P – ET – R) we derive uncertainty ranges for ΔS + ε, ranging -8 to 400 mm for 2017/18, 138 to 508 mm for 2018/19, 12 to 518 mm for 2019/20 and 3 to 445 mm for the average of the three years. The annual sums of ΔS + ε are 195 mm (2017/18), 323 mm (2018/19), 265 mm (2019/20), with the average derived for the three years being 261 mm. The sums of ΔS + ε therefore lie within the error ranges derived from the water balance estimates. Residuals in the May Moss water balances are thus most likely the result of measurement error, such as an underestimation of runoff, particularly of peak flow, evaporation of surface waters and changes in peat moisture.

4.4.2.2   Water balance variability

The intra-annual water balance tended to be characterised by a wet autumn and winter, with moisture surpluses (P – ET > 0) occurring in all years between September and March, while moisture deficits (P – ET < 0) were observed mainly, though not continuously, between April and August. The relative dominance of ET and R as hydrological losses from May Moss likewise varied seasonally, with the bog being more evaporative in summer due to higher

temperatures and longer daylight hours than during the autumn and winter months, in which baseflow is naturally higher and high runoff events occur more frequently (Evans et al., 1999; Holden and Burt, 2003b).

Summer water balances were variable, with deficits (P – ET) occurring in all summer months in 2018 and only slightly in August 2019, while 2020 lacked a deficit among the summer months. The variable nature of the summer water deficits thus appeared to characterise the water budget for the entire summer, with a severe loss in storage (ΔS) in summer 2018 (-207 mm), a small storage gain in summer 2019 (+13 mm) and a large storage gain in summer 2020 (+285 mm). Summer storage changes at May Moss thus showed considerably more variability than at an intact *Sphagnum* bog in central Sweden, where Kellner and Halldin, (2002) quantified negative water budgets of −99 mm and −50 mm for the growing seasons (24 May – 4 October) in 1996 and 1997, respectively.

The year 2017/18 was characterised by the summer 2018 drought and thus, unsurprisingly, had a negative annual ΔS of −255 mm and a summer ΔS of −207, highlighting a net loss of water from the bog, and accompanied by low precipitation and runoff, particularly in summer, and high ET. In addition, 2017/18 contained the largest residual (+450 mm) among the three years. Besides relating to measurement uncertainty or unknown outflows, the residual term may have also been related to exacerbated compression of the surface peat related to prolonged dry conditions and a reduction in summer water level (Kellner and Halldin, 2002; Bourgault et al., 2017). Kellner and Halldin (2002) found that changes in the water level only accounted for 60% of storage change, with the remaining 40% explained the swelling or shrinking due to "mire breathing". The following year (2018/19) had a positive storage change of +253 mm, suggesting a full recovery of the water table a year after an exceptionally dry summer relative to the water level at the start of the previous year (2017/18), and may highlight a relative resilience of intact bogs to seasonal droughts.

4.4.3 Hydro-meteorological influences on water table depth

Annual water tables were highly variable, but remained relatively shallow for most of the year, with annual average WTD ranging between −17 and −100 mm, similar to the average WTD reported for Moor House, where the WT remained within −50 mm 93% of the year (Evans et al., 1999). The scarcity of multi-year studies on bog hydrology which incorporate and directly quantify all components of the water balance, as well as other hydroclimate variables, has arguable limited our understanding of key drivers of WTD processes. While the average annual WTD appeared to be significantly related only with the average available

energy (Rn − G) (p < 0.05), analysis of correlations at monthly timescales reveals greater coupling between average WTD and VPD (p < 0.01), followed by the available energy (Rn − G) and PAR, reflective of the high correlations between VPD and Rn − G and PAR (p < 0.01). The considerable influence of VPD on WTD by driving ET losses has been observed by others (Price, 1991; Wang et al., 2020).

The extent of water table drawdown, here expressed as the minimum WTD, appears to be mainly a function of energy availability and VPD over annual and monthly timescales. Crucially, however, the magnitude of drawdown in summer is coupled with the incidence of days with a maximum temperature of at least 25°C – the temperature threshold which determines a heatwave in the region if maintained for at least three consecutive days. A higher incidence of days reaching 25°C is not necessarily reflective of overall higher summer energy or temperature or lower rainfall regimes but would likely cause a period of rapid evapotranspiration which could dramatically lower WTD. Indeed, total ET losses across June and July 2018 were 16 mm higher than the average sum for those months based on data between 2011 and 2020. This is reminiscent of Evans et al. (1999), who suggest a WTD threshold, at which point WTD becomes solely controlled by evaporation. The relationship thus suggests that the number of highly evaporative days in summer is a critical determinant for exceptionally deep seasonal WT drawdown.

The change in storage (ΔS), characterising the trend in WTD through a water balance deficit or surplus, was influenced slightly by precipitation over short-term monthly scales. However, across the summer, ΔS was strongly linked to water availability (P − ET) (p < 0.01), more so than with precipitation (p < 0.01) or ET (p < 0.01) alone, corroborating the analysis by Charman (2007) who found that summer water table variability is highly correlated with summer moisture deficit (P − ET), which in turn is driven by temperature in mid-latitude oceanic peatlands.

4.4.4 The 2018 heatwave and implications of climate change

The 2018 summer heatwave in the UK was the combined result of dominant anticyclonic circulation and high sea surface temperatures near the UK, culminating in the joint warmest summer on record since 1884 and resulting in widespread drought in the UK (McCarthy et al., 2019b; Turner et al., 2021). The summer of 2018 was a noteworthy event during the monitoring period as it was characterised by the deepest water table drawdown (−427 mm on 27/07/2018) observed among the ten summers monitored. Evans et al., (1999) reported a similar extreme WT drop of −420 mm at Moor House (central northern England) during the

1995 summer drought. Extreme water storage loss as seen in summer 2018 were not isolated events over the monitoring period, with even greater storage losses observed between March and May 2020 (ΔS = −295 mm). It is possible that summer 2020 would have seen a similar extreme WT drawdown event, if a large water surplus (P − ET) had not occurred in between June and August 2020 (+244 mm), with 151 mm of rainfall that month – four times the rainfall in June 2018. In addition, summer 2018 had considerably higher average temperatures, available energy (Rn − G), PAR and VPD (Table 4.4) which drove higher seasonal ET losses, resulting in a P − ET water deficit (Table 4.5) and consequently the severe negative ΔS. The relatively high incidence of warm evaporative days, here determined using incidences exceeding the daily 25°C threshold, was possibly the cause driving a WT drawdown that culminated at −427 mm depth.

Climate change has been predicted to increase the variability of the summer climate in Europe and increase the frequency of summer heatwaves (Seneviratne et al., 2006), with annual mean temperatures in the UK already shown to increase at a faster rate relative to the global mean (Kennedy-Asser et al., 2021). Peatlands can be surprisingly resilient to short-term meteorological events by regulating the water level relative to the surface by the process of "mire breathing" (Kellner and Halldin, 2002; Dise, 2009). We observed a complete offset in ΔS at May Moss in the year following the 2018 summer heatwave, demonstrating the resilience of an intact mire to mild drought (Dise, 2009; Page and Baird, 2016). In addition, the dominance of positive water balance residuals (ε) indicate that inputs exceed losses through outflows and storage change, implying that the mire has a predominantly positive water balance, as is necessary for the continued development of an active mire (Lindsay, 1995).

An increased frequency of summer heatwaves and drought (Seneviratne et al., 2006) has been associated with lower summer moisture availability and reduced carbon accumulation in mires (Charman et al., 2013), despite climatic warming potentially increasing net productivity and plant-derived soil carbon (Davidson and Janssens, 2006). From their simulation experiment on peat decomposition under a warming climate, Ise et al. (2008) highlight that a 4°C increase in temperature could result in 86% soil organic carbon loss from deep peat and conclude that peatlands will respond quickly to projected warming by losing labile organic carbon during dry periods. This corroborates Worrall et al. (2007) who suggest increased export of carbon from the UK uplands may be related to changes in rainfall and temperature regimes. The negative trend in local winter (−9%) and spring (−11%) precipitation between 1961 − 1990 and 2011 − 2020 could suggest that climatic warming

may hamper the full recharge in water storage generally observed in upland blanket mires over the winter months (Evans et al., 1999; Worrall et al., 2006), while increases in summer and spring precipitation observed for May Moss could be offset by enhanced evaporative losses under a warmer climate (Trenberth, 2011). The combined effect of drier and warmer (+0.6°C) winters, relative to 1961 – 1990, may also suggest that winter ET losses have increased at May Moss, corroborating Sottocornola and Kiely (2010) on enhanced winter ET with climate warming at an Atlantic blanket bog in southwestern Ireland, and reinforcing the vulnerability of winter recharge with climate change. Thus, despite the evidence of current short-term drought recovery and prevalent surface wetness at May Moss, enhanced winter drying and warming, as well as the negative annual ΔS observed in both 2017/18 and 2019/20, may thus highlight the hydrological vulnerability of UK blanket mires to climate change, particularly those located in drier areas of Britain (Wheeler, 2013), which could have exacerbating impacts on future carbon accumulation and loss.

4.5 CONCLUSION

A decade-long (2010/11 – 2019/20) energy and hydroclimate series facilitated the characterisation of the intact blanket bog, May Moss. The bog is in an unusually dry region for blanket mires, with average annual precipitation of 922 mm. Despite this, mean annual storage change of +1 mm over the ten-year period suggest that the bog is hydrologically well balanced, with inputs in equilibrium with outputs, and resilient to short-term impacts, such as the 2018 summer heatwave.

Annual water balances were computed for three consecutive hydrological years (2017/18, 2018/19, 2019/20), which comprised, on average, 930 mm of precipitation, 335 mm of evapotranspiration losses, 371 mm of runoff losses and a storage change of −7 mm, with the annual residual averaging at +268 mm. The positive residual implies that net outputs were not accounted for within the water balance. These residual "losses" are most likely derived from measurement error, in particular an underestimation of runoff, especially peak flow, evaporative losses from surface water or unaccounted changes in storage due to peat moisture loss, especially during severe drawdown events.

Average annual WTD is primarily related to average available energy (Rn – G), while monthly average WTD is driven mainly by VPD, which in turn is strongly coupled with available energy (Rn – G). Summer water availability (P – ET) is controlled more by precipitation than evapotranspiration and appears to be the key driver in summer ΔS. These findings may have

wider implications for palaeoclimate reconstructions based on changes in peat surface wetness, by confirming, at higher resolution, the control of summer moisture availability (P – ET) on summer average water table depth (Charman, 2007), although not on wider annual average water table depth, which is primarily driven by available energy (Rn – G). In addition, the extent of higher magnitude summer WT drawdown events, with potentially greater implications for hydrological functioning and carbon loss (Fenner and Freeman, 2011), appears to be driven by a higher incidence of warm, and therefore highly evaporative, days. The duration and extent of the 2018 summer drawdown thus appears to reflect the joint impact of low water availability (P – ET) and high incidence of highly evaporative days.

The high proportion of positive monthly storage changes and water balance residuals may suggest that May Moss has a positive water balance. In addition, storage losses observed over 2017/18 had recovered by the following year, verifying the relative resilience of intact mires to short-term drought events. Despite this, the trend of reducing winter and spring precipitation, enhanced winter warming, the location of May Moss on the lee side of the rain shadow barrier of the Pennines, and the predicted increase in the frequency of summer heatwaves across Europe (Seneviratne et al., 2006) could indicate that the water balance, and thus carbon stock, may be vulnerable to the effects of future climate change.

Chapter 5. Forest-to-bog restoration I. Hydrological functioning

ABSTRACT

Increased awareness of the deteriorating effects of afforestation of peatlands on carbon storage and water quality have prompted a rise in rewetting projects, with the aim of restoring the hydrological functioning of the peatland. Here, we analyse the impact of forest-to-bog restoration on the hydrological functioning of a formerly afforested blanket bog through a paired study with an adjacent intact blanket mire at May Moss, North York Moors, UK. Annual water balances, comprising precipitation, evapotranspiration, runoff, and storage change, as well as their residuals, are quantified for three hydrological years (2017/18, 2018/19 and 2019/20). Monthly water balance terms were similar between both sites, indicating that water balances resembled each other on intra-annual timescales. Baseflow made up a significantly higher proportion of total runoff at the recovering site (LG), compared to the intact bog (EB), which may be related to residual effects of former drainage and afforestation on enhancing lateral subsurface flow. Peak runoff was significantly reduced, and lag times extended at the restored site relative to the intact site, causing storm hydrographs to be considerably subdued and comparably less "flashy". Drought and post-drought hydrological behaviour at the two sites highlighted the rapid post-drought recovery of the intact blanket bog, while the restored site appeared to have lower moisture retention which reduced the level of recovery in the two years following a drought.

5.1 INTRODUCTION

Water-saturated conditions have facilitated the long-term accumulation of organic material, peat, in peatlands, making these wetlands the world's largest terrestrial carbon store, comprising between 500 and 700 Gt C, with northern peatlands sequestering an average of 18.6 g C m^{-2} yr^{-1} (Yu et al., 2010). However, peatland carbon sequestration and storage are sensitive to changes in the water balance, with peat accumulation requiring shallow near-surface water tables (Belyea and Clymo, 2001; Ratcliffe et al., 2018).

Peatlands have historically faced threats from large-scale drainage for the forestry, agriculture, and horticulture industries (Page and Baird, 2016). In the UK, peatlands are estimated to store 2302 Mt C (Billett et al., 2010). Large-scale afforestation of open mires,

most commonly with the North American species *Pinus contorta* (lodgepole pine) or *Picea sitchensis* (Sitka spruce), took place between the 1950s and the 1980s in the UK, with the aim of creating a national timber reserve (Hargreaves et al., 2003; Sloan et al., 2018a), and an estimated 9 – 10% of deep peat areas in the UK were afforested over this time period (Cannell et al., 1993; Tanneberger et al., 2017).

The drainage of peatlands, associated with afforestation, allows for the diffusion of air to greater depths within the peat (Cannell et al., 1993). Aeration of deep peat causes a reduction in the release of CH_4, produced as an end product of anaerobic respiration by methanogenic bacteria under normally anoxic conditions (Lai, 2009a), while also allowing the further oxidative decomposition of peat by bacteria and fungi resulting in heightened CO_2 emissions (Sloan et al., 2018a). In addition to changes in the greenhouse gas (GHG) balance, peatland drainage and afforestation leads to the consolidation, compaction and subsidence of peat (Anderson et al., 2000; Sloan et al., 2018b) due to the loss of water from large pore spaces due to initial lowering of the water table and the compressing weight of upper peat layers and tree stands (Sloan et al., 2018b). Afforestation has furthermore been related to a reduction in annual runoff, but an increase in peak flows (Anderson et al., 2000) and forms a considerable source for fluvial export of dissolved organic carbon (DOC) and nutrients (Cummins and Farrell, 2003; Marttila et al., 2018) and metal pollutants (Kaila et al., 2012; Asam et al., 2014a), thus having negative impacts on downstream water quality (Volk et al., 2002).

Increased awareness of the damaging effects of the drainage and afforestation of peatlands on carbon storage and water quality have motivated interest in rewetting projects, with the aim to recover the hydrological functioning of the peatland and re-establishing peat accumulation and carbon storage. The relative novelty of post-forestry restoration and the time scales (> 5 years) required to observe recovery, has meant that studies on the effects of restoration are still few in number. Drain blocking and other rewetting techniques result in an initial rise in water levels, sometimes returning to pristine levels (Wallage and Holden, 2011; Anderson and Peace, 2017), and have been linked to large reductions in discharge (Evans et al., 2018), though analysis of the extent of recovery comparable to pre-drainage levels is generally limited within the time-frame of the study. Rewetting has furthermore been related to a both a reduction and surge in storm runoff (Ballard et al., 2012; Menberu et al., 2018; Howson et al., 2021b), highlighting further uncertainty regarding the effectiveness of peatland rewetting in (re-)establishing key ecosystem services.

Here, we analyse the impact of forest-to-bog restoration on the hydrological functioning of a formerly afforested blanket bog 10 years post-restoration using a four-year paired hydrological study with an adjacent intact blanket mire at May Moss, North York Moors, UK. The analysis comprises a comparison in the water balances of the two catchments, storm hydrograph response to rainfall events and water table behaviour during seasonal drawdown and recharge.

5.2 METHODS

5.2.1 Study site

May Moss (54° 21' 4" N, 0° 39' 16" W, elev. 253 m) is the largest area of intact upland ombrotrophic blanket mire in the North York Moors (Chiverrell, 2001). The mire comprises two watershed basins with peat depths exceeding 5 m in thickness (Atherden, 1979), which form the headwater catchments of the northward draining Eller Beck (EB) and the adjacent southward draining Long Grain (LG) (Figure 1.4). The site is characterised by an average annual temperature of 8.1 ± 0.5°C, precipitation of 922 ± 109 mm yr^{-1} and evapotranspiration losses of 345 ± 32 mm yr^{-1}, based on a 10-year micrometeorological record spanning 01/10/2010 – 30/09/2020 (*Chapter 4*).

The intact area of blanket bog, dominating the EB catchment, has long been protected as a Site of Special Scientific Interest (SSSI) (Figure 1.4), now forming part of the North York Moors SSSI/Special Protection Area (SPA). The adjacent LG catchment to the east was afforested between 1975 and 1983 to form a Lodgepole pine (*Pinus contorta*) plantation, managed by the Forestry Commission. SITA-Trust *Enriching Nature* funding enabled the launch of a restoration process within the LG catchment between 2009 and 2012, which involved forest clearance, through a combination of felling and mulching or pulverising, and drain blocking with peat plugs and timber weirs, though the planting ridges and furrows were left intact and largely remain in place.

The EB and LG catchment areas and stream networks were delineated in ArcGIS and ArcHydro using an OS Terrain 5 DTM (Ordnance Survey, 2020). Spatial land cover datasets for the catchment areas were obtained from the Priority Habitat Inventory (Natural England, 2019) and the National Forest Inventory (Forestry Commission, 2019). Peat depth contours were projected upon the catchment map (Figure 1.3) using data from Atherden (1972). The EB catchment is dominated by intact blanket bog (64.0% of catchment area), classified as M18a (*Sphagnum magellanicum – Andromeda polifolia* sub-community), with some upland

heathland (H12a *Calluna vulgaris* sub-community) to the northeast, and felled recovering areas (23.4%) to the west and northeast of the catchment (Figure 1.4 and Table 1.1). The LG catchment is dominated by deforested, recovering blanket bog areas (56.8%), and smaller patches of upland heathland (H12a) (18.4%) to the north and some remaining active forestry plantation (15.7%) to the eastern border of the intact bog, as well as to the northeast and south of the catchment, with only a small proportion of intact blanket bog (5.3%) situated within the catchment (Figure 1.4 and Table 1.1).

5.2.2 Hydro-meteorological data collection and preparation

5.2.2.1 The May Moss meteorological station

The meteorological station on May Moss since 2010 has enabled the multi-year analysis of hydroclimate impacts on blanket bog hydrology. Hourly hydro-meteorological data have been collected since August 2010 at the May Moss station, comprising a micro-meteorological mast, rain gauge and water level sensor. The station is situated centrally on the intact bog, on the watershed of the EB catchment with an uninterrupted blanket bog cover wind fetch of over 240 m in all directions, and within 0.5 km of the LG catchment boundary. Hourly data were recorded using the Campbell Scientific CR1000 datalogger. Average, minimum, and maximum temperature (°C) and relative humidity (%) were measured at 0.4, 1.0, 2.0 and 3.0 m heights using four temperature and relative humidity sensors (Campbell Scientific CS215) and four rotary cup anemometers (Campbell Scientific 03102) were fixed at the same heights, facilitating vertical profile measurements of air temperature, relative humidity, and wind velocity. A net radiometer (NR-LITE2 Net Radiometer, Campbell Scientific), PAR-sensor (SKP215 Quantum Sensor, Campbell Scientific) and soil heat flux plate (HFP01, Campbell Scientific) were used to monitor energy fluxes. A rain gauge (ARG100, Campbell Scientific) collected hourly total precipitation (mm). Data gaps in the hydrometeorological time series were filled using largely linear regression (Peterson et al., 1998), where possible with adjacent sensors or otherwise with equivalent sensor data from the Fylingdales meteorological station. The methods used in the preparation of data collected between August 2010 and July 2021 from all sensors are detailed in *Chapter 3*.

Hourly air temperature, relative humidity and wind profiles, together with net radiation, photosynthetic active radiation and soil heat flux facilitated the quantification of hourly evapotranspiration using the Bowen ratio energy balance (BREB) method (*Chapters 3* and *4*), while a 1.8 m dipwell (MS) with a submersible vented pressure transducer (PDCR 1830, Campbell Scientific) next to the meteorological station allowed the analysis of hourly water

levels near the bog watershed contributing to the EB catchment. The May Moss hydro-meteorological data were analysed based on the UK hydrological year (1st October to 30th September) (e.g. in Holden and Burt (2003a); Worrall et al. (2015)). Hence, calendar years (1st January – 31st December) are referred to specifically as "calendar years", while the use of the simple terms "year" and "annual" refer to the hydrological year.

5.2.2.2   Water table depth

In March 2017, three additional dipwells with automatic watertight pressure transducers (HOBO U20 Water Level Logger, Onset) were installed: "EB" within the Eller Beck catchment, "LG" within the Long Grain catchment, and "GA" adjacent to a bog pool, Great Arc, within the Long Grain catchment (Figure 1.4). Hourly absolute pressures obtained from the loggers were converted to sensor depths using hourly atmospheric pressure (kPa) recorded using an equivalent pressure transducer housed within the May Moss meteorological station datalogger enclosure and the HOBOware Pro software (Onset). Sensor depths were then corrected to actual water levels (distance from the ground surface to the water surface) using linear regression between sensors depths and their respective manual measurements for dipwells MS (R^2 = 0.99, n = 9), EB (R^2 = 0.99, n = 9) LG (R^2 = 0.95, n = 9) and GA (R^2 = 0.997, n = 3). Thus, the hourly water level series of EB and LG span 14/03/2017 – 01/07/2021 and of GA spans 14/03/2017 – 10/03/2020. Due to their location near the centre of their respective catchment, the EB and LG dipwell water level series were used to compute monthly and annual storage change by calculating the loss or gain in water table depth between the first and last day of the month (monthly ΔS) and between the 1st October and 30th September (annual ΔS).

5.2.2.3   Runoff

Where the Eller Beck and Long Grain streams exit the area of deep peat, 90° v-notch weirs were installed in March 2017 to quantify hourly discharge and catchment runoff. Dipwells with pressure transducers (HOBO U20 Water Level Logger, Onset) were placed directly upstream from the weirs and absolute pressure series were likewise converted to sensor depths using the hourly May Moss atmospheric pressure series. Sensor depths were then corrected to head measurements (distance between the water surface and the v-notch of the weir) using linear regression between the sensor recorded depths and corresponding 20 manual head measurements taken in the field at the EB (R^2 = 0.91) and LG (R^2 = 0.95) weirs (Figure 5.1). Head measurements were converted to discharge using the Kindsvater-Shen equation (The British Standards Institution, 2017) (*Chapter 4*). Discharges (m^3 hr^{-1}) from EB

and LG were then divided by their respective catchment areas (EB = 0.63 km^2; LG = 1.53 km^2) to quantify catchment area-specific runoff (mm hr^{-1}) for the monitoring period lasting 14/03/2017 to 01/07/2021.
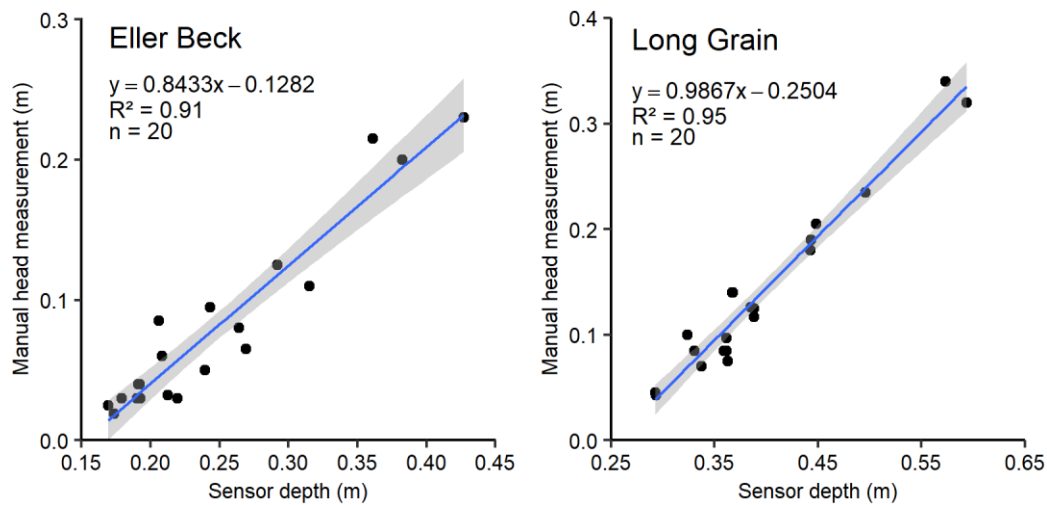
Figure 5.1. Linear regressions between sensor depths (m) and manual head measurements (m), used to model discharge series for Eller Beck (EB) and Long Grain (LG).

Both the EB and LG runoff series contained data gaps between 22/10/2017 and 01/02/2018, and the LG runoff series additionally had a data gap between 25/06/2018 and 03/07/2018, which amounted to a loss of 28% and 31% of the 2017/18 data for EB and LG runoff series, respectively. The longer gap spanning 22/10/2017 – 01/02/2018 was filled by linear regression of the EB and LG runoff series (corrected for unit area) with WTD data from the EB (R^2 = 0.39) and LG (R^2 = 0.23) dipwells, based on data spanning October – February from the affected and subsequent years (Figure 5.2). Runoff and WTD showed exponential relationships in both catchments, with shallower water levels relating to increasingly higher runoff (Figure 5.2). Here, LG generally showed greater runoff values for given water levels than EB, while EB presents a faster runoff response to water level change indicated by a steeper slope (-0.023) in the regression function compared to LG (-0.016) (Figure 5.2). The later gap in the LG runoff series (25/06/2018 – 03/07/2018) was filled by interpolating adjacent data points.
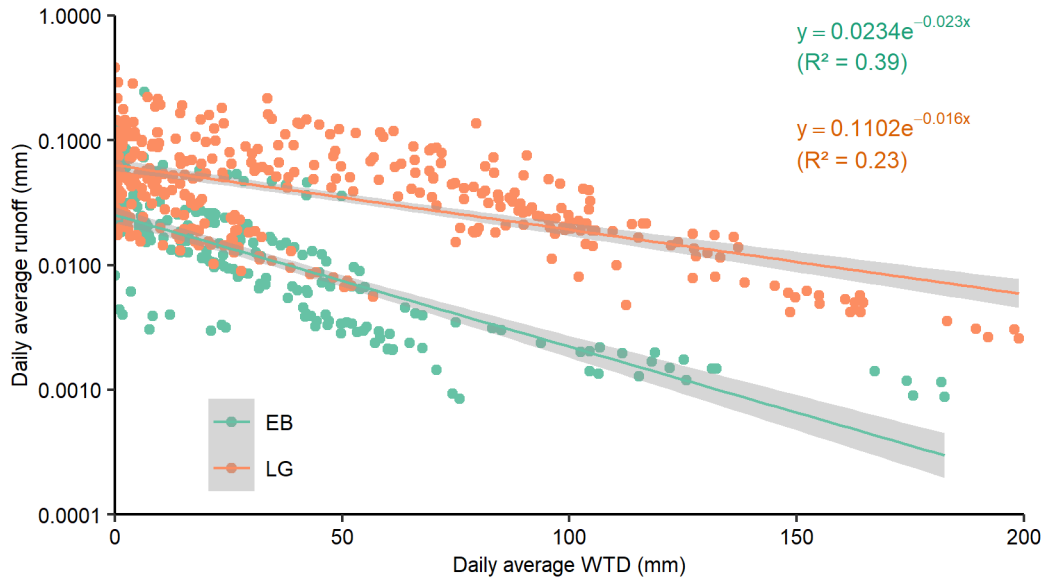
Figure 5.2. Linear regression between daily average water table depth (WTD) (mm) and runoff (mm) for the Eller Beck (EB) and Long Grain (LG) sites.

5.2.2.4   Water balance

The annual water balance equation for a bog may be simplified to:

$$P = ET - R - \Delta S \qquad (5.1)$$

where P is precipitation (mm), ET is evapotranspiration (mm), R is runoff (mm) and ΔS is the change in storage, here quantified as the change in water level between the start and end of the time interval. The equation was rearranged to solve for the residual, ε:

$$P - ET - R - \Delta S = \varepsilon \qquad (5.2)$$

A positive residual term, ε, implies that water gains (P) are exceeding water outflows ($ET + R$ and storage change (ΔS). The residual may represent measurement uncertainty or unknown outflow pathways (Isabelle et al., 2018; Safeeq et al., 2021), such as peat pipes (Holden and Burt, 2002c), or additional changes in storage associated with the swelling or shrinking of the underlying peat with "mire breathing" (Kellner and Halldin, 2002). The water balance terms, as well as annual residuals (ε), were summarised for the three complete hydrological years 2017/18, 2018/19 and 2019/20.

The analysis and comparison of water balance terms between the EB and LG catchments assumes that ET and P are consistent across sites. As the May Moss meteorological station was 262 m from one of the EB dipwells and 999 m from the LG dipwell, P and ET is assumed to equivalent at all dipwells. Water balance terms were analysed over monthly timescales to

minimise errors through potential hourly and daily differences in ET and P between the two sites and to minimise the effect of runoff and water level lag times on correlation analysis between water balance terms.

5.2.3   Runoff partitioning and storm flow analysis

The UK National River Flow Archive uses the 90th percentile (Q10) of runoff data to denote high flow events and the 5th percentile (Q95) to identify significant low flow (Marsh and Hannaford, 2008). The complete 2018/19 and 2019/20 runoff series for EB and LG were used to produce flow duration curves (FDC) and to identify the Q10 and Q95 thresholds for both catchments and the contributions of high (> Q10) and low (< Q95) runoff to total annual runoff.

The respective Q10 thresholds for each catchment were further used to identify storm events over the complete timeseries to assess and compare the responses of runoff parameters (Table 5.1) between EB and LG during storm events. Individual storm event hydrographs were selected by partitioning runoff into baseflow and quickflow (Howson et al., 2021b) using the R-package "EcoHydRology" (Fuka et al., 2018) and the complete hourly runoff series between 14/03/2017 and 01/07/2021. The storm hydrograph limits were selected where quickflow equalled zero prior to and following a runoff peak. Storm hydrographs were then selected for further parameter analysis based on the following criteria:

  I.   Storm hydrographs had to overlap between the two catchments
 II.   Peak flow had to occur under storm conditions (Q10) at both catchments
 III.   Storm conditions (Q10) had to persist > 1 hour in both catchments
 IV.   Hydrographs had to culminate in a single peak

Based on the above criteria, 40 storm events were selected and their hydrograph parameter (Table 5.1) data were collected for each catchment. To compare storm hydrographs between the EB and LG catchments, the distributions of the parameter data were assessed for normality using the Shapiro-Wilk test, which showed that all storm parameter data differed significantly from a normal distribution. The non-parametric Wilcoxon rank-sum test was therefore selected to compare storm responses between EB and LG.

Table 5.1. Storm hydrograph parameters and their description.

Parameter	Description
HG	Duration of hydrograph (time between successive zero quickflow)
PeakP	Maximum amount of precipitation (mm) received in an hour between previous zero quickflow and peak runoff
TotP	Total amount (mm) of precipitation during the hydrograph period (between successive zero quickflow)
PeakR	Peak runoff (R) rate (mm hr^{-1}) during the storm event
TotR	Total runoff (mm) during the hydrograph
TotBF	Total baseflow (mm) during the hydrograph
TotQF	Total quickflow(mm) during the hydrograph
BF:QF	Ratio of baseflow to quickflow
Lag-StartP-PeakR	Time (hrs) between the start of precipitation (after zero quickflow) and peak runoff during the hydrograph period
Lag-PeakP-PeakR	Time (hrs) between peak precipitation and peak runoff
Lag-BF-PeakR	Time (hrs) between the start of the hydrograph and peak runoff
Lag-PeakR-BF	Time (hrs) between peak runoff and the end of the hydrograph
Lag-PeakWT-PeakR	Time (hrs) between peak water table and peak runoff

5.2.4 Water levels and drawdown analysis

The water table series from the MS, EB and LG dipwells spanned the complete hydrological years 2017/18, 2018/19 and 2019/20, while the GA series included the first two of those years. Water level duration curves (WLDC) for the four dipwell series were thus based on the three complete years for MS, EB and LG and for the first two years for GA. Water table responses to water deficit and surplus were analysed and compared between MS, EB, LG and GA across 12 drawdown events (GA was included in nine events, as the series concluded on 10/03/2020) identified between 14/03/2017 and 01/07/2021. Data for each parameter (Table 5.2) for all four dipwells were assessed for normality in their distributions using the Shapiro-Wilk test, which found that distributions in parameters DE, Rise-Lag and Fall-Rate were significantly normal, while distributions in parameters Trough, Fall, Rise, Fall-Lag and Rise-Rate were significantly non-normal. To fulfil the assumptions of ANOVA on homogeneity of variance, Levene's test was used on parameters with normal distributions, while the Fligner-Killeen test was applied to non-normal parameters. Homogeneity of variance were found ($p > 0.05$) between the four dipwell series with all parameters and differences in the parameter (Table 5.2) means between the four dipwells were therefore tested using ANOVA.

Table 5.2. Water table drawdown parameters analysed for the MS, EB, LG and GA dipwell water level data for the twelve drawdown events.

Parameter	Description
DE	Total duration of the drawdown event (days)
Trough	The deepest water level (mm) reached during the drawdown event
Tot-Fall	The fall in water level (mm) between the pre-trough WL peak and the trough
Tot-Rise	The rise in water level (mm) between the trough and the post-trough WL peak
Fall-Lag	Lag time between the pre-peak water level and the trough (days)
Rise-Lag	Lag time between the trough and the post-peak water level (days)
Fall-Rate_WT	The rate of water level reduction per day during the LagFall period (mm day^{-1})
Rise-Rate_WT	The rate of water level increase per day during the LagRise period (mm day^{-1})

5.3 RESULTS

5.3.1 Catchment characteristics and hydroclimate

The hydroclimate series (Figure 5.3) at May Moss included hourly air temperature, precipitation (P), evapotranspiration (ET), as well as runoff (R) and storage change (ΔS) for the EB (0.63 km^2) and LG (1.53 km^2) catchments between March 2017 and June 2021, thus encompassing the complete hydrological years 2017/18, 2018/19 and 2019/20. Over the three years, annual air temperature averaged at 8.4 ± 0.3°C, average annual precipitation amounted to 930 ± 157 mm and annual evapotranspiration measured 335 ± 50 mm (Table 5.3). Across the three complete years, January, February and December were typically the coldest months, with average temperatures of 3.3, 3.4 and 3.7°C, respectively, while June, July and August were the warmest, averaging at 12.7, 15.1 and 14.8°C, respectively. May was, on average, the driest month of the year with a water deficit (P – ET) of −13 mm, followed by July (+5 mm) and April (+8 mm), while October (+97 mm) and November (+130 mm) tended to have the largest water surpluses (P – ET) (Table 5.4).

In both catchments, runoff tended to be lowest in May and July, and highest from October through to March, with high runoff also observed in June and August (Table 5.4). LG tended to exceed EB in runoff between winter and late spring (January – May), while EB had relatively higher runoff in the summer and autumn (June – November), with both catchments producing, on average, equal amounts of runoff in December. Water levels at the EB and LG dipwells were, on average, shallowest from November through to March, while April to October were characterised by considerably deeper water levels, particularly July, August and September. Average water levels were between 3 and 440% lower at the LG dipwell relative to the EB dipwell for all calendar months (Table 5.4).
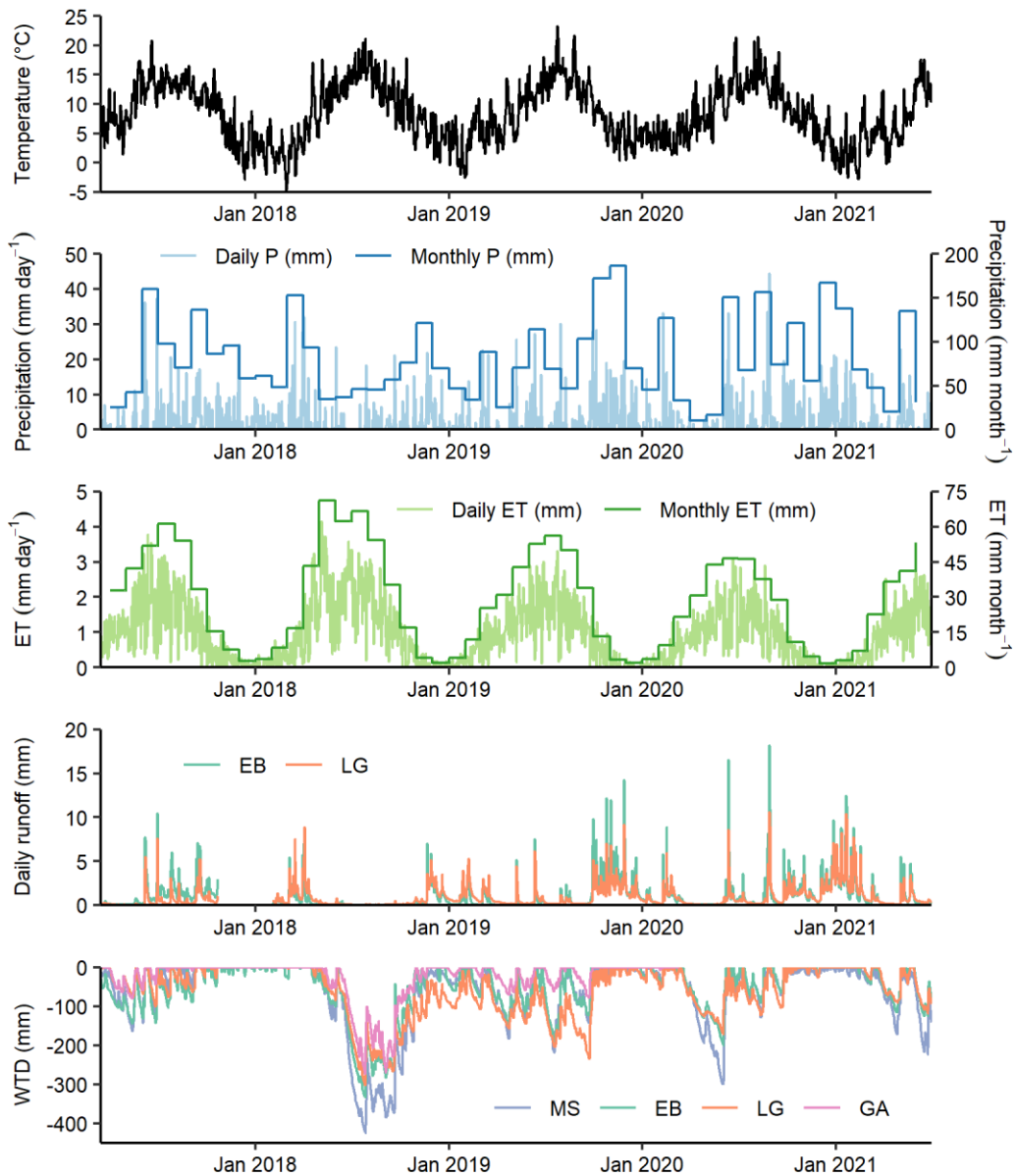
Figure 5.3. Average daily air temperature (°C), and daily and monthly total precipitation (mm) and evapotranspiration (ET) at the May Moss meteorological station. Daily total runoff (mm) at the Eller Beck (EB) and Long Grain (LG) weirs, and daily average water table depth (WTD) (mm) at the meteorological station (MS), Eller Beck (EB), Long Grain (LG) and Great Arc (GA) dipwells.

Table 5.3. Average annual temperature, °C (T), water balance components (P, ET, R and ΔS) (mm) and residuals (ε) (mm) for the Eller Beck (EB) and Long Grain (LG) catchments, and average water table depth (WTD) (mm) at the MS, EB, LG and GA dipwells. Summer (JJA) values are shown in brackets. Three-year averages are shown in the final row. More positive ΔS signifies greater water table recharge, while more positive residuals mean greater unaccounted "losses" of water.

Year	T	P	ET	R		ΔS		ε		WTD			
				EB	LG	EB	LG	EB	LG	MS	EB	LG	GA
2017/18	8.2 (14.8)	816 (128)	387 (183)	233 (29)	254 (31)	-166 (-152)	-198 (-156)	+361 (+69)	+373 (+70)	-100 (-267)	-76 (-200)	-68 (-178)	-52 (-137)
2018/19	8.7 (14.4)	865 (230)	331 (159)	211 (24)	287 (33)	+167 (+8)	+138 (-44)	+156 (+39)	+110 (+82)	-68 (-76)	-58 (-70)	-107 (-120)	-22 (-18)
2019/20	8.4 (13.5)	1110 (375)	287 (131)	558 (50)	397 (36)	-5 (+195)	-19 (+163)	+270 (-1)	+445 (+45)	-51 (-54)	-34 (-34)	-49 (-63)	-----
Avg.	8.4 (14.2)	930 (245)	335 (158)	334 (34)	313 (33)	-1 (+17)	-26 (-12)	+262 (+36)	+309 (+66)	-67 (-132)	-56 (-101)	-75 (-120)	-37 (-78)

Table 5.4. Average monthly air temperature, T (°C), precipitation, P (mm), evapotranspiration, ET (mm), available water (P − ET) (mm), and runoff (R) and average water table depth (WTD) for Eller Beck (EB) and Long Grain (LG), based on daily values from October 2017 − September 2020. Percentage difference (% diff) from EB to LG are shown for R and WTD values.

Month	T	P	ET	P − ET	R			WTD		
					EB	LG	% diff	EB	LG	% diff
January	3.3	51	4	47	22	25	14	-16	-31	-94
February	3.4	70	10	60	27	33	22	-16	-27	-69
March	4.2	91	21	70	28	36	29	-18	-30	-67
April	7.2	43	35	8	13	21	62	-70	-77	-10
May	10.2	40	53	-13	5	8	60	-91	-94	-3
June	12.7	101	54	47	27	23	-15	-55	-74	-35
July	15.1	61	56	5	9	7	-22	-144	-152	-6
August	14.8	83	47	36	28	19	-32	-104	-135	-30
September	11.7	78	33	45	15	12	-20	-105	-150	-43
October	9.0	112	15	97	52	34	-35	-37	-58	-57
November	5.4	135	5	130	67	52	-22	-10	-35	-250
December	3.7	66	2	64	42	42	0	-5	-27	-440

The hydroclimate series comprised a range of meteorological and hydrological events (Figure 5.3). After a comparably cold winter and wet spring, 2017/18 witnessed the substantial water level drawdown event in summer 2018 which culminated in the deepest water levels among the three hydrological years (Figure 5.3), and since monitoring began in August 2011 (*Chapter 3*). The deepest water levels were reached at the MS (−427 mm) nearest the watershed, followed by EB (−351 mm), LG (−307 mm) and GA (−280 mm) dipwells in June 2018, and water tables did not reach consistently shallow depths until well into autumn 2018 (Figure 5.3). The following winter witnessed a few smaller drawdown events, not observed in other years, interrupted by periods of high runoff (Figure 5.3). Likewise, Spring and Summer 2019 comprised several smaller drawdown events until end of September 2019, with water level depths falling to −224 mm at MS and −196 mm at EB in July, followed by −241 mm at LG and −90 mm at GA in September. The 2019/20 year began with a considerably wet autumn and winter, resulting in a period of high runoff and shallow water levels that lasted until the end of March. A further water table drawdown event commenced in April 2020, with water levels culminating in June at −314 mm at MS, −204 mm at EB and −177 mm at LG until a spike in precipitation facilitated recovery over autumn 2020 (Figure 5.3).

5.3.2 Water balance

5.3.2.1 *Closure and residuals*

The water balance equation was rearranged to assess water balance closure and quantify monthly and annual residuals (ε), with more positive residuals indicating greater net unaccounted "losses". Across 2017/18, 2018/19 and 2019/20, annual residuals amounted to +361, +156 and +270 mm at EB and +373, +110 and +445 mm at LG (Table 5.3), indicating

that net outputs or storage changes were not accounted for in both catchments. Monthly residuals, based on the three complete hydrological years ranged between −123 mm and +69 mm at EB (Mdn = 27 mm) and between −68 mm and +120 mm LG (Mdn = 26 mm). Positive residuals occurred in 75% of months across the three water years, again indicating that both catchments tended towards a water surplus and net monthly losses were not accounted for. A Wilcoxon rank-sum test indicated no significant difference in median monthly residuals between the two sites (W = 1316, p = 0.92).

Non-parametric Kendall's tests indicated a significant negative correlation between monthly residuals and ΔS at both EB (τ = −0.39, p < 0.001) and LG (τ = −0.34, p < 0.001). Residuals were also negatively correlated with ET at EB (τ = −0.25, p < 0.01) and LG (τ = −0.24, p < 0.05). In addition, residuals were negatively related to maximum monthly air temperature at EB (τ = −0.30, p < 0.01) and LG (τ = −0.25, p < 0.05). This implies that residuals became more positive, implying greater unaccounted losses, together with more negative ΔS and lower ET and temperatures. Kendall's tests further indicated that monthly residuals from either site were unrelated to precipitation and runoff (p > 0.05). The extent of water balance closure was further examined by partitioning the terms into monthly net water inputs (P − ET − R) and storage change (ΔS). Kendall's test showed monthly net inputs and ΔS to be significantly correlated for EB (τ = 0.56, p < 0.001) and LG (τ = 0.56, p < 0.001) (Figure 5.4), while Wilcoxon rank-sum tests revealed that monthly net inputs (P − ET − R) significantly exceeded storage change (ΔS) for both EB (W = 903, p < 0.01) and LG (W = 854, p < 0.01).
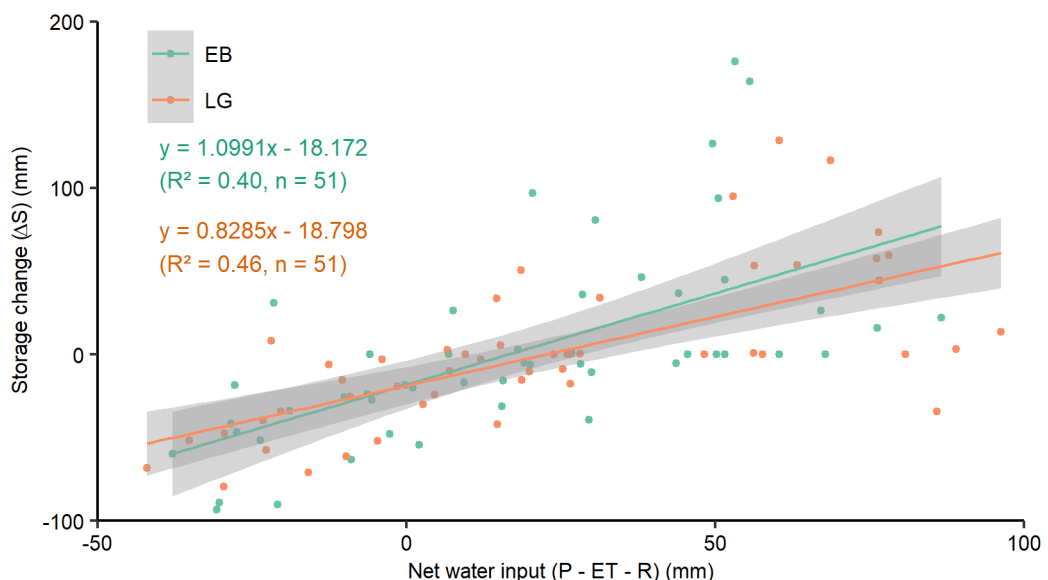
Figure 5.4. Linear regressions with 95% confidence interval showing the relationship between monthly net water input (P − ET − R) (mm) and storage change (ΔS) (mm) at Eller Beck (EB) and Long Grain (LG).

5.3.2.2 Catchment comparison

Among the three hydrological years, moisture availability (P − ET) was greatest in 2019/20, followed by 2018/19 and least in 2017/18. Annual R and ΔS followed similar trends at EB and LG over the three years (Table 5.3). Annual total runoff was highest in 2019/20 for both catchments and lowest in 2017/18 for LG and in 2018/19 for EB (Table 5.3). Annual runoff coefficients (R/P) were 0.29, 0.24 and 0.50 at EB (average = 0.34 ± 0.14) and 0.31, 0.33 and 0.36 at LG (average = 0.33 ± 0.02) for the hydrological years 2017/18, 2018/19 and 2019/20, respectively.

Annual ΔS was relatively similar between EB and LG, differing by a maximum of 32 mm (2017/18), though more positive in EB across all years. Among the three years, both catchments experienced their most negative annual ΔS in 2017/18, coinciding with the 2018 summer heatwave and an extreme water level drawdown event which lasted into the following year (2018/19). While EB appeared to have fully compensated for storage losses from 2017/18 (−166 mm) by the end of 2018/19 (+167 mm), LG regained 70% of the reduction in water storage from 2017/18 by the end of 2018/19 (Table 5.3). Storage change (ΔS) in 2019/20 was nearly negligible for both catchments, through slightly lower at LG than EB, while runoff was considerably higher, and more so at EB, compared to the previous two years (Table 5.3). Despite this variability, both catchments appeared relatively balanced in terms of their mean annual ΔS, with EB (-1 mm) closer to zero than LG (-26 mm) (Table 5.3). Mean summer ΔS was likewise close to zero for both catchments, but positive for EB (+17 mm), while negative for LG (-12 mm) (Table 5.3).

Water deficits (P < ET) occurred in April 2017, between May and August 2018, April and August 2019, April and May 2020, and April and June 2021 (Figure 5.5). EB and LG appeared relatively synchronous in their monthly water balance (Figure 5.5). The two catchments did not differ significantly in their monthly average WTDs (W = 1420.5, p = 0.4238) or monthly storage change (W = 1270, p = 0.8408). The median monthly WTD, based on monthly average WTD (2017/18 − 2019/20), was −32 mm at EB (IQR = −83 − −10) and -63 mm at LG (IQR = −112 − −15). Both EB and LG had a median monthly storage change (ΔS) of 0.0 mm, based on the 2017/18 − 2019/20 series, and monthly ΔS was ≥ 0 in 19 out of 36 months (52.8%) in both catchments, implying that storage change was generally balanced over the three-year period. Monthly ΔS was similarly significantly related to P (τ = 0.45, p < 0.001) and P − ET (τ = 0.45, p < 0.001) at EB, while at LG ΔS had a marginally stronger relationship to P (τ = 0.50,

p < 0.001) than to P − ET (τ = 0.47, p < 0.001). Monthly ΔS appeared unrelated to ET for both EB (τ = −0.07, p = 0.4695) and LG (τ = −0.08, p = 0.3888).
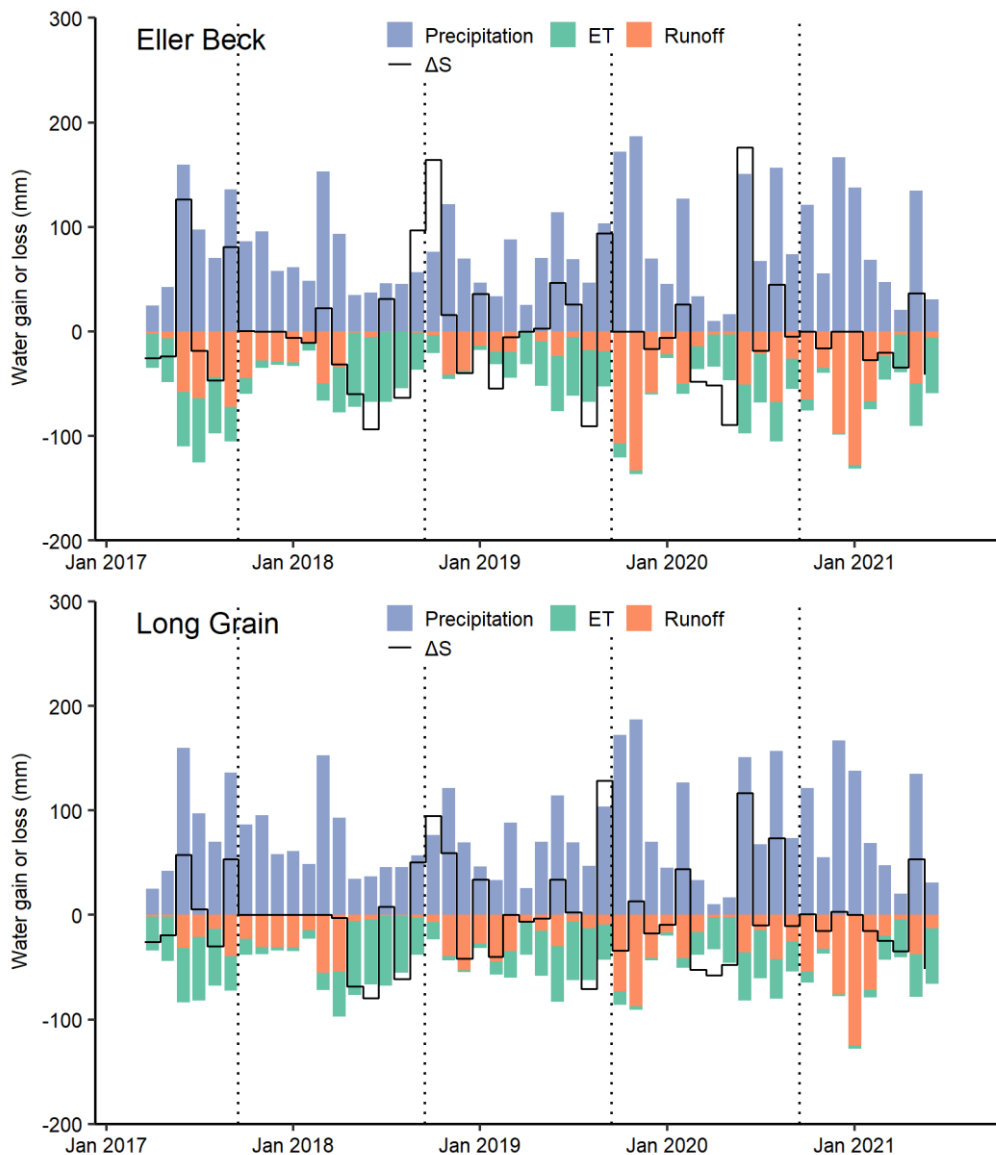
Figure 5.5. Monthly water balances (April 2017 – June 2021) for Eller Beck (EB) and Long Grain (LG), showing water gain through precipitation (P), water losses through evapotranspiration (ET) and runoff (R) and storage change (ΔS). Dotted lines mark hydrological years.

Monthly total runoff did not differ significantly (W = 1350, p = 0.743) between EB (Mdn = 20.6 mm, IQR = 5.4 − 38.8 mm) and LG (Mdn = 23.9 mm, IQR = 6.9 − 39.8 mm). Median net water inputs (P − ET − R) were positive at both EB (Mdn = 23.3 mm, IQR = −0.9 − 50.3 mm) and LG (Mdn = 21.9 mm, IQR = −6.0 − 54.1 mm). Monthly EB runoff (τ = 0.62, p < 0.001) appeared more responsive to precipitation than LG runoff (τ = 0.54, p < 0.001) (Figure 5.5). Conversely, monthly LG runoff (τ = −0.43, p < 0.001) appeared more limited by evapotranspiration than EB (τ = −0.31, p < 0.01). However, Kendall's tests showed monthly runoff from both catchments were more related to available water (P − ET), rather than

driven more by precipitation (P) or limited by evapotranspiration (ET) alone, with EB runoff (τ = 0.67, p < 0.001) and LG runoff (τ = 0.69, p < 0.001) showing similar strength in their correlation with available water (P – ET) (Figure 5.6). In addition, higher monthly runoff losses correlated significantly with greater water level recharge (ΔS) at EB (τ = 0.21, p < 0.05) and LG (τ = 0.24, p < 0.05). Monthly runoff coefficients (R/P) did not differ significantly between catchments (W = 1408, p = 0.4739), but appeared more strongly coupled with average WTD at EB (τ = 0.59, p < 0.001) than LG (τ = 0.44, p < 0.001), with exponential regressions indicating that LG tended towards higher runoff coefficients for any given WTD compared to EB, except for very shallow water levels where EB showed relatively higher R/P (Figure 5.7).
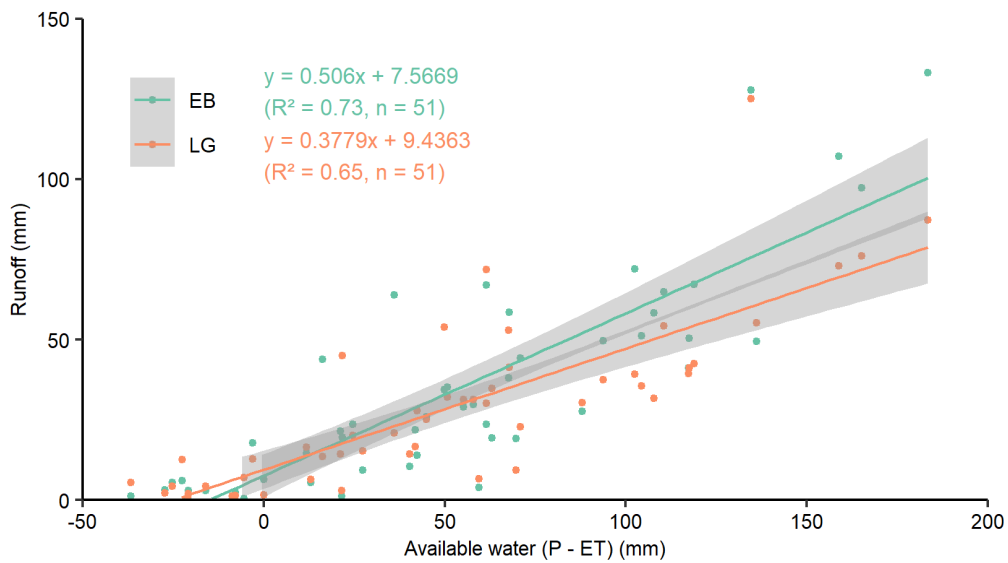
Figure 5.6. Linear regression with 95% confidence interval showing the relationship between monthly available water (P – ET) (mm) and runoff (mm) from the EB and LG catchments.
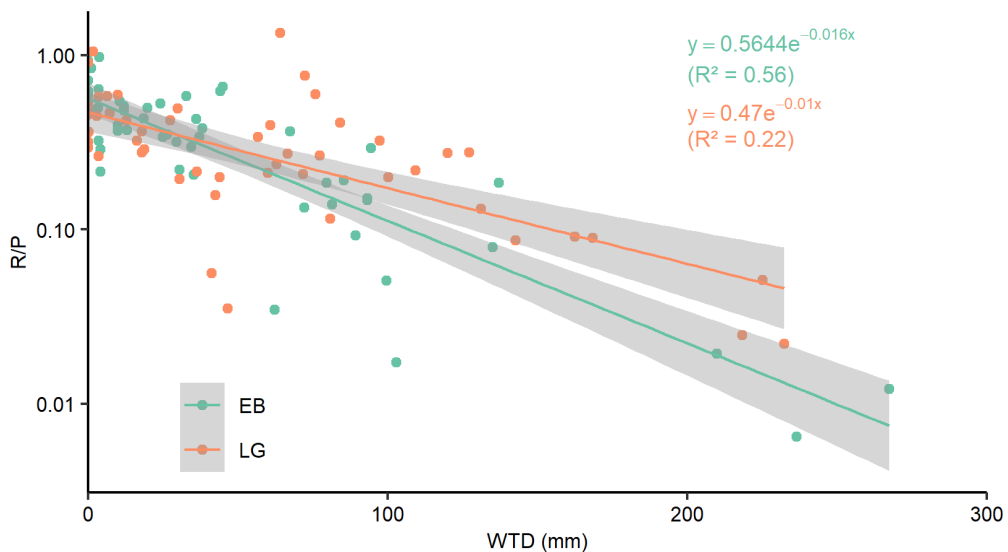
Figure 5.7. Exponential relationship between monthly average WTD (mm) (higher values signify deeper water tables) and runoff coefficients (R/P) at the EB and LG catchments.

5.3.3 Runoff

5.3.3.1 Runoff partitioning

Daily runoff in 2017/18, 2018/19 and 2019/20 averaged 0.64 ± 0.99 mm, 0.58 ± 1.07 mm, and 1.52 ± 2.34 mm respectively at EB (three-year average = 0.91 ± 1.65 mm day^{-1}) and 0.70 ± 0.96 mm, 0.79 ± 1.00 mm, and 1.09 ± 1.43 mm at LG (three-year average = 0.86 ± 1.16 mm day^{-1}). The partitioning of runoff into baseflow (BF) and quickflow (QF) was based on the original (without gap filling) paired hourly runoff series between March 2017 and June 2021 and allowed comparison of the BF:QF ratio between the catchments. For 2017/18, 2018/19 and 2019/20, mean BF:QF ratios were 1.9, 1.8 and 1.9 at EB, and 2.7, 3.5 and 2.3 at LG, respectively.

Based on the complete runoff series (14/03/2017 – 01/07/2021; precluding the gap-filled data), the median daily runoff was significantly higher (+22%) (W = 1011081, p-value < 0.01) at LG (Mdn = 0.44 mm day^{-1}) compared to EB (Mdn = 0.36 mm day^{-1}). The median daily quickflow was significantly higher (+13%) (W = 1022375, p-value < 0.05) at LG (Mdn = 0.054 mm day^{-1}) than EB (Mdn = 0.048 mm day^{-1}), and the median daily baseflow was likewise significantly greater (+32%) (W = 1002944, p-value < 0.01) at LG (Mdn = 0.37 mm day^{-1}) compared to EB (Mdn = 0.28 mm day^{-1}). Median daily BF:QF ratios were likewise significantly higher (+8%) (W = 955771, p-value < 0.001) at LG (Mdn = 5.3) compared to EB (Mdn = 4.9), denoting that baseflow made up a relatively higher proportion of total daily runoff at LG than at EB, while the later had proportionally greater quickflow.

In contrast to daily equivalents, monthly total baseflow (W = 1064, p-value = 0.9659) and quickflow (W = 1160, p-value = 0.4298) did not differ significantly between EB and LG. However, monthly BF:QF ranged 0.7 – 8.9 at EB and 1.1 – 13.0 at LG, and a Wilcoxon rank-sum test showed that BF:QF ratios were significantly higher (W = 737, p-value < 0.05) at LG (Mdn = 2.9) compared to EB (Mdn = 1.9), indicating that baseflow made up a relatively higher proportion of total monthly runoff at LG, compared to EB.

Computation of percentile flow thresholds were based on the complete series from 2018/19 – 2019/20. The 90th percentile (Q10) threshold for storm flow lay at 0.11 mm hr^{-1} for EB and at 0.10 mm hr^{-1} for LG. Based on the same years, storm flows (≥ Q10) made up a higher proportion of total annual runoff (mm per m^2) at EB (54%) compared to LG (43%). Conversely, extremely low runoff (≤ Q95) made up a higher proportion of total annual runoff at LG (0.20%) than at EB (0.04%), though the threshold for runoff ≤ Q95 was lower at EB (0.0006 mm hr^{-1}) than at LG (0.002 mm hr^{-1}) (Figure 5.8).
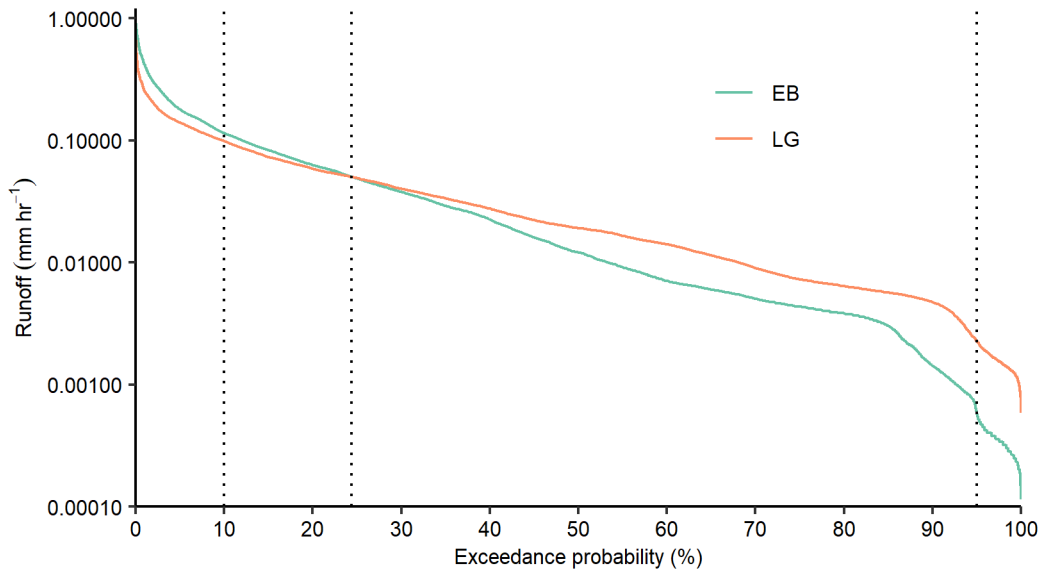
Figure 5.8. Flow duration curve (FDC) for the Eller Beck (EB) and Long Grain (LG) catchments, based on hourly runoff data from 01/10/2018 – 30/09/2020. Runoff (mm hr^{-1}) is per m^2 of catchment area. Dotted lines mark the high flow threshold (Q10), low flow threshold (Q95) and where EB and LG diverge (Q24.4). Note the log scale on the y-axis.

5.3.3.2   *Storm events*

Through the baseflow-quickflow partitioning, we identified 40 storm events with single-peak hydrographs which facilitated the comparison in storm response parameters between EB and LG. Hydrograph lengths (HG) ranged between 33 hours and 12 days and did not differ significantly (W = 779, p = 0.8436) between EB (Mdn = 97 hrs) and LG (Mdn = 91 hrs). While PeakR was significantly lower (-35%) at LG (Mdn = 0.24 mm hr^{-1}) that at EB (Mdn = 0.37 mm hr^{-1}) (W = 1113, p < 0.001), TotR did not differ significantly between the two catchments (W = 955, p = 0.1371). Likewise, no significant difference was found in TotBF (W = 846.5, p = 0.658), though EB (Mdn = 4.8 mm) released significantly more total quickflow (TotQF) during storm events than LG (Mdn = 3.4 mm) (W = 1041.5, p < 0.05) (Figure 5.9). Similarly, storm BF:QF ratios were significantly higher (+33%) at LG (Mdn = 2.0) than EB (Mdn = 1.5) (W = 549, p < 0.05), reiterating that LG released less quickflow during storm events than EB, though this did not result in differences in total runoff between the two sites.

Lag times were analysed between peak runoff and the start of rain (Lag-StartP-PeakR), peak rainfall (Lag-PeakP-PeakR) and the start (Lag-BF-PeakR) and end (Lag-PeakR-BF) of the hydrograph when quickflow was zero. Wilcoxon rank-sum tests revealed that LG had significantly longer lag times that EB for parameters Lag-StartP-PeakR (W = 529.5, p-value < 0.01), Lag-PeakP-PeakR (W = 321.5, p-value < 0.001) and Lag-BF-PeakR (W = 530, p-value <

0.01), while Lag-PeakR-BF did not differ significantly (W = 867.5, p-value = 0.519) between the two sites. In addition, RiseRate_R (W = 1315, p-value < 0.001) and FallRate_R (W = 517, p-value < 0.01) of the hydrograph were significantly faster at EB than at LG, signifying a flashier hydrograph at EB and a more subdued curve at LG.
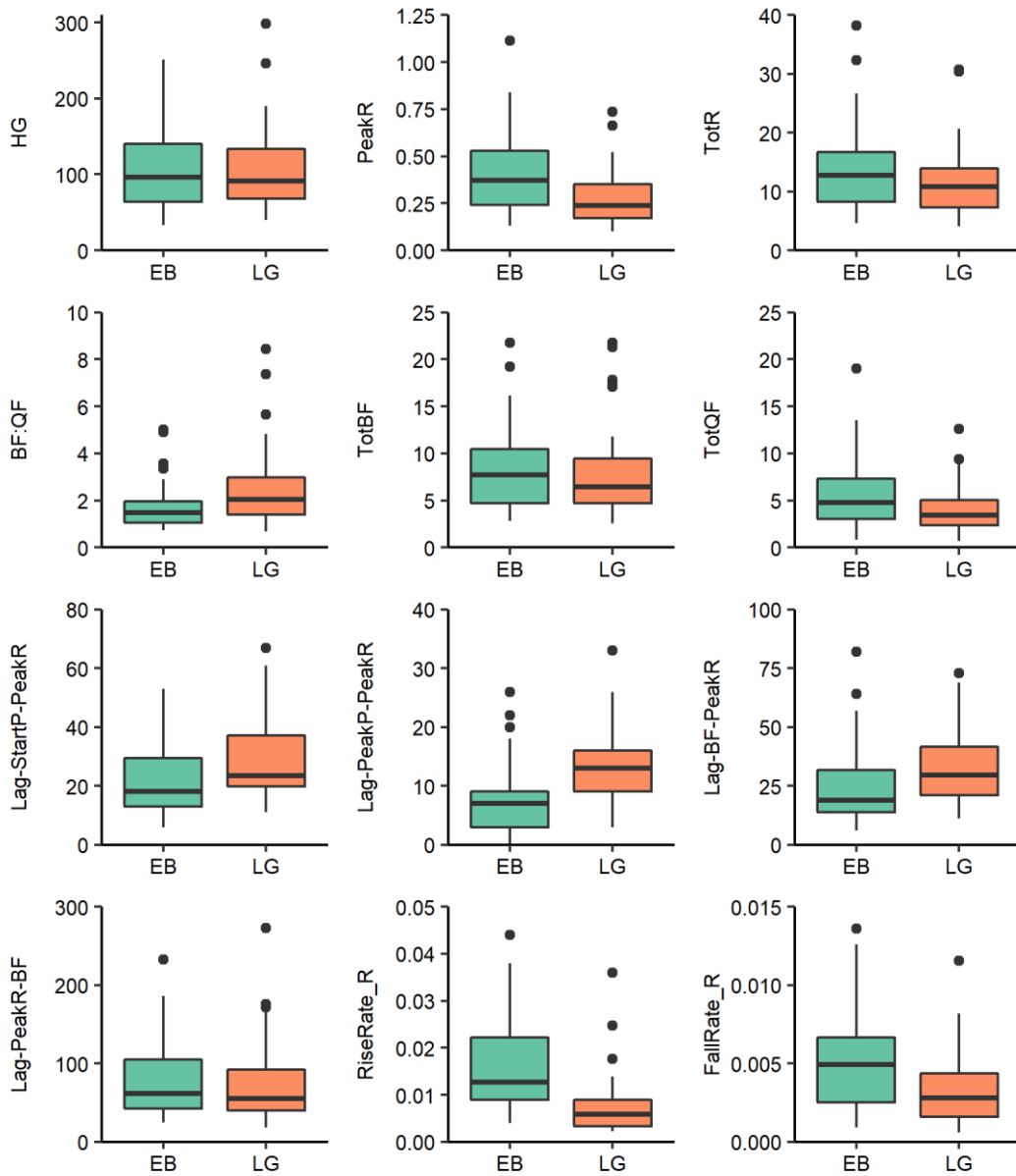
Figure 5.9. Comparison between Eller Beck (EB) and Long Grain (LG) storm response parameters. Refer to Table 5.1 for descriptions of parameters.

Among the 40 identified storm events, lag times (Lag-PeakWT-PeakR) between peak water level at the MS and EB dipwells and peak runoff at the EB weir and between peak water level at the LG and GA dipwells and peak runoff at the LG weir were analysed only where the water level was not zero at the start of the hydrograph, in order to avoid instances where the peat was already saturated at the beginning of the hydrograph. The number of events not rejected amounted 32 events for MS (80% of identified storm events), 9 events for EB (23%), 21

events for LG (53%) and 5 events for GA (13%). Lag-PeakWT-PeakR times increased in order from MS, EB, LG to GA (Figure 5.10). ANOVA tests indicated significant differences ($F_{(3,63)} = 4.16$, $p < 0.01$, w = 0.12) among the four dipwells, and a post-hoc Tukey test showed Lag-PeakWT-PeakR to be significantly longer at GA compared to EB ($p < 0.05$) and MS ($p < 0.01$), while no significant differences were found between the other dipwell sites.
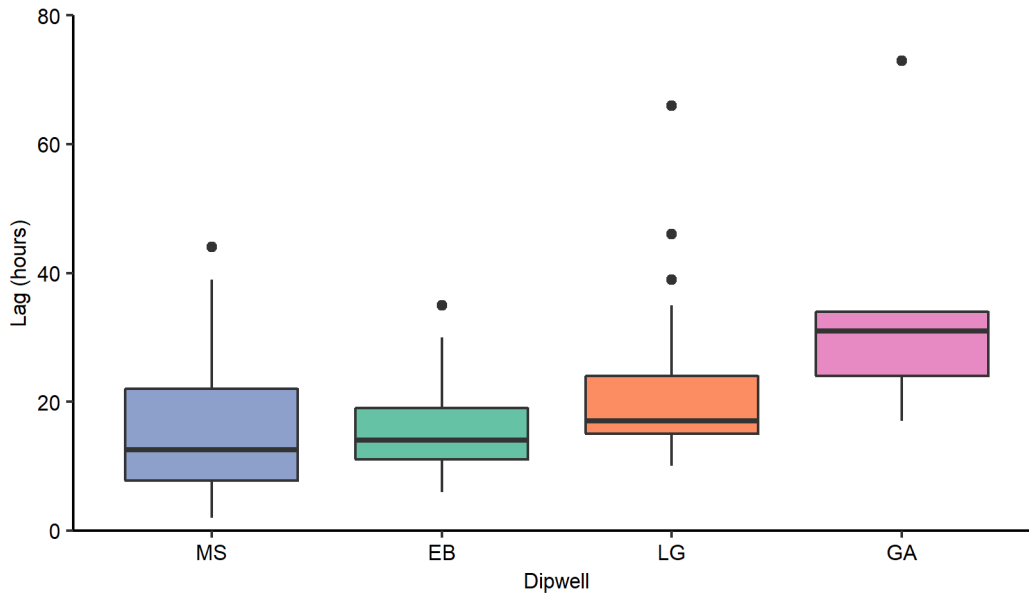
Figure 5.10. Mean and range of lag times (hours) between peak water level and peak catchment runoff. Data points numbered N(MS) = 32, N(EB) = 9, N(LG) = 21 and N(GA) = 5.

5.3.4   Water table

5.3.4.1   Dipwell comparison

Annual average WTDs were within 11 cm from the surface at all sites across all three years. The deepest summer water tables were recorded in 2017/18 at all sites (Table 5.3). Water levels averaged at −73 ± 99 mm at the MS dipwell, −56 ± 73 mm at the EB dipwell, −74 ± 71 mm at the LG dipwell, and −37 ± 58 mm at the GA dipwell, based on the three (two for GA) complete hydrological years. As the four water level series did not show homogeneity of variance (Fligner-Killeen: chi-squared = 425.66, df = 3, p-value < 0.001), a Kruskal-Wallis test was performed to assess for differences in median between the four series which confirmed a significant difference (Kruskal-Wallis: chi-squared = 379.21, df = 3, p-value < 0.001). A post-hoc pairwise Wilcoxon signed-rank test showed that median water tables at GA were significantly higher than at the other three sites ($p < 0.001$) and that EB dipwell water levels were significantly shallower than at MS and LG ($p < 0.001$). Water levels did not differ significantly between the MS and LG dipwells (p = 0.25).

Percentile water levels at the four dipwells revealed that water tables are within 5 cm from the surface for 60% of the time for the MS and EB dipwells, 45% of the time at LG dipwell and 75% of the time at GA dipwell (Figure 5.11). Kendall's tests indicated significant correlations between monthly average WTDs and available water (P – ET) in decreasing order of strength from EB ($\tau = 0.52$, $p < 0.001$), MS ($\tau = 0.46$, $p < 0.001$), GA ($\tau = 0.44$, $p < 0.001$) to LG ($\tau = 0.34$, $p < 0.001$) (Figure 5.12).
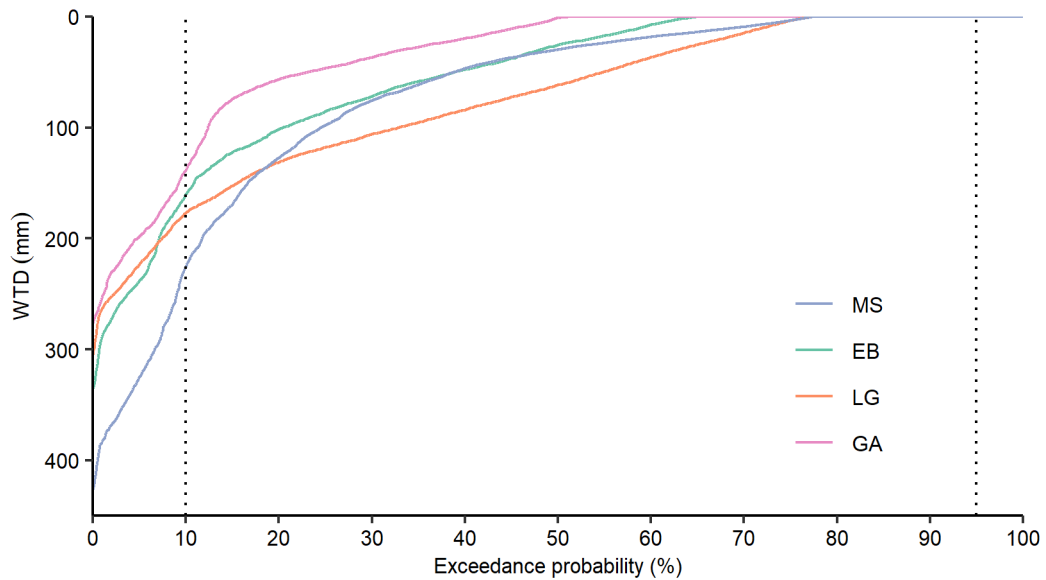
Figure 5.11. Water level duration curve (WLDC) for the meteorological station (MS), Eller Beck (EB), Long Grain (LG) and Great Arc (GA) dipwells. WLDCs for MS, EB and LG based on 2017/18, 2018/19 and 2019/20 data, and WLDC for GA based on 2017/18 and 2018/19 data.
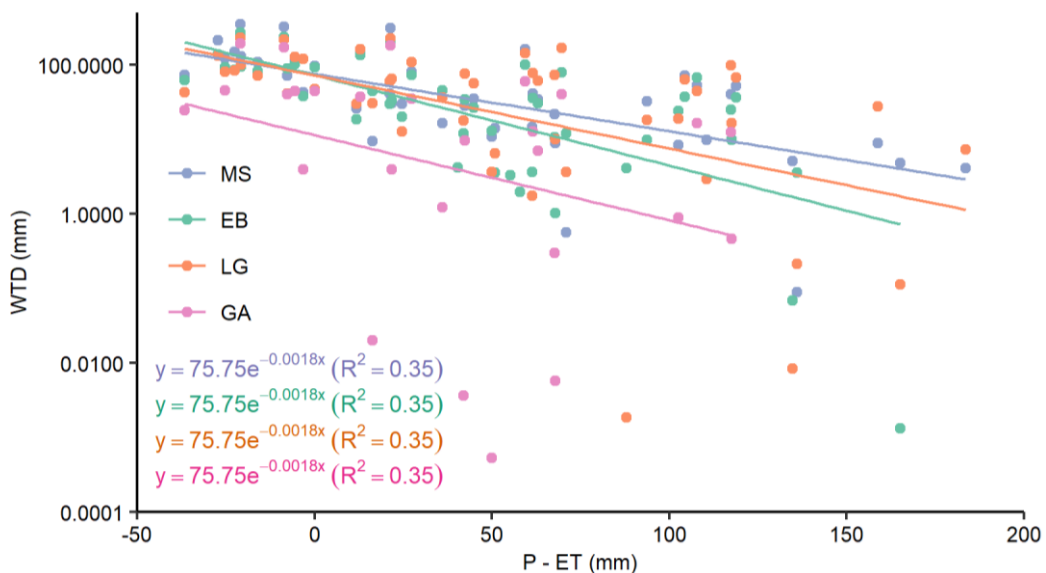
Figure 5.12. Relationship between available water (P – ET) (mm) and water table depth (WTD) (mm) at the MS, EB, LG and GA dipwells. WTD (mm) in log-scale, with higher values reflecting greater depths.

5.3.4.2 Drawdown events

Between March 2017 and June 2021, 12 drawdown events were identified, for which parameters (Table 5.2) were compared between the four dipwells (GA data existed for seven of these events). ANOVA tests indicated no significant differences among the four dipwells in terms of parameters DE ($p = 0.88$), Trough ($p = 0.0877$), Tot-Fall ($p = 0.172$), Fall-Lag ($p = 0.804$), Rise-Lag ($p = 0.982$), Rise-Rate_WT ($p = 0.563$), but significant differences in parameters Tot-Rise ($F_{(3,39)} = 3.59$, $p < 0.05$, $w = 0.15$), Fall-Rate_WT ($F_{(3,39)} = 3.50$, $p < 0.05$, $w = 0.15$). Subsequent Tukey tests highlighted that Fall-Rate_WT was faster, though not significantly, at MS compared with LG ($p = 0.0566$) and GA ($p = 0.0514$) and that Tot-Rise was significantly greater at MS compared to GA ($p < 0.05$).

5.4 DISCUSSION

5.4.1 Water balance residuals

The hydrological timeseries (14/03/2017 – 01/07/2021) encompassed precipitation, evapotranspiration, as well as runoff and water table depths for paired intact (EB) and restored (LG) catchments, facilitating the comparison of water balance components between the two sites. Both catchments tended towards positive water balance residuals, indicating an excess of inputs (precipitation) relative to outputs and storage change. Full water balance closure can be difficult to achieve, and residuals are commonly treated as a "drainage" or "leak" output term (Lapen et al., 2000; Rydin and Jeglum, 2013). The residuals from EB and LG could thus encompass a range of factors, such as genuine positive net inputs, as is generally required for the long-term development of active mire systems (Lindsay, 1995), measurement uncertainty around the quantified water balance components (Isabelle et al., 2018) and unidentified outflows which did not exit the peat ahead of the weir, such as by peat pipes (Holden and Burt, 2002c). The May Moss peat deposits accumulated on top of Jurassic sandstone bedrock (Atherden, 1979), making groundwater seepage a potential outflow route as well. Steam bed seepage to subsurface layers could likewise have contributed to positive residuals. The significant negative correlations between monthly residuals and storage change, evapotranspiration and temperature imply that greater unaccounted losses were associated with net water table drawdown, as well as cooler, less evaporative conditions. The contradiction in association with both greater water table drawdown and cooler, less evaporative conditions, suggests the presence of two separate "pathways" which could explain unaccounted water losses.

Firstly, the negative correlation between residuals and ET and temperature could imply an underestimation of evaporative losses in cooler months. This underestimation could be related to generally higher proportions of rejected Bowen ratios, used to quantify ET in the BREB method, during night-time hours (*Chapter 3*), which make up a higher proportion of days in winter. Peacock and Hess, (2004) have highlighted the risk of underestimating ET based on the assumption that night-time ET is zero, although others have indicated that night-time ET from ombrotrophic peats is largely negligible (Campbell and Williamson, 1997; Thompson et al., 1999; Shuttleworth, 2007), suggesting that the rejection of night-time ET should not have a considerable impact on annual totals. The absence of a significant correlation between residuals and storage change at the May Moss meteorological station (MS) (*Chapter 4*) situated near the watershed, further suggests that rather than being associated with an underestimation of ET, residuals may be related to an underestimation of runoff, as the EB and LG dipwells are situated further down their respective catchments and thus more closely coupled to changes in flow. Runoff tends to be higher in winter than summer, as lower evaporative losses and shallower water levels result in excess precipitation being rapidly directed away as runoff rather than maintain baseflow (Evans et al., 1999). The negative relationship between greater residuals and lower ET losses could therefore be suggestive of seasonal underestimations of runoff over the winter-half of the year. As runoff estimates were based on hourly recordings and upland blanket mires tend to be characterised by a rapid, "flashy" runoff regime (Holden and Burt, 2003b), it is highly likely than high runoff and especially peak flows were missed, leading to a systematic underestimation of annual runoff.

Secondly, the significant correlations between monthly residuals and storage change found at both sites, suggest that changes in peat moisture could account for a proportion of residuals (*Chapter 4*). Peat storage change encompasses both the fluctuation in water level as well as variations in peat moisture content (McCarter and Price, 2013), the latter of which we did not account for. Peat water content, especially in the shallow subsurface layer below hollows, can vary considerably (100 – 55%) in line with water level fluctuations, with Kellner and Halldin (2002) showing a reduction in peat water content from saturation (100%) to 55% related to a drop in water levels to 200 mm below the surface. As water levels, particularly in summer, were found to drop below 200 mm at both EB and LG, reductions in peat water content could likely have explained a proportion of positive residuals for both sites.

5.4.2 Runoff and storm response

Catchment characteristics that could have influenced variations in flow between the two catchments include stream order, relief, and size (Strahler, 1957; Brinson, 1993). Both Eller Beck and Long Grain are first-order upland headwater streams and should present similar "flashy" runoff behaviour (Flynn et al., 2021b). Surface elevation ranged approximately between 240 and 265 m in the EB catchment and between 245 and 285 m in the LG catchment (Figure 1.4), resulting in topographic relief of 25 m and 40 m, respectively. Steeper surface gradients typically drive higher overland runoff, while gentler slopes have been found to facilitate the development of underground peat pipes (Holden, 2009). However, at EB and LG the areas of deep peat are primarily located within the mid-lower reaches of the catchment, in an area of relatively low relief (Figure 1.3), suggesting that hydrological regimes associated with peat would be governed mainly within the low relief areas of both catchments. Finally, the LG catchment (1.53 km^2) is notably more than twice the size of the EB catchment (0.63 km^2), which could relate to differences in water travel time. Hydrological responses within such small catchments are known to be highly variable (Pilgrim et al., 1982; Stott, 1997), though more recent studies have found other parameters, such as rainfall intensity and hydraulic conductivity, to be of greater importance in influencing travel time than catchment size (Segura et al., 2012; Jutebring Sterte et al., 2021). To offset any potential linear relationships between catchment area and hydrological processes, such as travel time (Segura et al., 2012), runoff was corrected by catchment area (Hope et al., 1997; Worrall et al., 2012).

Annual runoff/rainfall coefficients at EB (0.34 ± 0.14) and LG (0.33 ± 0.02) resemble the mean runoff coefficient of 0.4 given for the Trout Beck catchment at Moor House NNR (Evans et al., 1999) and reflect the high proportion of precipitation that is transferred rapidly to streams by overland flow in upland peat catchments (Holden and Burt, 2003b). Daily total runoff, baseflow and quickflow were all significantly higher at the restored catchment (LG) compared to the intact catchment (EB), although this contrast did not translate to monthly timescales. Despite this, BF:QF ratios were significantly higher at the restored site at both daily and monthly timescales. This suggests that while runoff losses may be similar between the two sites, baseflow dominated runoff losses at the restored catchment (LG) and quickflow made up a relatively larger proportion of runoff at the intact site (EB). This contrast in BF:QF ratio was corroborated by the dominance of storm flow ($\geq$ Q10) at EB (54%) making up total annual runoff, compared to LG (43%), and the relatively higher proportions of low flow ($\leq$ Q95) which contributed to annual runoff at LG (0.20%) relative to EB (0.04%).

Relatively higher baseflow rates have likewise been documented at other post-drainage recovering blanket bog sites, compared to intact blanket bogs (Holden et al., 2017; Howson et al., 2021b). Holden et al. (2017) have suggested that these enhanced baseflow rates could be due to increased lateral subsurface flow, because of a larger presence of pipes and macropores caused by drainage and drying of peat (Holden et al., 2006). Similarly, Wallage and Holden (2011) found considerably lower peat bulk density and greater movement of water as throughflow related to 1.5 times higher hydraulic conductivity within the near-surface layer at a restored blanket bog compared to an undisturbed blanket bog in northern England. One explanation for a reduction in bulk density may be related to a rebound effect as peat compression is relieved upon rewetting (Hobbs, 1986). Higher proportions of baseflow relative to total runoff at the recovered site (LG) at May Moss could thus be indicative of residual effects of former drainage and subsequent recovery in enhancing hydraulic conductivity and thus throughflow within the near-surface peat layer.

Across the 40 analysed storm events, the intact site (EB) displayed significantly higher peak runoff, produced significantly more quickflow and had generally shorter lag times than the recovering site (LG). The intact site thus reflects the naturally "flashy" runoff behaviour of upland blanket bogs (Price, 1992b; Holden and Burt, 2003b), with most storm flow comprised of saturation excess overland flow (Holden and Burt, 2003b). The relative "flashy" nature of EB is further exemplified by the greater divergence between the Q10 and Q95 thresholds at EB than at LG, with a greater threshold divergence indicative of a more "flashy" runoff regime (Marsh and Hannaford, 2008; Flynn et al., 2021b). Drainage and afforestation are commonly associated with an increase in peak runoff (Anderson et al., 2000; Robinson et al., 2003; Ballard et al., 2012) and forest harvesting can lead to increases in baseflow (Robinson et al., 2003). Menberu et al. (2018) found that recently (< 5 years) post-forestry rewetted peatland had shorter residence times and higher and quicker peak flow rates compared to undisturbed peat catchments, while Wilson et al. (2010) noted a reduction in peak flows after drain blocking at a Welsh blanket bog. Our results thus suggest that peak runoff at the restored site (LG) has effectively been limited to rates below those of the intact site (EB), while lag times have generally increased. This runoff behaviour could stem from both hydrological recovery 10 years after restoration (Wilson et al., 2010), as well as residual effects of former drainage enhancing baseflow through higher near-surface hydraulic conductivity (Wallage and Holden, 2011).

5.4.3 Water level

Water levels at the GA dipwell (average = −37 ± 58 mm) were at the surface 75% of the time and were significantly shallower compared to the other three dipwells. This is unsurprising, as the GA dipwell was situated beside a sizeable bog pool with dominant *Sphagnum* cover, which was consistently inundated as observed from regular field visits. Nevertheless, the capacity of the restored catchment to sustain a bog pool, with water levels never dropping below −280 mm throughout the monitoring campaign, is indicative of restoration success (Tallis, 1994; Peacock et al., 2013b).

Water levels were at the surface 60% of the time at the MS and EB dipwells and 45% of the time at the LG dipwell, suggesting that, apart from at bog pools (GA), peat saturation was reached less often at the recovered site (LG) compared to the intact site (MS and EB). In addition, daily average water levels were significantly lower at LG dipwell (−74 ± 71 mm) compared to EB dipwell (−56 ± 73), although not differing significantly from the MS dipwell (−73 ± 99 mm). This corroborates the findings by Wallage and Holden (2011), who observed that water levels at a post-drainage restored blanket bog rose considerably upon rewetting but did not reach the surface as frequently (2%) as an intact bog (18%). Similarly, Haapalehto et al. (2014) observed that water levels at a forestry-drained boreal *Sphagnum* peatland recovered to pristine levels within 10 years post-restoration but noted some residual deviation in hydrological functioning related to artificial flow paths created by drainage. Thus, while restoration has clearly raised the water level at the recovering site (LG) to comparable levels at the intact bog (EB), surface water tables were still less frequently observed at the restored site, which may be related to greater hydraulic conductivity and thus lower water retention due to former drainage (Word et al., 2022).

5.4.4 Drought and post-drought recovery

Both catchments had net storage losses (ΔS) over the year 2017/18, driven by considerable storage deficits over the summer related to the severe impact of the 2018 heatwave which caused widespread drought across the UK (Turner et al., 2021). The deepest water tables were reached at the MS (−427 mm), followed by EB (−351 mm), LG (−307 mm) and GA (−280 mm) dipwells in June 2018. The MS dipwell was situated on the watershed of the EB catchment (Figure 1.4). Although the comparison in water level behaviour across 12 drawdown events showed little difference between the four dipwell sites, the analysis did highlight a considerably faster drawdown rate (Fall-Rate_WL) and greater total recharge (Tot-Rise) at the MS dipwell compared to other sites. The behaviour at the MS dipwell,

particularly during deep drawdown events, can most likely be related to its location near the watershed, an area with minimal slope. As lateral flow within peatlands generally slows with shallower slopes (Rydin and Jeglum, 2013), moisture loss due to evaporative demand would be less likely to be replenished by lateral flow at MS, resulting in quicker drawdown rates and a subsequent greater total recharge. However, this hypothesis would need to be verified by comparing hydraulic gradients across the mire catchment.

Storage losses over 2017/18 were 32 mm greater at LG, compared to EB, likely driven by greater annual runoff losses from the restored site, as annual runoff showed the next greatest annual discrepancy between the two sites (greater than the difference in annual residuals), with the annual runoff coefficients being 0.31 for LG and 0.29 for EB. Similarly to 2017/18, annual runoff losses in 2018/19 were greater at LG than at EB, with the latter appeared to have completely compensated storage losses by the end of 2018/19, while LG had recovered 70% of storage losses. The relatively higher runoff losses at the recovering site (LG) during the drought year, as well as the following year, may again confirm a reduced capacity to retain moisture, potentially due to higher hydraulic conductivity across the restored sites within the catchment (Wilson et al., 2010; Wallage and Holden, 2011; Word et al., 2022), but also highlights the impact of these altered peat properties to hydrological behaviour during drought and post-drought recovery.

Storage changes in 2019/20, a year characterised by considerable higher annual precipitation (1110 mm) compared to the previous two years, were near negligible at both catchments, suggesting that both sites had recovered their water balance from the effects of the 2018 summer heatwave. It is noteworthy, that EB had a runoff coefficient of 0.50 for 2019/20, compared to 0.36 at LG, indicating that the intact site (EB) released half of annual precipitation as runoff and nearly 1.5 times as much as the restored catchment (LG), which again alludes to subtle differences in the post-drought recovery between the two sites. The considerable increase in the annual runoff coefficient in 2019/20, two years following a severe drought summer, suggests that peat moisture in the EB catchment had fully recovered, resulting in more precipitation being directed away as saturation excess overland flow (Evans et al., 1999; Holden and Burt, 2003b). This corroborates the concept that the seasonal return of water levels to near surface-level over the winter months and thus the hydrological independence of summers and winters facilitate the rapid post-drought hydrological recovery of intact peatlands (Worrall et al., 2006). Conversely, the much lower runoff losses at LG in 2019/20 may be due to lower moisture retention during the previous two years as a result of previous drainage (Robinson et al., 2003; Holden et al., 2017) and

consequently may highlight a longer post-drought recovery process with the restored catchments (LG).

5.5 CONCLUSION

Here we used a four-year paired hydrological series, comprising precipitation, evapotranspiration, runoff, and water levels, to compare the hydrological functioning of a post-forestry restored blanket bog with that of an adjacent intact blanket mire based on a paired catchment approach. Water balances were computed for three complete hydrological years: 2017/18, 2018/19 and 2019/20, with an average of 930 mm of precipitation and 335 mm of evapotranspiration. Annual total runoff averaged 313 mm at the recovering catchment (LG) and 334 mm at the intact sites (EB). Annual storage change (ΔS) averaged at -27 mm at the recovering catchment (LG) and -1 mm at the intact sites (EB). While both catchments thus appear close to zero in their annual ΔS, particularly considering the drought event within the paired monitoring period, the difference in ΔS nevertheless suggests that the intact site is more hydrologically balanced than the recovering site. Annual water balance residuals indicated net unaccounted losses, which most likely derive from measurement error, in particular an under-sampling of winter high runoff events, underestimation of surface water evaporation or changes in peat moisture with water table drawdown in summer.

Water table depth (WTD) averaged at -74 mm near the centre of the recovering bog, resembling mean water levels measured at the watershed of the intact bog (-73 mm), but 32% lower that water levels measured in the centre of the intact bog (-56 mm). Nevertheless, the recovering site is able to support a sizeable bog pool, adjacent to which water levels averaged at -37 mm (GA dipwell). The difference in average water levels between the MS dipwell, at the watershed, and EB dipwells, within the centre of the bog, may be related to differences in rates and replenishment of subsurface lateral flow. Water tables were within 5 cm from the surface 60% of the time for the MS and EB dipwells, 45% of the time at LG dipwell and 75% of the time at the bog pool on the recovering site (GA dipwell). Thus, while restoration has raised the water level at the recovering site (LG), surface water tables were still less frequently observed than at the intact bog, which may be related to greater hydraulic conductivity and lower water retention as a result of former drainage.

Baseflow made up a significantly higher proportion of total runoff at the recovering site, compared to the intact bog, which may be related to residual effects of former drainage in

enhancing lateral subsurface flow. The comparison of storm runoff behaviour between the two sites indicates that the recovering catchments behaves less "flashy", with a relative reduction of peak runoff by 35%, longer lag times between the start/peak rain and peak runoff and a slower rise and fall rate in storm runoff. This would suggest that restoration techniques, including tree removal and drain-blocking, have been effective at reducing the relative intensity of storm runoff to levels below those observed at the adjacent intact catchment. The 2018 drought event and post-drought water balances emphasize the rapid hydrological recovery of an intact blanket mire following a summer with severe water table drawdown. In comparison, the restored site was characterised by relatively higher runoff/rainfall coefficients during the drought and subsequent year, suggesting lower water retention and a comparatively longer post-drought recovery process. Further research involving prolonged hydrological monitoring of post-forestry bog restoration is therefore necessary to establish their relative resilience to drought events and potential drying trends related to climate change.

Chapter 6. Forest-to-bog restoration II. Stream-water chemistry

ABSTRACT

Restoration of formerly forested peatlands aims to reverse the effects of forestry on the hydrological functioning with concomitant impacts on the water quality of stream-systems draining the peatlands. By removing the forestry and blocking ditches, restoration practitioners aim to raise the water tables and facilitate the (re-)establishment of 'pristine' hydrological and biogeochemical functioning. Using paired intact and post-forestry recovering catchments at May Moss, a relatively dry blanket bog on the North York Moors, a two-year water sampling campaign was carried out from 18/07/2018 to 27/08/2020, collecting stream-water samples every two-four days from streams draining the intact (EB) and restored (LG) sites. Water samples were analysed for dissolved organic carbon (DOC), dissolved nitrogen (DN), particulate organic carbon (POC), particulate nitrogen (PN), loss-on-ignition (LOI, %) and UV-vis absorbance. Powders collected by freeze drying the water samples were analysed for humic substances (HS) and 32 element concentrations measured by X-ray Fluorescence (XRF).

Stream-water DOC concentrations and discolouration were at significantly lower levels at the restored site, compared to the intact site, while POC concentrations were similar between both sites, which suggests that post-forestry restoration has been effective in limiting fluvial carbon loss below pristine levels. Reduced DOC concentrations may be related to enhanced flushing or changes in microbial activity and thus connected to impacts of previous forestry activities and drainage. In addition, residual effects of previous forestry activities are detectable for most analysed elements through their relative enrichment within the dry mass extracted from stream samples, including Na, Mg, Al, Si, S, Cl, K, Ca, Cr, Mn, Ni, Zn, Rb, Sr, Y, Zr, Ba and Hg, which are most likely related to disturbance of the upper peat profile and thus enhanced mixing with layers characterised by more mobile elements. Conversely, elements with strong sub-surface peat enrichment, including P, Cu, As and Pb, are at higher dry mass concentrations at the intact site, indicating that shallow sub-surface flow is likely dominant at both catchments. Despite relative element enrichments within the extracted dry mass, the relatively lower DOC concentrations and likely enhanced flushing mean that most elements are at reduced stream-water concentrations at the restored site,

relative to the intact bog. Residual impacts of forestry and harvesting operations are still detectable at the restored LG site through relatively enhanced stream-water concentrations of Al (twice as high as EB), S, Cl, Ca and Sr in stream samples, compared to the adjacent intact EB site. Thus, while the restored catchment presents lower stream-water DOC and equivalent POC concentrations compared with the adjacent catchment draining mostly intact blanket bog, it is uncertain whether this difference is due to the recovery of hydrological and biogeochemical processes or residual impacts of former disturbance to the peat profile and ecology. Further research is therefore key to assess linkages between peat disturbance, DOC production and mobilisation and stream-water chemistry.

6.1 INTRODUCTION

Increased awareness of the importance of intact peatlands as longer-term stores of global carbon and their role in regulating water quality has led to growth in the number of peatland restoration projects around the world. In the UK, upland blanket bogs have historically been used for forestry plantations, most commonly using Sitka spruce (*Picea sitchensis*) and lodgepole pine (*Pinus contorta*), with intense planting occurring between the 1950s and 1980s (Cannell et al., 1993; Sloan et al., 2018a). However, the drainage and afforestation of blanket bogs has been linked to severe peat subsidence, alteration of nutrient dynamics, changes in hydrological flow paths, and carbon loss through peat oxidation and decomposition (Byrne and Farrell, 2005; Lewis et al., 2013; Sloan et al., 2018a; b). In addition, drainage and forestry activities on peatlands have been associated with declines in water quality related to increases in the release of dissolved organic carbon (DOC), nutrients and metal pollutants into stream systems (Cummins and Farrell, 2003; Rodgers et al., 2010; Kaila et al., 2012; Asam et al., 2014b; Marttila et al., 2018), surface water acidification (Evans et al., 2014b), with implications for drinking water treatment (Ledesma et al., 2012; Ritson et al., 2014).

The water-courses draining peatlands, both intact and perturbed by human impacts, are typically of stronger yellow-brown colouration reflecting the concentrations of typically acidic dissolved organic carbon (DOC) in surface waters (Hope et al., 1997; Aitkenhead et al., 1999; Worrall et al., 2003). Humic and fulvic acids are examples of the complex and heterogenous mixtures of materials produced naturally within peatlands during humification, in which plant and animal remains are transformed through a range of biochemical and abiotic pathways (Zaccone et al., 2018). Patterns in the humification of peat are a complex series of responses to differences in the peat-forming vegetation,

hydroclimate, peat depth, trophic status, pH, and age. Production of humic compounds is heavily affected by variations in the water table given the association with the acrotelm – catotelm structure that typifies peatlands (Clymo et al., 1998). The acrotelm is the upper 'active' zone of peat sequences where fresh plant material is added and where most decay takes place. Beneath this, the catotelm extends, with minimal decay of organic matter (Ingram, 1978). Broadly, the acrotelm – catotelm boundary is often equivalent to water table depth and regulates the extent of aerobic and/or anaerobic conditions. However, these functional layers have diffuse boundaries and the active zone may vary both with time and space (Holden and Burt, 2003a; Morris et al., 2011). Perturbations of peatland water tables are further complicated by human intervention, both in the drainage activity in preparing for forestry and raising of water table implicit in restoring former peatlands from forestry, affecting a complex biogeochemical setting. The raising of water levels through post-forestry restoration has the capacity to reduce carbon loss as CO_2 from aerobic decomposition, however rewetting is also associated with an increase in methane (CH_4) emissions due to increased activity of methanogenic bacteria under anaerobic conditions. This has led to conflicting discourses on the relative benefits of peatland afforestation and restoration on greenhouse gas (GHG) emissions (Hargreaves et al., 2003), with some highlighting a risk of high methane emissions upon rewetting while simultaneously accumulating carbon (Hemes et al., 2018), while others have found peatland rewetting to encompass net benefits in GHG fluxes reducing climate warming (Günther et al., 2020).

Increasing concentrations of DOC have affected many surface waters across the northern hemisphere (Worrall et al., 2003; Evans et al., 2005). For peatland catchments, which are typically rich in DOC, these conditions most likely have a longer narrative spanning the acidification and paludification as peatlands established and begun accumulating over millennia (Barber, 1993). That said peatland streams drain towards systems often used for drinking water in many countries and high DOC concentrations has implications for water treatment processes (Ledesma et al., 2012). Heavy metals and other contaminants are transported with DOC and, if treated incorrectly, can produce carcinogens (Ledesma et al., 2012). Brown colour waters also invoke negative aesthetic concerns over colour, taste, and odour by the public in relation to both recreational and drinking waters (Volk et al., 2002).

As forest-to-bog restoration is a relatively recent activity, having developed only in the last three decades, studies on the biogeochemistry of restored ombrotrophic peatlands and their associated water-courses are still few in number. However, with awareness of the importance of peatlands increasing, the number of restoration projects is rising, and with

data from decade-old rewetting projects now available, the number of published studies on the impacts of forest-to-bog restoration on their biogeochemistry is now likewise increasing, e.g. Haapalehto et al. (2011, 2014); Koskinen et al., (2011, 2017); Kaila et al. (2016); Gaffney et al. (2018, 2020, 2021, 2022); Sloan et al. (2018a); Howson et al. (2021a); Pickard et al. (2021).

Some have observed sudden increases in nutrient loading and DOC release upon deforestation related to peat disturbance and high nutrient availability in brash (Koskinen et al., 2017; Gaffney et al., 2020). However, longer-term studies have generally noted reductions in nutrients within the shallow peat layer. For example, Haapalehto et al. (2011), who found that Ca, K, Mg and Mn in shallow (0 – 20 cm) peat core samples from a restored bog in Finland had reached comparable levels to a pristine bog 10 years after rewetting. Most studies however have focused on a limited number of water quality parameters and elements (e.g. Haapalehto et al., 2011, 2014; Gaffney et al., 2018, 2022; Howson et al., 2021)) with limited scope of intra-annual hydrological processes including drawdown and runoff events.

The paired catchment structure afforded by recent management of May Moss on the North York Moors provides an opportunity for a comprehensive comparison encompassing a wide range of water quality parameters and elements between tracts of intact (Eller Beck) and restored (Long Grain) blanket bog. Using the paired intact and forest-to-bog recovering catchments at May Moss thereby samples a SITA-Trust Enriching Nature funded peatland restoration initiative for a relatively dry blanket bog on the North York Moors. Hydro-meteorological data (e.g., temperature, windspeed, rainfall, the radiative regime, evapotranspiration (ET) and water tables) have been collected on the watershed on May Moss since August 2010 characterising the hydrological functioning of the intact blanket bog. Monitoring of hourly runoff from 14/03/2017 to 01/07/2021 facilitated water budgets for both catchments. Paralleling this extensive monitoring of peatland water tables and runoff for the two catchments, a two-year water sampling campaign was carried out 18/07/2018 to 27/08/2020 collecting stream-water samples every two days from systems draining the intact and restored sites. Here, we seek to assess the impacts of post-forestry restoration of a blanket bog on stream-water quality compared to an adjacent intact blanket mire, by quantifying stream-water concentrations of DOC, POC, humic substances (HS) and major element concentrations, both in terms of their dry mass and stream-water concentrations, followed by a comprehensive principal components analysis (PCA) in order to examine and

compare the relative response of a restored blanket bog to changes in hydrological condition, including a drought summer.

6.2 METHODS

6.2.1 Study site

The study site is May Moss, a water-shedding ombrotrophic blanket mire situated at ≈250 m O.D. within the North York Moors, UK (Figure 1.3). The mire comprises two basins draining a watershed feeding the headwaters of the Eller Beck (EB), draining largely intact blanket bog, and Long Grain (LG), draining for the most part former conifer plantations (Figure 1.4). Peat development was initiated at May Moss in these basins feeding Eller Beck and Long Grain approximately 9 ka during the early Holocene (Atherden, 1979). The peat then expanded to paludify, covering the watershed from 3.5 to 3 ka (Chiverrell, 2001). The deepest peats are > 5 m and centre in those basins, with > 2.5 – 3 m of ombrotrophic peat covering the watershed (Figure 1.3). A meteorological station, situated near the watershed of the EB catchment and the centre of the intact blanket bog area, provides hourly air temperature, relative humidity (Campbell Scientific CS215), and wind profiles (Campbell Scientific 03102) at 0.4, 1.0, 2.0 and 3.0 m height, in addition to hourly net radiation (NR-LITE2 Net Radiometer, Campbell Scientific), photosynthetic active radiation (SKP215 Quantum Sensor, Campbell Scientific), soil heat flux (HFP01, Campbell Scientific), atmospheric pressure (HOBO U20 Water Level Logger, ONSET) and precipitation (ARG100, Campbell Scientific). The meteorological array has thus facilitated the calculation of hourly evapotranspiration (ET) using the Bowen ratio energy balance (BREB) method (*Chapter 3*).

6.2.2 Hydrology

The hydrological series for both the EB and LG catchments comprised hourly runoff and WTD series spanning 14/03/2017 – 01/07/2021. V-notch weirs were installed at the stream exits for both blanket bog areas (Figure 1.4). Dipwells, containing automatic logging pressure transducers (HOBO U20 Water Level Logger, ONSET), were placed directly upstream of the weirs and facilitated the calculation of hourly discharge by calibrating the recorded sensor depths with manual head measurements at the weirs (*Chapter 5*). Catchment areas contributing to the EB and LG weir sites were delineated from an OS Terrain 5 DTM (Ordnance Survey, 2020) using ArcGIS. Hourly runoff (mm) normalised for catchment unit area were calculated by dividing hourly discharge by the catchment area.

Hourly water table depths (WTDs) across the EB and LG catchments were recorded using four waterproof pressure transducers (HOBO U20 Water Level Logger, ONSET and PDCR 1830, Campbell Scientific) inside perforated dipwells, with two sensors situated within each catchment: EB and MS on the intact site and LG and GA on the restored site (*Chapter 5*). A gap (43 days) in the MS WTD series in spring 2018 was filled by linear regression ($R^2 = 0.93$) with the EB WTD series (*Chapter 3*) and a gap (103 days) in the EB and LG runoff series were filled by linear regression (EB $R^2 = 0.32$; LG $R^2 = 0.28$) with the EB and LG WTD series (*Chapter 5*), respectively.

6.2.3   Water sample collection and preparation

Synchronous water samples ($\approx$ 1 L) were collected at the EB and LG weirs using automatic water samplers (ISCO Teledyne), each containing 24 bottles (1 L capacity), every two days from 18/07/2018 to 23/02/2020 and then every four days until 11/06/2020, with a final grab sample taken at each site on 27/08/2020. The ISCO samplers were embedded ≈0.3 m into the peat to ensure a cool sample storage chamber until collection every ≈48 days. A further 5 L grab sample was taken at each weir during the sample collection visits using heavy-duty PVC water carriers (5 L capacity), which were pre-rinsed three times with sample water before collection.

Within 72 hours of collection, ≈200 ml of the samples was measured for volume and vacuum-filtered using pre-combusted (450°C for 4 hours) Fisherbrand microglass fibre filters (0.7 μm pore size, 47 mm diameter). Glassware were rinsed between samples, to reduce cross-contamination between samples. The filtered waters were scanned immediately for their ultraviolet-visible (UV-Vis) absorbance spectra at 2 nm resolution using a UV-Vis spectrophotometer (Thermo Scientific Evolution 300), with a sample cuvette rinsed three times with double-distilled water and then three times with filtered sample prior to each scan. The filters were freeze-dried and subsequently stored at −20°C prior to particulate organic carbon (POC), total particulate carbon (PC) and total particulate nitrogen (PN) analysis. A 20 ml subsample of the filtered waters were placed in glass vials and acidified for preservation using 0.2 μL of 50% hydrochloric acid (HCl) (v/v), and then stored at 4°C until analysis for dissolved organic carbon (DOC) and dissolved nitrogen (DN).

The remaining ≈700 ml of unfiltered water sample was measured for volume and placed and placed inside resealable polyethylene bags and freeze-dried. The dried materials comprised typically a brown powder recovering both the particulate and dissolved load from the water. The water driven-off and collected in the 15 L ice chamber of the Mechatech LyoDry Midi

Freeze Dryer Condenser was consistently white/clear ice. The residual dry weights of the powders were then measured in preparation for NIRS and XRF analyses. The dry masses and compositions of the dry powders were expressed as concentrations by dividing by the original water volume of each freeze-dried sample.

Ten water samples from EB (two in April 2019 and eight in July 2019) and five samples from LG (all in July 2019) contained excessive amounts of algae, which had most likely been drawn up by the autosampler during extremely low flow conditions and potentially grown further inside the bottles. As the presence of algae was most likely representative of ponding behind the weir and the runoff, these samples could distort the water chemistry data and were therefore excluded from the study.

6.2.4   DOC and DN

The filtered and acidified water samples were analysed for DOC and DN using high-temperature catalytic oxidation (HTCO) on a Shimadzu TOC-V/TDN analyser. DOC and DN concentrations were determined from 5-point calibration curves using daily prepared standards of potassium hydrogen phthalate (KHP) and glycine, respectively. Injections with MilliQ water between sample injections ensured rinsing of the system and leucine injections after every 5 samples were used to ensure there was no drift during sample runs.

6.2.5   POC, PC and PN

Two core (Ø 4 mm) samples were taken from each freeze-dried filter, with one core analysed for POC and the other for PC and PN. Prior to analysis, the POC filter core was subjected to vapour phase de-carbonation using 12 N Analar Grade HCl (Yamamuro and Kayanne, 1995). The two filter cores were then analysed for POC, PC and PN using a Thermo Scientific FlashSmart Organic Elemental Analyser. A daily two-point calibration was performed using High Organic Sediment Standard OAS (Elemental Microanalysis Ltd), which was then analysed twice as an 'unknown'. The results for the 'unknown' were always within uncertainty limits of the certified value which are 7.17 ± 0.09% carbon and 0.57 ± 0.02% nitrogen. Certified values were determined by elemental analyser calibrated to Cystine 143d from the National Institute of Standards and Technology (NIST), Maryland, USA.

6.2.6   Analysis of near infrared spectra

Near infrared spectra (NIRS) were measured for all dried water samples using a Bruker MPA Fourier transform near-infrared spectrometer by diffuse reflectance using an integrating

sphere. Each sample was homogenised by grinding and lightly hand pressed on a microscope slide for each measurement. All NIR spectra are the product of 64 scans at an 8 cm^{-1} interval across the range 3595 – 12500 cm^{-1}. Sample spectra were processed through multiple regression of the NIR spectra for a selection of known composition end-member materials (EM-MR) (Russell et al., 2019) with equivalent NIR spectra derived for our unknown composition dried water samples. The selection of end-members was tailored to reflect the major components expected in the dried waters. This process included sensitivity (leave-out) analysis of the end-member selections to obtain the overall best fitting performance, defined by high R^2 of each sample multiple regression across the fitted end members.

The organic component of the dried waters was rationalised to three end members: fulvic acid (FA), humic acid (HA) and humin. The FA and HA end-member NIR spectra were derived from IHSS (International Humic Substances Society) Fulvic Acid standard III and Humic Acid standard III from the Suwannee River, and represent the fulvic and humic proportions of DOC. The humin end-member was a chemical extract from a May Moss dried peat sample, separated as the acid (HCl) and alkali (NaOH) insoluble material, and represents the less decomposed particulate organic matter (POM). Fitting of an end-member reflective of local sandstone bedrock produced poor fitting, which reflects the dominantly organic nature of the dried waters. Likewise, a biogenic silica end-member, essentially diatoms treated with H_2O_2 to remove any organic material, showed very poor fitting, a function of low biogenic silica content. Thus, neither a biogenic silica or mineral end member were used in the NIRS EM-MR calculations, which returned relative proportions (%) present in the dried water samples for i) fulvic acid (FA), ii) humic acid (HA) and iii) humin.

6.2.7 Analysis of UV-Vis absorbance spectra

Linear regressions between DOC concentration measured by high-temperature catalytic oxidation (HTCO) on a Shimadzu TOC-V/TDN analyser and UV-Vis absorbance spectra for the same samples were used to find the best-fit wavelength, identified as having the highest R^2 value, which best describes the DOC concentrations in the water samples of EB and LG. The ratios SUVA$_{254}$ and E4:E6 were computed and the Abs$_{400}$ (au m^{-1}) were analysed for each sample. SUVA$_{254}$ is the ratio of specific UV absorbance at 254 nm (measured in m^{-1}) to DOC concentration, which has been used to characterise the composition of DOC and specifically its aromaticity (Weishaar et al., 2003; Peacock et al., 2014, 2018), while the ratio E4:E6 (Abs$_{465}$:Abs$_{665}$) is used as a measure of the proportion of humic to fulvic acids in DOC (Thurman, 1985; Wallage et al., 2006) and was compared to NIRS-derived HA:FA ratios using

the Wilcoxon rank-sum test. The absorbance at wavelength 400 nm (Abs_{400}) is used to characterise the degree of water colouration (Wallage et al., 2006).

6.2.8   Major element chemistry

Concentrations of 32 elements (Na, Mg, Al, Si, P, S, Cl, K, Ca, Ti, V, Cr, Mn, Fe, Co, Ni, Cu, Zn, As, Br, Rb, Sr, Y, Zr, Sn, Sb, I, Ba, Hf, W, Hg and Pb) were determined for the dried water samples on a dry mass specific basis, using a Spectro XEPOS 3 Energy Dispersive X-ray fluorescence (XRF) analyser. The samples were hand pressed in 20 mm diameter pots and measured under a He atmosphere under combined Pd and Co excitation radiation and using a high resolution, low spectral interference silicon drift detector. Daily standardisation procedures provide a system check on the XRF analyser, with accuracy verified using 18 certified reference materials (Boyle et al., 2015). MM2016/4 is a vertical peat profile sampled with a 1.5 x 0.08 m dimension Russian-style peat corer, and was one of 5 profiles collected along the watershed of the intact May Moss peatland in 2016. The MM2016/4 profile located closest to the May Moss meteorological station provided element concentration data (Figure 6.1) measured by XRF and these data characterise the source area element composition of the intact peatland feeding the stream-waters draining the site.
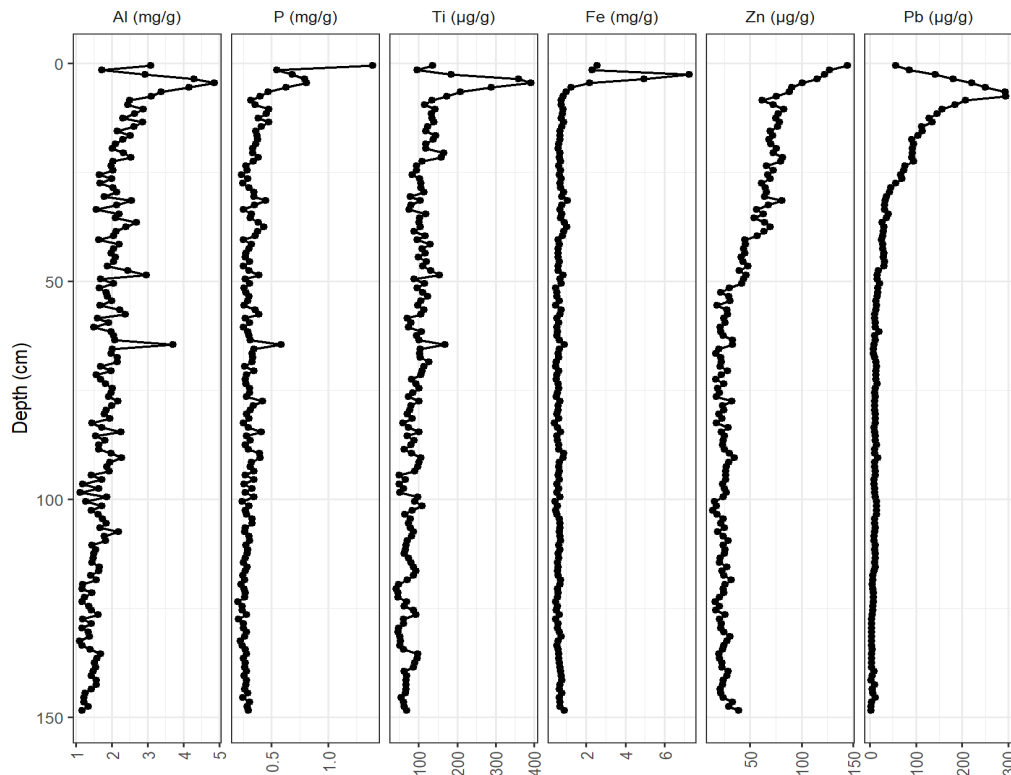
Figure 6.1. Select element concentrations with depth (cm) from the May Moss 2016/4 peat core taken from the intact peatland within ≈100 m of the May Moss meteorological station.

6.2.9   Building a loss-on-ignition model

A training set of 32 freeze-dried samples (16 from EB and 16 from LG) taken from the 5 L grab samples was used to assess the relationship between measured loss-on-ignition (LOI) and the NIR spectra. NIR and XRF scans were performed on these 32 samples prior to LOI. The training set was then dried at 105°C overnight and subjected to LOI combustion at 550°C for 4 hours using a Carbolite Gero (30 – 3000°C) furnace. Measured LOI values for the 32 samples were then regressed against their NIRS spectra using the software QUANT2 and optimised through first derivative and vector normalisation (SNV). The LOI model had a R^2 of 0.96 and was used to calculate a NIRS-inferred LOI for all the dried water samples (Figure 6.2). This LOI proportion was used to correct the humic substance and element concentrations for all samples.
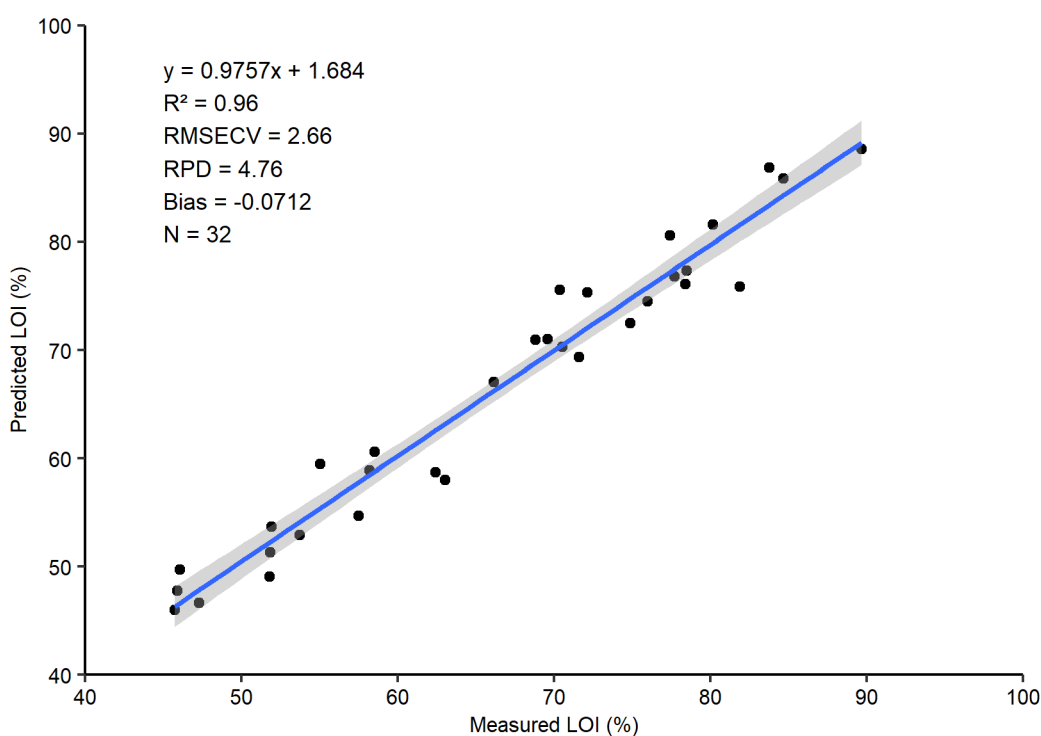
Figure 6.2. Comparison of measured and predicted LOI (%), LOI model performance.

Mass concentrations for FA, HA and humin were quantified by multiplying their NIRS-derived proportions by their respective sample dry weight concentrations (mg L^{-1}). Those values were then corrected for the sample LOI (%). Element concentrations (mg g^{-1}) derived by XRF were also corrected using the NIRS-inferred LOI in the onboard Spectro XEPOS 3 software, and ultimately expressed as mass concentrations per unit dry mass (μg g^{-1} or mg g^{-1}) and as mass concentrations per unit volume of water (μg L^{-1} or L g^{-1}) using the dry weight mass (g) and concentration (g L^{-1}), respectively, for each sample.

6.2.10 Statistics

Comparisons in water quality parameters were undertaken on temporal pairs of samples for EB and LG. For completeness, plots of the data as time series retain gaps where one or both sites did not collect a water sample or where samples were excluded due to containing excessive algae. As all parameters displayed non-Gaussian distributions, determined by Shapiro-Wilk normality tests, parameters were compared for significant differences between the two catchments using the Wilcoxon rank-sum test, with a significance threshold of $p < 0.05$. Due to their non-Gaussian distributions, homogeneity of variance among seasonal data was assessed using the Fligner-Killeen test, which has been determined as robust against departures from normality (Conover et al., 1981), and which confirmed that seasonal variances were non-homogenous. The Kruskal-Wallis test was therefore applied to examine the significance of seasonal differences among parameters. Correlations were tested using the non-parametric Kendall's rank sum test. Where multiple correlations were analysed on a matrix-basis, p-values were adjusted for the False Discovery Rate (FDR) using the Benjamini-Hochberg method (Benjamini and Hochberg, 1995), which is less conservative than the commonly used Bonferroni method and therefore less likely to reject true hypotheses (Pike, 2011). Statistical analyses were carried out in RStudio (Version 1.4.1717).

6.2.11 Principal components analysis

Patterns of variation between hydro-meteorological and water quality parameters were explored for each catchment using a principal components analysis (PCA). The catchments were analysed individually, and their complete datasets were reduced to matrices which contained only samples with data for all variables. Data were then normalised prior to analysis to have zero mean and unit variance by subtracting the mean and dividing by the standard deviation. Normalising data to their z-values allows the relative variation to be retained while avoiding scaling effects and is therefore commonly performed prior to PCA where variables are measured at different scales (Bridgham et al., 1998; Biester et al., 2012; Schreiber et al., 2014; Boothroyd et al., 2021). The number of principal components (PCs) for each catchment was based on the "broken stick" model (Jackson, 1993), where PCs with eigenvalues greater than those given by the model were retained. PC loadings were generated for all variables based on a correlation matrix using the software package PAST (v. 4.09) (Hammer et al., 2001). As PCA loadings are in effect correlation coefficients, loadings greater than $|0.5|$ are thus considered "high" and loadings between $|0.3|$ and $|0.5|$ are deemed "moderate" (Cohen, 1992).

6.3 RESULTS

6.3.1 Hydro-meteorology and the 2018 summer drought

The water sampling campaign spanned ≈2 years (18/07/2018 – 01/07/2020), during which water samples were collected every two or four days from both the EB and LG weir sampling points. The analytical methods targeted i) DOC, POC, DN and PN concentrations and C:N ratios based on liquid sample analysis, ii) quantification of humic substances (HS) using NIRS and iii) major and trace element concentrations by XRF (Table 6.1 and Table 6.2). The complete timeseries, including gaps, of stream-water concentrations of DOC, POC and HS, together with daily hydro-meteorological parameters, is depicted in Figure 6.3.

The sampling campaign commenced in the later period of the 2018 summer drought, and included the lowest water table depths recorded that summer for the LG dipwell (−307 mm) on 26/07/2018 and for the EB dipwell (−351 mm) on 27/07/2018 (Figure 6.3). We observed over the duration of the drought conditions, when water table drawdown lasted well into September 2018, that concentrations of DOC were particularly low and of POC were continuously high (Figure 6.3), and accompanied by spikes (with sometimes the maximum concentrations across the sampling campaign) in certain element concentrations, particularly Si, P, Mn, Fe, Co, As, Sn, Sb, Hf, W and Hg. Subsequent re-wetting in October 2018 was then associated with sudden rises in Na, Mg, Al, S, Ca, V, Zn, Sr and Pb (Figure 6.4 and Figure 6.5).

Non-parametric Kruskal-Wallis tests highlighted significant differences in seasonal runoff within the individual catchment PCA matrices ($p < 0.001$). For EB, average daily runoff increased in order spring < summer < autumn < winter and was significantly higher ($p < 0.001$) in winter compared to all other seasons, and autumn runoff was significantly higher than in summer ($p < 0.01$). For LG, average daily runoff increased in order summer < spring < autumn < winter and was significantly higher in winter compared to the other seasons ($p < 0.01$), and significantly lower in summer compared to all other seasons ($p < 0.001$).

Kruskal-Wallis tests also highlighted significant differences in WTD by season among all four dipwells within the PCA matrices. WTD depths were significantly shallower in winter, compared to all other seasons, and significantly lower in summer compared to spring across all dipwells ($p < 0.001$). In addition, daily average WTD in autumn was significantly shallower compared to summer for the EB dipwell ($p < 0.05$), and significantly shallower than in summer and significantly lower than in spring for the LG dipwell ($p < 0.05$).

160

Table 6.1. Median stream-water concentrations and ratios of parameters from paired samples, and p-values from Wilcoxon rank-sum tests between the two sites. For liquid-derived values (Type L) n = 208, for dry-mass-derived values (Type D) n = 166. Interquartile ranges (IQR) are shown in brackets. Significantly higher median values for Eller Beck are marked in blue and for Long Grain in red, while green marks parameters which did not differ significantly between catchments.

Parameter	Type	Eller Beck	Long Grain	p-value
Dry mass (mg L^{-1})	D	95.5 (72.8 – 112.5)	63.5 (48.3 – 79.4)	p < 0.001
DOC (mg L^{-1})	L	39.1 (29.0 – 47.6)	19.0 (13.8 – 29.1)	p < 0.001
POC (mg L^{-1})	L	2.0 (1.2 – 4.7)	1.9 (1.1 – 4.3)	p = 0.1971
PC (mg L^{-1})	L	2.1 (1.3 – 5.1)	2.0 (1.2 – 4.6)	p = 0.1391
DN (mg L^{-1})	L	1.4 (1.2 – 1.7)	0.8 (0.6 – 1.1)	p < 0.001
PN (mg L^{-1})	L	0.2 (0.1 – 0.3)	0.1 (0.1 – 0.2)	p < 0.001
DOC:DN	L	26.0 (20.5 – 31.3)	15.7 (13.3 – 24.3)	p < 0.001
POC:PN	L	12.2 (10.6 – 17.5)	14.4 (12.8 – 20.1)	p < 0.001
C:N	L	24.6 (21.0 – 29.4)	25.4 (21.2 – 29.2)	p = 0.9379
$SUVA_{254}$:DOC	L	5.5 (5.1 – 6.3)	5.4 (5.0 – 6.1)	p = 0.1599
E4:E6	L	5.9 (5.5 – 7.2)	6.5 (6.2 – 6.9)	p < 0.01
Abs_{400} (au m^{-1})	L	33.6 (28.0 – 41.3)	16.4 (10.9 – 24.6)	p < 0.001
HA (mg L^{-1})	D	31.0 (22.9 – 46.1)	10.8 (6.6 – 21.4)	p < 0.001
FA (mg L^{-1})	D	20.1 (10.9 – 35.6)	20.3 (11.6 – 28.6)	p = 0.6693
Humin (mg L^{-1})	D	9.0 (6.8 – 11.1)	6.8 (5.1 – 8.6)	p < 0.001
Na (mg L^{-1})	D	3.0 (2.2 – 4.2)	3.1 (2.3 – 3.9)	p = 0.8436
Mg (mg L^{-1})	D	0.5 (0.3 – 0.6)	0.5 (0.4 – 0.7)	p = 0.1759
Al (mg L^{-1})	D	0.2 (0.2 – 0.3)	0.5 (0.4 – 0.6)	p < 0.001
Si (mg L^{-1})	D	1.1 (0.8 – 1.5)	1.6 (1.2 – 2.2)	p < 0.001
P (mg L^{-1})	D	0.1 (0.0 – 0.2)	0.0 (0.0 – 0.1)	p < 0.001
S (mg L^{-1})	D	1.5 (1.1 – 2.5)	2.0 (1.5 – 2.6)	p < 0.01
Cl (mg L^{-1})	D	3.3 (2.3 – 4.6)	4.1 (3.2 – 5.4)	p < 0.001
K (mg L^{-1})	D	0.3 (0.2 – 0.5)	0.3 (0.2 – 0.4)	p = 0.09443
Ca (mg L^{-1})	D	0.6 (0.4 – 0.8)	1.0 (0.7 – 1.3)	p < 0.001
Ti (µg L^{-1})	D	5.1 (3.3 – 7.7)	2.8 (1.8 – 4.0)	p < 0.001
V (µg L^{-1})	D	2.3 (1.5 – 3.9)	1.7 (1.3 – 2.2)	p < 0.001
Cr (µg L^{-1})	D	3.9 (2.5 – 5.6)	2.9 (2.1 – 4.2)	p < 0.001
Mn (µg L^{-1})	D	69.1 (40.4 – 105.7)	54.9 (37.4 – 97.2)	p = 0.4858
Fe (mg L^{-1})	D	6.2 (3.6 – 10.0)	3.2 (1.9 – 6.3)	p < 0.001
Co (µg L^{-1})	D	13.7 (8.0 – 25.2)	7.3 (4.3 – 15.4)	p < 0.001
Ni (µg L^{-1})	D	13.4 (10.2 – 16.3)	11.9 (9.5 – 15.7)	p = 0.1425
Cu (µg L^{-1})	D	4.6 (2.7 – 7.8)	1.7 (1.3 – 3.0)	p < 0.001
Zn (µg L^{-1})	D	37.2 (20.2 – 56.4)	21.9 (14.8 – 29.0)	p < 0.001
As (µg L^{-1})	D	15.9 (11.6 – 20.3)	4.5 (2.8 – 7.5)	p < 0.001
Br (µg L^{-1})	D	83.1 (66.8 – 106.0)	58.9 (41.5 – 77.9)	p < 0.001
Rb (µg L^{-1})	D	2.0 (1.5 – 2.6)	1.6 (1.2 – 2.3)	p < 0.001
Sr (µg L^{-1})	D	13.4 (9.8 – 18.7)	15.9 (12.6 – 19.6)	p < 0.001
Y (µg L^{-1})	D	1.0 (0.8 – 1.5)	2.6 (1.9 – 3.6)	p < 0.001
Zr (µg L^{-1})	D	0.9 (0.7 – 1.4)	0.8 (0.6 – 1.2)	p < 0.05
Sn (µg L^{-1})	D	2.2 (1.1 – 3.8)	1.5 (0.0 – 2.8)	p < 0.001
Sb (µg L^{-1})	D	0.0 (0.0 – 2.2)	0.0 (0.0 – 0.8)	p < 0.001
I (µg L^{-1})	D	17.4 (11.8 – 23.8)	6.8 (1.9 – 11.9)	p < 0.001
Ba (µg L^{-1})	D	36.4 (20.4 – 47.9)	30.9 (22.4 – 43.9)	p = 0.2451
Hf (µg L^{-1})	D	0.5 (0.0 – 0.9)	0.3 (0.0 – 0.5)	p < 0.001
W (µg L^{-1})	D	0.6 (0.3 – 1.3)	0.2 (0.1 – 0.5)	p < 0.001
Hg (µg L^{-1})	D	0.1 (0.0 – 0.1)	0.0 (0.0 – 0.1)	p < 0.01
Pb (µg L^{-1})	D	18.0 (7.9 – 33.2)	3.5 (2.2 – 6.2)	p < 0.001

Table 6.2. Median and interquartile range (IQR) of LOI and dry mass concentrations of parameters from paired samples, and p-values from Wilcoxon rank-sum tests between the two sites. Each site n = 166. Interquartile ranges (IQR) are shown in brackets. Significantly higher median values for Eller Beck (EB) are marked in blue and for Long Grain (LG) in red, while green marks parameters which did not differ significantly between catchments.

Parameter	Eller Beck	Long Grain	p-value
LOI (%)	70.9 (64.6 – 79.1)	60.5 (55.7 – 67.6)	p < 0.001
HS (mg g^{-1})	708.8 (646.3 – 790.5)	605.1 (557.0 – 675.6)	p < 0.001
HA (mg g^{-1})	374.7 (289.1 – 473.7)	224.2 (125.7 – 280.0)	p < 0.001
FA (mg g^{-1})	244.7 (111.2 – 403.0)	295.8 (225.7 – 400.3)	p < 0.01
Humin (mg g^{-1})	93.6 (87.1 – 104.3)	101.7 (92.6 – 115.2)	p < 0.001
Na (mg g^{-1})	31.3 (24.7 – 42.8)	49.8 (38.9 – 64.3)	p < 0.001
Mg (mg g^{-1})	4.6 (3.8 – 6.5)	8.3 (6.3 – 10.7)	p < 0.001
Al (mg g^{-1})	2.4 (2.0 – 2.9)	7.1 (6.0 – 8.8)	p < 0.001
Si (mg g^{-1})	12.3 (8.9 – 16.2)	27.7 (21.8 – 35.8)	p < 0.001
P (mg g^{-1})	0.8 (0.4 – 1.6)	0.5 (0.4 – 0.9)	p < 0.001
S (mg g^{-1})	15.3 (11.8 – 28.3)	35.3 (18.0 – 47.2)	p < 0.001
Cl (mg g^{-1})	35.8 (27.4 – 46.3)	66.4 (51.4 – 80.9)	p < 0.001
K (mg g^{-1})	3.3 (2.4 – 4.8)	4.5 (3.0 – 6.8)	p < 0.001
Ca (mg g^{-1})	6.1 (4.9 – 8.5)	16.1 (11.4 – 21.4)	p < 0.001
Ti (µg g^{-1})	55.2 (39.9 – 80.1)	41.1 (34.4 – 51.5)	p < 0.001
V (µg g^{-1})	24.1 (15.6 – 39.9)	28.3 (19.9 – 35.2)	p = 0.4321
Cr (µg g^{-1})	39.1 (28.6 – 57.7)	44.9 (34.9 – 61.0)	p < 0.01
Mn (µg g^{-1})	779.6 (469.1 – 1129.8)	1083.5 (688.0 – 1595.3)	p < 0.001
Fe (mg g^{-1})	70.5 (40.1 – 98.5)	58.0 (36.5 – 86.2)	p < 0.01
Co (µg g^{-1})	154.8 (85.5 – 261.8)	131.0 (87.5 – 193.9)	p = 0.0721
Ni (µg g^{-1})	136.1 (110.6 – 167.8)	179.0 (138.1 – 266.9)	p < 0.001
Cu (µg g^{-1})	50.5 (31.8 – 82.2)	30.8 (21.0 – 40.1)	p < 0.001
Zn (µg g^{-1})	378.4 (230.4 – 643.8)	384.9 (207.0 – 488.7)	p < 0.05
As (µg g^{-1})	171.7 (142.7 – 197.4)	72.7 (57.6 – 91.9)	p < 0.001
Br (µg g^{-1})	908.4 (791.4 – 1045.0)	935.0 (826.6 – 1010.0)	p = 0.4991
Rb (µg g^{-1})	19.6 (16.0 – 26.1)	24.8 (19.9 – 32.1)	p < 0.001
Sr (µg g^{-1})	139.2 (113.8 – 181.3)	261.9 (188.5 – 335.2)	p < 0.001
Y (µg g^{-1})	12.3 (8.6 – 16.1)	43.8 (36.0 – 53.3)	p < 0.001
Zr (µg g^{-1})	11.1 (7.3 – 16.2)	13.8 (10.8 – 16.9)	p < 0.01
Sn (µg g^{-1})	22.6 (12.0 – 38.8)	23.0 (0.1 – 49.8)	p = 0.9968
Sb (µg g^{-1})	0.1 (0.1 – 21.0)	0.1 (0.1 – 10.9)	p = 0.2671
I (µg g^{-1})	190.5 (151.0 – 225.0)	109.0 (37.5 – 152.0)	p < 0.001
Ba (µg g^{-1})	350.5 (277.3 – 457.5)	528.5 (375.0 – 674.5)	p < 0.001
Hf (µg g^{-1})	5.7 (0.1 – 8.5)	4.3 (0.1 – 7.2)	p < 0.01
W (µg g^{-1})	6.2 (4.0 – 12.2)	3.8 (2.2 – 7.0)	p < 0.001
Hg (µg g^{-1})	0.6 (0.5 – 0.7)	0.8 (0.7 – 0.9)	p < 0.001
Pb (µg g^{-1})	199.6 (100.6 – 363.9)	56.8 (38.6 – 87.1)	p < 0.001
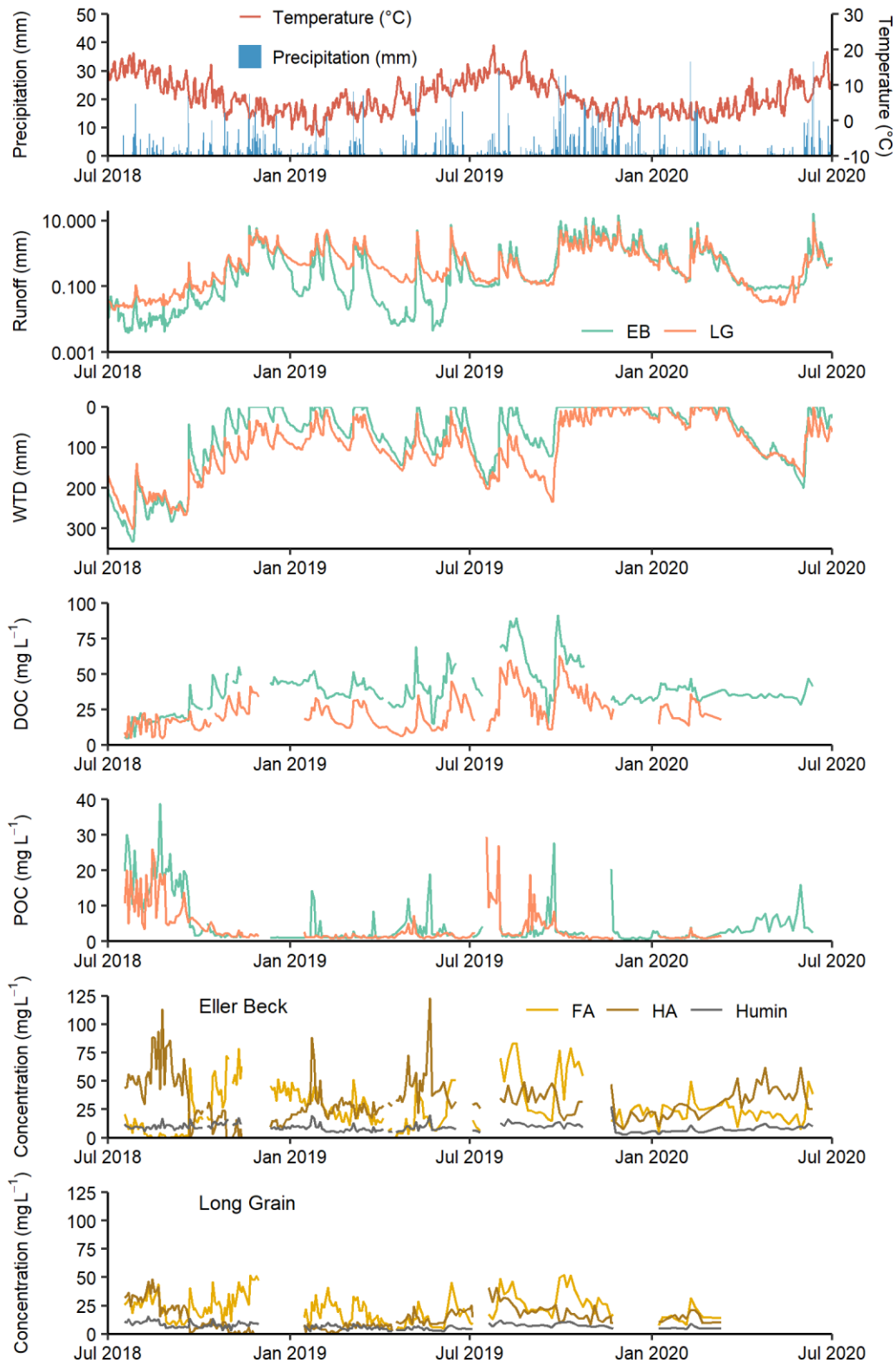
Figure 6.3 Complete hydro-meteorological and water chemistry timeseries showing daily average air temperature (°C) and total precipitation (mm), daily total runoff (mm), daily average water table depth (mm), DOC (mg L^{-1}), POC (mg L^{-1}), and humic substances concentrations (mg L^{-1}) for Eller Beck and Long Grain. Note that runoff (mm) is in log-scale to display very low runoff.
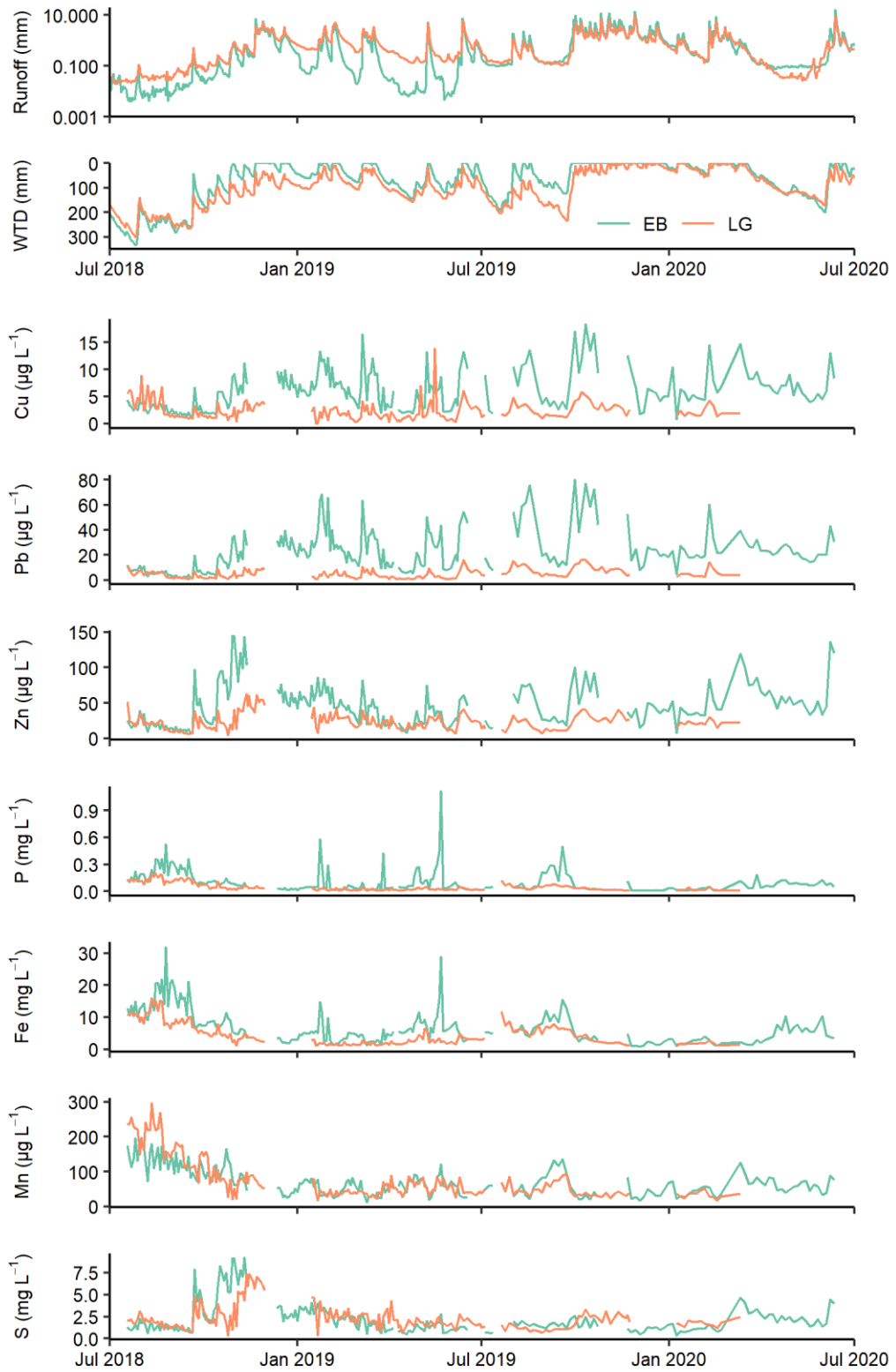
Figure 6.4. Timeseries of daily average runoff (mm), water table depth (WTD) and stream-water concentrations of select elements. Note that runoff (mm) is in log-scale to display very low runoff.
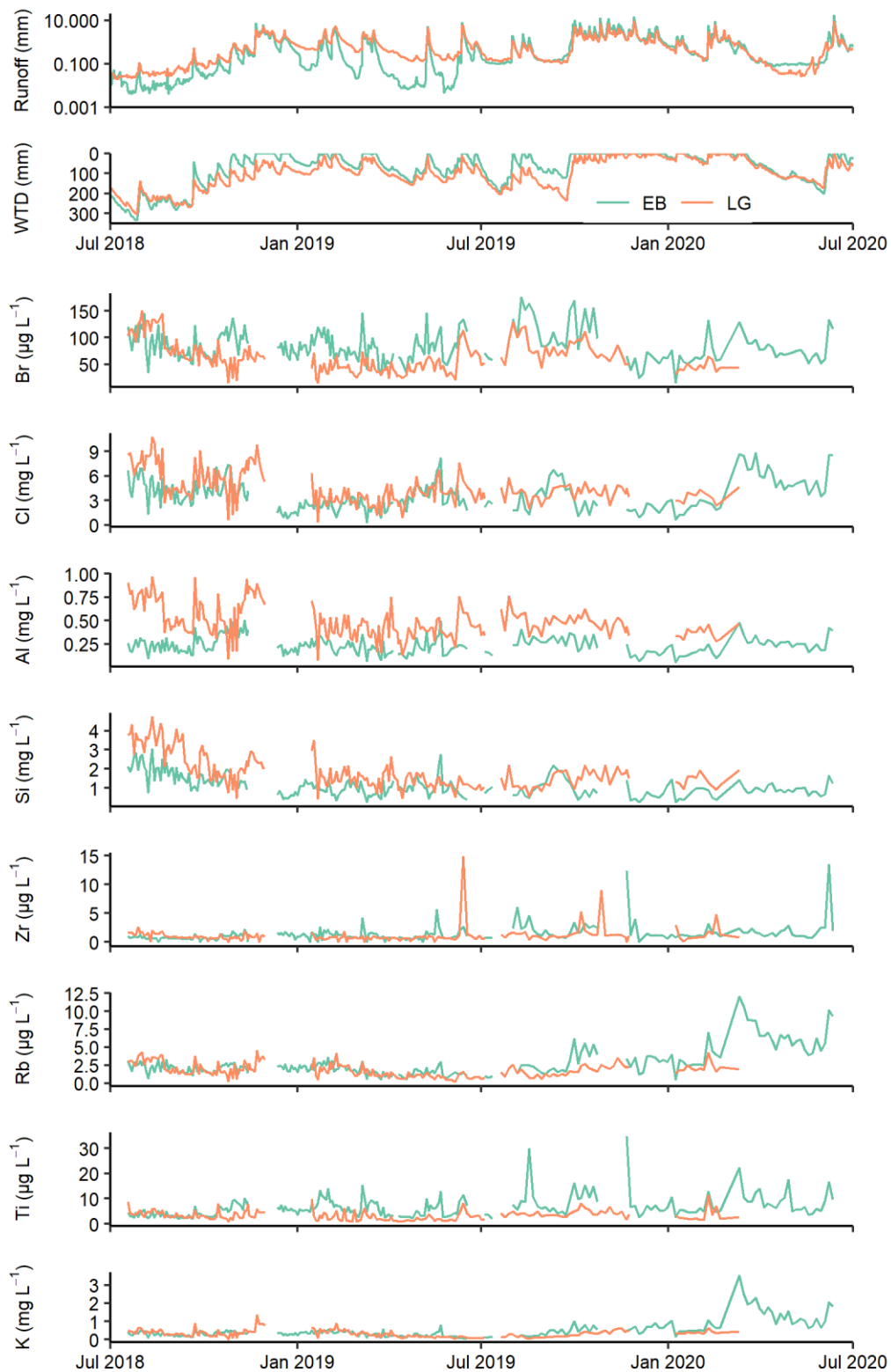
Figure 6.5. Timeseries of daily average runoff (mm), water table depth (WTD) and stream-water concentrations of select elements. Note that runoff (mm) is in log-scale to display very low runoff.

6.3.2   Parameters and element concentrations

DOC, DN, POC, PC and PN concentrations were quantified from 275 and 249 samples from

EB and LG, respectively, based on the water sampling campaign between 18/07/2018 and

165

27/08/2020. DOC concentrations ranged between 4.6 and 91.5 mg L^{-1} (mean = 39.3 mg L^{-1}, N = 275) at EB, and between 4.8 and 68.9 mg L^{-1} (mean = 23.7 mg L^{-1}, N = 249) at LG. POC concentrations varied between 0.6 and 38.8 mg L^{-1} (mean = 4.6 mg L^{-1}, N = 275) at EB, and between 0.6 and 29.4 mg L^{-1} (mean = 3.8 mg L^{-1}, N = 249) at LG. Wilcoxon rank-sum tests showed no significant differences between POC and PC for both EB (p = 0.4058) and LG (0.5171), indicating that POC dominates PC with minimal inorganic carbon.

Among paired data (n = 208), Wilcoxon rank-sum tests showed DOC concentrations were significantly lower (-51%) at LG (Med = 19.1 mg L^{-1}) compared to EB (Med = 39.1 mg L^{-1}) (W = 34538, p < 0.001), while POC concentrations did not differ significantly (W = 23214, p = 0.1971) between the catchments (Table 6.1). This discrepancy occurred across all seasons, except for spring, when EB samples had significantly higher POC concentrations than LG (p < 0.01, N = 45). DOC and POC were significantly and negatively correlated at both catchments, with a stronger inverse relationship found at EB (τ = −0.22, p < 0.001) than at LG (τ = −0.13, p < 0.01).

Kruskal-Wallis tests were used to assess for seasonal differences in DOC and POC concentrations. In EB, no significant seasonal differences were found for DOC (H(3) = 4.65, p = 0.1994), while for LG DOC concentrations were significantly lower in spring compared to all other seasons (H(3) = 32.27, p < 0.001). POC concentrations in EB were significantly lower in winter compared to all other seasons (H(3) = 109.8, p < 0.001), while for LG both summer and autumn POC concentrations were significantly higher than winter and spring concentrations (H(3) = 69.4, p < 0.001).

Various best-fit regression models (linear, logarithmic, power and exponential) showed that DOC and POC concentrations in stream water had positive power relationships with average daily runoff and exponentially declining relationships with WTD at both catchments (Figure 6.6). In both catchments, DOC concentrations increased with higher runoff and shallower water levels, suggesting a flushing effect driving greater DOC loss from the peat. Conversely, POC concentrations showed the opposite behaviour, indicating a dilution effect with higher runoff and particularly shallower water levels (Figure 6.6). Kendall's rank correlations indicated that DOC at EB showed a marginally stronger relationship with WTD (τ = −0.42, p < 0.001) than with average daily runoff (τ = 0.40, p < 0.001), conversely DOC at LG appears more driven by runoff (τ = 0.47, p < 0.001) than by WTD (τ = −0.36, p < 0.001). POC appeared more coupled with WTD than with runoff at both catchments, with stronger correlations observed at LG (WTD: τ = 0.51, p < 0.001; Runoff: τ = −0.45, p < 0.001) than EB (WTD: τ = 0.44,

$p < 0.001$; Runoff: $\tau = -0.31$, $p < 0.001$). These patterns are confirmed by respective R^2 coefficients for the regression equations (Figure 6.6).
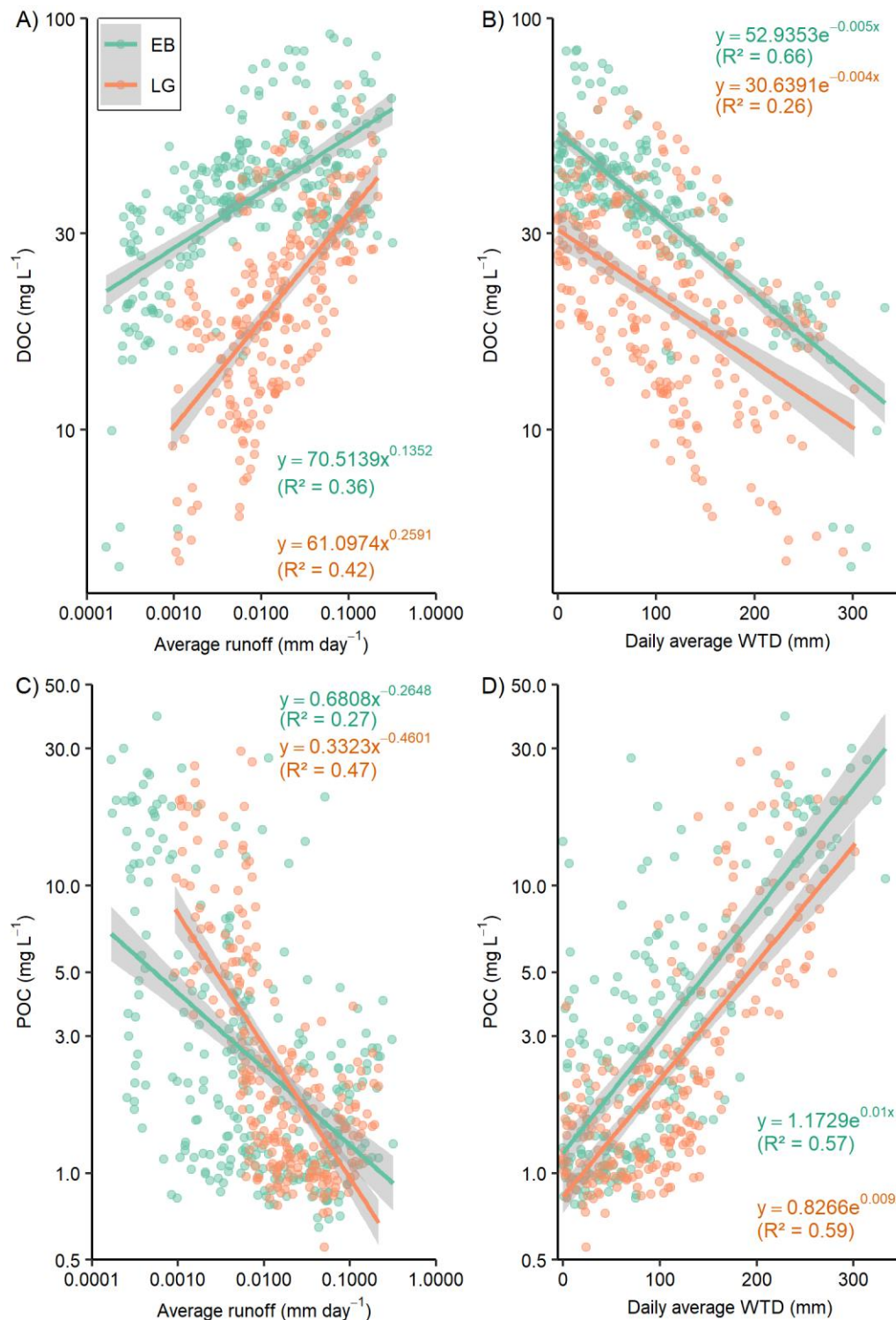
Figure 6.6. Regression models for Eller Beck (EB) and Long Grain (LG) between A) DOC (mg L-1) and daily average runoff (mm day-1), B) DOC (mg L-1) and daily average water table depth (WTD) (mm), C) POC (mg L-1) and daily average runoff (mm day-1), and D) POC (mg L-1) and daily average water table depth (WTD) (mm). R2 are adjusted. Note log scales on selected axes.

DN concentrations ranged between 0.8 and 3.7 mg L^{-1} (mean = 1.6 mg L^{-1}) at EB, and between 0.3 and 1.9 mg L^{-1} (mean = 0.9 mg L^{-1}) at LG, while PN concentrations varied between 0.1 and 2.7 mg L^{-1} (mean = 0.3 mg L^{-1}) at EB, and between 0.1 and 1.1 mg L^{-1} (mean = 0.2 mg L^{-1}) at LG. Among paired data (n = 208), Wilcoxon rank-sum tests showed that EB had significantly higher DN (W = 39291, $p < 0.001$) and PN (W = 27552, $p < 0.001$) concentrations than LG. C:N ((DOC + POC) : (DN + PN)) ratios ranged between 10.5 and 38.7 (mean = 24.4) at EB and between 12.2 and 40.8 (mean = 25.6) at LG, and did not differ significantly between catchments ($p = 0.9379$). However, when separated into dissolved and particulate ratios, EB showed significantly higher DOC:DN ratios (W = 39291, $p < 0.001$), while LG had significantly higher POC:PN ratios (W = 27552, $p < 0.001$) (Table 6.1), indicating that higher C:N ratios in stream-water samples were driven more by dissolved components at EB and by particulates at LG.

Wilcoxon rank-sum tests were carried out on the 166 paired XRF samples corrected for dry mass concentration (mg L^{-1}) from water samples, to assess stream-water concentrations of elements. LG had significantly higher median stream-water concentrations of Al, Si, Cl, Ca, Sr ($p < 0.001$) and S ($p < 0.05$), while EB had significantly higher concentrations of P, Ti, V, Cr, Fe, Co, Cu, Zn, As, Br, Rb, Y, Sn, Sb, I, Hf, W, Pb ($p < 0.001$), Hg ($p < 0.01$) and Zr ($p < 0.05$). Na ($p = 0.8436$), Mg ($p = 0.1759$), K ($p = 0.0944$), Mn ($p = 0.4858$), Ni ($p = 0.1425$) and Ba ($p = 0.2451$) did not differ significantly between catchments (Table 6.1).

In addition, Wilcoxon rank-sum tests were carried out on the 166 paired XRF samples, corrected for dry mass weight (mg) only, to compare the composition of the dry mass being exported by stream-water between the two sites and to account for potential dilution effects on stream-water concentrations, as median dry mass concentrations (mg L^{-1}) were significantly higher at EB compared to LG (W = 21121, $p < 0.001$) (Table 6.1). Dry masses from water samples derived from LG were significantly enriched in Na, Mg, Al, Si, S, Cl, K, Ca, Mn, Ni, Rb, Sr, Y, Ba, Hg ($p < 0.001$), Cr, Zr ($p < 0.01$) and Zn ($p < 0.05$) relative to EB. Conversely, EB dry masses were significantly enriched in P, Ti, Cu, As, I, W, Pb ($p < 0.001$), Fe and Hf ($p < 0.01$) compared to LG. Dry mass concentrations of elements V ($p = 0.4321$), Co ($p = 0.07214$), Br ($p = 0.4991$), Sn ($p = 0.9968$) and Sb ($p = 0.2671$) did not differ significantly between sites (Table 6.2).

6.3.3 DOC and POC fluxes

The complete runoff series, spanning 14/03/2017 – 01/07/2021, allowed us to estimate annual DOC and POC fluxes for 2018, 2019 and 2020 for each catchment. Daily DOC and POC

concentrations were estimated using the regression equations between measured concentrations and daily average runoff for each catchment, n = 275 samples for EB and n = 249 for LG (Figure 6.6). These DOC and POC concentrations (mg L^{-1}) were then multiplied by daily total discharge (L day^{-1}) to quantify daily loads (g C day^{-1}), which were divided by the catchment area to derive daily fluxes (mg C m^{-2} day^{-1}). Annual loads and fluxes for 2018, 2019 and 2020 were computed by summing the daily data for each year (Table 6.3). Both EB and LG had their lowest annual DOC and POC fluxes in 2018, amounting to 10.75 g m^{-2} yr^{-1} of DOC and 0.31 g m^{-2} yr^{-1} of POC from EB, and 8.38 g m^{-2} yr^{-1} of DOC and 0.36 g m^{-2} yr^{-1} from LG, which were associated with the lowest annual runoff among the three years (Table 6.3). DOC budgets were highest in 2019 for LG and 2020 for EB and coalesced with the lowest POC concentrations and highest POC loads and fluxes (Table 6.3). Annual DOC:POC ratios were high in all years at both catchments, particularly at EB (Table 6.3), highlighted the dominance of DOC in the total organic carbon (TOC) flux for both catchments.

Table 6.3. Total annual discharge (m^3 yr^{-1}) and runoff (mm m^{-2} yr^{-1}), and average annual concentration (mg L^{-1}), annual total load (T yr^{-1}) and fluxes (g m^{-2} yr^{-1}) of DOC and POC from the Eller Beck (EB) and Long Grain (LG) catchments.

Parameter	Eller Beck			Long Grain		
Year	2018	2019	2020	2018	2019	2020
Total discharge (m^3 yr^{-1})	135,983	269,523	287,651	410,350	596,722	548,048
Total runoff (mm m^{-2} yr^{-1})	216	427	456	268	390	358
DOC						
Avg. annual conc. (mg L^{-1})	35.75	39.91	43.10	20.61	24.39	23.42
Annual total load (T yr^{-1})	6.78	14.46	15.14	12.83	19.19	17.51
Annual flux (g m^{-2} yr^{-1})	10.75	22.93	24.01	8.38	12.54	11.44
POC						
Avg. annual conc. (mg L^{-1})	3.26	2.54	1.94	3.32	2.06	2.44
Annual total load (T yr^{-1})	0.20	0.33	0.37	0.54	0.72	0.68
Annual flux (g m^{-2} yr^{-1})	0.31	0.53	0.59	0.36	0.47	0.44
TOC flux (g m^{-2} yr^{-1})	11.06	23.46	24.60	8.74	13.01	11.88
DOC:POC conc. ratio	10.97	15.68	22.18	6.21	11.83	9.61
DOC:POC flux ratio	34.51	43.41	40.82	23.56	26.61	25.84

6.3.4 Humic substances

The water sampling campaign resulted in 227 samples from EB and 200 samples from LG which were analysed for NIRS to derive concentrations of humic substances (HS). End-member spectra for FA, HA and humin explained a high proportion of variation in the dried water samples. For EB, the end-member multiple regression (EM-MR) using those three end-members produced R^2 between 0.89 and 0.99 (mean = 0.93), while for LG the sample R^2 values ranged between 0.76 and 0.97 (mean = 0.87), indicating that humic substances made up a dominant proportion of the dry masses. While humin concentrations remained relatively constant across the monitoring period, with a coefficient of variation (CV) of 0.37

at both catchments, FA and HA were considerably more variable, though the extent of variation was inverse between catchments, with FA varying by CV = 0.59 at EB and CV = 0.75 at LG, and HA varying by CV = 0.74 at EB and CV = 0.55 at LG, indicating that FA concentrations were more variable at LG, while HA varied more at EB.

FA concentrations from EB ranged between 0.0 and 83.4 mg L^{-1} (mean = 25.8 mg L^{-1}), HA ranged between 0.0 and 123.1 mg L^{-1} (mean = 33.3 mg L^{-1}) and humin varied between 2.6 and 27.8 mg L^{-1} (mean = 9.0 mg L^{-1}). From LG, FA concentrations ranged between 2.9 and 63.9 mg L^{-1} (mean = 22.2 mg L^{-1}), HA ranged between 0.0 and 48.1 mg L^{-1} (mean = 14.0 mg L^{-1}) and humin varied between 2.2 and 15.6 mg L^{-1} (mean = 7.0 mg L^{-1}). Dry mass concentrations (mg g^{-1}) of HA were significantly higher at the intact site (EB) ($p < 0.001$), while dry mass concentrations of FA ($p < 0.01$) and humin ($p < 0.001$) were significantly higher for LG (Table 6.2). Conversely, liquid sample concentrations (mg L^{-1}) of FA did not differ significantly ($p = 0.6693$) between catchments and of humin became significantly more enriched ($p < 0.001$) at EB (Table 6.1), suggesting that both substances were affected by greater dilution at the recovering site.

Kruskal-Wallis tests were used to examine the seasonal variation in FA, HA and humin concentrations within individual catchments. FA concentrations were found to be significantly higher in autumn and winter than in spring and summer at EB (H(3) = 23.97, $p < 0.001$), while only the spring FA concentrations were significantly lower than during the rest of the year at LG (H(3) = 39.64, $p < 0.001$). Conversely, HA concentrations varied significantly by season, and were found to be significantly higher in spring and summer, compared to autumn and winter at EB (H(3) = 65.12, $p < 0.001$) and significantly higher in summer, compared to the rest of the year at LG (H(3) = 81.95, $p < 0.001$). Significantly higher HA concentrations in summer were likely driven by the high HA concentrations observed during the summer drought in 2018, particularly at EB, where a switch to dominance of FA was noticed upon post-drought rewetting (Figure 6.3). Similarly to HA, humin concentrations were significantly higher in summer and autumn, compared to winter and spring, at both EB (H(3) = 55.17, $p < 0.001$) and LG (H(3) = 58.50, $p < 0.001$).

Relationships between FA and HA and runoff and WTD were analysed by examining the best-fitting regression model between the substance concentrations and the hydrological variables. Regression models with FA and HA generally had lower R^2 values than the corresponding models with DOC and POC. For HA, the strongest fit was a logarithmic model with runoff and linear relationship with WTD, while FA presented a strongest fit with a power

function with runoff and a declining exponential function with WTD. For EB, FA showed considerably stronger relationships with runoff and WTD, indicated by higher R^2, than HA did, while FA at LG showed no relation to either hydrological variable (Figure 6.7).
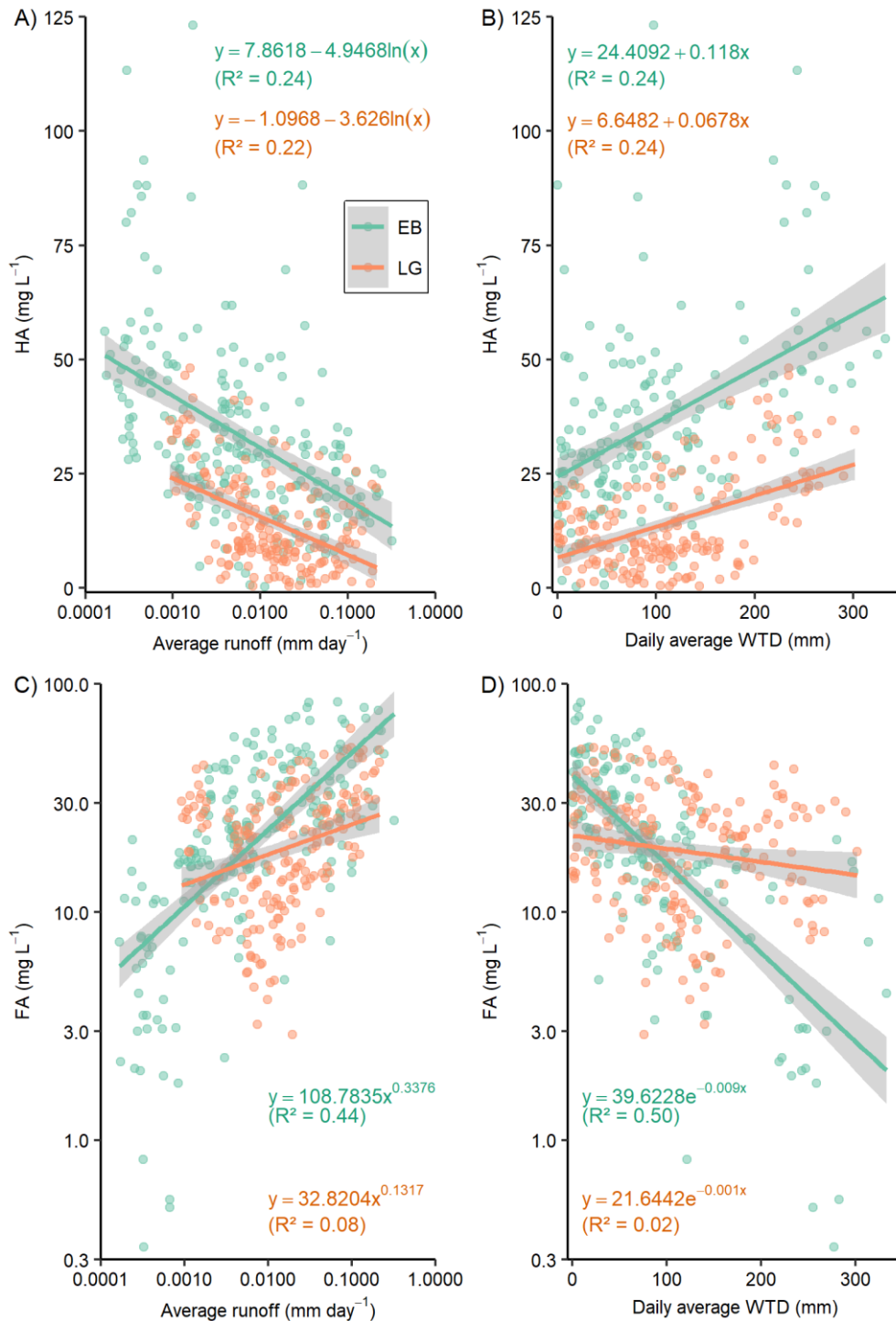
Figure 6.7. Regression models for Eller Beck (EB) and Long Grain (LG) between A) Humic acid (HA) (mg L^{-1}) and daily average runoff (mm day^{-1}), B) HA (mg L^{-1}) and daily average water table depth (WTD) (mm), C) Fulvic acid (FA) (mg L^{-1}) and daily average runoff (mm day^{-1}), and D) FA (mg L^{-1}) and daily average water table depth (WTD) (mm). R^2 are adjusted. Note log scales on most axes.

6.3.5   Water UV-Vis absorbance spectra

For both catchments, correlations between DOC concentration and UV-vis absorbance were strongest across the lower waveband and reduced towards higher wavelengths, with EB showing an exponential decline after ≈ 400 nm, while LG displayed a more gradual reduction in R^2 (Figure 6.8). EB absorbance spectra showed greater fitting at wavebands between 266 nm and 412 nm, while LG showed better fitting at lower and higher wavelengths (Figure 6.8). Linear regressions between DOC concentrations and absorbance spectra showed a strongest fit, based on highest R^2, for EB at Abs_{272} (R^2 = 0.88) and for LG at Abs_{242} (R^2 = 0.85). Abs_{254}, used to derive specific ultraviolet absorbance (SUVA) (Weishaar et al., 2003; Peacock et al., 2014; Strack et al., 2015), had R^2 values of 0.82 and 0.84 for EB and LG when fitted against DOC concentration, respectively (Figure 6.8). Median SUVA ratios (Abs_{254} : DOC) were 5.5 (IQR = 5.1 – 6.3) at EB and 5.4 (IQR = 5.0 – 6.1) at LG, but did not differ significantly between catchments (W = 20785, p = 0.1599).

Median Abs_{400} was significantly higher at EB (Med = 33.6 au m^{-1}, IQR = 28.0 – 41.3 au m^{-1}), compared to LG (Med = 16.4 au m^{-1}, IQR = 10.9 – 24.6) (W = 36281, p < 0.001), indicating considerably more colouration among EB samples than those from LG. These findings mirror the patterns found in the NIRS values for humic and fulvic acids in the dried water samples. In addition, Abs_{400} wavelengths were significantly correlated with DOC concentrations for both EB (τ = 0.56, p < 0.001) and LG (τ = 0.65, p < 0.001) (Figure 6.9).

Median E4:E6 ratios were significantly higher at LG (Med = 6.5, IQR = 6.2 – 6.9) compared to EB (Med = 5.9, IQR = 5.5 – 7.2) (W = 10619, p < 0.01), indicating higher proportions of humic to fulvic acids in LG stream-water samples, compared to EB. Conversely, NIRS-derived HA:FA ratios, based on the same sample group (n = 161), were significantly lower compared to E4:E6 ratios for both EB (Mdn = 1.4, IQR = 0.7 – 3.2) (W = 3894, p < 0.001) and LG (Mdn = 0.7, IQR = 0.3 – 1.1) (W = 21, p < 0.001), with median HA:FA ratios being significantly higher for EB compared to LG (W = 7040, p < 0.001), though the higher median EB HA:FA ratio was likely driven by high outliers (Max: 170.2) produced by occasionally very low (< 1 mg L^{-1}) FA concentrations. Considerable dissonance between E4:E6 and HA:FA ratios was furthermore found through a significant negative correlation between the two ratios at EB (τ = −0.51, p < 0.001) and a lack of correlation at LG (τ = 0.12, p < 0.05).
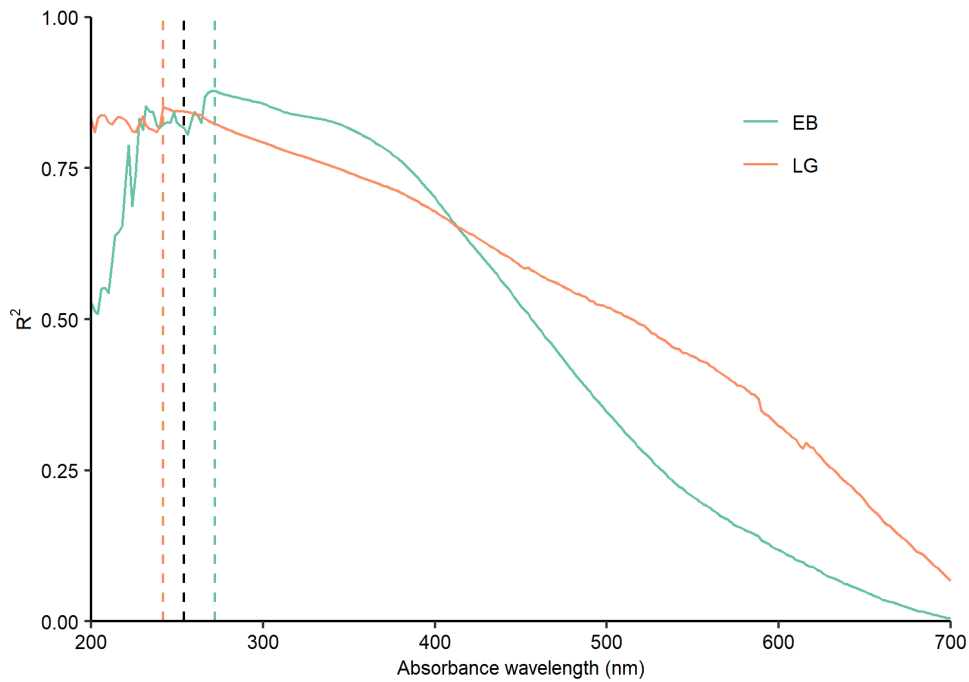
Figure 6.8. R^2 from linear regressions between DOC concentrations and UV-Vis absorbance wavelengths between 200 and 700 nm for Eller Beck (EB) (n = 275) and Long Grain (LG) (n = 249). The green and orange dashed lines mark the highest R^2 values for EB (Abs_{272}) and LG (Abs_{242}), respectively, and the black dashed line marks Abs_{254}.
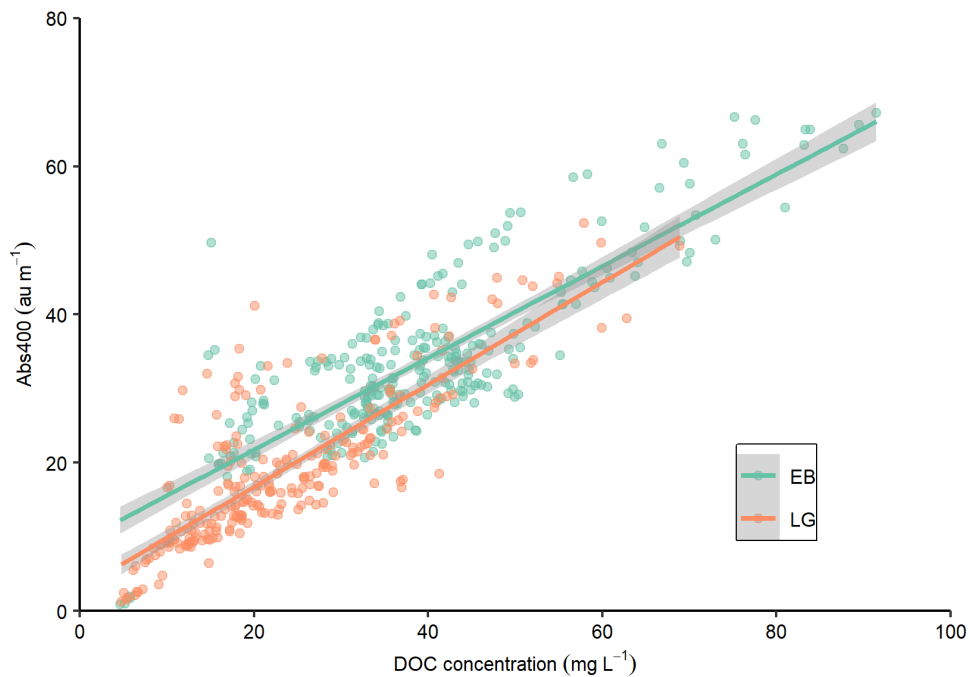
Figure 6.9. Relationship between DOC concentration (mg L^{-1}) and Abs400 (au m^{-1}) for Eller Beck (EB) (n = 275) and Long Grain (LG) (n = 249).

6.3.6   Associations between water quality parameters

The water sampling campaign resulted in the processing of 220 and 195 samples from EB and LG, respectively, for XRF analysis. Kendall's correlation tests were used to examine

correlations between hydro-meteorological variables at daily and weekly timescales with organic parameters and ratios in order to assess seasonal and hydrological relationships. For both EB and LG, stream-water DOC and DN concentrations and DOC:DN ratios appeared to be mainly limited by greater WTDs and driven by runoff, and were largely unrelated to temperature apart from DN from LG. Conversely, higher POC and PN concentrations and POC:PN ratios were related to deeper water tables, as well as higher weekly average temperatures and evaporative losses and, to a lesser extent, limited by runoff. At EB, C:N ratios were most strongly and negatively related to WTD but increased significantly with higher precipitation and runoff. In contrast, C:N ratios at LG appeared unrelated to WTD and runoff, and increased together with temperature, ET and precipitation (Table 6.4 and Table 6.5).

Table 6.4. Eller Beck Kendall's correlation coefficients between water quality parameters and daily (d) and weekly (wk) average hydro-meteorological parameters air temperature (T), evapotranspiration (ET), precipitation (P), runoff (R) and water table depth (WTD). FDR-adjusted p-values < 0.05 are highlighted in yellow, p-values < 0.01 are highlighted in red.

Parameter	T (d)	ET (d)	P (d)	R (d)	WTD (d)	T (wk)	ET (wk)	P (wk)	R (wk)	WTD (wk)
DOC (mg L^{-1})	-0.08	-0.10	0.15	0.40	-0.56	-0.07	-0.12	0.21	0.36	-0.43
POC (mg L^{-1})	0.37	0.36	0.04	-0.31	0.48	0.42	0.44	-0.03	-0.37	0.54
DN (mg L^{-1})	-0.03	-0.03	0.07	0.25	-0.28	0.01	-0.04	0.04	0.19	-0.17
PN (mg L^{-1})	0.34	0.33	0.02	-0.27	0.41	0.39	0.40	-0.02	-0.33	0.47
DOC:DN	-0.11	-0.13	0.12	0.34	-0.51	-0.13	-0.15	0.23	0.35	-0.45
POC:PN	0.34	0.29	0.05	-0.29	0.51	0.35	0.38	-0.03	-0.36	0.51
C:N	-0.07	-0.10	0.13	0.29	-0.40	-0.08	-0.11	0.24	0.29	-0.37
HA (mg L^{-1})	0.30	0.43	-0.04	-0.37	0.37	0.34	0.48	-0.15	-0.39	0.37
FA (mg L^{-1})	-0.21	-0.30	0.13	0.52	-0.56	-0.24	-0.33	0.28	0.48	-0.44
Hum (mg L^{-1})	0.20	0.11	0.10	-0.03	0.01	0.23	0.16	0.13	-0.09	0.16

Table 6.5. Long Grain Kendall's correlation coefficients between water quality parameters and daily (d) and weekly (wk) average hydro-meteorological parameters air temperature (T), evapotranspiration (ET), precipitation (P), runoff (R) and water table depth (WTD). FDR-adjusted p-values < 0.05 are highlighted in yellow, p-values < 0.01 are highlighted in red.

| Parameter	T (d)	ET (d)	P (d)	R (d)	WTD (d)	T (wk)	ET (wk)	P (wk)	R (wk)	WTD (wk)
DOC (mg L^{-1})	-0.05	-0.18	0.23	0.47	-0.36	-0.06	-0.17	0.44	0.41	-0.31
POC (mg L^{-1})	0.42	0.31	0.06	-0.45	0.52	0.47	0.40	-0.05	-0.54	0.62
DN (mg L^{-1})	-0.21	-0.28	0.19	0.57	-0.47	-0.21	-0.32	0.39	0.52	-0.42
PN (mg L^{-1})	0.40	0.27	0.08	-0.38	0.48	0.46	0.35	0.02	-0.47	0.58
DOC:DN	0.37	0.32	0.00	-0.50	0.45	0.40	0.40	-0.15	-0.54	0.48
POC:PN	0.28	0.15	0.03	-0.43	0.47	0.30	0.21	-0.13	-0.50	0.51
C:N	0.27	0.14	0.16	0.05	0.04	0.29	0.19	0.25	0.03	0.05
HA (mg L^{-1})	0.44	0.34	0.06	-0.30	0.22	0.48	0.45	0.01	-0.33	0.23
FA (mg L^{-1})	0.06	-0.12	0.21	0.22	-0.13	0.05	-0.11	0.40	0.16	-0.06
Hum (mg L^{-1})	0.19	-0.01	0.17	0.00	0.08	0.21	0.03	0.28	-0.07	0.16

Stream-water concentrations of HA increased with higher temperatures and, particularly at EB, with higher ET and lower water tables, while reducing significantly with runoff (Table 6.4 and Table 6.5). At EB, higher FA concentrations were significantly and strongly related to higher runoff, shallower water tables and lower temperature and ET (Table 6.4), while being driven significantly only by precipitation and, to a lesser extent, runoff at LG (Table 6.5). Humin concentration showed relatively weak correlations with all included parameters but increased most strongly and significantly with temperature at EB (Table 6.4) and with weekly total precipitation at LG (Table 6.5).

6.3.7 Principal components analysis

Relationships between hydro-meteorological variables and concentrations of DOC, POC, DN, PN, humic substances (HS) and selected elements were further explored independently for each catchment using a principal components analysis (PCA). The Kaiser-Meyer-Olkin (KMO) values were 0.86 for EB and 0.88 for LG, thus verifying the sampling adequacy for the analysis as "excellent" (Kaiser, 1974). Bartlett's test of sphericity for the EB ($\chi^2(1431) = 27269$, $p < 0.001$) and the LG matrices ($\chi^2(1431) = 24022$, $p < 0.001$) indicated that correlations between variables were sufficiently large for PCA to capture significant variance in the data. Based on the "broken stick" model (Jackson, 1993), four significant principal components (PCs) were retained for EB and three for LG (Figure 6.10).
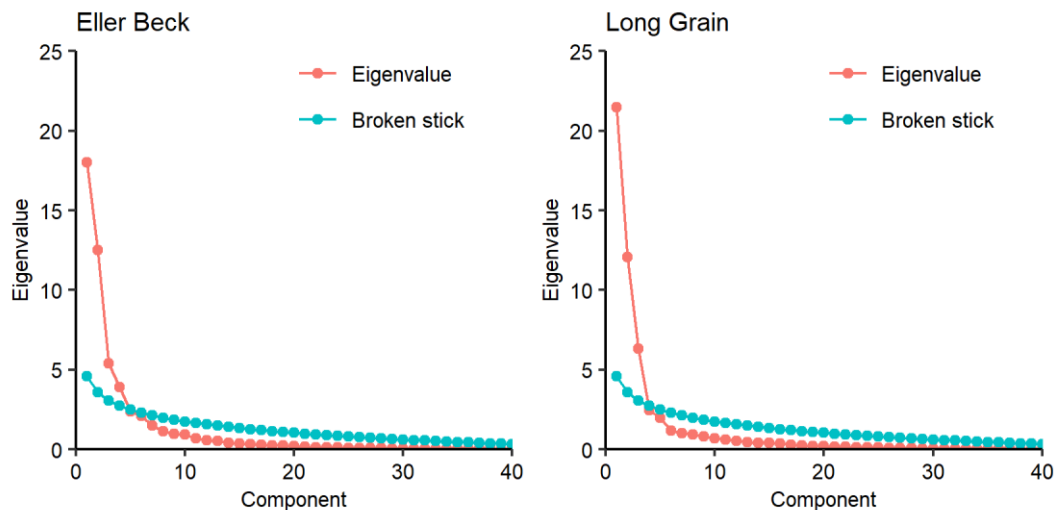

Figure 6.10. Scree plots for Eller Beck and Long Grain showing eigenvalues for each component (red) and eigenvalues expected under the "broken stick" model (blue).

175

Table 6.6. The loadings for variables on the principal components and their associated % variance and eigenvalues from PCA on Eller Beck and Long Grain correlation matrices. High loadings (>|0.5|) are emphasised in bold.

Variable	Eller Beck				Long Grain		
	PC1	PC2	PC3	PC4	PC1	PC2	PC3
% variance	33.3	23.2	10.0	7.3	39.7	22.4	11.7
Eigenvalue	18.0	12.5	5.4	3.9	21.5	12.1	6.3
T (w)	**0.670**	0.196	0.120	-0.158	**0.703**	-0.323	0.349
ET (w)	**0.696**	0.101	0.187	-0.011	**0.585**	-0.458	0.304
Prec (w)	-0.400	0.225	0.324	-0.125	-0.023	**0.685**	0.370
R (d)	**-0.530**	0.093	0.393	0.101	-0.257	**0.733**	0.221
R (w)	**-0.567**	-0.077	0.399	0.082	-0.383	**0.651**	0.140
MS/LG WTD (d)	**0.921**	-0.012	-0.044	-0.009	**0.679**	**-0.611**	-0.114
EB/GA WTD (d)	**0.948**	-0.053	-0.025	-0.025	**0.727**	**-0.505**	-0.072
MS/LG WTD (w)	**0.899**	0.074	-0.061	-0.028	**0.732**	**-0.528**	-0.073
EB/GA WTD (w)	**0.927**	0.049	-0.021	-0.051	**0.755**	-0.453	-0.079
Dry mass	0.297	**0.861**	0.250	-0.064	**0.885**	0.384	0.169
POC	**0.821**	0.178	0.339	0.066	**0.778**	-0.328	0.076
PN	**0.693**	0.320	0.344	0.174	**0.848**	-0.234	0.053
PC	**0.824**	0.191	0.340	0.065	**0.767**	-0.332	0.074
DOC	**-0.736**	0.375	0.202	-0.214	-0.119	**0.711**	**0.576**
DN	-0.304	0.361	-0.072	**0.619**	-0.248	**0.764**	0.233
POC:PN	**0.828**	0.020	0.261	0.032	**0.619**	**-0.541**	0.144
DOC:DN	**-0.701**	0.088	0.202	**-0.595**	0.051	0.316	**0.593**
C:N	**-0.543**	0.073	0.287	**-0.703**	0.225	0.232	**0.671**
LOI	**-0.799**	-0.113	0.494	-0.026	-0.155	0.414	**0.800**
HA	**0.687**	0.238	0.472	0.179	**0.706**	-0.225	**0.525**
FA	**-0.693**	**0.568**	-0.021	-0.258	0.394	**0.830**	0.158
Humin	0.124	**0.839**	0.152	-0.117	**0.752**	**0.523**	0.077
Na	0.065	**0.697**	**-0.633**	-0.194	**0.507**	**0.527**	-0.481
Mg	0.034	**0.676**	**-0.658**	-0.211	**0.513**	0.449	**-0.637**
Al	-0.016	**0.906**	-0.332	0.021	**0.746**	0.479	-0.309
Si	**0.755**	0.404	-0.203	-0.036	**0.814**	-0.013	-0.388
P	**0.632**	0.391	0.237	0.059	**0.897**	-0.215	0.028
S	-0.213	**0.605**	**-0.686**	-0.155	0.079	**0.652**	**-0.666**
Cl	0.428	0.485	-0.412	0.397	**0.761**	0.274	-0.367
K	-0.185	0.302	-0.225	**0.845**	0.265	**0.626**	-0.498
Ca	-0.157	**0.734**	**-0.602**	-0.013	0.317	**0.674**	**-0.588**
Ti	-0.477	**0.595**	0.275	0.340	0.443	**0.590**	0.270
V	**-0.667**	**0.596**	0.145	0.170	0.223	**0.909**	0.149
Cr	-0.134	0.246	0.098	0.409	0.198	0.187	-0.215
Mn	**0.810**	0.313	-0.283	0.007	**0.900**	-0.259	-0.209
Fe	**0.866**	0.317	0.181	-0.111	**0.929**	-0.238	0.151
Co	**0.830**	0.338	0.285	-0.113	**0.928**	-0.197	0.158
Ni	-0.156	0.268	0.236	0.216	0.094	0.100	-0.168
Cu	**-0.666**	**0.580**	0.305	0.134	0.483	**0.522**	0.176
Zn	**-0.579**	**0.695**	-0.329	0.068	0.109	**0.883**	-0.324
As	0.031	**0.765**	**0.519**	-0.041	**0.912**	0.137	0.316
Br	-0.106	**0.877**	0.129	-0.152	**0.866**	0.291	0.257
Rb	-0.171	0.422	-0.077	**0.798**	**0.593**	**0.556**	-0.252
Sr	-0.276	**0.780**	-0.424	-0.251	0.497	**0.590**	**-0.516**
Y	**-0.535**	**0.692**	0.316	-0.108	**0.932**	0.017	0.153
Zr	-0.305	0.436	0.287	0.337	0.177	0.338	0.320
Sn	0.369	0.339	0.215	-0.180	**0.817**	-0.005	-0.054
Sb	0.422	0.250	-0.104	-0.145	**0.820**	-0.052	-0.078
I	0.141	**0.776**	0.324	-0.151	**0.686**	0.183	**0.516**
Ba	0.105	**0.746**	-0.138	-0.283	**0.740**	0.140	-0.215
Hf	**0.636**	0.471	0.324	0.022	**0.918**	-0.072	0.139
W	0.312	0.144	0.056	-0.099	**0.647**	0.011	0.001
Hg	**0.779**	0.335	0.096	-0.131	**0.856**	-0.048	-0.030
Pb	**-0.676**	**0.552**	0.429	0.015	0.251	**0.783**	0.486

For EB, the first four statistically-significant PCs together accounted for a combined 73.8% of the variance in the data. PC1, summarising 33.3% variance (eigenvalue = 18.0), had high positive loadings (> 0.5) for temperature, ET and WTD variables, together with particulates (POC, PC, PN, POC:PN) and HA, and elements Si, P, Mn, Fe, Co, Hf and Hg, and weaker positive loadings (< 0.3) for dry mass, Cl, Sn, Sb and W. Conversely, PC1 had high negative loadings (< −0.5) for runoff variables, DOC, DOC:DN, LOI, FA, and elements V, Cu and Pb, with weaker negative loadings (> −0.3) for precipitation, DN, Ti and Zr (Figure 6.11). PC1 thus appears to represent the variance in water quality parameters with water availability along a left-to-right (Figure 6.11) spectrum from "dry" (low WTD) to "wet" (high runoff) conditions.

PC2 from the EB matrix accounted for 23.2% variance (eigenvalue = 12.5) and had high positive loadings for dry mass and humin, as well as Na, Mg, Al, Cl, Ca, Ti, Zn, As, Br, Sr, Y, Zr, I and Br, and moderate positive loadings for DOC, DN, PN, Si, P, Cl, K, Mn, Fe, Co, Rb, Zr, Sn, Hf and Hg, suggesting that PC2 summarises a grouping a elements closely associated with the release of dry mass and DOC. PC3 explained 10.0% variance (eigenvalue = 5.4) and is characterised by the highest negative loading for S, accompanied by secondary high negative loadings for Na, Mg and Ca, against a high (though secondary) positive loading for As (Figure 6.11). PC4 accounted for 7.3% (eigenvalue = 3.9) of the variance and contained high positive loadings for DN and elements K and Rb, with weaker positive loadings for Cl, Ti, Cr and Zr, against strong negative loadings for DOC:DN and C:N ratios, indicating that PC4 has characterised the association of elements with nitrogen. Ni was the only element among the EB matrix with a maximum loading of < |0.3|, indicating disassociation from the main four PCs, but was most aligned with a positive loading for PC2 and with insoluble organic matter.

For LG, the first three statistically-significant components together explained 73.8% of the variance in the data. PC1 accounted for 39.7 % (eigenvalue = 21.5) of the variance and contained high positive loadings for temperature, ET and WTD – indicative of dry conditions with deeper WTD – as well as for dry mass, particulates (POC, PC, PC, POC:PN), HA and humin, and elements Na, Mg, Al, Si, P, Cl, Mn, Fe, Co, As, Br, Rb, Y, Sn, Sb, I, Ba, Hf, W and Hg, with weaker positive loadings for FA, Ca, Ti, Cu and Sr. Conversely to EB, PC1 in LG did not have high negative loadings of variables, with the strongest negative loading with weekly runoff (−0.38), suggesting that PC1 was primarily an indicator of variables associated with dry conditions (Figure 6.11).

PC2 from the LG matrix explained 22.4% (eigenvalue = 12.1) of the variance and consisted of high positive loadings for precipitation and runoff – characterising wet, high flow conditions

– together with high loadings for DOC, DN and FA, and elements Na, S, K, Ca, Ti, V, Cu, Zn, Rb, Sr and Pb, and weaker positive loadings for dry mass, DOC:DN, LOI, Mg, Al and Zr. In addition, PC2 had strong negative loadings for WTD and POC:PN and weak negative loadings for temperature, ET, POC and PC (Figure 6.11). PC2 thus appears to group parameters with high positive loadings together with indicators of wet, high flow conditions (precipitation and runoff) and distinguishes these from dry, low flow conditions and reductions in particulates which were associated positively for PC1.

LG PC3 summarised 11.7% (eigenvalue = 6.3) of variance, and was characterised by high positive loadings for DOC, DOC:DN, C:N, LOI, HA and element I, with weak positive loadings for temperature, ET and precipitation and elements As, Zr and Pb. Conversely, PC3 had high negative loadings of Mg, S, Ca and Sr, with weak negative loadings of Na, Al, Si, Cl, K and Zn. Elements Cr and Ni both had maximum loadings below < │0.3│ for the three PCs, indicating that these elements were largely disassociated from PC retained from the LG matrix, but had their strongest negative loadings with PC3.

Water quality parameters, which were strongly associated with dry conditions in both catchments, indicated by loadings > │0.5│, were particulates (POC, PC, PN, POC:PN) and HA, and elements Si, P, Mn, Fe, Co, Hf and Hg. Conversely, parameters strongly associated with wet conditions in both catchments comprised DOC, FA and elements V, Cu and Pb. Both catchments also separate two groupings of elements on PC3, with positive loadings for precipitation, LOI and HA together with elements As, I and Pb against negative loadings of Na, Mg, Al, S, Cl, Ca, Zn and Sr, suggesting that the affinity for some elements to bind to organic matter during runoff and precipitation events is similar for both catchments.

The most striking difference between the PCs of EB and LG is the association of water quality parameters with either runoff or WTD, i.e. wet or dry conditions. For EB the associations occur over a spectrum across PC1, suggesting that water quality parameters aligned either with wet or dry conditions. For LG, this association with hydrological condition is separated by PC1 and PC2, suggesting that there is considerable overlap for most parameters between dry and wet conditions. In addition, DN and elements K and Rb separate strongly in EB as PC4, while for LG they align with other positive loadings on PC2, indicative of wet, high flow conditions.
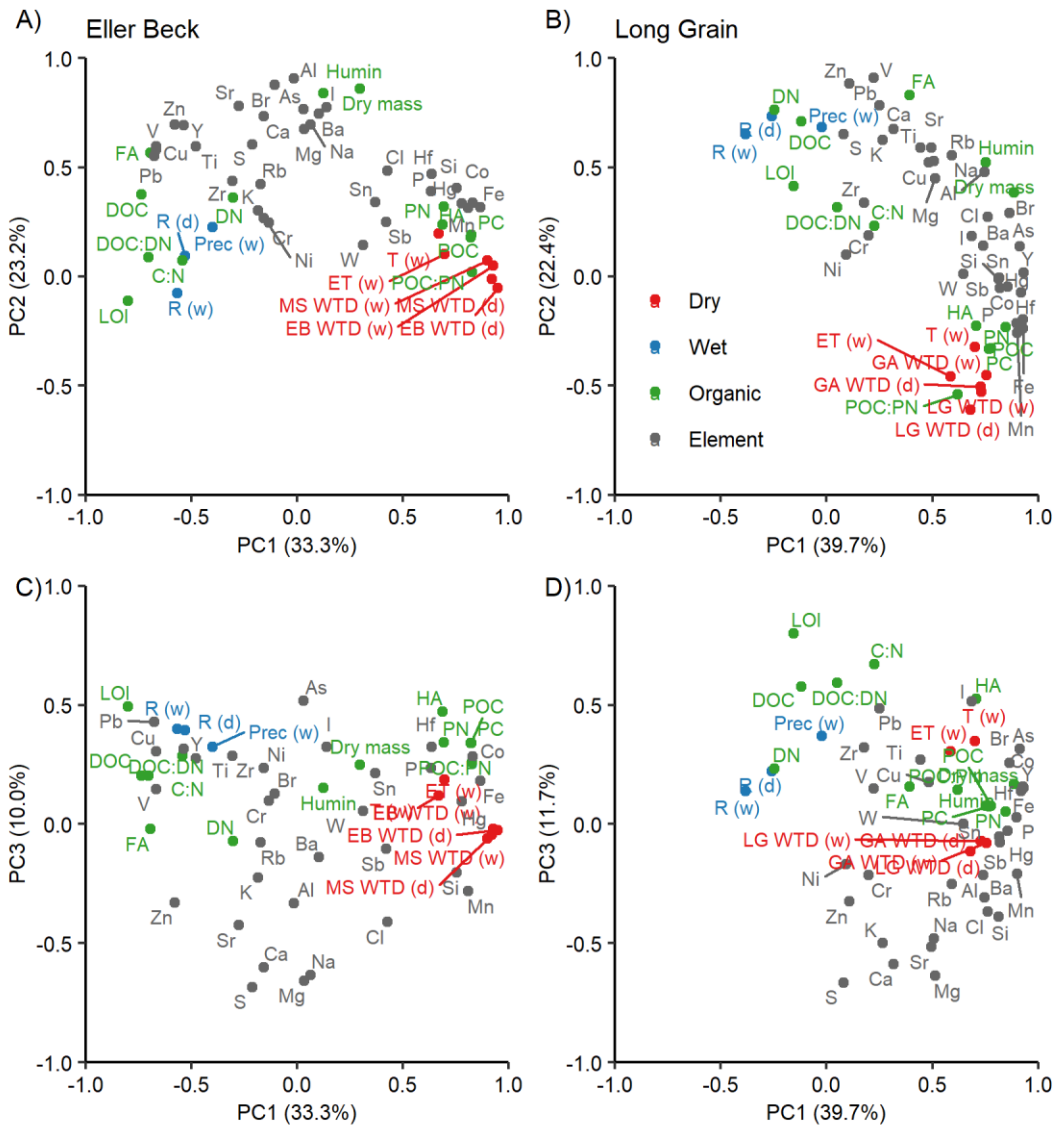
Figure 6.11. Loadings plots from principal components analysis (PCA) for components 1, 2 and 3, based on the Eller Beck (EB) (A and C) and Long Grain (LG) (B and D) correlation matrices. Colours indicate broad groupings into hydro-meteorological variables (blue), biophyllic parameters (green) and pure elements (grey).

6.4 Discussion

6.4.1   Stream-water organic carbon budgets and characterisation

The aim here was to evaluate the impacts of blanket bog restoration from former afforestation on stream-water quality by comparing intact (EB) and restored (LG) catchments based on a 2-year water sampling campaign (18/07/2018 – 27/08/2020), facilitated by a paired hydrological series (*Chapter 5*). Afforestation and drainage of peatlands are well-known to facilitate the further decomposition of peat and loss of stored carbon through the emission of CO_2 from the peat to the atmosphere (Cannell et al., 1993; Byrne and Farrell, 2005). For example, in a study based on the Mullaghareirk Mountains in southern Ireland,

(Jovani-Sancho et al., 2021) found that the afforestation of peatlands with Sitka spruce (*Picea sitchensis*) or lodgepole pine (*Pinus contorta*) resulted in the underlying peat becoming a net source of atmospheric carbon, although the reduction or complete ceasing of methane (CH_4) emission with lowered water levels also needs to be accounted for within drained peatland carbon budgets (Hargreaves et al., 2003; Strack and Waddington, 2007). Forestry activities have been related to increased export of DOC related to Fe reduction as well as high nitrogen and low C:N ratios due to greater microbial activity (Nieminen et al., 2015), with elevated stream-water DOC causing greater water discolouration (Armstrong et al., 2010). In addition, forestry activities have been linked with a higher release of particulate organic matter, including POC, as direct result of increased disruption through on-site activity such as ploughing, tree planting and harvesting (Finnegan et al., 2014; Palviainen et al., 2014; Ryder et al., 2014; Sloan et al., 2018a).

Forest-to-bog restoration, which typically involves deforestation followed by the removal of trees and brash and the blocking of drains, aims to reverse the rate of peat decomposition and related fluvial exports of organic matter by re-establishing a shallow water table (Parry et al., 2014). Upon rewetting, DOC concentrations have been found to either increase or decrease in the short-term, with Gaffney et al. (2020) observing considerable increases in DOC over the summer following rewetting and Howson et al. (2021) noting higher DOC concentrations in porewater samples at a forest-to-bog restoration site in Scotland, compared to a nearby intact blanket bog. Conversely, reduced DOC concentrations upon rewetting have been linked with short-term increases in flushing (Wallage et al., 2006), and Höll et al. (2009) identified significantly lower DOC concentrations in shallow (4 cm depth) pore-waters in a restored peatland 20 years after rewetting, compared to a drained site, related to a reduction in the rate of peat decomposition with the re-establishment of shallow water levels.

6.4.1.1 DOC and POC concentrations and fluxes

The data from May Moss highlight significantly lower DOC concentration at the restored site (LG, Med = 19.1 mg L^{-1}), 10 years following restoration, compared to the intact site (EB, Med = 39.1 mg L^{-1}), which resulted in considerable difference in annual TOC fluxes, ranging 8.74 – 13.01 g m^{-2} yr^{-1} at LG and 11.06 – 24.60 g m^{-2} yr^{-1} at EB. At both sites, TOC was mainly driven by DOC and characterised by high annual DOC:POC ratios, corroborating others on the relative dominance of DOC in the carbon budget within upland peat catchments (Dawson et al., 2002). Headwater streams draining peats tend to have naturally high concentrations of

DOC, which have reportedly risen over the past decades attributed to a range of causes (Evans et al., 2005). High concentrations of DOC at both catchments at May Moss were thus not surprising. However, the significantly higher concentrations from EB resembled more the maximum DOC concentrations (24.59 – 46.14 mg L^{-1}) measured at headwater peatland streams in the South Pennines, UK (Pawson et al., 2012), although they were considerably lower than median DOC concentrations (58.3 mg L^{-1}) measured at eroding peat gullies (Clay et al., 2012). DOC concentration at LG were more comparable to mean DOC concentrations (22 mg L^{-1}) measured in an upland peat catchment in the Harz mountains, Germany (Birkel et al., 2017).

POC concentrations did not differ significantly between catchments, with median concentrations of 2.0 mg L^{-1} measured for EB and 1.9 mg L^{-1} at LG, and were relatively low, compared to some peatland headwaters in northern England with average POC concentrations ranging 1.63 – 4.97 mg L^{-1} (Pawson et al., 2012). As high POC concentrations tend be associated with higher sediment fluxes due to peat erosion (Evans and Warburton, 2005; Parry et al., 2014; Shuttleworth et al., 2015; Worrall et al., 2017), our relatively low concentrations of POC reflect the minimal peat erosion observed at both catchments.

DOC and POC fluxes were quantified for 2018, 2019 and 2020. It must be noted here that the use of extrapolated datasets for the quantification of these annual fluxes is based on imperfect regression with runoff and are therefore likely to contain a high level of error both due to the regression equation (Wilson et al., 2011a) and the underestimation of runoff implicit in hourly measurements (*Chapter 5*). Nevertheless, across the monitoring period since March 2017, the lowest annual DOC fluxes at both EB (10.75 g m^{-2} yr^{-1}) and LG (8.38 g m^{-2} yr^{-1}) occurred in 2018, a year that was characterised by a severe summer drought (Turner et al., 2021) and that resulted in deep water table drawdown in both catchments (*Chapter 5*). The year 1995, another year with a prominent summer drought (Walker and Smithers, 1998), was likewise associated with a reduced flux in DOC (7.0 g m^{-2} yr^{-1}) from a peat catchment in the North Pennines attributed to a reduction in microbial activity and thus DOC production under more acidic conditions (Scott et al., 1998). TOC fluxes at EB and LG during non-drought years (2019 and 2020) were lower compared to an estimate from Moor House (37.1 g m^{-2} yr^{-1}) in the North Pennines in 1999 (Worrall et al., 2003), while positioned above and below, respectively, of estimates from sites in NE Scotland (191 kg ha^{-1} yr^{-1} = 19.1 g m^{-2} yr^{-1}) and Mid-Wales (121 kg ha^{-1} yr^{-1} = 12.1 g m^{-2} yr^{-1}) (Dawson et al., 2002). Interestingly, DOC fluxes from EB resembled more a drained site (23.5 g C m^{-2} yr^{-1}), while LG was comparable to a non-drained (7.9 g C m^{-2} yr^{-1}) peat catchment in the Flow Country, Scotland

(Pickard et al., 2022). The large year-on-year variation in DOC fluxes observed at EB thus highlights the value of multi-year DOC flux estimates to capture the range in annual DOC fluxes from upland peat catchments (Billett et al., 2010).

6.4.1.2   Characterisation of DOC

The significant disparity in DOC concentrations between the intact (EB) and restored (LG) sites was furthermore reflected in their relative UV-Vis absorbances. The close association between DOC and UV-Vis absorbance spectra is often used to derive information such as the degree of water discolouration and the relative proportions of humic and fulvic acids (E4:E6) (Peacock et al., 2014). Higher E4:E6 ratios at the restored site were juxtaposed against significantly lower NIRS-derived stream-water HA:FA ratios, complicating a valid interpretation of humic substances characterisation of DOC and may be due to the measured materials (i.e. liquid, filtered samples to derive E4:E6 vs post-freeze-dried total dry mass NIRS-based HA:FA) or method to derive the ratios. Higher E4:E6 ratios at a restored bog were similarly reported by others (Wilson et al., 2011a; Gaffney et al., 2018), indicating a reduction in the export of humic substances while (Wallage et al., 2006) found significantly lower E4:E6 ratios associated with drain blocking, indicating a more humified DOC source.

SUVA ratios were similarly high at both EB (Med = 5.5) and LG (Med = 5.4), indicative of similarly high levels of aromaticity of DOC (Zheng et al., 2018), and were comparable to an undisturbed peatland (Bois-de-Bell) (mean = 5.52) in Quebec, Canada (Strack et al., 2015). Linear regressions between absorbance wavelengths and DOC concentrations showed a best-fit for wavelengths at 272 nm and 242 nm for EB and LG, respectively. Both catchments presented a steady decline in fitting between absorbance and DOC towards higher wavelengths, as described by (Peacock et al., 2014), which has been attributed to the exponential reduction in the absorbance of HA, a major component of DOC, towards higher wavelengths (Wang and Hsieh, 2001; Peacock et al., 2013a).

Abs_{400}, used to characterise the degree of discolouration in water samples, was significantly correlated with DOC concentrations at EB and LG, corroborating the close association observed between water colour and DOC (Wallage et al., 2006; Wallage and Holden, 2010). The median Abs_{400} from stream-water samples at the recovering site (LG) (Mdn = 16.4 au m^{-1}) were significantly lower than samples from the intact site (EB) (Mdn = 33.6) but resembled the median Abs_{400} (14.6 au m^{-1}) from shallow peat pore-waters an intact blanket peat catchment in northern England (Wallage et al., 2006). Similar to the findings of Wallage et

al. (2006), Abs_{400} were significantly lower at the recovering peatland (LG) relative to the intact site (EB), indicating reduced levels of discolouration at LG.

6.4.1.3   Residual effects of forestry on stream-water organic carbon

Stream-water chemistry may not necessarily be directly representative of upstream peat composition, however catchments containing highly organic soils and peats generally have higher stream-water concentrations of DOC (Hope et al., 1997; Aitkenhead et al., 1999), and close coupling between stream-water and shallow pore-water for DOC have been demonstrated (Clark et al., 2005). While DOC can be mineralized within the stream (Richey et al., 2002), there is also possibility of autochthonous in-stream production of DOC, although allochthonous DOC tends to dominate in peat-draining streams (Eatherall et al., 2000). We may therefore presume that stream-water DOC is representative of DOC concentrations within shallow peat. As the comparative analysis between the two sites was based on a paired catchment approach, with environmental influences assumed to be consistent across both catchments and runoff corrected by unit of catchment area, we regard the differences in DOC, as well as other parameters, between the two catchments as indicative of differences in the processes affecting the relative availability and/or mobilisation of DOC, as well as other parameters, within the catchment.

The significantly lower DOC concentrations and discolouration at LG are suggestive that deforestation, drain-blocking and rewetting have been effective in limiting fluvial carbon loss and colouration to levels below those of an adjacent intact blanket mire. This would corroborate others on the effects of drain-blocking on lowering stream DOC concentrations and discolouration in peatlands (Wallage et al., 2006; Armstrong et al., 2010; Wilson et al., 2011). However, the significant contrast in DOC and colour between the two sites may also hint at underlying residual effects of previous forestry activities and subsequent rewetting.

Analysis of the relationships between DOC and POC with runoff and WTD indicates clear similarities and differences in behaviour between the two catchments (Figure 6.6). In both catchments, POC concentrations increased with lower runoff and deeper water levels, suggesting that POC was prone to dilution (Dawson et al., 2002), which is plausible given the low concentrations measured in both streams (EB median = 2.0 mg L^{-1}; LG median = 1.9 mg L^{-1}). In both catchments, water level was more important than runoff in determining POC concentration, and the two catchments resembled each other in their POC behaviour with water level, indicated by their similar slope (EB = 0.01; LG = 0.009) in the regression models

(Figure 6.6). This would imply that the processes releasing POC, such as peat erosion (Evans and Lindsay, 2010), were comparable (and limited) between both sites.

In contrast to POC, we observe that DOC concentrations increased with higher runoff and shallower water levels in both catchments (Figure 6.6), suggesting a flushing effect which drives greater DOC loss from the peat during high flow conditions (Worrall et al., 2002), with EB releasing higher DOC concentrations than LG in both instances. However, while WTD predicted a greater proportion of variation in DOC at EB, runoff was more important at LG (Figure 6.6). The variation in response to WTD may be the result of a more established gradient in mobile DOC along the intact peat column at EB (with more mobile DOC nearer the surface), while distributions within the upper peat column at LG could still be more mixed owing to former disturbance.

Moreover, the regression slopes indicate that DOC concentrations at LG increase faster in response to higher runoff than in EB, though runoff rates would need to rise well above 1.0 mm day^{-1} for the two catchments to intersect in their DOC response to runoff (Figure 6.6). This differing rate in response to runoff could be a function of the contrast in catchment size, with the larger area of LG leading to greater volumes and velocities in runoff which could drive more rapid changes in the transport and flushing of DOC (Coch et al., 2020). Alternatively, preferential flowpaths across the intact peat at EB could be more established (Holden and Burt, 2003a), resulting in a more gradual change in DOC concentration in stream water, while flowpaths at LG may be subject to more variation both vertically and laterally owing to former disturbance across and down the peat profile.

Reduced stream-water DOC concentrations at the recovering site could thus be related to changes in DOC production, release and/or transportation processes within the peat (Wallage et al., 2006) associated with previous ploughing activities and tree growth. The resulting disturbances to the peat profile likely have led to enhanced hydraulic connectivity through a higher proportion of macropores related to drainage within the upper peat layers and thus higher baseflow observed at the LG catchment (*Chapter 4*), which may be causing enhanced and persistent flushing and thus higher dilution of DOC at the recovering site (Wallage et al., 2006). While several studies have pointed out the increased release of suspended sediment and POC following peatland forestry harvesting (Finnegan et al., 2014; Palviainen et al., 2014; Ryder et al., 2014), we found no significant differences in POC concentrations between the intact (EB) and restored (LG) sites, which suggests that POC release has most likely recovered at LG.

Despite finding comparable C:N ratios in stream-water between the intact and restored sites, median DOC:DN ratios, which would reflect more directly the microbial activity than the particulate ratio, were significantly lower in stream-water at the restored site (LG). Decomposition tends to reduce soil C:N ratios, as a greater release of carbon as CO_2 results in a relative reduction of carbon to nitrogen in the soil (Biester et al., 2012), which could point towards higher levels of peat decomposition at the recovering site (LG). This relationship is furthermore reflected in the general positive correlation between C:N ratio and fluvial DOC concentration (Aitkenhead and McDowell, 2000), although Kaila et al. (2016) observed no relationship between the degree of decomposition and DOC release, suggesting that carbon mobilization is more related to microbially mediated redox reactions than the direct microbial breakup of organic matter (Grybos et al., 2009). As water levels tended to be lower for most of the year at the recovering site (LG), relative to the intact bog (EB) (*Chapter 5*), the lower incidence of reducing conditions within the near-surface peat layer may thus be a limiting factor for the release of DOC (Grybos et al., 2009). Alternatively, previous disturbance of microbial communities may still be impacting on microbially-driven processes (Andersen et al., 2013), including redox reactions, with consequences for DOC production. Lower stream-water DOC concentrations at the restored site (LG) may thus be reflective of processes including enhanced flushing, resulting in greater dilution of DOC as well as changes in microbial activity related to lower average water levels, although these hypotheses would need to be verified by further analysis e.g., comparing pore-water concentrations of DOC between the intact and recovering sites.

6.4.2 Major element concentrations

6.4.2.1 Dry mass composition

Dry mass concentrations of elements revealed relative differences in terms of the composition of the dry masses extracted from the water samples. Dry masses from stream-waters at the restored site (LG) were significantly enriched in NIRS-derived FA and humin and XRF-derived element concentrations of Na, Mg, Al, Si, S, Cl, K, Ca, Cr, Mn, Ni, Zn, Rb, Sr, Y, Zr, Ba and Hg. Conversely, EB dry masses were relatively enriched in HA as well as P, Ti, Fe, Cu, As, I, Hf, W and Pb and had significantly higher LOI (%). Dry mass concentrations of V, Co, Br, Sn and Sb were at comparable levels between both sites. The significantly higher LOI and higher proportions of HA relative to FA within the dry mass suggest that the intact site (EB) has a higher organic and more humified DOC load, while the restored site (LG) showed greater proportions of mineral elements with lower LOI (%) and greater quantities of Al, Si,

K, Rb, Y and Zr. The restored site thus appears more mineral rich, despite also having a highly-organic dry mass load.

Heavy metals Ti, Fe, Cu, As and Pb were significantly enriched, relative to crustal averages, within the dry mass load from the intact site (EB). Cu, As and Pb are dust-derived elements in peat, meaning their accumulation within the peat profile is related to atmospheric deposition related to anthropogenic industrial and post-industrial pollution which has resulted in a strong down-core profile with high enrichment within the shallow sub-surface peat layer (Cloy et al., 2005, 2008, 2009; Tipping et al., 2010), likewise detected at May Moss (Figure 6.1). Iron, derived from mineral aerosols derived from the weathering (Shotyk, 1997), is another element with a strong surface peak in the peat profile of the intact Moss (Figure 6.1) and also had elevated concentrations within the EB dry masses, relative to the restored catchment (LG). In contrast Zn shows a more diffuse peat profile (Figure 6.1), reflecting greater mobility and down-core migration of the element (Shotyk, 1988; Shotyk et al., 1990; Broder and Biester, 2017). This would indicate, from a source perspective, a strong contribution of surface peat layers to the stream-water chemistry with a prevalence of saturation-excess overland flow (Holden and Burt, 2002a) at the intact site. The significantly higher loading of P within dry mass at the intact site (EB) is again reflective of the strong surface peak in phosphorus within the intact peat profile (Figure 6.1) furthermore implying dominant surface runoff as well as efficient phosphorus release to the stream system (Worrall et al., 2016).

The relative enrichments of elements showing a more diffuse vertical profile, such as Zn and Mn (Novak et al., 2011), together with the relative depletion of elements with strong surface enrichment, such as P, Cu, As, Pb, at the restored site (LG) could thus be a function of disturbance to the shallow peat profile and the lack of a well-developed near surface acrotelm geochemical structure. While heavy metal loadings within dry masses at the restored site are still high compared to crustal averages, they are at significantly lower concentrations relative to the intact bog, which points towards either a difference in flow paths, most likely greater subsurface throughflow facilitated by higher incidence of macropores and pipes as a result of drainage (Holden et al., 2006), or that surface peats sustaining flows towards the LG stream are more mixed in composition as a function of disturbance, e.g. ploughing and ditching, during previous forestry activities, or a combination of both factors.

6.4.2.2   Residual element enrichment following restoration

While a significant proportion of elements were enriched within the dry mass load at the restored site, the opposite was observed in terms of water sample concentrations. A greater number of elements within our analysis occurred at significantly reduced aqueous concentration at the restored tract (LG) relative to water samples from the intact site (EB). Few elements (Na, Mg, K, Mn, Ni) were at comparable stream-water concentrations between the two sites, while Al, Si, S, Cl, Ca and Sr remained significantly enriched at the restored tract (LG). As the intact site (EB) was relatively enriched in stream-water concentrations of dry mass and DOC, while POC was at comparable concentrations, we may infer that the dry mass load was tightly bound to DOC. The dilution-effect at the restored catchment (LG) may therefore have been a key driver in the reduced stream-water concentration of most elements, particularly those strongly associated with the DOC flux, such as As and Pb (Broder and Biester, 2017).

The relative enrichments stream-water concentrations of Al, Si, S, Cl, Ca and Sr at the restored site (LG), 10 years after rewetting, suggest that either dilution did not have as much of an effect on their concentrations, compared to other elements, or that they truly occur at enriched levels within the recovering peat (LG). Elevated concentrations of Al, S and Ca were similarly found in surface- and shallow pore-waters following forest-to-bog restoration in the Flow Country, Scotland (Gaffney et al., 2018), while elevated Al concentrations have been measured in blanket bog lakes situated in catchments draining active conifer plantation forestry (Drinan et al., 2013). Furthermore, a study by Evans et al. (2014b) which analysed surface water quality in 51 sites across the North York Moors, found that conifer plantations had exacerbated acidification, leading to threefold higher Al concentrations, as well as fivefold increases in nitrate, compared to non-planted moorland. High Al concentrations may be related to the release from needle decomposition upon forestry clear-cutting (Kaila et al., 2012; Asam et al., 2014a) and disturbance through ploughing of shallow peat (Muller and Tankéré-Muller, 2012). In terms of element concentration recovery following rewetting, it took 10 years for Ca concentrations to return to pristine levels at a restored peatland in Finland (Haapalehto et al., 2011), while Gaffney et al. (2018) found that Al and Ca concentrations reduced to levels comparable to an intact bog 17 years post-restoration, suggesting that Al and Ca concentrations within the restored catchments (LG) may still be in the process of recovery.

The proximity of May Moss to the east coast ($\approx$ 12 km) possibly resulted in the 'sea-salt effect' (Evans et al., 2001) on tree-stands, with the coastal influence on the biogeochemistry of May Moss indicated by relatively high Cl concentrations at both EB (Med = 3.3 mg L^{-1}) and LG (Med = 4.1 mg L^{-1}). The 'sea-salt effect' has been associated with forestry plantations, where marine base cations, such as Na and Mg from chloride ions, displace existing cations, such as Al and Ca, on soil exchange sites, resulting in acidification of runoff (Evans et al., 2001). In addition, legacy effects of atmospheric scavenging of S (Fowler et al., 1989; Neal et al., 2008) by tall forestry conifers likely resulted in S enrichment at LG. Similarly, Ca and Sr have been documented to become concentrated in trees, leading to enrichment in upper soil layers (Poszwa et al., 2000; Schmitt and Stille, 2005). In oceanic peat bogs, the dominant source of Sr has been found to be sea salt (Shotyk, 1997), supporting the marine influence on enrichment of element concentrations by former forestry.

Higher concentrations of Si in ombrotrophic peat have been related to a greater degree of decomposition related to the selective loss of organic matter due to mineralization and an increase in particle density (Biester et al., 2012), and Sr has likewise been related to decomposition (Broder and Biester, 2017). The release of S in peat with water table drawdown has been widely reported, particularly in reference to drought (Tipping et al., 2003; Clark et al., 2005; Fenner and Freeman, 2011). With lowering of the water table, sulphur species are oxidised into more mobile sulphate (Fenner and Freeman, 2011), which has contributed to higher S concentration in pore-waters in forestry and recently restored bogs in the Flow Country (Gaffney et al., 2018), with increased concentrations of sulphur pollutants association with a reduction in *Sphagnum* growth (Ferguson et al., 1978). Gaffney et al. (2018) observed a complete recovery of S concentrations to pristine levels within 17 years post-restoration, which again suggests that S concentrations are in the process of reducing at LG. Elevated concentrations of Al, Si, S, Cl, Ca and Sr may thus represent a legacy effect 10 years post-rewetting, derived from the absorption and soil enrichment of some elements (Al, Cl, Ca) by previous forestry, as well as the release of others (Si, Sr, S) related to greater decomposition of peat.

6.4.3 PCA associations between hydro-meteorological variables, water quality parameters and elements

Principal components analysis (PCA) was used here to examine associations among water quality parameters and a wide array of elements and their relation to possible controlling hydro-meteorological and seasonal variables. While peatland stream-water concentrations

of DOC (Fraser et al., 2001; Koehler et al., 2009; Clay et al., 2012), POC (Robroek et al., 2010; Pawson et al., 2012; Worrall et al., 2014) and selected elements, particularly the nutrients (Cundill et al., 2007; Nieminen et al., 2017a) and metal pollutants (Rothwell et al., 2005; Tipping et al., 2006; Novak and Pacherova, 2008), have been widely analysed and reported. Comprehensive studies that include a fuller and wide array of parameters and elements, such by Broder and Biester (2017) remain scarce.

6.4.3.1 Cool, wet conditions

EB and LG both showed clear associations between certain water quality parameters and hydrological conditions through loadings on PC1 and PC2. Loadings together with WTD and runoff indicated relative associations of parameters and elements with drier and wetter conditions, respectively. Cooler, wetter conditions were thus characterised by negative loadings of PC1 for the intact site and by positive loadings on PC2 for the restored site. Both catchments thus displayed clear association of DOC, DN, LOI, FA and metal elements Ti, V, Cu, Zn and Pb with higher runoff and greater precipitation, and these differentiate to the opposite loadings displayed for temperature, ET and WTD.

DOC concentrations are generally understood to be low in winter and spring but increase in summer and autumn due to enhanced biological activity within the upper peat layer, rather than be associated with high runoff (Clay et al., 2012; Muller and Tankéré-Muller, 2012). Our results, however, found no significant differences in DOC concentrations between seasons, apart from spring DOC being significantly lower compared to the rest of the year at LG. In addition, we observed that DOC concentrations had highly significant, through negative, correlations with WTD, and highly significant positive correlations with runoff, rather than with temperature, at both catchments. As DOC concentrations were considerably lower at the start of the water sampling campaign, during the 2018 summer drought, we consider these strong inverse relationships with WTD and runoff may have been augmented by the considerably lower DOC concentrations observed during this dry period, followed by the rise in concentrations as drought conditions subsided and the water table rebounded (Figure 6.3). This supports previous work showing a serious curtailment of DOC release under drought conditions (Clark et al., 2005, 2012), such as the suppression of DOC in summer 2018 and subsequent DOC release with post-drought rewetting (Ritson et al., 2017). Indeed, DOC export from an upland peat catchment in Germany was found to be considerably higher during wetter conditions in 2014, compared to a drier period in 2013 (Birkel et al., 2017). FA make up a high proportion of DOC and are soluble under both base and acidic conditions

(Charman, 2002; Rydin and Jeglum, 2013), making them highly mobile, and were likewise associated with high DOC and runoff.

The close association between DOC and DN potentially reflects the strong positive correlations that have been observed between DOC and ammonium (Daniels et al., 2012), and suggests that the DN from both EB and LG may be dominated by ammonium rather than nitrate. Ammonium release from peatlands has been related to low gully density, while higher nitrate concentration has been associated with high gully density which allows greater water table drawdown, aeration and nitrification (Daniels et al., 2012). The ceasing of nitrification and nitrate mobilization from peat upon rewetting due to anoxic conditions has also been noted elsewhere (Kaila et al., 2016), suggesting that if water levels are sufficiently close to the bog surface for most of the year they could limit nitrate production, for example at our restored site (LG).

The release of metal elements Ti, V, Cu, Zn and Pb under high runoff conditions was likely driven by flushing of DOC, which has been demonstrated to facilitate the mobilisation of metals from the more enriched shallow peat layers in peat moorlands (Rothwell et al., 2007). Rothwell et al. (2007) concluded that the release of Pb, Ti and V is driven by DOC, while metals with a low affinity for organic matter, such as Zn, are continuously leached into peatland fluvial systems. Cu and Zn have furthermore been shown to form strong bonds with FA (Pokrovsky et al., 2005), while the high association between Pb release and organic matter, particularly DOC, and under high runoff conditions has also been highlighted by others (Jordan et al., 1997; Broder and Biester, 2015).

6.4.3.2   Warm, dry conditions

Deeper water tables displayed positive loadings that grouped with warmer temperatures and greater ET losses on PC1 for EB and PC2 for LG. These parameters, indicating warmer and drier conditions, and had moderate and positive loadings together with particulates (POC, PC, PN, POC:PN) and HA and elements Si, P, Cl, Mn, Fe, Co, Hf and Hg, against negative loadings for runoff and precipitation. Indeed, enhanced stream-water concentrations of Si, P, Cl, Mn, Fe, Co, Hf and Hg were observed during the 2018 drought and during water table drawdown affecting both catchments, indicating a similar export behaviour with drawdown at both the intact and restored sites. POC concentrations and suspended sediment in peat catchments have generally been reported to increase with greater discharge (Hillier, 2001; Pawson et al., 2012). Here, we observed the opposite, with POC concentrations negatively

related to runoff and positively correlated with deeper water levels at both catchments, which might reflect a reduction in dilution with lower runoff.

Higher Si concentrations have been linked to increased decomposition of the organic load with lower water levels (Biester et al., 2012), while enhanced P release under warm and drier conditions could be the result of increased litter, particularly from *Calluna* (Worrall et al., 2016), reflective of the strong surface peak in the intact peat of May Moss (Figure 6.1). Mn and Fe are notably redox-sensitive, with their abundance related to the dissolving and reducing power of HA (Shotyk, 1988). Fe(III) oxyhydroxides have been documented to accumulate at the peat surface during dry periods, which may then be leached as Fe by bacterial reductive dissolution of these oxyhydroxydes during sudden moisture availability, with Fe forming a binding agent for the additional release of Mn (Novak et al., 2011). Hg mobilization has been likewise associated with lower WTD related to enhanced peat decomposition and oxidation-induced production of methylmercury (Haynes et al., 2017).

6.4.3.3   Patterns in the dry mass geochemistry

PC2 shared several similarities between the intact and restored sites. Both catchments indicated moderate and high positive loadings for dry mass, DOC, DN, FA and humin and elements Na, Mg, Al, S, Ca, Ti, K, V, Cu, Zn, Sr and Pb, with the intact site (EB) also showing high loadings for As, Br, Y, I and Ba. The grouping was coupled with a weak positive loading for precipitation for the intact site (EB), indicating that that PC2 summarised strong affiliations of some elements with DOC release upon rewetting. For the recovering site (LG), this grouping was clearly related to enhanced runoff and precipitation, as already discussed.

The strong affiliation between the export of metals and DOC had been widely discussed (Rothwell et al., 2005, 2007; Tipping et al., 2006; Novak and Pacherova, 2008; Warnken et al., 2009; Novak et al., 2011), and Warnken et al. (2009) have indicated that the presence of DOC, particularly during phases of rewetting, can increase the solubility of metals, such as Fe, due to the formation of dissolved complexes with fulvic acid. Similarly, Broder and Biester, (2015) observed a sharp rise in Pb concentrations upon rewetting, related to the sudden mobilisation of the Pb pool which accumulates within the shallow peat layer due to microbial decomposition or mineralization, as well as the legacy of atmospheric fallout, while Rothwell et al. (2007) additionally noted a strong coupling between Ti and V release together with DOC.

PC2 also included positive loadings for highly mobile elements, such as Na, Mg, Cl, Ca, Zn, Br, Sr and Rb (Shotyk, 1997; Broder and Biester, 2017), particularly at the intact site. For the

intact site this suggests a strong disassociation of highly mobile elements from runoff and WTD. Conversely, these elements as well as dry mass, loaded highly for both PC1 and PC2 for the restored site (LG). Those PCs do not correlate with each other (Jollife and Cadima, 2016), suggesting a strong overlap in their release under both drier and wetter conditions, which may have been induced by greater mixing of the surface peat layer through previous forestry activity.

6.4.3.4 Drought and post-drought rewetting

PC3 likewise revealed similar behaviour between the two catchments, and this involved positive loadings for temperature, ET, precipitation, runoff, LOI, HA and As, I and Pb against high negative loadings for Na, Mg, S, Ca and Sr. The contrast in the response of As and S together during and after the 2018 summer drought indicate that PC3 summarises the drought and post-drought rewetting behaviour at both EB and LG. Stream-water concentrations were found to considerably depleted in terms of Na, Mg, S, Ca, Zn and Sr concentrations during the 2018 summer drought, but rose sharply upon rewetting. These elements are known to be highly mobile within peat, leading to their vertical migration within the peat profile (Shotyk, 1997; Broder and Biester, 2017). The reduction of these elements under drought conditions thus accentuates the impact of low water levels on the continued leaching of these elements, as observed under normal high water level conditions.

We observed considerable depletion in S within stream-water samples collected during the drought, followed by rapid enrichment with precipitation events at both catchments. The mobilisation of sulphur in peatlands is tightly bound to variations in water levels. Water table drawdown during droughts facilitate the oxidation of reduced sulphur into sulphate (SO_4^{2-}), causing a reduction in pH which reduces the solubility of DOC (Clark et al., 2005). As already highlighted, DOC concentrations were considerably reduced during the 2018 summer drought at both catchments, a phenomenon likewise observed by others (Chapman et al., 2005; Clark et al., 2005, 2012). Increased flushing of DOC upon post-drought rewetting is a widely observed phenomena (Worrall et al., 2006; Fenner and Freeman, 2011; Clark et al., 2012; Broder and Biester, 2015; Ritson et al., 2017), and has been related to enhanced phenol oxidase activity during drought conditions, reducing concentrations of phenolic compounds which in effect stimulates microbial growth resulting in breakdown of organic matter and DOC production which is later released during rewetting (Fenner and Freeman, 2011). Conversely, Clark et al. (2012) have related an increase in DOC release upon rewetting to drought-induced acidification, enhancing DOC solubility, rather than microbial activity. As

both catchments showed a clear and comparable distinction in parameters associations with PC3, the restored site (LG) appears to show a similar drought and post-drought rewetting behaviour to the intact site (EB).

6.4.3.5   Seasonal availability of N, K and Rb

For EB, PC4 accounted for 7.3% of variation on the data, with high loadings for DN, K and Rb. N and K are macronutrients and their availability is thus affected by their seasonal uptake by plants. Rb, although not a nutrient, is also affected by seasonal plant uptake (Dahlqvist et al., 2007) and is contained within Sphagnum tissue at relatively consistent ratios to K within the shallow peat layer (Vinichuk et al., 2010). K and Rb showed maximum concentrations during a spring flood event, associated with their seasonal enrichment in the topsoil (Dahlqvist et al., 2007). Similarly, exports of K, Rb and nitrate in a headwater draining an ombrotrophic peatland in the Harz Mountains, Germany, were considerably higher in autumn and during snowmelt, related to deposition during the previous winter with their enrichment in the upper peat layer reflecting low winter biological activity relative to spring and summer (Broder and Biester, 2017).

As the grouping made up of DN, K and Rb contributed high loadings to a significant principal component at EB, this may reflect that the seasonal uptake of these macronutrients and associated elements has a considerable influence on their intra-annual concentrations in runoff from EB. These three elements did not form a significant principal component by themselves for LG, but instead had high loadings for PC2, indicative of cool, wet conditions. The separation in behaviour of DN, K and Rb from other PCs at EB, compared to LG, potentially reflects that this grouping is more strongly subject to seasonal availability and depletion for the intact peatland (Broder and Biester, 2017), whereas damage to the acrotelm layer at the restored site would have encouraged greater mixing of the upper peat profile and a mobility affected by flushing rather than biological activity. Significantly higher dry mass concentrations of K and Rb could furthermore indicate their relative enrichment within peat at the restored site (LG). Gaffney et al. (2018) observed that shallow- and pore-water ammonium concentrations, while reducing gradually after an initial spike upon rewetting, took 17 years to reach levels comparable to an intact bog, while K concentrations recovered to pristine levels within 11 years post-restoration. Relatively higher pore-water concentrations of DN and K at a restored peatland (LG) may thus diminish a seasonal variation in their fluvial export, compared to adjacent intact peatlands (EB) where nutrient concentrations are likely to be more limited.

6.5 CONCLUSION

Stream-water DOC concentrations and discolouration were at significantly lower levels at the restored site (LG), compared to the intact site (EB), with DOC in LG at half the concentration measured at EB, while POC concentrations were similar between both sites, which suggests that post-forestry restoration has been effective in limiting losses of fluvial carbon to below the levels seen at the intact site. Alternatively, the difference in DOC may be the result of enhanced seasonal flushing or changes in microbial activity at LG and thus associated with impacts of former forestry and peatland drainage. In addition, residual impacts of former forestry activities are detectable for most analysed elements through their relative enrichment in the dry mass samples extracted from the stream waters, including Na, Mg, Al, Si, S, Cl, K, Ca, Cr, Mn, Ni, Zn, Rb, Sr, Y, Zr, Ba and Hg, which are most likely related to disturbance of the upper peat profile and thus enhanced mixing with layers containing more mobile elements. Conversely, elements with strong near-surface enrichment in peat profiles, including P, Cu, As and Pb, are at higher dry mass concentrations at the intact site, indicating that shallow sub-surface flows are the dominant flux to water courses from both catchments. Despite relative element enrichments of elements within the extracted dry mass, the lower relative DOC concentrations and likely enhanced flushing mean that most elements are at reduced stream-water concentrations at the restored site, relative to the intact bog. Residual impacts of forestry and harvesting operations are still detectable at the restored peatland (LG) expressed as enhanced stream-water concentrations of Al (twice as high as EB), S, Cl, Ca and Sr in the stream samples, compared to the adjacent intact peatland (EB). Thus, while the LG catchment presents lower stream-water DOC and equivalent POC concentrations compared to the adjacent EB catchment draining mostly intact blanket bog, it is uncertain whether this difference is due to the recovery of hydrological and biogeochemical processes or residual impacts of former disturbance to the peat profile and ecology. Further research is therefore necessary to assess linkages between peat disturbance, DOC production and mobilisation and stream-water chemistry.

Chapter 7. Synthesis

7.1 RESEARCH AIM AND OBJECTIVES

Peatlands have received increasing attention in recent decades for their long-term carbon storage and sequestration, particularly within the context of climate change, as well as other ecosystem services such as flow regulation and drinking water provision (Orr et al., 2008). Peatland restoration is viewed as a means to re-establish previous ecosystem services, such as reducing present carbon losses related to peatland drainage and other anthropogenic pressures and return them to a state of being a net carbon sink to enhance carbon storage in an effort to mitigate climate change (Bonn et al., 2016). While understanding of the negative effects of drainage on peatland carbon storage, flow regimes and ecology is not new (Conway and Millar, 1960; Burke, 1975; Lavers and Haines-Young, 1997), and research into restoration practices has been developing rapidly over the past decades (Phillips et al., 1981; Shuttleworth et al., 2015), post-forestry peatland restoration is still relatively novel, with best practices still being developed and the long-term trajectory of ecosystem recovery still largely unknown (Anderson and Peace, 2017; Gaffney et al., 2022). This has led to calls for further research into the mechanisms and timeframes involved in their recovery (Martin-Ortega et al., 2014; Alderson et al., 2019; Glenk et al., 2021), particularly in combination with baseline or control sites (Andersen et al., 2017), to assess their relative success in re-establishing hydrological and biogeochemical functioning.

The dual aims of this research were 1) to use a long time series of hydrometeorological monitoring to assess the hydrological functioning on an intact upland ombrotrophic mire, and 2) to examine the effects of peatland restoration from former conifer plantation on blanket bog hydrological functioning and water quality. The study was centred on May Moss, a 1.5 km^2 ombrotrophic blanket mire in the eastern North York Moors protected as part of the North York Moors SSSI/Special Protection Area (SPA) and managed by Forestry England, Natural England. The study was carried out using a paired catchment approach, comparing a 0.63 km^2 catchment dominated by intact blanket bog (Eller Beck, EB) with an adjacent 1.53 km^2 catchment (Long Grain, LG) where most of the forestry had been removed and blanket bog restoration techniques had been applied. These management actions including tree removal, mulching and drain blocking to improve water retention within the peatland as a whole. The main objectives of this research focused on:

I.   Quantifying and characterising the hydrological functioning and drivers governing the intact blanket bog and the main catchment draining it (Eller Beck) using a 10-year hydro-meteorological timeseries (20/08/2010 – 01/07/2021) (*Chapter 4*)

II.   A critical comparison of the hydrological functioning of the paired intact and restored catchments using a four-year hydrological series (14/03/2017 – 01/07/2021) including runoff and water table depths (WTDs) 10 years after initial restoration (*Chapter 5*)

III.   Evaluating the impacts of restoration on stream-water quality by comparing the intact and restored catchments using on two-year water sampling campaign (18/07/2018 – 27/08/2020), facilitated by the paired hydrological series from *Chapter 5* (*Chapter 6*)

7.2   SUMMARY AND KEY RESULTS

7.2.1   Chapter 3

This research was based on a decade worth of hydro-meteorological data from the May Moss meteorological station, situated near the watershed on the intact blanket mire. The hourly series included 3 m vertical profiles for air temperature, relative humidity and wind speed profiles, as well as soil heat flux (G), net radiation (Rn) and photosynthetic active radiation (PAR). Together these data facilitated the calculation of hourly evapotranspiration (ET) losses from the bog surface using the Bowen ratio energy balance (BREB) method for a 10-year period. Maintaining data arrays like the May Moss station is challenging, and approaches were needed to address data gaps and problems using adjacent UK Met Office MIDAS station records. However, long-term, high-resolution ET series are rare for upland ombrotrophic blanket bogs, primarily due to the wind fetch requirements, cost and maintenance involved in setting up a system for BREB and even more so for eddy covariance (EC) (Drexler et al., 2004).

Examples of long-term ET estimates from ombrotrophic peatlands includes the 19-year long series by Worrall et al. (2015), centred on an upland blanket bog at Moor House NNR in the North Pennines, UK. However, the authors used the method by White (1932) to derive daily ET from diel changes in WTD, a method which has been found to account for 50% variation in ET and thus restrains the accuracy of those estimates of daily ET (Fahle and Dietrich, 2014). Other multiyear ET measurements have been based on an Atlantic blanket bog in southwestern Ireland (Sottocornola and Kiely, 2010) and a shrub-covered bog in southern

Ontario, Canada (Lafleur et al., 2005), while many other studies have focused solely on growing season ET (e.g., Campbell and Williamson, 1997; Thompson et al., 1999; Kellner, 2001; Gerling et al., 2019; Wang et al., 2020). To our knowledge, we provide here the first long-term, high-resolution ET series for an upland blanket bog in the UK, based on an energy balance method.

7.2.2 Chapter 4

A decade-long (2010/11 – 2019/20) energy and hydroclimate series facilitated the characterisation of the intact blanket bog, May Moss. The bog is in an unusually dry region for blanket mires, with average annual precipitation of 922 mm, and has an annual mean air temperature of 8.1°C (2010/11 – 2019/20). Historical temperature and precipitation records, derived from nearby weather stations, reveal that the latest decade (2011 – 2020) is on average 0.3°C warmer, driven by a 0.6°C warming of average winter temperatures, when compared with the 1961 – 1990 reference period (Figure 7.1). Average annual total precipitation over 2011 – 2020 has increased by 3% compared to the 1961 – 1990 reference, driven by wetter summers (+17%) and autumns (+15%), while winter (−9%) and spring (−11%) months have become drier (Figure 7.1).
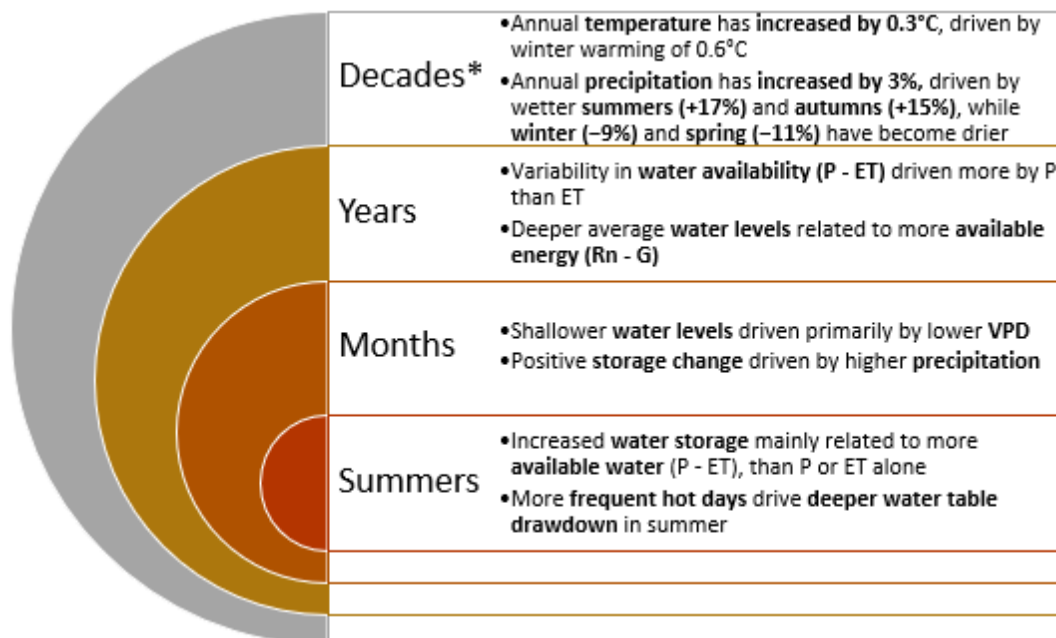

Figure 7.1. Hydro-meteorological trends and influences on the water balance at May Moss. *Decadal trends were measured between the 1961 – 1990 reference baseline, derived from nearby weather stations, and the most recent monitored decade (2011 – 2020) at May Moss.

Despite the relatively low annual precipitation, mean annual storage change of +1 mm over the ten-year period suggest that the bog is hydrologically well balanced, with inputs in equilibrium with outputs, and resilient to short-term impacts, such as the 2018 summer heatwave. Annual water balances were computed for three consecutive hydrological years (2017/18, 2018/19, 2019/20), which comprised, on average, 930 mm of precipitation, 335 mm of evapotranspiration losses, 371 mm of runoff losses and a storage change of −7 mm, with the annual residual averaging at +268 mm. The positive residual implies that net outputs within the water balance were not accounted for. These residual "losses" are most likely derived from measurement error, in particular an underestimation of peak flow, evaporative losses from surface water or unaccounted changes in storage due to peat moisture loss, especially during severe drawdown events.

Average annual WTD is primarily related to average available energy (Rn – G), while monthly average WTD is driven mainly by VPD (Figure 7.1), which in turn is strongly coupled with available energy (Rn – G). Summer water availability (P – ET) is controlled more by precipitation than evapotranspiration and appears to be the key driver in summer ΔS (Figure 7.1). In addition, the extent of higher magnitude summer WT drawdown events appears to be driven by a higher incidence of warm, and therefore highly evaporative, days (Figure 7.1). The duration and extent of the 2018 summer drawdown thus appears to reflect the joint impact of low water availability (P – ET) and greater incidence of highly evaporative days. The high proportion of positive monthly storage changes and water balance residuals may suggest that May Moss has a positive water balance. In addition, storage losses observed over 2017/18 had recovered by the following year, verifying the relative resilience of intact mires to short-term drought events. Despite this, the current local trend of reducing winter and spring precipitation, enhanced winter warming, the location of May Moss on the lee side of the rain shadow barrier of the Pennines, and the predicted increase in the frequency of summer heatwaves across Europe (Seneviratne et al., 2006) could indicate that the water balance, and thus carbon stock, may be vulnerable to the effects of future climate change.

7.2.3 Chapter 5

Here we used a four-year paired hydrological series (March 2017 – July 2021), comprising precipitation, evapotranspiration, runoff, and water levels, to compare the hydrological functioning of a post-forestry restored blanket bog with that of an adjacent intact blanket mire based on a paired catchment approach. Water balances were computed for three complete hydrological years: 2017/18, 2018/19 and 2019/20, with an average of 930 mm of

precipitation and 335 mm of evapotranspiration. Annual total runoff averaged 313 mm at the recovering catchment (LG) and 334 mm at the intact sites (EB). Annual storage change (ΔS) averaged at -27 mm at the recovering catchment (LG) and -1 mm at the intact sites (EB). While both catchments thus appear close to zero in their annual ΔS, particularly considering the drought event within the paired monitoring period, the difference in ΔS nevertheless suggests that the intact site is more hydrologically balanced than the recovering site.

WTD averaged at -74 mm near the centre of the recovering bog (LG), resembling mean water levels measured at the watershed of the intact bog (MS) (-73 mm), but 32% lower that water levels measured in the centre of the intact bog (EB) (-56 mm) (Figure 7.2). Nevertheless, the recovering site is able to support a sizeable bog pool, adjacent to which water levels averaged at -37 mm (GA). The difference in average water levels between the MS dipwell, at the watershed, and EB dipwells, within the centre of the bog, may be related to differences in rates and replenishment of subsurface lateral flow. Water tables were within 5 cm from the surface 60% of the time for the MS and EB dipwells, 45% of the time at LG dipwell and 75% of the time at the bog pool on the recovering site (GA) (Figure 7.2). Thus, while restoration has raised the water level at the recovering site (LG), surface water tables were still less frequently observed than at the intact bog, which may be related to greater hydraulic conductivity and lower water retention as a result of former drainage.

Baseflow made up a significantly higher proportion of total runoff at the recovering site, compared to the intact bog (Figure 7.2), which may be related to residual effects of former drainage in enhancing lateral subsurface flow. The comparison of storm runoff behaviour between the two sites indicates that the recovering catchments behaves less "flashy" (Figure 7.2), with a relative reduction of peak runoff by 35%, longer lag times between the start/peak rain and peak runoff and a slower rise and fall rate in storm runoff. This would suggest that restoration techniques, including tree removal and drain-blocking, have been effective at reducing the relative intensity of storm runoff to levels below those observed at the adjacent intact catchment. The 2018 drought event and post-drought water balances emphasize the rapid hydrological recovery of an intact blanket mire following a summer with severe water table drawdown. In comparison, the restored site was characterised by relatively higher runoff/rainfall coefficients during the drought and subsequent year, suggesting lower water retention and a comparatively longer post-drought recovery process.

Figure 7.2. Key findings in the analysis of post-forestry blanket bog water levels, runoff and stream-water chemistry at May Moss and implications of hydro-meteorological processes for bog restoration.

7.2.4   Chapter 6

A two-year water sampling campaign between summer 2018 and summer 2020 involved the collection of water samples every two-four days from streams draining the paired intact and restored sites. Water samples were analysed for dissolved organic carbon (DOC), dissolved nitrogen (DN), particulate organic carbon (POC), particulate nitrogen (PN), loss-on-ignition and UV-vis absorbance. Powders collected by freeze drying the water samples were analysed for humic substances and 32 element concentrations measured by X-ray Fluorescence. The water quality timeseries analysis was supported by the four-year paired hydrological

monitoring programme on the two catchments, which facilitated the calculation of fluxes within the stream-water.

Stream-water DOC in the recovering bog was at half the concentration compared to the intact bog (Figure 7.2), and water discolouration was likewise significantly lower at the restored site, whereas POC concentrations were similar between both sites. While reduced stream-water DOC in the recovering site may suggest a reduction in DOC loss associated with bog restoration, the reduction may also be the result of enhanced seasonal flushing or changes in microbial activity and thus associated with impacts of former forestry and peatland drainage.

In addition, residual impacts of former forestry activities are detectable for most analysed elements through their relative enrichment in the dry mass samples extracted from the stream waters, including Na, Mg, Al, Si, S, Cl, K, Ca, Cr, Mn, Ni, Zn, Rb, Sr, Y, Zr, Ba and Hg, which are most likely related to disturbance of the upper peat profile and thus enhanced mixing with layers containing more mobile elements (Figure 7.2). Conversely, elements with strong near-surface enrichment in peat profiles, including P, Cu, As and Pb, are at higher dry mass concentrations at the intact site, indicating that shallow sub-surface flows are the dominant flux to water courses from both catchments. Despite relative element enrichments of elements within the extracted dry mass, the lower relative DOC concentrations and likely enhanced flushing mean that most elements are at reduced stream-water concentrations at the restored site, relative to the intact bog.

Residual impacts of forestry and harvesting operations are still detectable at the restored peatland expressed as enhanced stream-water concentrations of Al (twice as high as the intact site), S, Cl, Ca and Sr in the stream samples, compared to the adjacent intact peatland (Figure 7.2). Thus, while the recovering Long Grain catchment presents lower stream-water DOC and equivalent POC concentrations compared to the adjacent Eller Beck catchment draining mostly intact blanket bog, it is uncertain whether this difference is due to the recovery of hydrological and biogeochemical processes or residual impacts of former disturbance to the peat profile and ecology.

7.3 FUTURE RESEARCH FOR MAY MOSS AND BEYOND

Forest-to-bog restoration is still a developing area of research, and this thesis has highlighted the need and scope for further study at May Moss and beyond. Expanding the range and depth of analysis at May Moss, as described above, would provide further invaluable data

on the extent of post-forestry recovery on blanket mires. However, May Moss is an example of (small-scale) forest-to-bog restoration, situated within a much larger upland area and catchments. To further assess the impact of post-forestry rewetting within headwater catchments, such as Long Grain, monitoring setups could be developed across larger geographical scales. This could range from regional studies across the North York Moors to assess, for example, water table response to meteorological events and stream-water quality (Evans et al., 2014b), to encompassing the larger catchment to which the Eller Beck (River Esk) and Long Grain (Upper Derwent) headwaters contribute. The following section highlights key areas to further expand and build on the research presented here.

Water balance residuals varied extensively over the monitoring period, highlighting scope for greater accuracy of measurement of the terms. Residuals were most likely derived from measurement error (Kellner and Halldin, 2002; Isabelle et al., 2018), such as an underestimation of runoff, in particular peak flow, evaporative losses from surface water or unaccounted changes in storage due to peat moisture loss, especially during severe drawdown events. As runoff was recorded at hourly intervals and upland peat catchments are inherently "flashy" with short hydrograph lag times, it is highly likely that we underestimated runoff, especially peak flow, under storm conditions, leading to systematic underestimations of fluvial fluxes for parameters such as DOC and POC. This source of error could be addressed by carrying out short-term high-resolution flow recording and sampling campaigns under forecasted storm flow conditions (Rothwell et al., 2007; Wilson et al., 2011b). Alternatively, the collection of average, minimum and maximum flow rates at hourly intervals would allow more precise, high-resolution interpolation of runoff, with consequent improvement in the estimation of other fluxes. Another way of assessing and comparing storm runoff events would be to apply a unit hydrograph model, which estimates the direct runoff hydrograph resulting from given excess rainfall and assumes uniform rainfall across the catchment (Moore, 1985; Jakeman et al., 1990). This research has also raised questions as to the resilience of the water balance of May Moss to short-term events, such as heatwaves and droughts, as well as long-term changes in water availability as a result of climate change, which can only be addressed through continued long-term monitoring, particularly of water levels, vegetation and other surface moisture parameters.

Differences in baseflow estimates and storm runoff response between the two catchments are thought to derive from differences in their peat characteristics and preferential flowpaths, as a result of former drainage and disturbance in Long Grain, although differences in catchment characteristics, such as size and relief, may have also influenced their relative

hydrological behaviour. These uncertainties could be addressed in several ways. The addition of further dipwells with automatic water level loggers would allow greater spatial density to the current WTD array and provide further information on hydrological connectivity across both catchments. Peat cores from the restored site could provide greater peat characterisations (e.g. bulk density, hydraulic conductivity, macropores), degree of damage to the peat profile, level of degradation and nutrient and heavy metal loading. This could also involve an examination of peat bulk density, to validate hypotheses of enhanced hydraulic conductivities at the restored site. These analyses would thereby provide key information on the linkages between peat disturbance, DOC production and mobilisation and stream-water chemistry.

The peatland carbon budgets were here only examined by analysing temporal trends in stream-water concentrations of DOC and POC, measured at one location in each stream. Stream-water DOC concentrations were thus assumed to reflect DOC mobilised and transported from the peat. However, in-stream concentrations of DOC were likely influenced by further in-stream autochthonous DOC production or mineralisation to CO_2 (Moody et al., 2013). A sampling campaign involving a sequence of upstream samples may give further indication to downstream net production or consumption of DOC, thus providing better estimates of net DOC loss from peat, and further means of comparison between the intact and recovering catchment. In addition, there is further scope in assessing the net impact of post-forestry blanket bog restoration on the peatland's carbon balance – an area of research which is receiving increasing attention, though difficult to implement due to the range of measurements required. This could involve a comparison of the greenhouse gases (GHG) CO_2, CH_4 and N_2O fluxes between adjacent intact, restored as well as afforested sites (Yamulki et al., 2013), supplemented by respective net peat (and carbon) accumulation measurements. This extension to the present study would serve to provide further information on the net impact of peatland rewetting on atmospheric carbon concentrations and mitigation potential for climate change.

7.4 WIDER CONTEXT OF RESEARCH

7.4.1 Palaeoclimatic research

The quantification of hourly ET, precipitation, and energy balance parameters over a 10-year period, which also included a severe drought in summer 2018, facilitated the analysis of the hydro-meteorological controls over annual water table variability. These results

corroborated to some extent the findings by Charman (2007), who concluded that the summer water deficit (P – ET) was the main parameter controlling water table depths based on palaeoclimatic reconstructions of peat surface wetness using palaeoenvironment methods (e.g., testate amoebae and plant macrofossil stratigraphy). These palaeo-environmental techniques use subfossil records typically at 5-10 mm vertical and sub-decadal resolution using ecological transfer functions calibrated to the present-day environmental preferences of taxa to infer past changes in peatland water table depth (Barber, 1993). The work at May Moss offered a broader and higher-resolution analysis of the effects of monthly, summer and annual temperature, precipitation, water deficit (P – ET), available energy (Rn – G) and vapour pressure deficits (VPD). The summer water deficit (P – ET) was indeed a significant control on average summer WTD, but even more so on summer water storage deficits (ΔWTD) in peat. Given the importance of summers to the life cycles of amoebic protozoa (testate amoebae) and peatland plants (Mitchell et al., 2008; Väliranta et al., 2012), the May Moss data suggest that for a dry but still relatively humid oceanic bog, any changes in 5 to 10 year average bog surface wetness would reflect changes in the summer water deficit.

7.4.2   The future of May Moss under climate change

The extent of summer water table drawdown at May Moss was primarily driven by the frequency of highly evaporative days. Given that the past decade has had a much greater occurrence of regional heatwaves compared to the reference period 1961 – 1990 (Figure 4.7) and the frequency of summer heatwaves in Europe is predicted to increase with climate change (Seneviratne et al., 2006), we may expect that an increase in the frequency of severe water table drawdown events within ombrotrophic peats will follow. Intact mires are considered relatively resilient to short-term droughts due to an inherent decoupling in hydrological condition between summer and winter in which summer moisture losses are fully recovered over the winter months (Worrall et al., 2006; Holden and Rose, 2011). These circumstances were a feature of the hydrological functioning at May Moss, where the water balance recovered fully the losses observed over the 2018 drought by the following year (*Chapters 4* and *5*). However, the trend of warmer and drier winters observed for the May Moss area, when comparing the recent decade 2011 – 2020 to 1961 – 1990 (*Chapter 4*), does point to an increased risk of winter rewetting being ultimately unable to offset summer moisture loss. Considering that annual precipitation at May Moss is already close to the threshold ($\approx$1000 mm yr^{-1}) recommended for sustained mire development (Lindsay et al.,

1988), a higher incidence of more evaporative days in summer leading to more frequent and more severe water table drawdown coupled with a reduced capacity to recover moisture loss over the winter could thus have severe consequences for the water balance of May Moss, as well as other ombrotrophic peatlands close to the annual precipitation threshold generally necessary for mire development and experiencing this trend in warmer, drier winters. The short-term climatic trend observed at May Moss compares well with the study by Clark et al. (2010), who used a series of bioclimate models to assess the vulnerability of blanket bogs in the UK to climate change, finding that their bioclimatic space reduced in 7 out of 8 models, particularly in the eastern regions of Northumbria, the North York Moors and Orkney. Similarly, but on a larger scale, Swindles et al. (2019) showed that most European peatlands included in their analysis were found to be subject to widespread drying over the past 300 years due to combined pressures including climatic drying, warming and direct human impacts, and as a result are moving away from their longer-term hydrological baselines, with the potential to change from a carbon sink to a source.

The impact climate change will have on May Moss is nevertheless largely unknown. The peatland's carbon store will depend on whether enhanced primary productivity and carbon sequestration under warmer temperatures will exceed carbon losses related to drying and enhanced peat decomposition (Moore, 2002; Davidson and Janssens, 2006). Despite the water budget of May Moss appearing balanced at present (*Chapters 4* and *5*), a trend towards warmer, drier winters and a consequent drying of the bog itself effect on could also be exacerbated through positive feedback loops. In addition to affecting net carbon emissions, changes in precipitation and temperature regimes and their implications for peat surface wetness have the potential to increase fire risk (Hogg et al., 1992) and facilitate tree encroachment and plant succession, further exacerbating drying, decomposition, and carbon emissions (Laiho, 2006; Clark et al., 2010; Kokkonen et al., 2019). Previous research has highlighted that May Moss has endured a variable climate and fluctuating water levels over the past 200 years (Chiverrell, 2001), and the ten years of hydro-meteorological data presented here have indicated a resilience to severe drought events. However, current climatic trends nevertheless raise questions on the resilience of May Moss to projected changes in temperature and precipitation regimes with climate change and what thresholds could jeopardise the long-term endurance of the mire.

7.4.3 Impacts of restoration of hydrological functioning and water quality

Chapters 5 and *6* focused on the catchment comparison between the intact blanket mire (Eller Beck) and the restored bog (Long Grain) in terms of runoff and water table behaviour (*Chapter 5*), based on a four-year paired runoff and water level series, and stream-water chemistry, based on a two-year water sampling campaign. Peatland restoration aims to reverse the effects of former disturbance on hydrological and biogeochemical functioning, primarily by ensuring a predominantly shallow water table (Quinty and Rochefort, 2003). In addition, a reduction in peak flow and lengthening of lag times is often cited as a key aim of peatland restoration to reduce downstream flood risk as part of a suite of natural flood management and slow-the-flow initiatives (Parry et al., 2014; Shuttleworth et al., 2019). Addressing this aim, the restoration activities at Long Grain appeared successful in limiting peak runoff and reducing the "flashiness" of storm runoff at the restored catchment, relative to the intact catchment, Eller Beck. While water levels near the centre the restored bog (LG) were found to be significantly lower than near the centre of the intact site (EB) they resembled a site by the watershed on the intact mire (MS) and were found to be near the surface (< 5 cm depth) for close to half the year (45%). These patterns and differences have been observed in equivalent comparisons by others (Wallage and Holden, 2011; Haapalehto et al., 2014). That said, the restored site is able to sustain a large bog pool with near-surface water levels for most of the year (75%) (*Chapter 5*), indicative of strong water retention and recovery of peatland water level functioning (Tallis, 1994; Peacock et al., 2013b). Although a comparison in annual storage change indicated that the restored site could take longer to recover from severe drought events (summer 2018), annual summer drawdown behaviour otherwise resembled the intact site. In summary, the hydrological dynamics across May Moss, both Eller Beck and Long Grain catchments, suggest behaviour that indicates a good level and direction to hydrological recovery within the restored catchment.

In *Chapter 6*, differences between the restored and intact sites were assessed in terms of their stream-water chemistry. In both catchments, DOC dominated the stream-water organic carbon, with minimal POC, as is commonly the case with headwaters that drain peat-dominated catchments (Hope et al., 1997; Aitkenhead et al., 1999). Stream-water DOC concentrations were significantly lower at the restored site. Although this may seem surprising and indicate that restoration has been effective in inhibiting fluvial carbon loss, relative to the intact site, it may also suggest underlying differences in the rate of DOC production between the two sites and/or reflect more efficient flushing of available DOC stocks within the restored tracts of peatland. While most geochemical elements were at

reduced concentrations within the DOC load carried in the stream-water at Long Grain, analysis of dry mass concentrations revealed significant enrichment of most elements. The most likely driver of this would be the mixing of the upper peat profile as a direct result of disturbance related to previous forestry (e.g., ploughing and ditch construction) and restoration activities. Enrichment of some elements, for example Al, in both stream-water and dry mass concentrations at the restored site likewise hint at legacy effects of former disturbance (Gaffney et al., 2018). Conversely, other metal pollutants, including copper, arsenic and lead, were significantly enriched at the intact site, most likely related to their strong near-surface enrichment in the intact peat profile and dominant shallow sub-surface flow. Disturbance and mixing of the upper peat profile at the restored site may thus have had a diluting effect on the export of element with strong surface peat enrichment. This pattern is similarly reflected in the relatively lower stream-water concentrations of phosphorus at the restored site, which shows strong surface enrichment in intact peat sequences, and could indicate the geochemical structure and functioning of peat within the restored catchment has not yet re-acquired that patterning.

7.4.4 Implications of climate change for forest-to-bog restoration at May Moss and other blanket mires

Peatland restoration has been advocated as an effective mitigation strategy for combating both the causes and impacts of climate warming, with many governments aiming to achieve net zero emissions in the coming decades (Glenk et al., 2021). The England Peat Action Plan, as part of the UK government's 25 Year Environment Plan, has set out the government's aim to fund the restoration of 35,000 ha of peatland by 2025 (UK Government, 2021), as part of the government's commitment to reach Net Zero by 2050. The restoration of all UK peatlands has been estimated to cost between £8.4 to £21.3 billion, though these would be far outweighed by the estimated carbon benefits of £109 billion, meaning that peatland restoration is classed as a "Very High" value mitigation approach (UK Government, 2021). The appreciation of peatland restoration as a mitigation strategy has also been more broadly reflected within the latest IPCC WGIII report Climate Change 2022 on the Mitigation of Climate Change, in which peatland restoration has been included as a means to offset carbon emissions (IPCC, 2022). The report highlights that agriculture, forestry and other land uses were responsible for 22% [13 GtCO$_2$-eq] of anthropogenic GHG emissions in 2019, but suggest that the conservation, improved management, and restoration of ecosystems, including peatlands, could offset between 4.2 and 7.4 GtCO$_2$-eq yr^{-1} (IPCC, 2022).

Rising DOC loss from peatlands has partly been associated with climatic warming. DOC concentrations in stream-water in the intact catchment were similarly high as other upland peat sites in the UK (Clay et al., 2012; Pawson et al., 2012). While Worrall et al. (2007) have related higher DOC export to enhanced peat decomposition driven by an increase in the frequency of summer droughts, Freeman et al. (2004) have suggested that enhanced DOC loss is most likely related to higher atmospheric CO_2 driving greater DOC production from root exudates due to higher productivity rates. Wilson et al. (2016) furthermore predict that DOC decomposition within the surface peat layer will form the main emitter of carbon under a warming climate. The lower DOC concentrations in the recovering catchment may seem unexpected and suggest recovery, given previous peat disturbance through forestry which is generally linked with enhanced fluvial carbon loss (Koskinen et al., 2017; Gaffney et al., 2020), though as previously discussed they may be the result of residual effects of former drainage such as differences in DOC production and mobilisation or enhanced flushing by higher baseflow. Further research should therefore investigate linkages between peat disturbance and hydraulic conductivity in rewetted peat catchments.

The raising of water levels through post-forestry restoration has the capacity to reduce carbon loss as CO_2 from aerobic decomposition, however rewetting is also associated with an increase in methane (CH_4) emissions due to increased activity of methanogenic bacteria under anaerobic conditions (Cannell et al., 1993). This has previously led to conflicting discourses on the relative benefits of peatland afforestation and restoration on greenhouse gas emissions (Cannell et al., 1993; Hargreaves et al., 2003), with some highlighting a risk of high methane emissions upon rewetting while simultaneously accumulating carbon (Hemes et al., 2018), while others have found peatland rewetting to encompass net benefits in GHG fluxes and carbon storage, mitigating climate warming (Günther et al., 2020). With many forestry plantations on peatlands within Western Europe approaching the end of their first rotation, there have been calls for greater evidence-based decision to assess sites for their suitability for restocking or restoration (Andersen et al., 2017). Given the drying trend observed at May Moss over the 20th century owing to the adjacent forestry or climate change (Atherden, 1972; Chiverrell, 2001), relatively low average annual precipitation (< 1000) and the trend of warmer, drier winters presented here (*Chapter 4*), it may be questioned whether post-forestry bog restoration is a viable option in terms of the potential large-scale carbon emission which could be released from a drying peatland, or whether continued forestry would offer greater carbon savings through reduced methane emissions and short-term carbon storage in conifer trees and forest soil (Cannell et al., 1993). However, previous

research has also highlighted the endurance of May Moss through variations in climate, leading to fluctuating water levels, over the past 200 years (Chiverrell, 2001), and the ten years of hydro-meteorological data presented here have indicated a hydrological resilience to severe drought events both within the intact and recovering catchments (*Chapter 4* and *5*) (Figure 7.2). The future endurance of May Moss will thus most likely depend on how shifts in temperature and precipitation regimes due to climate change will impact the water balances within the two catchments of May Moss, with adjacent active forestry likely contributing additional water stress at both sites. Given the current hydrological resilience displayed at May Moss and relative reductions in storm runoff intensity and fluvial carbon loss in the recovering catchment of Long Grain within a decade of rewetting, this research advocates further and larger-scale forest-to-bog restoration, particularly of sites most at risk of drying, in order to sustain future hydrological resilience and ensure net carbon storage under a changing climate.

7.5 KEY MESSAGES

- The intact blanket bog of May Moss displays significant resilience to short-term drought events, however hydro-meteorological data over the past decades highlight a trend of increasingly warmer and drier winters, which could render the water balance, particularly the extent of winter recharge, vulnerable to climate change.

- Blanket bog restoration within the Long Grain catchment has been effective in limiting peak runoff and extending lag times, in effect rendering storm runoff less "flashy" compared to the Eller Beck catchment, dominated by intact blanket mire.

- Carbon concentrations and discolouration of stream-water were significantly lower in the recovering Long Grain compared to the intact Eller Beck catchment.

- Long-term monitoring is essential to assess trends in peatland functioning, particularly water table variability, and the extent of post-restoration ecosystem recovery attainable.

- Hydrological resilience to short-term events and relative reductions in storm runoff intensity and fluvial carbon loss within a decade of rewetting advocate further and larger-scale forest-to-bog restoration, particularly of sites most at risk of drying, to sustain future hydrological resilience under a changing climate.

References

Abtew, W. and Melesse, A., (2013) *Evaporation and evapotranspiration: measurement and estimations*. Dordrecht: Springer.

Aitkenhead, J.A., Hope, D. and Billett, M.F., (1999) The relationship between dissolved organic carbon in stream water and soil organic carbon pools at different spatial scales. *Hydrological Processes*, 13, pp.1289–1302.

Aitkenhead, J.A. and McDowell, W.H., (2000) Soil C:N ratio as a predictor of annual riverine DOC flux at local and global scales. *Global Biogeochemical Cycles*, 14(1), pp.127–138.

Alderson, D.M., Evans, M.G., Shuttleworth, E.L., Pilkington, M., Spencer, T., Walker, J. and Allott, T.E.H., (2019) Trajectories of ecosystem change in restored blanket peatlands. *Science of the Total Environment*, 665, pp.785–796.

Allen, R.G., Pereira, L.S., Howell, T.A. and Jensen, M.E., (2011) Evapotranspiration information reporting: I. Factors governing measurement accuracy. *Agricultural Water Management*, 98, pp.899–920.

Allen, R.G., Pereira, L.S., Raes, D. and Smith, M., (1998) *Crop Evapotranspiration*. *FAO Irrigation and Drainage Paper No. 56*.

Allen, R.G., Smith, M., Pereira, L.S. and Perrier, A., (1994a) An Update for the Calculation of Reference Evapotranspiration. *ICID Bulletin*, 43(2), pp.35–92.

Allen, R.G., Smith, M., Perrier, A. and Pereira, L.S., (1994b) An Update for the Definition of Reference Evapotranspiration. *ICID Bulletin*, 43(2), pp.1–34.

Andersen, R., Chapman, S.J. and Artz, R.R.E., (2013) Microbial communities in natural and disturbed peatlands: A review. *Soil Biology and Biochemistry*, 57, pp.979–994.

Andersen, R., Farrell, C.A., Graf, M., Muller, F., Calvar, E., Frankard, P., Caporn, S. and Anderson, P., (2017) An overview of the progress and challenges of peatland restoration in Western Europe. *Restoration Ecology*, 252, pp.271–282.

Anderson, A.R., Ray, D. and Pyatt, D.G., (2000) Physical and hydrological impacts of blanket bog afforestation at Bad a' Cheo, Caithness: The first 5 years. *Forestry*, 73(5), pp.467–478.

Anderson, R., (2010) *Restoring afforested peat bogs: results of current research*. Forest Research, Research Note FCRN006.

Anderson, R. and Peace, A., (2017) Ten-year results of a comparison of methods for restoring afforested blanket bog. *Mires and Peat*, 19(6), pp.1–23.

Armstrong, A., Holden, J., Kay, P., Francis, B., Foulger, M., Gledhill, S., McDonald, A.T. and Walker, A., (2010) The impact of peatland drain-blocking on dissolved organic carbon loss and discolouration of water; results from a national survey. *Journal of Hydrology*, 381, pp.112–120.

Artz, R., Chris, E., Ian, C., Mark, H., Matt, S.-C., Mike, P., Peter, J., David, C., Andrew, M., Katherine, R. and Weyl, R., (2019) *The State of UK Peatlands: an update*. [online] Available at: http://archive.jncc.gov.uk/page-6563.

Asam, Z.-Z., Nieminen, M., Kaila, A., Laiho, R., Sarkkola, S., O'Connor, M., O'Driscoll, C., Sana, A., Rodgers, M., Zhan, X. and Xiao, L., (2014a) Nutrient and heavy metals in decaying harvest residue needles on drained blanket peat forests. *European Journal of Forest Research*, 133, pp.969–982.

Asam, Z.-Z., Nieminen, M., O'Driscoll, C., O'Connor, M., Sarkkola, S., Kaila, A., Sana, A., Rodgers, M., Zhan, X. and Xiao, L., (2014b) Export of phosphorus and nitrogen from lodgepole pine (Pinus contorta) brash windrows on harvested blanket peat forests. *Ecological Engineering*, 64, pp.161–170.

Atherden, M.A., (1972) *A contribution to the vegetation and land use history of the eastern-central north York Moors*. Durham University.

Atherden, M.A., (1979) Late Quaternary Vegetational History of the North York Moors VII. Pollen Diagrams from the Eastern-Central Area. *Journal of Biogeography*, 6(1), pp.63–83.

Bacon, K.L., Baird, A.J., Blundell, A., Bourgault, M.-A., Chapman, P.J., Dargie, G., Dooling, G.P., Gee, C., Holden, J., Kelly, T., McKendrick-Smith, K.A., Morris, P.J., Noble, A., Palmer, S.M., Quillet, A., Swindles, G.T., Watson, E.J. and Young, D.M., (2017) Questioning ten common assumptions about peatlands. *Mires and Peat*, 19(12), pp.1–23.

Ballard, C.E., McIntyre, N. and Wheater, H.S., (2012) Effects of peatland drainage management on peak flows. *Hydrology and Earth System Sciences*, 16, pp.2299–2310.

Barber, K.E., (1993) Peatlands as scientific archives of past biodiversity. *Biodiversity and Conservation*, 2, pp.474–489.

Bathurst, J., Birkinshaw, S., Johnson, H., Kenny, A., Napier, A., Raven, S., Robinson, J. and Stroud, R., (2018) Runoff, flood peaks and proportional response in a combined nested and paired forest plantation/peat grassland catchment. *Journal of Hydrology*, 564, pp.916–927.

Bay, R.R., (1967) Evapotranspiration from two peatland watersheds. *IAHS, ed. geochemistry precipitation, evapotranspiration, soil-moisture, hydrometry. General Assembly of Bern, UVESCO/IAHS*, 78, pp.300–307.

Bell, M.C., Ritson, J.P., Verhoef, A., Brazier, R.E., Templeton, M.R., Graham, N.J.D., Freeman, C. and Clark, J.M., (2018) Sensitivity of peatland litter decomposition to changes in temperature and rainfall. *Geoderma*, 331, pp.29–37.

Belyea, L.R. and Clymo, R.S., (2001) Feedback control of the rate of peat formation. *Proceedings of the Royal Society of London. Series B: Biological Sciences*, 268, pp.1315–1321.

Benjamini, Y. and Hochberg, Y., (1995) Controlling the False Discovery Rate: A Practical and Powerful Approach to Multiple Testing. *Journal of the Royal Statistical Society. Series B (Methodological)*, 57(1), pp.289–300.

Biester, H., Hermanns, Y.-M. and Martinez Cortizas, A., (2012) The influence of organic matter decay on the distribution of major and trace elements in ombrotrophic mires - a case study from the Harz Mountains. *Geochimica et Cosmochimica Acta*, 84, pp.126–136.

Billett, M.F., Charman, D.J., Clark, J.M., Evans, C.D., Evans, M.G., Ostle, N.J., Worrall, F., Burden, A., Dinsmore, K.J., Jones, T., McNamara, N.P., Parry, L., Rowson, J.G. and Rose, R., (2010) Carbon balance of UK peatlands: current state of knowledge and future research challenges. *Climate Research*, 45, pp.13–29.

Birkel, C., Broder, T. and Biester, H., (2017) Nonlinear and threshold-dominated runoff generation controls DOC export in a small peat catchment. *Journal of Geophysical Research: Biogeosciences*, 122, pp.498–513.

Bonn, A., Allott, T., Evans, M., Joosten, H. and Stoneman, R. eds., (2016) *Peatland restoration and ecosystem services: science, policy and practice*. Cambridge: Cambridge University Press.

Bonnett, S.A.F., Ostle, N. and Freeman, C., (2006) Seasonal variations in decomposition processes in a valley-bottom riparian peatland. *Science of The Total Environment*, 370, pp.561–573.

Bonnett, S.A.F., Ross, S., Linstead, C. and Maltby, E., (2009) *A review of techniques for monitoring the success of peatland restoration*. *University of Liverpool. Natural England Commissioned Reports, Number 086*.

Boothroyd, I.M., Worrall, F., Moody, C.S., Clay, G.D., Abbott, G.D. and Rose, R., (2021) Sulfur constraints on the carbon cycle of a blanket bog peatland. *Journal of Geophysical Research: Biogeosciences*, 126(8), p.20.

Bourgault, M.-A., Larocque, M. and Garneau, M., (2017) Quantification of peatland water storage capacity using the water table fluctuation method. *Hydrological Processes*, 31(5), pp.1184–1195.

Bowen, I.S., (1926) The ratio of heat losses by conduction and by evaporation from any water surface. *Physical Review*, 27, pp.779–787.

Boyle, J.F., Chiverrell, R.C. and Schillereff, D., (2015) Approaches to water content correction and calibration for μXRF core scanning: comparing X-ray scattering with simple regression of elemental concentrations. In: I.W. Croudace and R.G. Rothwell, eds., *Micro-XRF Studies of Sediment Cores*. Dordrecht: Springer, pp.373–390.

Bragg, O.M. and Tallis, J.H., (2001) The sensitivity of peat-covered upland landscapes. *CATENA*, 42, pp.345–360.

van Breemen, N., (1995) How Sphagnum bogs down other plants. *TREE*, 10(7), pp.270–275.

Bridgham, S.D., Pastor, J., Dewey, B., Weltzin, J.F. and Updegraff, K., (2008) Rapid carbon response of peatlands to climate change. *Ecology*, 89, pp.3041–3048.

Bridgham, S.D., Pastor, J., Updegraff, K., Malterer, T.J., Johnson, K., Harth, C. and Chen, J., (1999) Ecosystem Control over Temperature and Energy Flux in Northern Peatlands. *Ecological Applications*, 9(4), pp.1345–1358.

Bridgham, S.D., Updegraff, K. and Pastor, J., (1998) Carbon, nitrogen, and phosphorus mineralization in northern wetlands. *Ecology*, 79(5), pp.1545–1561.

Broder, T. and Biester, H., (2015) Hydrologic controls on DOC, As and Pb export from a polluted peatland-the importance of heavy rain events, antecedent moisture conditions and hydrological connectivity. *Biogeosciences*, 12, pp.4651–4664.

Broder, T. and Biester, H., (2017) Linking major and trace element concentrations in a headwater stream to DOC release and hydrologic conditions in a bog and peaty riparian zone. *Applied Geochemistry*, 87, pp.188–201.

Brown, A.E., Zhang, L., McMahon, T.A., Western, A.W. and Vertessy, R.A., (2005) A review of paired catchment studies for determining changes in water yield resulting from alterations in vegetation. *Journal of Hydrology*, 310, pp.28–61.

Brümmer, C., Black, T.A., Jassal, R.S., Grant, N.J., Spittlehouse, D.L., Chen, B., Nesic, Z., Amiro, B.D., Arain, M.A., Barr, A.G., Bourque, C.P.A., Coursolle, C., Dunn, A.L., Flanagan, L.B., Humphreys, E.R., Lafleur, P.M., Margolis, H.A., McCaughey, J.H. and Wofsy, S.C., (2012) How climate and vegetation type influence evapotranspiration and water use efficiency in Canadian forest, peatland and grassland ecosystems. *Agricultural and Forest Meteorology*, 153, pp.14–30.

Burke, W., (1975) Effect of drainage on the hydrology of blanket bog. *Irish Journal of Agricultural Research*, 14(2), pp.145–162.

Byrne, K.A. and Farrell, E.P., (2005) The effect of afforestation on soil carbon dioxide emissions in blanket peatland in Ireland. *Forestry: An International Journal of Forest Research*, 78(3), pp.217–227.

Campbell, D.I. and Williamson, J.L., (1997) Evaporation from a raised peat bog. *Journal of Hydrology*, 193, pp.142–160.

Campbell Scientific, (2005) *Bowen Ratio Instrumentation Instruction Manual*.

Campbell Scientific, (2010) *ARG100 Tipping Bucket Raingauge*. Loughborough, UK: Campbell Scientific Inc.

Campbell Scientific, (2016) *NR-Lite2 Net Radiometer User Guide*.

Cannell, M.G.R., Dewar, R.C. and Pyatt, D.G., (1993) Conifer Plantations on Drained Peatlands in Britain: a Net Gain or Loss of Carbon? *Forestry*, 66(4), pp.353–369.

Chapman, P.J., Clark, J.M., Heathwaite, A.L., Adamson, J.K. and Lane, S.N., (2005) Sulphate controls on dissolved organic carbon dynamics in blanket peat: Linking field and laboratory evidence. *Dynamics and Biogeochemistry of River Corridors and Wetlands*, 294, p.9.

Charman, D.J., (2002) *Peatlands and environmental change*. Chichester: Wiley.

Charman, D.J., (2007) Summer water deficit variability controls on peatland water-table changes: implications for Holocene palaeoclimate reconstructions. *The Holocene*, 17(2), pp.217–227.

Charman, D.J., Beilman, D.W., Blaauw, M., Booth, R.K., Brewer, S., Chambers, F.M., Christen, J.A., Gallego-Sala, A.V., Harrison, S.P., Hughes, P.D.M., Jackson, S.T., Korhola, A., Mauquoy,

D., Mitchell, F.J.G., Prentice, I.C., van der Linden, M., de Vleeschouwer, F., Yu, Z.C., Alm, J., Bauer, I.E., Corish, Y.M.C., Garneau, M., Hohl, V., Huang, Y., Karofeld, E., le Roux, G., Loisel, J., Moschen, R., Nichols, J.E., Nieminen, T.M., MacDonald, G.M., Phadtare, N.R., Rausch, N., Sillasoo, Ü., Swindles, G.T., Tuittila, E.-S., Ukonmaanaho, L., Väliranta, M., van Bellen, S., van Geel, B., Vitt, D.H. and Zhao, Y., (2013) Climate-related changes in peatland carbon accumulation during the last millennium. *Biogeosciences*, 10, pp.929–944.

Chiverrell, R.C., (2001) A proxy record of late Holocene climate change from May Moss, northeast England. *Journal of Quaternary Science*, 16(1), pp.9–29.

Ciais, P., Sabine, C., Bala, G., Bopp, L., Brovkin, V., Canadell, J., Chhabra, A., DeFries, R., Galloway, J., Heimann, M., Jones, C., Quéré, C. le, Myneni, R.B., Piao, S. and Thornton, P., (2013) Carbon and Other Biogeochemical Cycles. In: T.F. Stocker, D. Qin, G.-K. Plattner, M. Tignor, S.K. Allen, J. Boschung, A. Nauels, Y. Xia, V. Bex and P.M. Midgley, eds., *Climate Change 2013: The Physical Science Basis. Contribution of Working Group I to the Fifth Assessment Report of the Intergovernmental Panel on Climate Change*. Cambridge, United Kingdom and New York, NY, USA: Cambridge University Press, pp.465–570.

Clark, J.M., Chapman, P.J., Adamson, J.K. and Lane, S.N., (2005) Influence of drought-induced acidification on the mobility of dissolved organic carbon in peat soils. *Global Change Biology*, 11, pp.791–809.

Clark, J.M., Gallego-Sala, A.V., Allott, T.E.H., Chapman, S.J., Farewell, T., Freeman, C., House, J.I., Orr, H.G., Prentice, I.C. and Smith, P., (2010) Assessing the vulnerability of blanket peat to climate change using an ensemble of statistical bioclimatic envelope models. *Climate Research*, 45, pp.131–150.

Clark, J.M., Heinemeyer, A., Martin, P. and Bottrell, S.H., (2012) Processes controlling DOC in pore water during simulated drought cycles in six different UK peats. *Biogeochemistry*, 109, pp.253–270.

Clay, G.D., Dixon, S., Evans, M.G., Rowson, J.G. and Worrall, F., (2012) Carbon dioxide fluxes and DOC concentrations of eroding blanket peat gullies. *Earth Surface Processes and Landforms*, 37, pp.562–571.

Cloy, J.M., Farmer, J.G., Graham, M.C. and MacKenzie, A.B., (2009) Retention of As and Sb in ombrotrophic peat bogs: Records of As, Sb, and Pb deposition at four Scottish sites. *Environmental Science and Technology*, 43, pp.1756–1762.

Cloy, J.M., Farmer, J.G., Graham, M.C., MacKenzie, A.B. and Cook, G.T., (2005) A comparison of antimony and lead profiles over the past 2500 years in Flanders Moss ombrotrophic peat bog, Scotland. *Journal of Environmental Monitoring*, 7, pp.1137–1147.

Cloy, J.M., Farmer, J.G., Graham, M.C., MacKenzie, A.B. and Cook, G.T., (2008) Historical records of atmospheric Pb deposition in four Scottish ombrotrophic peat bogs: An isotopic comparison with other records from western Europe and Greenland. *Global Biogeochemical Cycles*, 222, pp.1–16.

Clymo, R.S., Turunen, J. and Tolonen, K., (1998) Carbon accumulation in peatland. *Oikos*, 81(2), pp.368–388.

Coch, C., Ramage, J.L., Lamoureux, S.F., Meyer, H., Knoblauch, C. and Lantuit, H., (2020) Spatial Variability of Dissolved Organic Carbon, Solutes, and Suspended Sediment in Disturbed Low Arctic Coastal Watersheds. *Journal of Geophysical Research: Biogeosciences*, 125, p.18.

Cohen, J., (1992) A power primer. *Psychological Bulletin*, 112(1), pp.155–159.

Conover, W.J., Johnson, M.E. and Johnson, M.M., (1981) A comparative study of tests for homogeneity of variances, with applications to the outer continental shelf bidding data. *Technometrics*, 23(4), pp.351–361.

Conway, V.M. and Millar, A., (1960) The hydrology of some small peat-covered catchments in the northern Pennines. *Journal of the Institution of Water Engineers*, 14(6), pp.415–424.

Creevy, A.L., Payne, R.J., Andersen, R. and Rowson, J.G., (2020) Annual gaseous carbon budgets of forest-to-bog restoration sites are strongly determined by vegetation composition. *Science of The Total Environment*, 705, p.11.

Cris, R., Buckmaster, S., Bain, C. and Bonn, A. eds., (2012) *UK Peatland Restoration - Demonstrating Success.* Edinburgh: IUCN UK National Committee Peatland Programme.

Crow, S.E. and Wieder, R.K., (2005) Sources of CO_2 emission from a northern peatland: Root respiration, exudation, and decomposition. *Ecology*, 86(7), pp.1825–1834.

Cummins, T. and Farrell, E.P., (2003) Biogeochemical impacts of clearfelling and reforestation on blanket-peatland streams II. Major ions and dissolved organic carbon. *Forest Ecology and Management*, 180, pp.557–570.

Cundill, A.P., Chapman, P.J. and Adamson, J.K., (2007) Spatial variation in concentrations of dissolved nitrogen species in an upland blanket peat catchment. *Science of the Total Environment*, 373, pp.166–177.

Cunliffe, A.M., Baird, A.J. and Holden, J., (2013) Hydrological hotspots in blanket peatlands: Spatial variation in peat permeability around a natural soil pipe. *Water Resources Research*, 49, pp.5342–5354.

Dahlqvist, R., Andersson, K., Ingri, J., Larsson, T., Stolpe, B. and Turner, D., (2007) Temporal variations of colloidal carrier phases and associated trace elements in a boreal river. *Geochimica et Cosmochimica Acta*, 71, pp.5339–5354.

Daniels, S.M., Evans, M.G., Agnew, C.T. and Allott, T.E.H., (2012) Ammonium release from a blanket peatland into headwater stream systems. *Environmental Pollution*, 163, pp.261–272.

Davidson, E.A. and Janssens, I.A., (2006) Temperature sensitivity of soil carbon decomposition and feedbacks to climate change. *Nature*, 440, pp.165–173.

Dawson, J.J.C., Billett, M.F., Neal, C. and Hill, S., (2002) A comparison of particulate, dissolved and gaseous carbon in two contrasting upland streams in the UK. *Journal of Hydrology*, 257, pp.226–246.

Dedysh, S.N., (2002) Methanotrophic bacteria of acidic Sphagnum peat bogs. *Microbiology*, 71(6), pp.638–650.

Dise, N.B., (2009) Peatland Response to Global Change. *Science*, 326(5954), pp.810–811.

Drexler, J.Z., Snyder, R.L., Spano, D. and Paw U, K.T., (2004) A review of models and micrometeorological methods used to estimate wetland evapotranspiration. *Hydrological Processes*, 18, pp.2071–2101.

Drinan, T.J., Graham, C.T., O'Halloran, J. and Harrison, S.S.C., (2013) The impact of catchment conifer plantation forestry on the hydrochemistry of peatland lakes. *Science of the Total Environment*, 443, pp.608–620.

Dunfield, P., Knowles, R., Dumont, R. and Moore, T., (1993) Methane production and consumption in temperate and subarctic peat soils: Response to temperature and pH. *Soil Biology and Biochemistry*, 25(3), pp.321–326.

Eatherall, A., Warwick, M.S. and Tolchard, S., (2000) Identifying sources of dissolved organic carbon on the River Swale, Yorkshire. *The Science of the Total Environment*, 251–252, pp.173–190.

Edwards, K., (2014) *The fluid flow calculations website. V-Notch (Triangular) Weir Calculator: Discharge and Head Calculations, Equations, and Guidelines for water flow measurement in streams and channels.* [online] LMNO Engineering, Research, and Software, Ltd. Available at: https://www.lmnoeng.com/Weirs/vweir.php [Accessed 1 Dec. 2021].

Eigner, J., (1975) Naturschutz und Landschaftspflege in Schleswig-Holsteinischen Mooren. *TELMA*, 5, pp.227–239.

Elkington, T., Dayton, N., Jackson, D.L. and Strachan, I.M., (2001) *Field Guide To Mires and Heaths*. *Joint Nature Conservation Committee*.

Erwin, K.L., (2009) Wetlands and global climate change: the role of wetland restoration in a changing world. *Wetlands Ecology and Management*, 17, pp.71–84.

Escobedo, J.F., Gomes, E.N., Oliveira, A.P. and Soares, J., (2009) Modeling hourly and daily fractions of UV, PAR and NIR to global solar radiation under various sky conditions at Botucatu, Brazil. *Applied Energy*, 86, pp.299–309.

Evans, C.D., Bonn, A., Holden, J., Reed, M.S., Evans, M.G., Worrall, F., Couwenberg, J. and Parnell, M., (2014a) Relationships between anthropogenic pressures and ecosystem functions in UK blanket bogs: Linking process understanding to ecosystem service valuation. *Ecosystem Services*, 9, pp.5–19.

Evans, C.D., Chadwick, T., Norris, D., Rowe, E.C., Heaton, T.H.E., Brown, P. and Battarbee, R.W., (2014b) Persistent surface water acidification in an organic soil-dominated upland region subject to high atmospheric deposition: The North York Moors, UK. *Ecological Indicators*, 37, pp.304–316.

Evans, C.D., Chapman, P.J., Clark, J.M., Monteith, D.T. and Cresser, M.S., (2006) Alternative explanations for rising dissolved organic carbon export from organic soils. *Global Change Biology*, 12, pp.2044–2053.

Evans, C.D., Jones, T.G., Burden, A., Ostle, N., Zieliński, P., Cooper, M.D.A., Peacock, M., Clark, J.M., Oulehle, F., Cooper, D. and Freeman, C., (2012) Acidity controls on dissolved organic carbon mobility in organic soils. *Global Change Biology*, 18(11), pp.3317–3331.

Evans, C.D., Monteith, D.T. and Cooper, D.M., (2005) Long-term increases in surface water dissolved organic carbon: Observations, possible causes and environmental impacts. *Environmental Pollution*, 137, pp.55–71.

Evans, C.D., Monteith, D.T. and Harriman, R., (2001) Long-term variability in the deposition of marine ions at west coast sites in the UK Acid Waters Monitoring Network: Impacts on surface water chemistry and significance for trend determination. *Science of the Total Environment*, 265, pp.115–129.

Evans, C.D., Peacock, M., Green, S.M., Holden, J., Chapman, P.J., Lebron, I., Callaghan, N., Grayson, R. and Baird, A.J., (2018) The impact of ditch blocking on fluvial carbon export from a UK blanket bog. *Hydrological Processes*, 32, pp.2141–2154.

Evans, M.G., Burt, T.P., Holden, J. and Adamson, J.K., (1999) Runoff generation and water table fluctuations in blanket peat: evidence from UK data spanning the dry summer of 1995. *Journal of Hydrology*, 221, pp.141–160.

Evans, M.G. and Lindsay, J., (2010) Impact of gully erosion on carbon sequestration in blanket peatlands. *Climate Research*, 45, pp.31–41.

Evans, M.G. and Warburton, J., (2005) Sediment budget for an eroding peat-moorland catchment in northern England. *Earth Surface Processes and Landforms*, 30, pp.557–577.

Evans, M.G. and Warburton, J., (2010) *Geomorphology of upland peat: erosion, form and landscape change*. Chichester: Wiley-Blackwell.

Fahle, M. and Dietrich, O., (2014) Estimation of evapotranspiration using diurnal groundwater level fluctuations: Comparison of different approaches with groundwater lysimeter data. *Water Resources Research*, 50, pp.273–286.

Fenner, N. and Freeman, C., (2011) Drought-induced carbon loss in peatlands. *Nature Geoscience*, 4, pp.895–900.

Ferguson, P., Lee, J.A. and Bell, J.N.B., (1978) Effects of sulphur pollutants on the growth of Sphagnum species. *Environmental Pollution*, 16, pp.151–162.

Ferretto, A., Brooker, R., Matthews, R. and Smith, P., (2021) Climate change and drinking water from Scottish peatlands: Where increasing DOC is an issue? *Journal of Environmental Management*, 300(113688), p.11.

Field, R.H., Buchanan, G.M., Hughes, A., Smith, P. and Bradbury, R.B., (2020) The value of habitats of conservation importance to climate change mitigation in the UK. *Biological Conservation*, 248(108619), p.10.

Finnegan, J., Regan, J.T., O'Connor, M., Wilson, P. and Healy, M.G., (2014) Implications of applied best management practice for peatland forest harvesting. *Ecological Engineering*, 63, pp.12–26.

Flynn, R., Mackin, F. and Renou-Wilson, F., (2021a) *Towards the Quantification of Blanket Bog Ecosystem Services to Water*. *EPA Research Report 378 Towards*.

Flynn, R., McVeigh, C., Mackin, F. and Wilson, F.R., (2021b) Sources of stream base flow in blanket peat covered catchments. *Journal of Hydrology*, 603(126965), p.13.

Foken, T., (2008) The energy balance closure problem: an overview. *Ecological Applications*, 18(6), pp.1351–1367.

Forestry Commission, (2019) *National Forest Inventory Woodland England*. [online] Available at: https://data-forestry.opendata.arcgis.com/ [Accessed 8 Apr. 2021].

Foster, M., (2012) *Restoration of North York Moors bog hailed big success*. [online] Available at: https://www.thenorthernecho.co.uk/news/9871418.restoration-north-york-moors-bog-hailed-big-success/ [Accessed 1 Mar. 2022].

Fowler, D., Cape, J.N., Unsworth, M.H., Mayer, H., Crowther, J.M., Jarvis, P.G., Gardiner, B. and Shuttleworth, W.J., (1989) Deposition of atmospheric pollutants on forests. *Philosophical Transactions of the Royal Society of London. Series B, Biological Sciences*, 324(1223), pp.247–265.

Fowler, H.J. and Kilsby, C.G., (2002) Precipitation and the North Atlantic Oscillation: A study of climatic variability in Northern England. *International Journal of Climatology*, 22, pp.843–866.

Fraser, C.J.D., Roulet, N.T. and Moore, T.R., (2001) Hydrology and dissolved organic carbon biogeochemistry in an ombrotrophic bog. *Hydrological Processes*, 15, pp.3151–3166.

Freeman, C., Evans, C.D., Monteith, D.T., Reynolds, B. and Fenner, N., (2001a) Export of organic carbon from peat soils. *Nature*, 412, pp.785–785.

Freeman, C., Fenner, N., Ostle, N.J., Kang, H., Dowrick, D.J., Reynolds, B., Lock, M.A., Sleep, D., Hughes, S. and Hudson, J., (2004) Export of dissolved organic carbon from peatlands under elevated carbon dioxide levels. *Nature*, 430, pp.195–198.

Freeman, C., Ostle, N. and Kang, H., (2001b) An enzymic 'latch' on a global carbon store. *Nature*, 409, p.149.

Frolking, S., Talbot, J., Jones, M.C., Treat, C.C., Kauffman, J.B., Tuittila, E.-S. and Roulet, N., (2011) Peatlands in the Earth's 21st century climate system. *Environmental Reviews*, 19, pp.371–396.

Fuka, D.R., Walter, M.T., Archibald, J.A., Steenhuis, T.S. and Easton, Z.M., (2018) *Package 'EcoHydRology': A community modeling foundation for eco-hydrology*.

Gaffney, P.P.J., Hancock, M.H., Taggart, M.A. and Andersen, R., (2018) Measuring restoration progress using pore- and surface-water chemistry across a chronosequence of formerly afforested blanket bogs. *Journal of Environmental Management*, 219, pp.239–251.

Gaffney, P.P.J., Hancock, M.H., Taggart, M.A. and Andersen, R., (2020) Restoration of afforested peatland: Immediate effects on aquatic carbon loss. *Science of the Total Environment*, 742(140594), p.13.

Gaffney, P.P.J., Hancock, M.H., Taggart, M.A. and Andersen, R., (2021) Catchment water quality in the year preceding and immediately following restoration of a drained afforested blanket bog. *Biogeochemistry*, 153, pp.243–262.

Gaffney, P.P.J., Hancock, M.H., Taggart, M.A. and Andersen, R., (2022) Restoration of afforested peatland: Effects on pore- and surface-water quality in relation to differing harvesting methods. *Ecological Engineering*, 177(106567), p.13.

Gallego-Sala, A.V. and Prentice, I.C., (2013) Blanket peat biome endangered by climate change. *Nature Climate Change*, 3, pp.152–155.

García-Rodríguez, A., García-Rodríguez, S., Díez-Mediavilla, M. and Alonso-Tristán, C., (2020) Photosynthetic active radiation, solar irradiance and the CIE standard sky classification. *Applied Sciences (Switzerland)*, 10, p.14.

Gerling, L., Weber, T.K.D., Reineke, D., Durner, W., Martin, S. and Weber, S., (2019) Eddy covariance based surface-atmosphere exchange and crop coefficient determination in a mountainous peatland. *Ecohydrology*, 12, p.14.

Gilvear, D.J. and Bradley, C., (2000) Hydrological monitoring and surveillance for wetland conservation and management; a UK perspective. *Physics and Chemistry of the Earth, Part B: Hydrology, Oceans and Atmosphere*, 25(7-8), pp.571–588.

Glatzel, S., Kalbitz, K., Dalva, M. and Moore, T., (2003) Dissolved organic matter properties and their relationship to carbon dioxide efflux from restored peat bogs. *Geoderma*, 113, pp.397–411.

Glenk, K., Faccioli, M., Martin-Ortega, J., Schulze, C. and Potts, J., (2021) The opportunity cost of delaying climate action: Peatland restoration and resilience to climate change. *Global Environmental Change*, 70(102323), p.14.

Glenk, K. and Martin-Ortega, J., (2018) The economics of peatland restoration. *Journal of Environmental Economics and Policy*, 7(4), pp.345–362.

Grybos, M., Davranche, M., Gruau, G., Petitjean, P. and Pédrot, M., (2009) Increasing pH drives organic matter solubilization from wetland soils under reducing conditions. *Geoderma*, 154, pp.13–19.

Günther, A., Barthelmes, A., Huth, V., Joosten, H., Jurasinski, G., Koebsch, F. and Couwenberg, J., (2020) Prompt rewetting of drained peatlands reduces climate warming despite methane emissions. *Nature Communications*, 11(1644), p.5.

Haapalehto, T., Kotiaho, J.S., Matilainen, R. and Tahvanainen, T., (2014) The effects of long-term drainage and subsequent restoration on water table level and pore water chemistry in boreal peatlands. *Journal of Hydrology*, 519, pp.1493–1505.

Haapalehto, T.O., Vasander, H., Jauhiainen, S., Tahvanainen, T. and Kotiaho, J.S., (2011) The effects of peatland restoration on water-table depth, elemental concentrations, and vegetation: 10 years of changes. *Restoration Ecology*, 19(5), pp.587–598.

Hammer, Ø., Harper, D.A.T. and Ryan, P.D., (2001) PAST: Paleontological statistics software package for education and data analysis. *Palaeontologia Electronica*, 4(1), p.9.

Hancock, M.H., Klein, D. and Cowie, N.R., (2020) Guild-level responses by mammalian predators to afforestation and subsequent restoration in a formerly treeless peatland landscape. *Restoration Ecology*, 28(5), pp.1113–1123.

Hargreaves, K.J., Milne, R. and Cannell, M.G.R., (2003) Carbon balance of afforested peatland in Scotland. *Forestry*, 76(3), pp.299–317.

Haynes, K.M., Kane, E.S., Potvin, L., Lilleskov, E.A., Kolka, R.K. and Mitchell, C.P.J., (2017) Mobility and transport of mercury and methylmercury in peat as a function of changes in water table regime and plant functional groups. *Global Biogeochemical Cycles*, 31, pp.233–244.

Hemes, K.S., Chamberlain, S.D., Eichelmann, E., Knox, S.H. and Baldocchi, D.D., (2018) A Biogeochemical Compromise: The High Methane Cost of Sequestering Carbon in Restored Wetlands. *Geophysical Research Letters*, 45, pp.6081–6091.

Hemond, H.F., (1980) Biogeochemistry of Thoreau's Bog, Concord, Massachusetts. *Ecological Monographs*, 50(4), pp.507–526.

Hillier, S., (2001) Particulate composition and origin of suspended sediment in the R. Don, Aberdeenshire, UK. *Science of The Total Environment*, 265, pp.281–293.

Hobbs, N.B., (1986) Mire morphology and the properties and behaviour of some British and foreign peats. *Quarterly Journal of Engineering Geology*, 19, pp.7–80.

Hogg, E.H., Lieffers, V.J. and Wein, R.W., (1992) Potential Carbon Losses From Peat Profiles: Effects of Temperature, Drought Cycles, and Fire. *Ecological Applications*, 2(3), pp.298–306.

Holden, J., (2005) Controls of soil pipe frequency in upland blanket peat. *Journal of Geophysical Research: Earth Surface*, 110, p.11.

Holden, J., (2009) Topographic controls upon soil macropore flow. *Earth Surface Processes and Landforms*, 34, pp.345–351.

Holden, J. and Burt, T.P., (2002a) Infiltration, runoff and sediment production in blanket peat catchments: Implications of field rainfall simulation experiments. *Hydrological Processes*, 16, pp.2537–2557.

Holden, J. and Burt, T.P., (2002b) Laboratory experiments on drought and runoff in blanket peat. *European Journal of Soil Science*, 53(4), pp.675–690.

Holden, J. and Burt, T.P., (2002c) Piping and pipeflow in a deep peat catchment. *CATENA*, 48, pp.163–199.

Holden, J. and Burt, T.P., (2003a) Hydrological studies on blanket peat: the significance of the acrotelm-catotelm model. *Journal of Ecology*, 91, pp.86–102.

Holden, J. and Burt, T.P., (2003b) Runoff production in blanket peat covered catchments. *Water Resources Research*, 39(7), p.9.

Holden, J., Evans, M.G., Burt, T.P. and Horton, M., (2006) Impact of Land Drainage on Peatland Hydrology. *Journal of Environmental Quality*, 35, pp.1764–1778.

Holden, J., Green, S.M., Baird, A.J., Grayson, R.P., Dooling, G.P., Chapman, P.J., Evans, C.D., Peacock, M. and Swindles, G.T., (2017) The impact of ditch blocking on the hydrological functioning of blanket peatlands. *Hydrological Processes*, 31, pp.525–539.

Holden, J. and Rose, R., (2011) Temperature and surface lapse rate change: a study of the UK's longest upland instrumental record. *International Journal of Climatology*, 31, pp.907–919.

Holden, J., Smart, R.P., Dinsmore, K.J., Baird, A.J., Billett, M.F. and Chapman, P.J., (2012) Natural pipes in blanket peatlands: Major point sources for the release of carbon to the aquatic system. *Global Change Biology*, 18, pp.3568–3580.

Höll, B.S., Fiedler, S., Jungkunst, H.F., Kalbitz, K., Freibauer, A., Drösler, M. and Stahr, K., (2009) Characteristics of dissolved organic matter following 20 years of peatland restoration. *Science of The Total Environment*, 408, pp.78–83.

Hope, D., Billett, M.F. and Cresser, M.S., (1997) Exports of organic carbon in two river systems in NE Scotland. *Journal of Hydrology*, 193, pp.61–82.

Hornibrook, E.R.C., Longstaffe, F.J. and Fyfe, W.S., (1997) Spatial distribution of microbial methane production pathways in temperate zone wetland soils: Stable carbon and hydrogen isotope evidence. *Geochimica et Cosmochimica Acta*, 61(4), pp.745–753.

House, J.I., Orr, H.G., Clark, J.M., Gallego-Sala, A.V., Freeman, C., Prentice, I.C. and Smith, P., (2010) Climate change and the British Uplands: Evidence for decision-making. *Climate Research*, 45, pp.3–12.

Howson, T., Chapman, P.J., Shah, N., Anderson, R. and Holden, J., (2021a) A comparison of porewater chemistry between intact, afforested and restored raised and blanket bogs. *Science of the Total Environment*, 766, p.144496.

Howson, T., Chapman, P.J., Shah, N., Anderson, R. and Holden, J., (2021b) The effect of forest-to-bog restoration on the hydrological functioning of raised and blanket bogs. *Ecohydrology*, 14, p.19.

Hu, S., Zhao, C., Li, J., Wang, F. and Chen, Y., (2014) Discussion and reassessment of the method used for accepting or rejecting data observed by a Bowen ratio system. *Hydrological Processes*, 28, pp.4506–4510.

Humphreys, E.R., Lafleur, P.M., Flanagan, L.B., Hedstrom, N., Syed, K.H., Glenn, A.J. and Granger, R., (2006) Summer carbon dioxide and water vapor fluxes across a range of northern peatlands. *Journal of Geophysical Research: Biogeosciences*, 111(G04011), p.16.

Hurrell, J.W., Kushnir, Y., Ottersen, G. and Visbeck, M., (2003) An overview of the North Atlantic Oscillation. In: *Geophysical Monograph Series*. p.35.

Ingram, H.A.P., (1967) Problems of Hydrology and Plant Distribution in Mires. *Journal of Ecology*, 55(3), pp.711–724.

Ingram, H.A.P., (1978) Soil layers in mires: function and terminology. *Journal of Soil Science*, 29, pp.224–227.

Ingram, H.A.P., (1982) Size and shape in raised mire ecosystems: A geophysical model. *Nature*, 297, pp.300–303.

IPCC, (2022) Summary for Policymakers. In: P.R. Shukla, J. Skea, R. Slade, A. al Khourdajie, R. van Diemen, D. McCollum, M. Pathak, S. Some, P. Vyas, R. Fradera, M. Belkacemi, A. Hasija, G. Lisboa, S. Luz and J. Malley, eds., *Climate Change 2022: Mitigation of Climate Change. Contribution of Working Group III to the Sixth Assessment Report of the Intergovernmental Panel on Climate Change*. Cambridge, UK and New York, USA.

Isabelle, P.-E., Nadeau, D.F., Rousseau, A.N. and Anctil, F., (2018) Water budget, performance of evapotranspiration formulations, and their impact on hydrological modeling of a small boreal peatland-dominated watershed. *Canadian Journal of Earth Sciences*, 55, pp.206–220.

Ise, T., Dunn, A.L., Wofsy, S.C. and Moorcroft, P.R., (2008) High sensitivity of peat decomposition to climate change through water-table feedback. *Nature Geoscience*, 1, pp.763–766.

IUCN, (2022) *Peatland Code (Version 1.2)*. International Union for Conservation of Nature (IUCN) UK Peatland Programme.

Jackson, D.A., (1993) Stopping rules in principal components analysis: a comparison of heuristical and statistical approaches. *Ecology*, 74(8), pp.2204–2214.

Jakeman, A.J., Littlewood, I.G. and Whitehead, P.G., (1990) Computation of the instantaneous unit hydrograph and identifiable component flows with application to two small upland catchments. *Journal of Hydrology*, 117(1-4), pp.275–300.

Jollife, I.T. and Cadima, J., (2016) Principal component analysis: A review and recent developments. *Philosophical Transactions of the Royal Society A: Mathematical, Physical and Engineering Sciences*, 374(20150202), p.16.

Joosten, H., (2009) The Global Peatland CO2 Picture: Peatland status and drainage related emissions in all the countries of the world. *Wetlands International*. [online] Available at: http://www.wetlands.org/LinkClick.aspx?fileticket=fcVE4EMiG%2Fw%3D&tabid=56.

Joosten, H., Tanneberger, F. and Moen, A. eds., (2017) *Mires and peatlands of Europe: Status, distribution and conservation*. Stuttgart: Schweizbart Science Publishers.

Jordan, R.N., Yonge, D.R. and Hathhorn, W.E., (1997) Enhanced mobility of Pb in the presence of dissolved natural organic matter. *Journal of Contaminant Hydrology*, 29, pp.59–80.

Jovani-Sancho, A.J., Cummins, T. and Byrne, K.A., (2021) Soil carbon balance of afforested peatlands in the maritime temperate climatic zone. *Global Change Biology*, 27, pp.3681–3698.

Jutebring Sterte, E., Lidman, F., Lindborg, E., Sjöberg, Y. and Laudon, H., (2021) How catchment characteristics influence hydrological pathways and travel times in a boreal landscape. *Hydrology and Earth System Sciences*, 25, pp.2133–2158.

Kaila, A., Asam, Z.-Z., Koskinen, M., Uusitalo, R., Smolander, A., Kiikkilä, O., Sarkkola, S., O'Driscoll, C., Kitunen, V., Fritze, H., Nousiainen, H., Tervahauta, A., Xiao, L. and Nieminen, M., (2016) Impact of re-wetting of forestry-drained peatlands on water quality—a laboratory approach assessing the release of P, N, Fe, and dissolved organic carbon. *Water, Air, & Soil Pollution*, 227(292), p.15.

Kaila, A., Asam, Z.-Z., Sarkkola, S., Xiao, L., Laurén, A., Vasander, H. and Nieminen, M., (2012) Decomposition of harvest residue needles on peatlands drained for forestry - Implications for nutrient and heavy metal dynamics. *Forest Ecology and Management*, 277, pp.141–149.

Kaiser, H.F., (1974) An index of factorial simplicity. *Psychometrika*, 39, pp.31–36.

Kalbitz, K., Schmerwitz, J., Schwesig, D. and Matzner, E., (2003) Biodegradation of soil-derived dissolved organic matter as related to its properties. *Geoderma*, 113, pp.273–291.

Kellner, E., (2001) Surface energy fluxes and control of evapotranspiration from a Swedish Sphagnum mire. *Agricultural and Forest Meteorology*, 110, pp.101–123.

Kellner, E. and Halldin, S., (2002) Water budget and surface-layer water storage in a Sphagnum bog in central Sweden. *Hydrological Processes*, 16, pp.87–103.

Kendon, M., McCarthy, M., Jevrejeva, S., Matthews, A., Sparks, T. and Garforth, J., (2020) State of the UK Climate 2019. *International Journal of Climatology*, 40S1, pp.1–69.

Kennedy-Asser, A.T., Andrews, O., Mitchell, D.M. and Warren, R.F., (2021) Evaluating heat extremes in the UK Climate Projections (UKCP18). *Environmental Research Letters*, 16(014039), p.10.

Klavins, M. and Purmalis, O., (2013) Properties and structure of raised bog peat humic acids. *Journal of Molecular Structure*, 1050, pp.103–113.

Koehler, A.-K., Murphy, K., Kiely, G. and Sottocornola, M., (2009) Seasonal variation of DOC concentration and annual loss of DOC from an Atlantic blanket bog in South Western Ireland. *Biogeochemistry*, 95(2-3), pp.231–242.

Kokkonen, N.A.K., Laine, A.M., Laine, J., Vasander, H., Kurki, K., Gong, J. and Tuittila, E.-S., (2019) Responses of peatland vegetation to 15-year water level drawdown as mediated by fertility level. *Journal of Vegetation Science*, 30, pp.1206–1216.

Kondolf, G.M. and Matthews, W.V.G., (1991) Unmeasured Residuals in Sediment Budgets: A Cautionary Note. *Water Resources Research*, 27(9), pp.2483–2486.

Koskinen, M., Sallantaus, T. and Vasander, H., (2011) Post-restoration development of organic carbon and nutrient leaching from two ecohydrologically different peatland sites. *Ecological Engineering*, 37, pp.1008–1016.

Koskinen, M., Tahvanainen, T., Sarkkola, S., Menberu, M.W., Laurén, A., Sallantaus, T., Marttila, H., Ronkanen, A.-K., Parviainen, M., Tolvanen, A., Koivusalo, H. and Nieminen, M., (2017) Restoration of nutrient-rich forestry-drained peatlands poses a risk for high exports of dissolved organic carbon, nitrogen, and phosphorus. *Science of the Total Environment*, 586, pp.858–869.

Lafleur, P.M., (2008) Connecting atmosphere and wetland: energy and water vapour exchange. *Geography Compass*, 2(4), pp.1027–1057.

Lafleur, P.M., Hember, R.A., Admiral, S.W. and Roulet, N.T., (2005) Annual and seasonal variability in evapotranspiration and water table at a shrub-covered bog in southern Ontario, Canada. *Hydrological Processes*, 19, pp.3533–3550.

Lafleur, P.M., Roulet, N.T. and Admiral, S.W., (2001) Annual cycle of CO2 exchange at a bog peatland. *Journal of Geophysical Research Atmospheres*, 106(D3), pp.3071–3081.

Lai, D.Y.F., (2009a) Methane Dynamics in Northern Peatlands: A Review. *Pedosphere*, 19(4), pp.409–421.

Lai, D.Y.F., (2009b) Modelling the effects of climate change on methane emission from a northern ombrotrophic bog in Canada. *Environmental Geology*, 58, pp.1197–1206.

Laiho, R., (2006) Decomposition in peatlands: Reconciling seemingly contrasting results on the impacts of lowered water levels. *Soil Biology and Biochemistry*, 38, pp.2011–2024.

Laine, A.M., Byrne, K.A., Kiely, G. and Tuittila, E.-S., (2009) The short-term effect of altered water level on carbon dioxide and methane fluxes in a blanket bog. *Suo*, 60(3-4), pp.65–83.

Lapen, D.R., Price, J.S. and Gilbert, R., (2000) Soil water storage dynamics in peatlands with shallow water tables. *Canadian Journal of Soil Science*, 80, pp.43–52.

Lapen, D.R., Price, J.S. and Gilbert, R., (2005) Modelling two-dimensional steady-state groundwater flow and flow sensitivity to boundary conditions in blanket peat complexes. *Hydrological Processes*, 19, pp.371–386.

Lavers, C.P. and Haines-Young, R.H., (1997) Displacement of dunlin Calidris alpina schinzii by forestry in the Flow Country and an estimate of the value of moorland adjacent to plantations. *Biological Conservation*, 79, pp.87–90.

Ledesma, J.L.J., Köhler, S.J. and Futter, M.N., (2012) Long-term dynamics of dissolved organic carbon: Implications for drinking water supply. *Science of the Total Environment*, 432, pp.1–11.

Leifeld, J. and Menichetti, L., (2018) The underappreciated potential of peatlands in global climate change mitigation strategies. *Nature Communications*, 9(1071), p.7.

Lelieveld, J., Crutzen, P.J. and Dentener, F.J., (1998) Changing concentration, lifetime and climate forcing of atmospheric methane. *Tellus, Series B: Chemical and Physical Meteorology*, 50(2), pp.128–150.

Letts, M.G., Comer, N.T., Roulet, N.T., Skarupa, M.R. and Verseghy, D.L., (2000) Parametrization of peatland hydraulic properties for the Canadian land surface scheme. *Atmosphere - Ocean*, 38(1), pp.141–160.

Lewis, C., Albertson, J., Zi, T., Xu, X. and Kiely, G., (2013) How does afforestation affect the hydrology of a blanket peatland? A modelling study. *Hydrological Processes*, 27, pp.3577–3588.

Limpens, J., Berendse, F., Blodau, C., Canadell, J.G., Freeman, C., Holden, J., Roulet, N. and Rydin, H., (2008) Peatlands and the carbon cycle: from local processes to global implications – a synthesis. *Biogeosciences*, 5, pp.1475–1491.

Lindsay, R., (1995) *Bogs: the ecology, classification and conservation of ombrotrophic mires*. Edinburgh: Scottish Natural Heritage.

Lindsay, R.A., Charman, D.J., Everingham, F., O'Reilly, R.M., Palmer, M.A., Rowell, T.A. and Stroud, D.A., (1988) *The Flow Country: the peatlands of Caithness and Sutherland*. Peterborough: Joint Nature Conservation Committee.

Loisel, J., Gallego-Sala, A.V., Amesbury, M.J., Magnan, G., Anshari, G., Beilman, D.W., Benavides, J.C., Blewett, J., Camill, P., Charman, D.J., Chawchai, S., Hedgpeth, A., Kleinen, T., Korhola, A., Large, D., Mansilla, C.A., Müller, J., van Bellen, S., West, J.B., Yu, Z., Bubier, J.L., Garneau, M., Moore, T., Sannel, A.B.K., Page, S.E., Väliranta, M., Bechtold, M., Brovkin, V., Cole, L.E.S., Chanton, J.P., Christensen, T.R., Davies, M.A., de Vleeschouwer, F., Finkelstein, S.A., Frolking, S., Gałka, M., Gandois, L., Girkin, N., Harris, L.I., Heinemeyer, A., Hoyt, A.M., Jones, M.C., Joos, F., Juutinen, S., Kaiser, K., Lacourse, T., Lamentowicz, M., Larmola, T., Leifeld, J., Lohila, A., Milner, A.M., Minkkinen, K., Moss, P., Naafs, B.D.A., Nichols, J., O'Donnell, J., Payne, R., Philben, M., Piilo, S., Quillet, A., Ratnayake, A.S., Roland, T.P., Sjögersten, S., Sonnentag, O., Swindles, G.T., Swinnen, W., Talbot, J., Treat, C., Valach, A.C. and Wu, J., (2021) Expert assessment of future vulnerability of the global peatland carbon sink. *Nature Climate Change*, 11, pp.70–77.

Lunt, P.H., Fyfe, R.M. and Tappin, A.D., (2019) Role of recent climate change on carbon sequestration in peatland systems. *Science of The Total Environment*, 667, pp.348–358.

Marsh, T.J. and Hannaford, J. eds., (2008) *UK Hydrometric Register. Hydrological data UK series.*

Martin-Ortega, J., Allott, T.E.H., Glenk, K. and Schaafsma, M., (2014) Valuing water quality improvements from peatland restoration: Evidence and challenges. *Ecosystem Services*, 9, pp.34–43.

Marttila, H., Karjalainen, S.M., Kuoppala, M., Nieminen, M.L., Ronkanen, A.-K., Kløve, B. and Hellsten, S., (2018) Elevated nutrient concentrations in headwaters affected by drained peatland. *Science of the Total Environment*, 643, pp.1304–1313.

Matilainen, A., Gjessing, E.T., Lahtinen, T., Hed, L., Bhatnagar, A. and Sillanpää, M., (2011) An overview of the methods used in the characterisation of natural organic matter (NOM) in relation to drinking water treatment. *Chemosphere*, 83, pp.1431–1442.

Mazzola, V., Perks, M.P., Smith, J., Yeluripati, J. and Xenakis, G., (2021) Seasonal patterns of greenhouse gas emissions from a forest-to-bog restored site in northern Scotland: Influence of microtopography and vegetation on carbon dioxide and methane dynamics. *European Journal of Soil Science*, 72(3), pp.1332–1353.

McCarter, C.P.R. and Price, J.S., (2013) The hydrology of the Bois-des-Bel bog peatland restoration: 10 years post-restoration. *Ecological Engineering*, 55, pp.73–81.

McCarthy, M., Armstrong, L. and Armstrong, N., (2019a) A new heatwave definition for the UK. *Weather*, 74(11), pp.382–387.

McCarthy, M., Christidis, N., Dunstone, N., Fereday, D., Kay, G., Klein-Tank, A., Lowe, J., Petch, J., Scaife, A. and Stott, P., (2019b) Drivers of the UK summer heatwave of 2018. *Weather*, 74(11), pp.390–396.

Menberu, M.W., Haghighi, A.T., Ronkanen, A.-K., Marttila, H. and Kløve, B., (2018) Effects of Drainage and Subsequent Restoration on Peatland Hydrological Processes at Catchment Scale. *Water Resources Research*, 54, pp.4479–4497.

Met Office, (2021a) MIDAS Open: UK daily rainfall data, v202107. *NERC EDS Centre for Environmental Data Analysis*. [online] Available at: http://dx.doi.org/10.5285/d6bcf4171c2f4754a7455d00deda0f72 [Accessed 5 May 2021].

Met Office, (2021b) MIDAS Open: UK daily temperature data, v202107. *NERC EDS Centre for Environmental Data Analysis*. [online] Available at: http://dx.doi.org/10.5285/92e823b277cc4f439803a87f5246db5f.

Met Office, (2021c) MIDAS Open: UK hourly rainfall data, v202107. *NERC EDS Centre for Environmental Data Analysis*. [online] Available at: http://dx.doi.org/10.5285/f7ae919f96b44a1c9695f40a9cf988dd.

Met Office, (2021d) MIDAS Open: UK hourly weather observation data, v202107. *NERC EDS Centre for Environmental Data Analysis*. [online] Available at: http://dx.doi.org/10.5285/3bd7221d4844435dad2fa030f26ab5fd.

Meyer, A., Tarvainen, L., Nousratpour, A., Björk, R.G., Ernfors, M., Grelle, A., Kasimir Klemedtsson, Å., Lindroth, A., Räntfors, M., Rütting, T., Wallin, G., Weslien, P. and Klemedtsson, L., (2013) A fertile peatland forest does not constitute a major greenhouse gas sink. *Biogeosciences*, 10, pp.7739–7758.

Mitchell, E.A.D., Charman, D.J. and Warner, B.G., (2008) Testate amoebae analysis in ecological and paleoecological studies of wetlands: Past, present and future. *Biodiversity and Conservation*, 17, pp.2115–2137.

Monteith, D.T., Stoddard, J.L., Evans, C.D., de Wit, H.A., Forsius, M., Høgåsen, T., Wilander, A., Skjelkvåle, B.L., Jeffries, D.S., Vuorenmaa, J., Keller, B., Kopécek, J. and Vesely, J., (2007)

Dissolved organic carbon trends resulting from changes in atmospheric deposition chemistry. *Nature*, 450, pp.537–540.

Monteith, J.L., (1965) Evaporation and environment. *Symposia of the Society for Experimental Biology*, 19, pp.205–234.

Moody, C.S., Worrall, F., Evans, C.D. and Jones, T.G., (2013) The rate of loss of dissolved organic carbon (DOC) through a catchment. *Journal of Hydrology*, 492, pp.139–150.

Moore, P.A., Pypker, T.G. and Waddington, J.M., (2013) Effect of long-term water table manipulation on peatland evapotranspiration. *Agricultural and Forest Meteorology*, 178–179, pp.106–119.

Moore, P.D., (1989) The ecology of peat-forming processes: a review. *International Journal of Coal Geology*, 12, pp.89–103.

Moore, P.D., (2002) The future of cool temperate bogs. *Environmental Conservation*, 29(1), pp.3–20.

Moore, R.J., (1985) The probability-distributed principle and runoff production at point and basin scales. *Hydrological Sciences Journal*, 30(2), pp.273–297.

Moore, T., Blodau, C., Turunen, J., Roulet, N. and Richard, P.J.H., (2005) Patterns of nitrogen and sulfur accumulation and retention in ombrotrophic bogs, eastern Canada. *Global Change Biology*, 11, pp.356–367.

Morris, P.J., Waddington, J.M., Benscoter, B.W. and Turetsky, M.R., (2011) Conceptual frameworks in peatland ecohydrology: looking beyond the two-layered (acrotelm-catotelm) model. *Ecohydrology*, 4, pp.1–11.

Muller, F.L.L., Chang, K.C., Lee, C.L. and Chapman, S.J., (2015) Effects of temperature, rainfall and conifer felling practices on the surface water chemistry of northern peatlands. *Biogeochemistry*, 126, pp.343–362.

Muller, F.L.L. and Tankéré-Muller, S.P.C., (2012) Seasonal variations in surface water chemistry at disturbed and pristine peatland sites in the Flow Country of northern Scotland. *Science of the Total Environment*, 435–436, pp.351–362.

Murphy, T., Hanley, M., Ellis, J. and Lunt, P., (2019) Deviation between projected and observed precipitation trends greater with altitude. *Climate Research*, 79, pp.77–89.

Natural England, (2019) *Priority Habitat Inventory (North) (England)*. [online] Available at: https://naturalengland-defra.opendata.arcgis.com/ [Accessed 8 Apr. 2021].

Neal, C., Lofts, S., Evans, C.D., Reynolds, B., Tipping, E. and Neal, M., (2008) Increasing iron concentrations in UK upland waters. *Aquatic Geochemistry*, 14, pp.263–288.

Nieminen, M., Koskinen, M., Sarkkola, S., Laurén, A., Kaila, A., Kiikkilä, O., Nieminen, T.M. and Ukonmaanaho, L., (2015) Dissolved Organic Carbon Export from Harvested Peatland Forests with Differing Site Characteristics. *Water, Air, & Soil Pollution*, 226(181), p.12.

Nieminen, M., Sallantaus, T., Ukonmaanaho, L., Nieminen, T.M. and Sarkkola, S., (2017a) Nitrogen and phosphorus concentrations in discharge from drained peatland forests are increasing. *Science of the Total Environment*, 609, pp.974–981.

Nieminen, M., Sarkkola, S. and Laurén, A., (2017b) Impacts of forest harvesting on nutrient, sediment and dissolved organic carbon exports from drained peatlands: A literature review, synthesis and suggestions for the future. *Forest Ecology and Management*, 392, pp.13–20.

Novak, M. and Pacherova, P., (2008) Mobility of trace metals in pore waters of two Central European peat bogs. *Science of the Total Environment*, 394, pp.331–337.

Novak, M., Zemanova, L., Voldrichova, P., Stepanova, M., Adamova, M., Pacherova, P., Komarek, A., Krachler, M. and Prechova, E., (2011) Experimental evidence for mobility/immobility of metals in peat. *Environmental Science and Technology*, 45, pp.7180–7187.

Novák, V., (2012) *Evapotranspiration in the soil-plant-atmosphere system*. *Progress in Soil Science*. Dordrecht: Springer Netherlands.

Ohmura, A., (1982) Objective criteria for rejecting data for Bowen ratio flux calculations. *Journal of Applied Meteorology*, 21, pp.595–598.

Oke, T.R., (1987) *Boundary layer climates*. Second ed. Methuen.

Oliphant, A., Susan, C., Grimmond, B., Schmid, H.P. and Wayson, C.A., (2006) Local-scale heterogeneity of photosynthetically active radiation (PAR), absorbed PAR and net radiation as a function of topography, sky conditions and leaf area index. *Remote Sensing of Environment*, 103, pp.324–337.

Ordnance Survey, (2020) *OS Terrain 5 [ASC geospatial data]*. [online] Available at: https://digimap.edina.ac.uk [Accessed 29 Mar. 2021].

Orr, H.G., Wilby, R.L., Hedger, M.M. and Brown, I., (2008) Climate change in the uplands: A UK perspective on safeguarding regulatory ecosystem services. *Climate Research*, 37, pp.77–98.

Ortega-Farias, S.O., Cuenca, R.H. and Ek, M., (1996) Daytime variation of sensible heat flux estimated by the bulk aerodynamic method over a grass canopy. *Agricultural and Forest Meteorology*, 81, pp.131–143.

Page, S.E. and Baird, A.J., (2016) Peatlands and Global Change: Response and Resilience. *Annual Review of Environment and Resources*, 41, pp.35–57.

Palviainen, M., Finér, L., Laurén, A., Launiainen, S., Piirainen, S., Mattsson, T. and Starr, M., (2014) Nitrogen, phosphorus, carbon, and suspended solids loads from forest clear-cutting and site preparation: Long-term paired catchment studies from eastern Finland. *Ambio*, 43, pp.218–233.

Parry, L.E., Holden, J. and Chapman, P.J., (2014) Restoration of blanket peatlands. *Journal of Environmental Management*, 133, pp.193–205.

Pawson, R.R., Evans, M.G. and Allott, T.E.H., (2012) Fluvial carbon flux from headwater peatland streams: Significance of particulate carbon flux. *Earth Surface Processes and Landforms*, 37, pp.1203–1212.

Payero, J.O., Neale, C.M.U., Wright, J.L. and Allen, R.G., (2003) Guidelines for validating Bowen ratio data. *Transactions of the ASAE*, 46(4), pp.1051–1060.

Peacock, C.E. and Hess, T.M., (2004) Estimating evapotranspiration from a reed bed using the Bowen ratio energy balance method. *Hydrological Processes*, 18, pp.247–260.

Peacock, M., Burden, A., Cooper, M., Dunn, C., Evans, C.D., Fenner, N., Freeman, C., Gough, R., Hughes, D., Hughes, S., Jones, T., Lebron, I., West, M. and Zieliński, P., (2013a) Quantifying dissolved organic carbon concentrations in upland catchments using phenolic proxy measurements. *Journal of Hydrology*, 477, pp.251–260.

Peacock, M., Evans, C.D., Fenner, N. and Freeman, C., (2013b) Natural revegetation of bog pools after peatland restoration involving ditch blocking—The influence of pool depth and implications for carbon cycling. *Ecological Engineering*, 57, pp.297–301.

Peacock, M., Evans, C.D., Fenner, N., Freeman, C., Gough, R., Jones, T.G. and Lebron, I., (2014) UV-visible absorbance spectroscopy as a proxy for peatland dissolved organic carbon (DOC) quantity and quality: considerations on wavelength and absorbance degradation. *Environmental Science: Processes & Impacts*, 16, pp.1445–1461.

Peacock, M., Jones, T.G., Futter, M.N., Freeman, C., Gough, R., Baird, A.J., Green, S.M., Chapman, P.J., Holden, J. and Evans, C.D., (2018) Peatland ditch blocking has no effect on dissolved organic matter (DOM) quality. *Hydrological Processes*, 32, pp.3891–3906.

Peichl, M., Sagerfors, J., Lindroth, A., Buffam, I., Grelle, A., Klemedtsson, L., Laudon, H. and Nilsson, M.B., (2013) Energy exchange and water budget partitioning in a boreal minerogenic mire. *Journal of Geophysical Research: Biogeosciences*, 118, pp.1–13.

Penman, H.L., (1948) Natural evaporation from open water, bare soil and grass. *Proceedings of the Royal Society of London. Series A, Mathematical and Physical Sciences*, 193(1032), pp.120–145.

Perez, P.J., Castellvi, F., Ibañez, M. and Rosell, J.I., (1999) Assessment of reliability of Bowen ratio method for partitioning fluxes. *Agricultural and Forest Meteorology*, 97, pp.141–150.

Peterson, T.C., Easterling, D.R., Karl, T.R., Groisman, P., Nicholls, N., Plummer, N., Torok, S., Auer, I., Boehm, R., Gullett, D., Vincent, L., Heino, R., Tuomenvirta, H., Mestre, O., Szentimrey, T., Salinger, J., Førland, E.J., Hanssen-Bauer, I., Alexandersson, H., Jones, P. and Parker, D., (1998) Homogeneity adjustments ofin situ atmospheric climate data: a review. *International Journal of Climatology*, 18, pp.1493–1517.

Phillips, J., Yalden, D. and Tallis, J.H., (1981) *Peak Dsitrict Moorland Erosion Study: Phase 1 Report*. Bakewell: Peak Park Joint Planning Board.

Pickard, A.E., Branagan, M., Billett, M.F., Andersen, R. and Dinsmore, K.J., (2022) Effects of peatland management on aquatic carbon concentrations and fluxes. *Biogeosciences*, 19, pp.1321–1334.

Pike, N., (2011) Using false discovery rates for multiple comparisons in ecology and evolution. *Methods in Ecology and Evolution*, 2, pp.278–282.

Pilgrim, D.H., Cordery, I. and Baron, B.C., (1982) Effects of catchment size on runoff relationships. *Journal of Hydrology*, 58, pp.205–221.

Pokrovsky, O.S., Dupré, B. and Schott, J., (2005) *Fe-Al-organic colloids control of trace elements in peat soil solutions: Results of ultrafiltration and dialysis. Aquatic Geochemistry*, .

Poszwa, A., Dambrine, E., Pollier, B. and Atteia, O., (2000) A comparison between Ca and Sr cycling in forest ecosystems. *Plant and Soil*, 225(1-2), pp.299–310.

Potschin, M.B. and Haines-Young, R.H., (2011) Ecosystem services: Exploring a geographical perspective. *Progress in Physical Geography*, 35(5), pp.575–594.

Pravia, A., Andersen, R., Artz, R.R.E., Boyd, K., Cowie, N.R. and Littlewood, N.A., (2020) Moth responses to forest-to-bog restoration. *Mires and Peat*, 26, pp.1–19.

Price, J.S., (1991) Evaporation from a blanket bog in a foggy coastal environment. *Boundary-Layer Meteorology*, 57, pp.391–406.

Price, J.S., (1992a) Blanket bog in Newfoundland. Part 1. The occurrence and accumulation of fog-water deposits. *Journal of Hydrology*, 135, pp.87–101.

Price, J.S., (1992b) Blanket bog in Newfoundland. Part 2. Hydrological processes. *Journal of Hydrology*, 135, pp.103–119.

Price, J.S., Edwards, T.W.D., Yi, Y. and Whittington, P.N., (2009) Physical and isotopic characterization of evaporation from Sphagnum moss. *Journal of Hydrology*, 369, pp.175–182.

Priestley, C.H.B. and Taylor, R.J., (1972) On the assessment of surface heat flux and evaporation using large-scale parameters. *Monthly Weather Review*, 100, pp.81–92.

Quinty, F. and Rochefort, L., (2003) *Peatland restoration guide*. 2nd ed. Québec: Canadian Sphagnum Peat Moss Association and New Brunswick Department of Natural Resources and Energy.

Ratcliffe, J.L., Payne, R.J., Sloan, T.J., Smith, B., Waldron, S., Mauquoy, D., Newton, A., Anderson, A.R., Henderson, A. and Andersen, R., (2018) Holocene carbon accumulation in the peatlands of northern Scotland. *Mires and Peat*, 23, pp.1–30.

Reed, M.S., Allen, K., Attlee, A., Dougill, A.J., Evans, K.L., Kenter, J.O., Hoy, J., McNab, D., Stead, S.M., Twyman, C., Scott, A.S., Smyth, M.A., Stringer, L.C. and Whittingham, M.J., (2017) A place-based approach to payments for ecosystem services. *Global Environmental Change*, 43, pp.92–106.

Reed, M.S., Bonn, A., Evans, C., Joosten, H., Bain, B., Farmer, J., Emmer, I., Couwenberg, J., Moxey, A., Artz, R., Tanneberger, F., von Unger, M., Smyth, M., Birnie, R., Inman, I., Smith, S., Quick, T., Cowap, C., Prior, S. and Lindsay, R.A., (2013) *Towards the development of a UK Peatland Code: Payments for Ecosystem Services (PES) Pilot Research Project*. *Department for Environment, Food and Rural Affairs (Defra)*. London.

Richey, J.E., Melack, J.M., Aufdenkampe, A.K., Ballester, V.M. and Hess, L.L., (2002) Outgassing from Amazonian rivers and wetlands as a large tropical source of atmospheric CO_2. *Nature*, 416, pp.617–620.

Ritson, J.P., Brazier, R.E., Graham, N.J.D., Freeman, C., Templeton, M.R. and Clark, J.M., (2017) The effect of drought on dissolved organic carbon (DOC) release from peatland soil and vegetation sources. *Biogeosciences*, 14, pp.2891–2902.

Ritson, J.P., Graham, N.J.D., Templeton, M.R., Clark, J.M., Gough, R. and Freeman, C., (2014) The impact of climate change on the treatability of dissolved organic matter (DOM) in upland water supplies: A UK perspective. *Science of the Total Environment*, 473–474, pp.714–730.

Robinson, M., Cognard-Plancq, A.L., Cosandey, C., David, J., Durand, P., Führer, H.W., Hall, R., Hendriques, M.O., Marc, V., McCarthy, R., McDonnell, M., Martin, C., Nisbet, T., O'Dea, P., Rodgers, M. and Zollner, A., (2003) Studies of the impact of forests on peak flows and baseflows: A European perspective. *Forest Ecology and Management*, 186, pp.85–97.

Robroek, B.J.M., Smart, R.P. and Holden, J., (2010) Sensitivity of blanket peat vegetation and hydrochemistry to local disturbances. *Science of the Total Environment*, 408, pp.5028–5034.

Rodgers, M., O'Connor, M., Healy, M.G., O'Driscoll, C., Asam, Z.-Z., Nieminen, M., Poole, R., Müller, M. and Xiao, L., (2010) Phosphorus release from forest harvesting on an upland blanket peat catchment. *Forest Ecology and Management*, 260, pp.2241–2248.

Rothwell, J.J., Evans, M.G., Daniels, S.M. and Allott, T.E.H., (2007) Baseflow and stormflow metal concentrations in streams draining contaminated peat moorlands in the Peak District National Park (UK). *Journal of Hydrology*, 341, pp.90–104.

Rothwell, J.J., Robinson, S.G., Evans, M.G., Yang, J. and Allott, T.E.H., (2005) Heavy metal release by peat erosion in the Peak District, southern Pennines, UK. *Hydrological Processes*, 19, pp.2973–2989.

Runkle, B.R.K., Wille, C., Gažovič, M., Wilmking, M. and Kutzbach, L., (2014) The surface energy balance and its drivers in a boreal peatland fen of northwestern Russia. *Journal of Hydrology*, 511, pp.359–373.

Russell, F.E., Boyle, J.F. and Chiverrell, R.C., (2019) NIRS quantification of lake sediment composition by multiple regression using end-member spectra. *Journal of Paleolimnology*, 62, pp.73–88.

Ryder, E., de Eyto, E., Dillane, M., Poole, R. and Jennings, E., (2014) Identifying the role of environmental drivers in organic carbon export from a forested peat catchment. *Science of the Total Environment*, 490, pp.28–36.

Rydin, H. and Jeglum, J.K., (2013) *The Biology of Peatlands*. Oxford University Press.

Safeeq, M., Bart, R.R., Pelak, N.F., Singh, C.K., Dralle, D.N., Hartsough, P. and Wagenbrenner, J.W., (2021) How realistic are water-balance closure assumptions? A demonstration from the southern sierra critical zone observatory and kings river experimental watersheds. *Hydrological Processes*, 35(e14199), p.16.

Schlesinger, W.H. and Bernhardt, E.S., (2013) *Biogeochemistry: an analysis of global change*. 3rd ed. Academic Press.

Schmitt, A.D. and Stille, P., (2005) The source of calcium in wet atmospheric deposits: Ca-Sr isotope evidence. *Geochimica et Cosmochimica Acta*, 69(14), pp.3463–3468.

Schreiber, N., Garcia, E., Kroon, A., Ilsøe, P.C., Kjær, K.H. and Andersen, T.J., (2014) Pattern Recognition on X-ray Fluorescence Records from Copenhagen Lake Sediments Using Principal Component Analysis. *Water, Air, & Soil Pollution*, 225(2221), p.11.

Scott, M.J., Jones, M.N., Woof, C. and Tipping, E., (1998) Concentrations and fluxes of dissolved organic carbon in drainage water from an upland peat system. *Environment International*, 24(5-6), pp.537–546.

Segura, C., James, A.L., Lazzati, D. and Roulet, N.T., (2012) Scaling relationships for event water contributions and transit times in small-forested catchments in Eastern Quebec. *Water Resources Research*, 48(W07502), p.21.

Seneviratne, S.I., Lüthi, D., Litschi, M. and Schär, C., (2006) Land-atmosphere coupling and climate change in Europe. *Nature*, 443, pp.205–209.

Shotyk, W., (1988) Review of the inorganic geochemistry of peats and peatland waters. *Earth Science Reviews*, 25, pp.95–176.

Shotyk, W., (1997) Atmospheric deposition and mass balance of major and trace elements in two oceanic peat bog profiles, northern Scotland and the Shetland Islands. *Chemical Geology*, 138, pp.55–72.

Shotyk, W., Wayne Nesbitt, H. and Fyfe, W.S., (1990) The behaviour of major and trace elements in complete vertical peat profiles from three Sphagnum bogs. *International Journal of Coal Geology*, 15, pp.163–190.

Shotyk, W., Wayne Nesbitt, H. and Fyfe, W.S., (1992) Natural and antropogenic enrichments of trace metals in peat profiles. *International Journal of Coal Geology*, 20, pp.49–84.

Shuttleworth, E.L., Evans, M.G., Hutchinson, S.M. and Rothwell, J.J., (2015) Peatland restoration: Controls on sediment production and reductions in carbon and pollutant export. *Earth Surface Processes and Landforms*, 40, pp.459–472.

Shuttleworth, E.L., Evans, M.G., Pilkington, M., Spencer, T., Walker, J., Milledge, D. and Allott, T.E.H., (2019) Restoration of blanket peat moorland delays stormflow from hillslopes and reduces peak discharge. *Journal of Hydrology X*, 2(100006), p.14.

Shuttleworth, W.J., (2007) Putting the 'vap' into evaporation. *Hydrology and Earth System Sciences*, 11(1), pp.210–244.

Singh, R.K., Liu, S., Tieszen, L.L., Suyker, A.E. and Verma, S.B., (2012) Novel approach for computing photosynthetically active radiation for productivity modeling using remotely sensed images in the Great Plains, United States. *Journal of Applied Remote Sensing*, 6.

Sloan, T.J., Payne, R.J., Anderson, A.R., Bain, C., Chapman, S., Cowie, N.R., Gilbert, P., Lindsay, R., Mauquoy, D., Newton, A.J. and Andersen, R., (2018a) Peatland afforestation in the UK and consequences for carbon storage. *Mires and Peat*, 23(1), pp.1–17.

Sloan, T.J., Payne, R.J., Anderson, A.R., Gilbert, P., Mauquoy, D., Newton, A.J. and Andersen, R., (2018b) Ground surface subsidence in an afforested peatland fifty years after drainage and planting. *Mires and Peat*, 23(6), pp.1–12.

Smart, R.P., Holden, J., Dinsmore, K.J., Baird, A.J., Billett, M.F., Chapman, P.J. and Grayson, R., (2013) The dynamics of natural pipe hydrological behaviour in blanket peat. *Hydrological Processes*, 27, pp.1523–1534.

Sottocornola, M. and Kiely, G., (2010) Energy fluxes and evaporation mechanisms in an Atlantic blanket bog in southwestern Ireland. *Water Resources Research*, 46(W11524), p.13.

Strack, M. and Waddington, J.M., (2007) Response of peatland carbon dioxide and methane fluxes to a water table drawdown experiment. *Global Biogeochemical Cycles*, 21(GB1007), p.13.

Strack, M., Zuback, Y., McCarter, C. and Price, J.S., (2015) Changes in dissolved organic carbon quality in soils and discharge 10years after peatland restoration. *Journal of Hydrology*, 527, pp.345–354.

Strahler, A.N., (1957) Quantitative analysis of watershed geomorphology. *Eos, Transactions American Geophysical Union*, 38(6), pp.913–920.

Strobl, K., Moning, C. and Kollmann, J., (2020) Positive trends in plant, dragonfly, and butterfly diversity of rewetted montane peatlands. *Restoration Ecology*, 28(4), pp.796–806.

Swindles, G.T., Morris, P.J., Mullan, D.J., Payne, R.J., Roland, T.P., Amesbury, M.J., Lamentowicz, M., Turner, T.E., Gallego-Sala, A.V., Sim, T., Barr, I.D., Blaauw, M., Blundell, A., Chambers, F.M., Charman, D.J., Feurdean, A., Galloway, J.M., Gałka, M., Green, S.M., Kajukało, K., Karofeld, E., Korhola, A., Lamentowicz, Ł., Langdon, P., Marcisz, K., Mauquoy, D., Mazei, Y.A., McKeown, M.M., Mitchell, E.A.D., Novenko, E., Plunkett, G., Roe, H.M., Schoning, K., Sillasoo, Ü., Tsyganov, A.N., van der Linden, M., Väliranta, M. and Warner, B., (2019) Widespread drying of European peatlands in recent centuries. *Nature Geoscience*, 12, pp.922–928.

Swinnen, W., Broothaerts, N. and Verstraeten, G., (2019) Modelling long-term blanket peatland development in eastern Scotland. *Biogeosciences*, 16, pp.3977–3996.

Tallis, J.H., (1994) Pool-and-Hummock Patterning in a Southern Pennine Blanket Mire II. The Formation and Erosion of the Pool System. *The Journal of Ecology*, 824, p.789.

Tallis, J.H., (1998) Growth and degradation of British and Irish blanket mires. *Environmental Reviews*, 6(2), pp.81–122.

Tanneberger, F., Tegetmeyer, C., Busse, S., Barthelmes, A., Shumka, S., Mariné, A.M., Jenederdjian, K., Steiner, G.M., Essl, F., Etzold, J., Mendes, C., Kozulin, A., Frankard, P., Milanović, Ganeva, A., Apostolova, I., Alegro, A., Delipetrou, P., Navrátilová, J., Risager, M., Leivits, A., Fosaa, A.M., Tuominen, S., Muller, F., Bakuradze, T., Sommer, M., Christanis, K., Szurdoki, E., Oskarsson, H., Brink, S.H., Connolly, J., Bragazza, L., Martinelli, G., Aleksāns, O., Priede, A., Sungaila, D., Melovski, L., Belous, T., Saveljić, D., de Vries, F., Moen, A., Dembek, W., Mateus, J., Hanganu, J., Sirin, A., Markina, A., Napreenko, M., Lazarević, P., Stanová, V.Š., Skoberne, P., Pérez, P.H., Pontevedra-Pombal, X., Lonnstad, J., Küchler, M., Wüst-Galley, C., Kirca, S., Mykytiuk, O., Lindsay, R. and Joosten, H., (2017) The peatland map of Europe. *Mires and Peat*, 19(22), pp.1–17.

The British Standards Institution, (2017) *BS ISO 1438:2017*.

Thompson, M.A., Campbell, D.I. and Spronken-Smith, R.A., (1999) Evaporation from natural and modified raised peat bogs in New Zealand. *Agricultural and Forest Meteorology*, 95, pp.85–98.

Thornthwaite, C.W., (1948) An approach toward a rational classification of climate. *Geographical Review*, 38(1), pp.55–94.

Thurman, E.M., (1985) *Organic Geochemistry of Natural Waters*. Dordrecht: Springer.

Tipping, E., Lawlor, A.J., Lofts, S. and Shotbolt, L., (2006) Simulating the long-term chemistry of an upland UK catchment: Heavy metals. *Environmental Pollution*, 141, pp.139–150.

Tipping, E., Rothwell, J.J., Shotbolt, L. and Lawlor, A.J., (2010) Dynamic modelling of atmospherically-deposited Ni, Cu, Zn, Cd and Pb in Pennine catchments (northern England). *Environmental Pollution*, 158, pp.1521–1529.

Tipping, E., Smith, E.J., Lawlor, A.J., Hughes, S. and Stevens, P.A., (2003) Predicting the release of metals from ombrotrophic peat due to drought-induced acidification. *Environmental Pollution*, 123, pp.239–253.

Todd, B., Macdonald, N., Chiverrell, R.C., Caminade, C. and Hooke, J.M., (2013) Severity, duration and frequency of drought in SE England from 1697 to 2011. *Climatic Change*, 121, pp.673–687.

Trenberth, K.E., (2011) Changes in precipitation with climate change. *Climate Research*, 47, pp.123–138.

Trenberth, K.E., Dai, A., Rasmussen, R.M. and Parsons, D.B., (2003) The changing character of precipitation. *Bulletin of the American Meteorological Society*, 84(9), pp.1205–1217.

Turner, N., (1757) *An essay on draining and improving peat bogs; in which their nature and properties are fully considered*. London: Baldwin and Pew.

Turner, S., Barker, L.J., Hannaford, J., Muchan, K., Parry, S. and Sefton, C., (2021) The 2018/2019 drought in the UK: a hydrological appraisal. *Weather*, 76(8), pp.248–253.

Twine, T.E., Kustas, W.P., Norman, J.M., Cook, D.R., Houser, P.R., Meyers, T.P., Prueger, J.H., Starks, P.J. and Wesely, M.L., (2000) Correcting eddy-covariance flux underestimates over a grassland. *Agricultural and Forest Meteorology*, 1033, pp.279–300.

Udo, S.O. and Aro, T.O., (1999) Global PAR related to global solar radiation for central Nigeria. *Agricultural and Forest Meteorology*, 97, pp.21–31.

UK Government, (2021) *England Peat Action Plan*. [online] Available at: www.gov.uk/official-documents.

Unland, H.E., Houser, P.R., Shuttleworth, W.J. and Yang, Z.L., (1996) Surface flux measurement and modeling at a semi-arid Sonoran Desert site. *Agricultural and Forest Meteorology*, 82, pp.119–153.

Väliranta, M., Blundell, A., Charman, D.J., Karofeld, E., Korhola, A., Sillasoo, Ü. and Tuittila, E.-S., (2012) Reconstructing peatland water tables using transfer functions for plant macrofossils and testate amoebae: A methodological comparison. *Quaternary International*, 268, pp.34–43.

Vinichuk, M., Johanson, K.J., Rydin, H. and Rosén, K., (2010) The distribution of 137Cs, K, Rb and Cs in plants in a Sphagnum-dominated peatland in eastern central Sweden. *Journal of Environmental Radioactivity*, 101, pp.170–176.

Volk, C., Wood, L., Johnson, B., Robinson, J., Zhu, H.W. and Kaplan, L., (2002) Monitoring dissolved organic carbon in surface and drinking waters. *Journal of Environmental Monitoring*, 4, pp.43–47.

Waddington, J.M., Morris, P.J., Kettridge, N., Granath, G., Thompson, D.K. and Moore, P.A., (2015) Hydrological feedbacks in northern peatlands. *Ecohydrology*, 8, pp.113–127.

Walker, S. and Smithers, H.A., (1998) A review of the 1995-96 drought in the North West. *Water and Environment Journal*, 12, pp.273–279.

Wallage, Z.E. and Holden, J., (2010) Spatial and temporal variability in the relationship between water colour and dissolved organic carbon in blanket peat pore waters. *Science of The Total Environment*, 408, pp.6235–6242.

Wallage, Z.E. and Holden, J., (2011) Near-surface macropore flow and saturated hydraulic conductivity in drained and restored blanket peatlands. *Soil Use and Management*, 27, pp.247–254.

Wallage, Z.E., Holden, J. and McDonald, A.T., (2006) Drain blocking: An effective treatment for reducing dissolved organic carbon loss and water discolouration in a drained peatland. *Science of The Total Environment*, 367, pp.811–821.

Wang, G.S. and Hsieh, S.T., (2001) Monitoring natural organic matter in water with scanning spectrophotometer. *Environment International*, 26, pp.205–212.

Wang, K. and Dickinson, R.E., (2012) A review of global terrestrial evapotranspiration: Observation, modeling, climatology, and climatic variability. *Reviews of Geophysics*, 502, p.54.

Wang, M., Wu, J. and Lafleur, P., (2020) Comparison of energy fluxes between an undisturbed bog and an adjacent abandoned peatland pasture. *Agricultural and Forest Meteorology*, 291(108086), p.11.

Warnken, K.W., Lawlor, A.J., Lofts, S., Tipping, E., Davison, W. and Zhang, H., (2009) In situ speciation measurements of trace metals in headwater streams. *Environmental Science and Technology*, 43, pp.7230–7236.

Watras, C.J., Morrison, K.A., Rubsam, J.L. and Buffam, I., (2017) Estimates of evapotranspiration from contrasting Wisconsin peatlands based on diel water table oscillations. *Ecohydrology*, 10(e1834), p.12.

Weishaar, J.L., Aiken, G.R., Bergamaschi, B.A., Fram, M.S., Fujii, R. and Mopper, K., (2003) Evaluation of specific ultraviolet absorbance as an indicator of the chemical composition and reactivity of dissolved organic carbon. *Environmental Science and Technology*, 37, pp.4702–4708.

Wessel, D.A. and Rouse, W.R., (1994) Modelling evaporation from wetland tundra. *Boundary-Layer Meteorology*, 68, pp.109–130.

Wheeler, D., (2013) Regional weather and climates of the British Isles - Part 4: North East England and Yorkshire. *Weather*, 68(7), pp.184–190.

White, W.N., (1932) A method of estimating ground-water supplies based on discharge by plants and evaporation from soil: Results of investigations in Escalante Valley, Utah. *Water Supply Paper 659 - A*, p.105.

Williamson, J.L., Tye, A., Lapworth, D.J., Monteith, D., Sanders, R., Mayor, D.J., Barry, C., Bowes, M., Bowes, M., Burden, A., Callaghan, N., Farr, G., Felgate, S., Fitch, A., Gibb, S., Gilbert, P., Hargreaves, G., Keenan, P., Kitidis, V., Juergens, M., Martin, A., Mounteney, I., Nightingale, P.D., Pereira, M.G., Olszewska, J., Pickard, A., Rees, A.P., Spears, B., Stinchcombe, M., White, D., Williams, P., Worrall, F. and Evans, C., (2021) Landscape controls on riverine export of dissolved organic carbon from Great Britain. *Biogeochemistry*, 2, p.22.

Wilson, L., Wilson, J., Holden, J., Johnstone, I., Armstrong, A. and Morris, M., (2010) Recovery of water tables in Welsh blanket bog after drain blocking: Discharge rates, time scales and the influence of local conditions. *Journal of Hydrology*, 391, pp.377–386.

Wilson, L., Wilson, J., Holden, J., Johnstone, I., Armstrong, A. and Morris, M., (2011a) Ditch blocking, water chemistry and organic carbon flux: Evidence that blanket bog restoration reduces erosion and fluvial carbon loss. *Science of the Total Environment*, 409, pp.2010–2018.

Wilson, L., Wilson, J., Holden, J., Johnstone, I., Armstrong, A. and Morris, M., (2011b) The impact of drain blocking on an upland blanket bog during storm and drought events, and the importance of sampling-scale. *Journal of Hydrology*, 404, pp.198–208.

Wilson, R.M., Hopple, A.M., Tfaily, M.M., Sebestyen, S.D., Schadt, C.W., Pfeifer-Meister, L., Medvedeff, C., McFarlane, K.J., Kostka, J.E., Kolton, M., Kolka, R.K., Kluber, L.A., Keller, J.K., Guilderson, T.P., Griffiths, N.A., Chanton, J.P., Bridgham, S.D. and Hanson, P.J., (2016) Stability of peatland carbon to rising temperatures. *Nature Communications*, 7(13723), p.10.

Word, C.S., McLaughlin, D.L., Strahm, B.D., Stewart, R.D., Varner, J.M., Wurster, F.C., Amestoy, T.J. and Link, N.T., (2022) Peatland drainage alters soil structure and water retention properties: Implications for ecosystem function and management. *Hydrological Processes*, 36, pp.1–12.

Worrall, F., Burt, T.P. and Adamson, J., (2006) Long-term changes in hydrological pathways in an upland peat catchment - recovery from severe drought? *Journal of Hydrology*, 321, pp.5–20.

Worrall, F., Burt, T.P., Adamson, J., Reed, M., Warburton, J., Armstrong, A. and Evans, M.G., (2007) Predicting the future carbon budget of an upland peat catchment. *Climatic Change*, 85, pp.139–158.

Worrall, F., Burt, T.P., Clay, G.D. and Moody, C.S., (2015) A 19-year long energy budget of an upland peat bog, northern England. *Journal of Hydrology*, 520, pp.17–29.

Worrall, F., Burt, T.P. and Howden, N.J.K., (2014) The fluvial flux of particulate organic matter from the UK: Quantifying in-stream losses and carbon sinks. *Journal of Hydrology*, 519, pp.611–625.

Worrall, F., Burt, T.P., Jaeban, R.Y., Warburton, J. and Shedden, R., (2002) Release of dissolved organic carbon from upland peat. *Hydrological Processes*, 16, pp.3487–3504.

Worrall, F., Davies, H., Bhogal, A., Lilly, A., Evans, M.G., Turner, K., Burt, T.P., Barraclough, D., Smith, P. and Merrington, G., (2012) The flux of DOC from the UK - Predicting the role of soils, land use and net watershed losses. *Journal of Hydrology*, 448–449, pp.149–160.

Worrall, F., Gibson, H.S. and Burt, T.P., (2008) Production vs. solubility in controlling runoff of DOC from peat soils – The use of an event analysis. *Journal of Hydrology*, 358, pp.84–95.

Worrall, F., Moody, C.S., Clay, G.D., Burt, T.P. and Rose, R., (2016) The total phosphorus budget of a peat-covered catchment. *Journal of Geophysical Research: Biogeosciences*, 121, pp.1814–1828.

Worrall, F., Moody, C.S., Clay, G.D., Burt, T.P. and Rose, R., (2017) The flux of organic matter through a peatland ecosystem: The role of cellulose, lignin, and their control of the ecosystem oxidation state. *Journal of Geophysical Research: Biogeosciences*, 122, pp.1655–1671.

Worrall, F., Reed, M., Warburton, J. and Burt, T.P., (2003) Carbon budget for a British upland peat catchment. *Science of The Total Environment*, 312, pp.133–146.

Xu, J., Morris, P.J., Liu, J. and Holden, J., (2018) PEATMAP: Refining estimates of global peatland distribution based on a meta-analysis. *CATENA*, 160, pp.134–140.

Yallop, A.R., Clutterbuck, B. and Thacker, J., (2010) Increases in humic dissolved organic carbon export from upland peat catchments: The role of temperature, declining sulphur deposition and changes in land management. *Climate Research*, 45, pp.43–56.

Yamamuro, M. and Kayanne, H., (1995) Rapid direct determination of organic carbon and nitrogen in carbonate-bearing sediments with a Yanaco MT-5 CHN analyzer. *Limnology and Oceanography*, 40(5), pp.1001–1005.

Yamulki, S., Anderson, R., Peace, A. and Morison, J.I.L., (2013) Soil CO2 CH4 and N2O fluxes from an afforested lowland raised peatbog in Scotland: Implications for drainage and restoration. *Biogeosciences*, 10, pp.1051–1065.

Ye, R., Jin, Q., Bohannan, B., Keller, J.K., McAllister, S.A. and Bridgham, S.D., (2012) pH controls over anaerobic carbon mineralization, the efficiency of methane production, and methanogenic pathways in peatlands across an ombrotrophic–minerotrophic gradient. *Soil Biology and Biochemistry*, 54, pp.36–47.

Yeloff, D.E., Labadz, J.C., Hunt, C.O., Higgitt, D.L. and Foster, I.D.L., (2005) Blanket peat erosion and sediment yield in an upland reservoir catchment in the southern Pennines, UK. *Earth Surface Processes and Landforms*, 30, pp.717–733.

Yu, Z., Loisel, J., Brosseau, D.P., Beilman, D.W. and Hunt, S.J., (2010) Global peatland dynamics since the Last Glacial Maximum. *Geophysical Research Letters*, 37(L13402), p.5.

Zaccone, C., Plaza, C., Ciavatta, C., Miano, T.M. and Shotyk, W., (2018) Advances in the determination of humification degree in peat since Achard (1786): Applications in geochemical and paleoenvironmental studies. *Earth-Science Reviews*, 185, pp.163–178.

Zheng, Y., Waldron, S. and Flowers, H., (2018) Fluvial dissolved organic carbon composition varies spatially and seasonally in a small catchment draining a wind farm and felled forestry. *Science of the Total Environment*, 626, pp.785–794.